

Low-temperature cryocooling

PROEFSCHRIFT

ter verkrijging van de graad van doctor
aan de Technische Universiteit Eindhoven,
op gezag van de Rector Magnificus, prof.dr. R.A. van Santen,
voor een commissie aangewezen door het College
voor Promoties in het openbaar te verdedigen op
woensdag 27 oktober 2004 om 16.00 uur

door

Irina Tanaeva

geboren te Moskou, Rusland

Dit proefschrift is goedgekeurd door de promotoren:

prof.dr. A.T.A.M. de Waele

en

prof.dr. G. Thummes

CIP-DATA LIBRARY TECHNISCHE UNIVERSITEIT EINDHOVEN

Tanaeva, Irina

Low-temperature cryocooling / by Irina Tanaeva. -
Eindhoven : Technische Universiteit Eindhoven, 2004. –

Proefschrift.

ISBN 90-386-2005-5

NUR 924

Trefw.: cryogene techniek / thermodynamica / pulsbus koelers / regeneratoren /
superfluiditeit

Subject headings: cryogenics / pulse-tube refrigerators / cryocoolers / regenerators /
superfluid helium

Drukwerk: Universiteitsdrukkerij TUE

Omslag: Paul Verspaget

Foto: Jacques Dam

To my parents

Моим родителям посвящается

CONTENTS

Chapter 1.	INTRODUCTION	1
1.1.	Cryocoolers and their applications	1
1.2.	General introduction to pulse-tube refrigerators (PTRs)	2
1.3.	Introduction to this thesis	4
	References	6
Chapter 2.	THEORETICAL ASPECTS OF PULSE-TUBE REFRIGERATORS	7
2.1.	Two types of the PTR, depending on the gas compression method	7
2.2.	The operation principle of pulse-tube refrigerators	9
2.3.	Cooling power	12
2.4.	Coefficient of performance	
2.5.	Multistage pulse-tube refrigerators	20
2.6.	The main components of the PTR and their functions	22
2.6.1.	Compressor	22
2.6.2.	Rotary valve	24
2.6.3.	Heat exchangers	25
2.6.4.	Regenerator	27
2.6.4.1.	Regenerator and its function	27
2.6.4.2.	Temperature profile in the regenerator with an ideal gas	28
2.6.4.3.	Non-ideal gas effects in the regenerator	31
2.6.4.4.	Regenerator losses	35
2.6.5.	Pulse tube	36
2.6.5.1.	Velocities of the gas at the hot and at the cold ends	36
2.6.5.2.	Pulse tube losses	38
2.6.6.	Flow straighteners	38
2.6.7.	1 st orifice	40
2.6.8.	Double-inlet orifice	41
2.6.9.	Minor orifice	41
2.7.	Conclusions	41
	References	42

Chapter 3.	PRACTICAL ASPECTS OF PULSE-TUBE REFRIGERATORS, PART I	45
3.1.	^4He and ^3He as working fluids in the PTR	45
3.2.	Three-stage PTR (PTR1)	45
3.3.	Two-stage PTR (PTR2)	48
3.3.1.	Experimental set-up	48
3.3.2.	Material fixation in the regenerator	50
3.3.3.	Regenerator flow resistance	52
3.3.4.	Orifices optimum	55
3.3.5.	Cooling power	59
3.4.	Rotary valve	59
3.4.1.	Conventional rotary valve (valve 1)	60
3.4.2.	Modified conventional rotary valve (valve 2)	64
3.4.3.	'No-contact' rotary valve (valve 3)	68
3.4.3.1.	The construction of a 'no-contact' rotary valve	68
3.4.3.2.	The maximum leak rate	70
3.4.3.3.	The power loss	71
3.4.3.4.	The influence of the shape of the radial channel in the rotor on the shape of the pressure wave in the PTR	72
3.5.	Conclusions	75
	References	78
 Chapter 4.	 PRACTICAL ASPECTS OF PULSE-TUBE REFRIGERATORS, PART II	 79
4.1.	Design of the new three-stage PTR	79
4.2.	New tree-stage PTR (PTR3)	82
4.3.	Experimental results with ^4He	87
4.3.1.	Optimum frequency	87
4.3.2.	2 nd stage improvement	89
4.3.3.	Improvement of the 3 rd stage	92
4.3.3.1.	The length of the pulse tube	92
4.3.3.2.	Two different types of ErNi in the 3 rd stage regenerator	94
4.3.4.	Cooling power of PTR3. Comparison of PTR3 with PTR1	95
4.3.5.	The performance of PTR3, driven by 4 kW and 2 kW compressors	97
4.4.	^3He experiments	99
4.5.	Conclusions and discussions	102
	References	104

Chapter 5.	HEAT CAPACITIES AND MAGNETIC MOMENTS OF POTENTIAL REGENERATOR MATERIALS AT LOW TEMPERATURES	105
5.1.	Selection of magnetic materials	105
5.2.	The samples preparation and their magnetic moments	107
5.2.1.	Preparation procedure	107
5.2.2.	Magnetic moments measurements	107
5.3.	Heat capacity measurements	109
5.3.1.	The experimental set-up and technique	109
5.3.2.	Results	112
5.4.	The optimum quantity of regenerator material	115
5.5.	Preliminary ^4He test with GdAlO_3 in the 3 rd stage regenerator of PTR3	118
5.6.	Conclusions	118
	References	119
Chapter 6.	SUPERFLUID VORTEX COOLER	121
6.1.	Operation principle of the SVC	121
6.1.1.	Fountain effect	121
6.1.2.	Vortex cooling effect	124
6.1.3.	Superfluid vortex cooler	125
6.2.	Conceptual design of the SVC	125
6.2.1.	Diameters of superleaks and capillaries	125
6.2.2.	Thermal losses in the SVC	128
6.2.2.1.	Heat conduction	128
6.2.2.2.	Heat transport with the normal flow	128
6.2.2.3.	Dissipation in the capillaries	132
6.3.	The experimental set-up and results	133
6.3.1.	Experimental set-up	133
6.3.2.	Results of the measurements	134
6.3.3.	Cooling power	140
6.4.	Conclusions	142
	References	142
Chapter 7.	THE SUPERFLUID VORTEX COOLER, INTEGRATED WITH A PULSE-TUBE REFRIGERATOR	145
7.1.	The integration of the SVC with the PTR	145
7.1.1.	The SVC and the PTR before the integration	145
7.1.2.	Filling capillaries	146
7.1.3.	The integration of the SVC with the PTR	147
7.2.	Experimental results	149
7.3.	Conclusions and suggestions	150
	References	151

Contents

Chapter 8. SUMMARY	153
APPENDIX	155
SAMENVATTING	161
КРАТКОЕ СОДЕРЖАНИЕ	163
AKNOWLEDGMENTS	167
CURRICULUM VITAE	169

CHAPTER 1

INTRODUCTION

An increased need in cryogenic temperatures in research and high technology during the last decade caused a rapid development of cryocoolers. Some cryocooler applications are briefly described in this chapter. Most of the applications require high efficiency and reliability of a cooler as well as its long lifetime and a low cost. A new concept of cryocooler, the pulse-tube refrigerator (PTR), meets many of these requirements. The main emphasis of this thesis is made on PTRs. In this chapter a short review on the history of PTRs is presented. A general description of the content of this thesis is given as well.

1.1 CRYOCOOLERS AND THEIR APPLICATIONS

This thesis deals with various aspects of low-temperature cryocooling. Cryocoolers are refrigerating machines, which are able to achieve and to maintain cryogenic temperatures, *i.e.* temperatures below 120 K. At this temperature methane and the so-called permanent gases, such as nitrogen, oxygen, and argon, begin to liquefy. According to the second law of thermodynamics, the work, required to reach and to maintain low temperatures, increases with the decrease of a desired low temperature (see Chapter 2). For example, to provide 1 W of refrigeration at 80 K requires at least 2.6 W of the input power, while to provide 1 W of refrigeration at 4 K requires at least 72 W of power.

At low temperatures the properties of many materials undergo considerable modifications. It is a matter of experimental observations and experience that a given change in properties often seems to be related more to the factor by which the absolute temperature is varied than to the actual magnitude of the variation [1].

From all said above it is clear, that the lower the temperature the more difficult it is to obtain a unit of a temperature decrease. However, these difficulties make the process of obtaining low temperatures very attractive and challenging.

The main goal of cryocoolers development is not only to reach and to maintain low temperatures, but also to make the process of obtaining low temperatures, and therefore, the cryocoolers, more efficient and reliable. The application area of cryocoolers is very large. As the temperature decreases, the thermal noise decreases as well. Therefore, one major application of cryocoolers is cooling of various detectors for space, military, environmental, and commercial purposes (e.g. infrared detectors for Earth observation, night vision, missile guidance, gamma ray detectors, and bolometers for astrophysics, etc.). The other large application area of cryocoolers is for cryopumping for high and clean vacuum (semiconductor industry, particle acceleration, etc.).

Some metallic elements, intermetallic compounds, and alloys exhibit the phenomenon of superconductivity at low temperatures. This phenomenon can be

described as the absence of electrical resistance. The range of crytical temperatures (the temperatures, at which materials become superconductive) varies between a few tenth of a mK to 110 K for the Bi-2223 superconductor. All superconductors for applications have to be cooled, thus providing a lot of possibilities for using cryocoolers. A good example of a device, containing a superconducting magnet, is a magnetic resonance imaging (MRI) system. The substitution of the helium bath, surrounding the magnet, with a cryocooler, will make the system smaller and cheaper [2]. Another option is to use a cryocooler for reducing the boil-off of helium, which would make the MRI system cheaper as well.

In addition to the applications, mentioned above, cryocoolers are also used in transportation and storage of liquid gases and other products, as well as for cryosurgery, agriculture, and biology.

1.2. GENERAL INTRODUCTION TO PULSE-TUBE REFRIGERATORS (PTRs)

Most of the applications require a cooler to be efficient, reliable, to have a long lifetime, a low cost, and to operate without interference with an object to be cooled. However, the presence of moving parts in the cold area of most of cryocoolers makes it difficult to meet all these requirements. A new concept of a cryocooler, the pulse-tube refrigerator (PTR), satisfies many of these requirements. A PTR is a closed-cycle regenerative mechanical cooler. The main distinction of PTRs from other closed-cycle mechanical coolers, such as Stirling coolers or Gifford-McMahon (GM) coolers[3], is that the PTR has no moving parts in the low-temperature region, and, therefore, has a long lifetime and low mechanical and magnetical interferences. The operating principle of the PTR is based on the displacement and the expansion of gas in the pulse tube that results in the reduction of the temperature. Usually the PTR uses helium as a working fluid. The working fluid undergoes an oscillating flow and an oscillating pressure. A typical average pressure in a PTR is 10 to 25 bar, and a typical pressure amplitude is 2 to 7 bar. A piston compressor (in case of a Stirling type PTR) or a combination of a compressor and a set of switching valves (GM type PTR) are used to create pressure oscillations in a PTR. The regenerator of a PTR stores the heat of the gas in its material during a half of a cycle, and, therefore, must have a high heat capacity, compared to the heat capacity of the gas.

Pulse-tube refrigerators have their origin in an observation that W. E. Gifford made, while working on the compressor in the late 1950's. He noticed that a tube, which branched from the high-pressure line and was closed by a valve, was hotter at the valve than at the branch. He recognised that there was a heat pumping mechanism that resulted from pressure pulses in the line. Thus, in 1963 Gifford together with his research assistant R. C. Longworth introduced the Pulse-Tube Refrigerator, which nowadays is known as the Basic Pulse-Tube Refrigerator (BPTR) [4]. Note, that the BPTR has not so much in common with the modern PTRs. The cooling principle of the BPTR is the surface heat pumping, which is based on the exchange of heat between the working gas and the pulse-tube walls. However, in modern pulse-tube coolers the heat pumping mechanism, in most cases, is a negative effect, which has to be avoided.

The lowest temperature, reached by Gifford and Longworth with the BPTR, was 124 K with a single-stage PTR and 79 K with a two-stage PTR (see FIG. 1.1) [5].

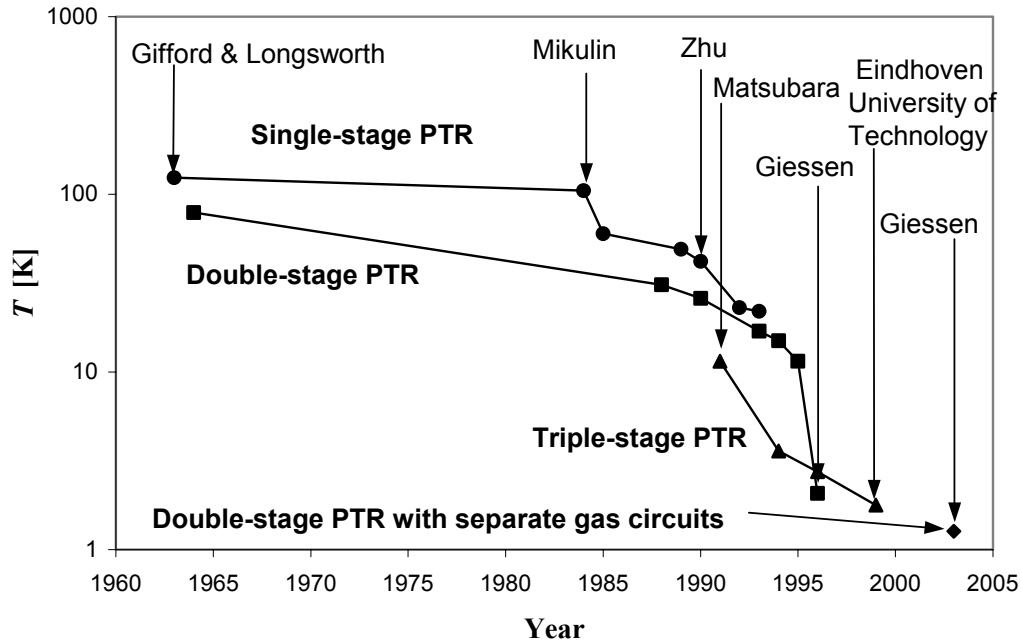


Figure 1.1. History of a lowest temperature, reached with a PTR.

The main breakthrough came in 1984, when Mikulin and his co-workers invented the Orifice Pulse Tube Refrigerator (OPTR) [6]. A flow resistance, the orifice, was inserted at the warm end of the pulse tube to allow some gas to pass to a large reservoir. With a single-stage configuration of the OPTR Mikulin achieved a low temperature of 105 K, using air as the working gas. Soon afterwards R. Radebaugh reached 60 K with a similar device, using helium [7]. For the first time since the invention of the PTR its performance became comparable to the Stirling cooler.

After that the development of the PTR went really fast. In 1990 Zhu *et al.* connected the warm end of the pulse tube with the main gas inlet by a tube, containing the second orifice [8]. Thus, a part of the gas could enter the pulse tube from the warm end, bypassing the regenerator. Because of this effect such a configuration of the PTR was called the Double-Inlet Pulse-Tube Refrigerator (DPTR). In 1994 Y. Matsubara used this configuration to reach a temperature as low as 3.6 K with a three-stage PTR [9]. The same year the Low Temperature Group of Eindhoven University of Technology began the research on the PTR. In 1999 with a three stage DPTR a temperature of 1.78 K was reached in our research group [10]. For several years this temperature remained the record lowest temperature, reached with PTRs. However, in 2003 the group of Professor G. Thummes from Giessen University has developed a double-circuit $^3\text{He}/^4\text{He}$ PTR that has achieved 1.27 K [11].

Nowadays, PTRs are used for many applications, described in section 1.1, and provide cooling powers from a few tenths of a mW at 2 K [11] up to around 200 W at 80 K [12]. The efficiency of PTRs is mostly as high as the efficiency of other coolers. Therefore, PTRs are beginning to replace other cryocoolers. However, a lot of research still has to be done in order to improve the performance and to explore the possibilities of PTRs even further.

1.3. INTRODUCTION TO THIS THESIS

The main emphasis of this thesis is made on pulse-tube refrigerators. The explanation of their operation principle is given in Chapter 2. There the loss mechanisms and the efficiency of PTRs are treated as well.

This research work is for a great part experimental. One of the goals is to explore the physics and the technology of PTRs, operating near its lowest temperature region. For that our research group has developed three multistage PTRs, using both ^4He and ^3He as the working fluids. The first one, a three-stage PTR (PTR1) had been built before my research has started. A lowest temperature of 1.78 K was reached with PTR1, using ^3He . At that time (1999) it was the lowest temperature, ever reached with a PTR. A number of experiments have been carried out with PTR1 within the work, described in this thesis. A cooling power of 160 mW at 4.2 K has been reached.

The second PTR (PTR2) has been obtained by eliminating one stage from PTR1 (see FIG. 1.2). By doing this we have obtained a two-stage PTR and have decreased the amount of variables, needed to be adjusted, when investigating and modifying certain components of the PTR. In particular a lot of work has been done on improving the rotary valve, responsible for generating pressure oscillations in the PTR. The work, done on PTR1 and PTR2, is described in Chapter 3.

Chapter 4 is dedicated to the third PTR (PTR3), which has been designed by scaling down PTR1 by 50%. The main requirements for the design of PTR3 have been small size and weight, flexibility, little input power, and small amount of working gas and regenerator material. The performance of PTR3 is required to be at least comparable to the performance of PTR1.

As it has already been mentioned in section 1.1 the material of the regenerator of a PTR must have a high heat capacity to provide good heat storage conditions. Below 20 K the heat capacities of most regenerator materials rapidly decrease,

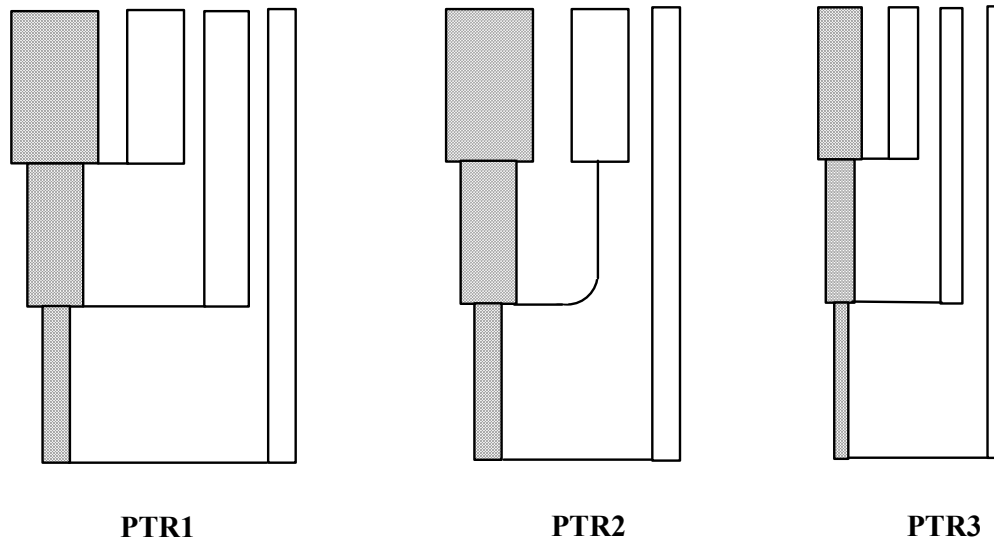


Figure 1.2. Schematic drawings of PTR1, PTR2, and PTR3. PTR2 is obtained by eliminating one stage from PTR1. The volume of PTR3 is 50% of the volume of PTR1.

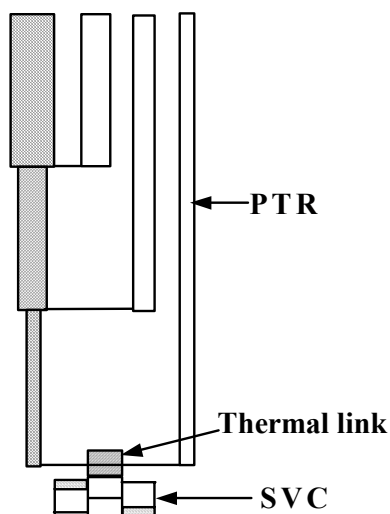


Figure 1.3. Schematic drawing of a SVC, integrated with a PTR.

whereas the heat capacity of helium increases and has a maximum at a temperature of around 10 K. This obstacle for reaching low temperatures has been overcome by using rare-earth magnetic materials in the coldest part of the regenerator. These materials have a magnetic phase transitions below 20 K, accompanied by an increase in their heat capacities. However, finding a good material for sub-4 K application is still a challenge. In collaboration with the University of Tsukuba in Japan we have investigated potentially better regenerator materials for the sub-4 K temperature region. Heat capacities of a number of samples of rare-earth oxides of perovskite structure have been measured between 1.5 and 10 K. The measurements and their results are presented in Chapter 5.

Theoretically, the lowest temperature attainable with a ^3He PTR is just above 1 K. However, this temperature can be reduced further, if we use a PTR as a precooler for another cooling device. In Chapter 6 a superfluid vortex cooler (SVC) is described. A SVC is a cooling device, the operation of which is based on the special properties of superfluid helium (He II). He II is helium below λ line (2.17 K at the saturated vapor pressure). It can be considered as a combination of two components: the normal component, which behaves just like any other viscous fluid, and the superfluid component, which has zero viscosity and entropy. The SVC is small, simple, has no moving parts, and is gravity independent. It is capable of reaching temperatures as low as 0.65 K. If we integrate the SVC with a PTR (see FIG. 1.3), a compact, cryogen-free cooler with no moving parts in the cold area, which cools from room temperature to temperatures below 1 K, can be obtained.

First a number of experiments, in which the SVC has been precooled by a liquid helium bath, have been carried out. This work is discussed in Chapter 6. After that the SVC has been integrated with a PTR. This research has been done in collaboration with Giessen University in Germany. The results of the integration are given in Chapter 7.

REFERENCES

1. McClintock, P. V. E., Meredith, D. J., Wigmore, J. K., "Matter at low temperatures", John Wiley & Sons, New York, 1984.
2. Good, J., Hodgson, S., Mitchell, R., and Hall, R., "Helium free magnets and research systems", *Cryocoolers* **12**, 2003, pp. 813-816.
3. Walker, G., "Cryocoolers", Plenum Press, New York and London, 1983.
4. Gifford, W.E. and Longworth, R. C., "Pulse tube refrigeration", *Trans. ASME*, 1964, pp. 264-268.
5. Longworth, R. C., "An experimental investigation of pulse tube refrigeration heat pumping rates", *Advances in Cryogenic Engineering* **12**, 1967, pp. 608-618.
6. Mikulin, E.I., Tarasov, A.A., and Shkrebyonock, M., P., "Low-temperature expansion pulse tubes", *Advances in Cryogenic Engineering* **29**, 1984, pp. 629-637.
7. Radebaugh, R., Zimmerman, J., Smith, D., R., and Louie, B., "Comparison of three types of pulse tube refrigerators: New methods for reaching 60 K", *Advances in Cryogenic Engineering* **31**, 1986, pp. 779-789.
8. Zhu, Sh., Wu, P., and Chen, Zh., "Double inlet pulse tube refrigerators: an important improvement", *Cryogenics* **30**, 1990, pp. 514-520.
9. Matsubara, Y. and Gao, J., L., "Novel configuration of three-stage pulse tube refrigerator for temperatures below 4 K", *Cryogenics* **34**, 1994, pp. 259-262.
10. Xu, M. Y., Waele, A. T. A. M. de, and Ju, Y. L., "A Pulse Tube Refrigerator Below 2 K", *Cryogenics* **39**, 1999, pp. 865-869.
11. Jiang, N., Lindemann, U., Giebeler, F., and Thummes, G., "A ^3He pulse tube cooler operating down to 1.27 K", *Cryogenics* **44**, 2004, pp. 809-816.
12. Zia, J. H., "Design and operation of a 4 kW liner motor driven pulse tube cryocooler", *Advances in Cryogenic Engineering* **49**, 2004, pp. 1309-1317.

CHAPTER 2.

THEORETICAL ASPECTS OF PULSE-TUBE REFRIGERATORS

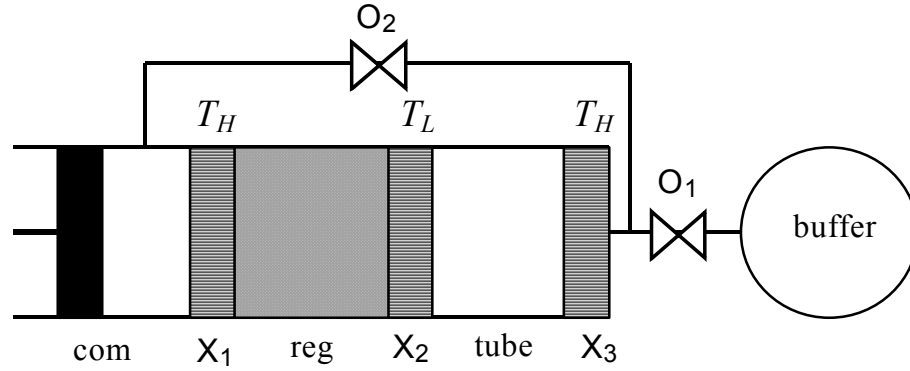
In this chapter some theoretical aspects of pulse-tube refrigerators are treated. The operation principle of the PTR is explained. The function of the main components of the PTR and the losses, produced in them, are discussed.

2.1. TWO TYPES OF THE PTR, DEPENDING ON THE GAS COMPRESSION METHOD

There are two types of PTRs: a Stirling-type PTR (FIG. 2.1(a)) and a GM-type PTR (FIG. 2.1(b)). The type of a PTR is determined by the way the pressure oscillations are generated. In the GM-type PTR a compressor produces continuous high and low pressures and uses a rotary valve to generate pressure oscillations in the pulse tube. In the Stirling-type PTR pressure oscillations are created by the movement of a piston, directly connected to the pulse tube and controlled by a linear motor.

Now we will describe the main components of the GM-type PTR. From left to right the pulse-tube system in FIG. 2.1(b) consists of a compressor (com), a room temperature heat exchanger or an after-cooler (X_1), a rotary valve (r.v.), a regenerator (reg), a low-temperature heat exchanger (X_2), a pulse tube (tube), another room temperature heat exchanger (X_3), two orifices (O_1 and O_2), and a buffer volume (buffer). The compressed gas enters the regenerator at room temperature T_H . The regenerator consists of a porous material with a high heat capacity. The function of the regenerator is to store heat, taking it from the gas, when it flows from the compressor to the tube, and reject this heat back to the gas, when the gas flows from the tube to the compressor. After passing the regenerator the gas enters the pulse tube, which is just a tube with the heat exchangers X_2 and X_3 on its two ends. At the low-temperature end T_L the cold heat exchanger X_2 is used to extract the heat from the cooling object. The hot heat exchanger X_3 rejects this heat to the surroundings. The orifices O_1 and O_2 are simply flow resistances, which can be represented by adjustable needle valves, orifices, capillaries, or the like. The buffer volume is a reservoir, the volume of which is typically 10 times larger than the volume of the pulse tube. The pressure in the buffer is practically constant and close to the average pressure in the pulse tube. The combination of the orifice O_1 and the buffer provides a phase difference between the flow of the gas in the tube and the pressure. This phase difference is necessary for the efficient performance of the PTR. The

a



b

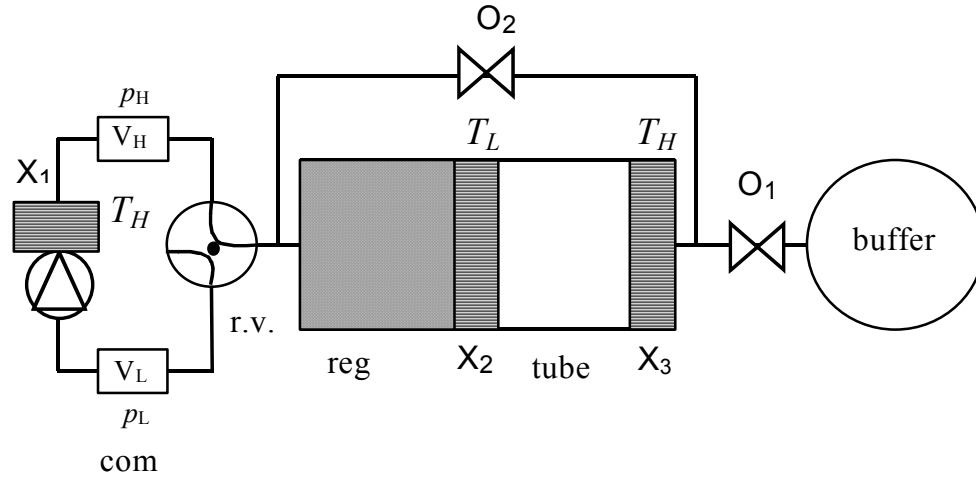


Figure 2. 1. Two types of the PTR. (a) A Stirling-type PTR. From left to right it consists of a compressor (com), an aftercooler (X_1), a regenerator (reg), a cold heat exchanger (X_2), a pulse tube (tube), a hot heat exchanger (X_3), an orifice (O_1), and a buffer. Orifice O_2 connects the hot end of the regenerator and the hot end of the pulse tube. (b) A GM-type PTR. Except for the compressor - rotary valve (r.v.) combination, the main components of the GM-type PTR are the same as of the Stirling PTR.

function of the double-inlet orifice O_2 is to reduce the irreversible entropy production in the regenerator, which leads to losses. It allows some gas to bypass the regenerator and to enter the pulse tube via X_3 .

The choice of the gas compression method depends on the intended temperature range. In the case of a single-stage pulse-tube cooler for the 20 to 80 K range the Stirling type compressor is more appropriate. It has a high efficiency, which results in a lower total weight. Typically the driving frequency of the Stirling type PTR is 25 to 50 Hz.

On the other hand, to attain temperatures below 20 K, the systems are usually operated at lower frequencies (1-5 Hz). The density of the gas at a constant pressure increases with the decrease of its temperature. Hence, to provide a certain volume of the gas at low temperature several times larger volume should be compressed at room

temperature. The lower the desired cold-end temperature of a cooler, the larger volume of the gas has to be compressed and expanded at room temperature. In the Stirling compressor, if the driving frequency is lower than 7 Hz, the piston's resonance condition will require the piston to be heavier and the spring to be less stiff. Under this condition, it is difficult to stabilise the piston against changes in pressure or gravity.

In addition to that the frequency defines the diffusion depth in the working gas and the regenerator material. The diffusion depth, d , is given by the following equation

$$d = \sqrt{\frac{k}{\pi \nu C}}, \quad (2.1)$$

where k is the heat conductivity, ν is the frequency, and C is the volumetric heat capacity of the regenerator material. From the equation 2.1 it is easily seen, that when increasing the frequency, the diffusion depth decreases; and the heat storage in the regenerator degrades. Hence, the regenerator material with a small particle size or fine-mesh screens have to be used in the high-frequency PTRs. However, multistage pulse tubes are required to reach temperatures of liquid helium range and below. Large temperature difference over the regenerator requires a rather large length of it. In this case a high operating frequency means a big pressure drop in the regenerator, which leads to a poor performance of a system.

Therefore, the GM-type PTR is more suitable for temperatures below 20K. However, there is still an interest in achieving low temperatures with the Stirling-type compressors [1, 2]. It is especially important for space applications. It is impossible to use a large water-cooled G-M type compressor in space. In addition to that, as it will be shown later, most losses in the G-M type PTRs originate from the compressor and the rotary valve.

2.2. THE OPERATION PRINCIPLE OF PULSE-TUBE REFRIGERATORS

The operation principle of PTRs will be explained on the example of the orifice pulse-tube refrigerator (OPTR). We consider a small gas parcel, which during a cycle travels from the regenerator through X_2 into the pulse tube and back. To make the explanation easier several assumptions are made. The flow in the tube is considered to be one-dimensional without turbulence or mixing. The processes in the tube are adiabatic. There is no heat conduction in the tube and no heat exchange between the gas and the tube walls. The heat exchangers are ideal, so their temperatures are constant and the heat exchange is perfect.

The pressure in the pulse tube is considered to be cyclic with a shape according to FIG. 2.2a. The cycle is divided in 4 steps. We will assume, that the orifice O_1 is closed during the steps 1 and 3 and open during the steps 2 and 4.

Step 1. The compression step. The system is connected to the high-pressure side of the compressor. The pressure in the pulse tube rises from the low pressure p_L to the high-pressure p_H . The orifice is closed.

Step 2. The orifice is open. As the pressure in the buffer is close to the average pressure

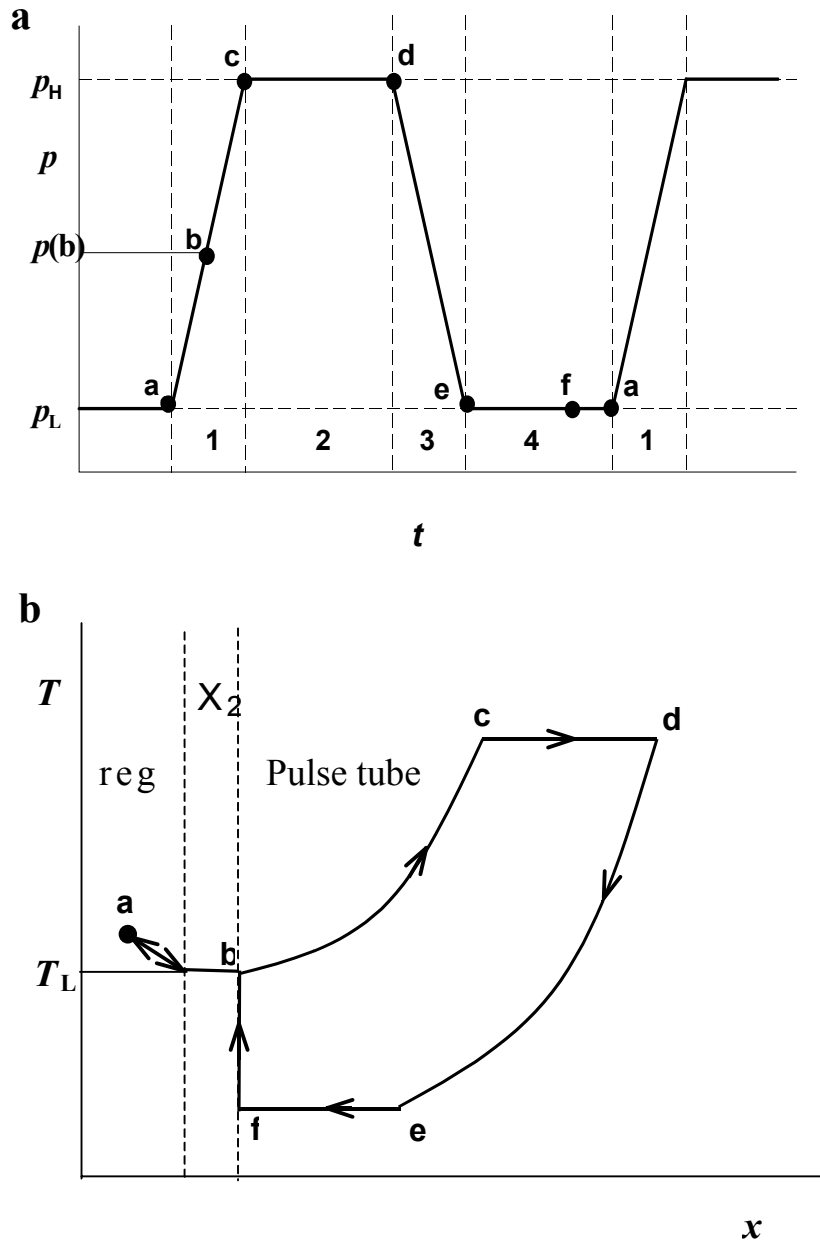


Figure 2. 2. (a) Idealized form of the pressure in a pulse tube as a function of time. The cycle is divided into 4 steps. The pressure rises from a low pressure, p_L , to a high pressure, p_H , during the compression step 1 (from a to c via b), remains at a value of p_H during the step 2 (from c to d), decreases from p_H to p_L during the expansion step 3 (from d to e), and is equal to p_L during the step 4 (from e to a via f). (b) Temperature of a gas particle as a function of position in the regenerator, X_2 , and the pulse tube in the OPTR for a p - t dependence, given in FIG. 2.2a.

in the system, the pressure in the pulse tube is now higher than the pressure in the buffer. Hence, the gas flows from the tube to the buffer. As the rotary valve is still open to the high-pressure side of the compressor, the pressure in the tube remains at the value of p_H .

Step 3. The expansion step. The system is connected to the low-pressure side of the compressor. The pressure in the pulse tube decreases from p_H to p_L , while the orifice is closed.

Step 4. The orifice is open again. Now the pressure in the buffer is higher than the pressure in the pulse tube. So the gas flows from the buffer into the tube. As the rotary valve is still open to the low-pressure side of the compressor, the pressure in the tube remains constant at p_L .

We now follow a gas element, which is inside the regenerator at the start of the cycle (point **a** on FIG. 2.2a and FIG. 2.2b).

Step 1: from **a** via **b** to **c**. When the pressure rises, the gas element moves through the regenerator in the direction of the heat exchanger X_2 (from **a** to **b**). According to the assumptions above, the heat exchange is perfect, and the temperature of the gas element is equal to the local temperature of the regenerator. At point **b** the gas element leaves X_2 and enters the tube with the temperature T_L . From **b** to **c** the gas element is compressed adiabatically, while it moves towards the orifice. Its temperature rises together with the pressure.

Step 2: from **c** to **d**. The gas element moves to the right. The pressure is constant, so the temperature is constant as well.

Step 3: from **d** to **e**. The orifice is closed and the expansion takes place. Gas moves back in the direction of X_2 . As it is thermally isolated, its temperature drops together with the pressure. The gas element entered the pulse tube at some intermediate pressure, $p(b)$, after the cycle had already started (see FIG. 2.2a). At the end of the expansion step the pressure of the gas element, $p(e)$, is equal to p_L (FIG. 2.2a). As $p(e) < p(b)$, the temperature of the gas element at the end of step 3 is below T_L .

Step 4: from **e** via **f** to **a**. The expansion stops, and the orifice is open again. The gas continues flowing in the direction of X_2 . From **e** to **f**: the pressure is constant, so the temperature is constant as well. At point **f** the gas parcel enters X_2 with $T < T_L$. When passing X_2 the gas extracts heat from it and warms up to the temperature T_L . That is when

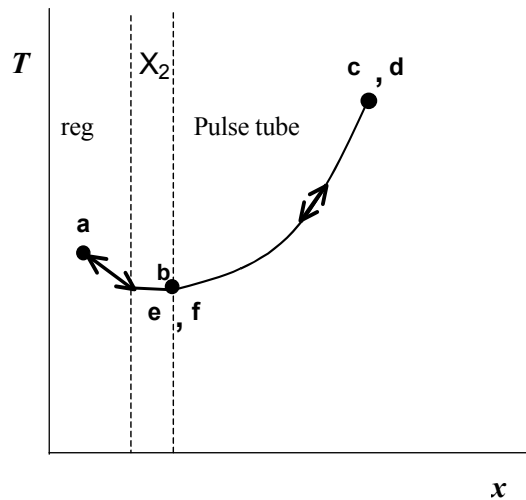


Figure 2. 3. Temperature of a gas particle as a function of position in the regenerator, X_2 , and the pulse tube in the BPTR for a p - t dependence, given in FIG. 2.2a.

the cooling takes place. The amount of heat, which the gas takes away from the heat exchanger, is the cooling power. In the remaining time of the cycle the gas element moves inside the regenerator to its original position.

There is a certain amount of gas, entering the pulse tube from the cold end and going out of it during a cycle; and a certain amount of gas entering the pulse tube and going out of it during a cycle at the hot end. But there is also some gas, which never leaves the pulse tube. This gas forms the so-called gas piston. The name is related to the moving displacer in the Stirling and G-M coolers.

The absence of the gas flow at the hot end means that the PTR operates in the basic mode. This can be illustrated in FIG. 2.3. In the explanation of the operation principle of the OPTR we have assumed that the orifice is open during steps 2 and 4. In basic mode O_1 is always closed. Considering the adiabatic pulse tube, nothing happens during step 2 and step 4. Hence, no cooling takes place.

2.3. COOLING POWER

In this section we assume a harmonic time dependence of the pressure in the pulse tube

$$p_t = p_0 + p_1 \cos \omega t, \quad (2.2)$$

where p_0 is the average pressure, p_1 is the pressure amplitude, and ω is the angular frequency, related to the cycle time, t_c , and the frequency, ν , by

$$\omega = 2\pi\nu = \frac{2\pi}{t_c}. \quad (2.3)$$

The volume flow of the gas, \dot{V}_H , at the hot end of the pulse tube, is determined by the pressure oscillations δp

$$\delta p = p_1 \cos \omega t, \quad (2.4)$$

and the resistance of the orifice R_1

$$\dot{V}_H = \frac{\delta p}{R_1}. \quad (2.5)$$

The heat, extracted from the cooling object at the cold end of the pulse tube, is rejected to the surroundings by the hot heat exchanger. Therefore, when the gas passes the hot heat exchanger from the pulse tube into the buffer, its temperature T_g is higher than the temperature of the heat exchanger T_H [3]

$$T_g = T_H + 2T_H \frac{R}{C_p} \frac{\delta p}{p_0}, \quad (2.6)$$

where R is the molar ideal gas constant, and C_p is the heat capacity of the gas at a constant pressure. When the gas returns to the pulse tube, its temperature is equal to the temperature of the heat exchanger: $T_g = T_H$. The heat exchange rate between the gas and the heat exchanger is given by

$$\dot{Q}_H = \dot{n}_H C_p (T_g - T_H), \quad (2.7)$$

where \dot{n}_H is the molar flow rate at the hot end of the pulse tube, given by

$$\dot{n}_H = \frac{p_0 \dot{V}_H}{RT_H}. \quad (2.8)$$

Integrating \dot{Q}_H in equation 2.7 over a cycle and dividing by the cycle time, gives the average heat exchange rate in the hot heat exchanger

$$\bar{\dot{Q}}_H = \overline{\dot{V}_H \delta p} = \frac{1}{2} V_1 p_1, \quad (2.9)$$

where V_1 is the amplitude of the volume flow of the gas passing the orifice during a cycle.

The displacement of the gas at the cold end of the pulse tube is equal to the displacement of the gas at the hot end plus an additional term due to the compressibility of the gas in the tube. Thus, the volume of the gas displaced at the cold end of the tube is

$$\dot{V}_L = \dot{V}_H + \frac{C_V}{C_p} \frac{V_t}{p_0} \frac{dp_t}{dt}, \quad (2.10)$$

where V_t is a volume of the tube. Because of the dp_t/dt term, the gas flow is no longer in phase with the pressure in the pulse tube.

From FIG. 2b it is seen that the gas enters the pulse tube with the temperature, equal to the temperature of the cold heat exchanger, $T_g = T_L$. However, when the gas comes back from the pulse tube its temperature is lower than T_L

$$T_g = T_L + T_L \frac{R}{C_p} \frac{p_1}{p_0} \frac{2}{1 + \alpha^2} (\cos \omega t - \alpha \sin \omega t). \quad (2.11)$$

where α is the gas piston parameter, expressed as follows

$$\alpha = \frac{C_V}{C_p} R_1 \frac{V_t}{p_0} \omega. \quad (2.12)$$

The heat exchange rate between the gas and the cold heat exchanger is

$$\dot{Q}_L = \dot{n}_L C_p (T_g - T_L), \quad (2.13)$$

where \dot{n}_L is the molar flow rate of the gas at the cold end of the pulse tube, given by

$$\dot{n}_L = \frac{p_0 \dot{V}_L}{RT_L}. \quad (2.14)$$

The average heat exchange rate in the cold heat exchanger or the cooling power of the PTR can be found by integrating equation 2.13 over a cycle and dividing it by the cycle time

$$\overline{\dot{Q}_L} = \overline{\dot{V}_L \delta p} = \frac{1}{2} V_1 p_1. \quad (2.15)$$

The cooling power per cycle depends on the pressure amplitude in the pulse tube and the amount of the gas, passing the cold heat exchanger during a cycle. The total cooling power of the PTR is the heat, exchanged per cycle, multiplied by the frequency of the pressure oscillations.

The cooling power, described by equation 2.15, is valid only for an ideal gas. Above 30-40 K helium, which is a usual working gas in the close-cycled regenerative coolers, can for convenience be considered as an ideal gas. Below this temperature this approximation is no longer valid. That means, that the energy flows in the PTR are no longer functions of the temperature only, but also functions of the pressure. This results in an additional term $T_L \alpha_v$ in the expression for the cooling power of the PTR:

$$\overline{\dot{Q}_L} = T_L \alpha_v \overline{\dot{V}_L \delta p}, \quad (2.16)$$

where α_v is the volumetric thermal expansion coefficient. The product of T_L and α_v is plotted via temperature in FIG. 2.4. Here it is shown that, above 30 K, the value of $(T \alpha_v)$ is close to 1, which is the value for an ideal gas.

2.4. COEFFICIENT OF PERFORMANCE

The coefficient of performance (COP) is an important characteristic of a cryocooler, describing its efficiency and used for comparing. It is defined as the average cooling power $\overline{\dot{Q}_L}$ divided by the average work input in the system P

$$COP = \frac{\overline{\dot{Q}_L}}{P}. \quad (2.17)$$

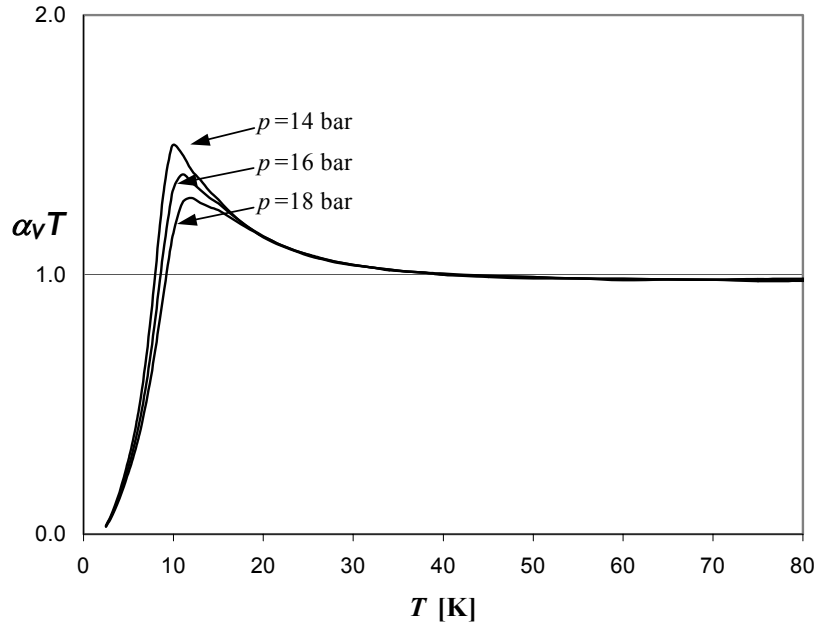


Figure 2. 4. The products of the temperature, T , and volumetric expansion coefficient, α_v as functions of temperature at various pressures.

The COP for coolers in general can be calculated by applying the 1st and the 2nd law of thermodynamics to a system in the steady state, containing a complete cryocooler. FIG. 2.5 represents a cryocooler with a cooling power \dot{Q}_L at a temperature T_L , which

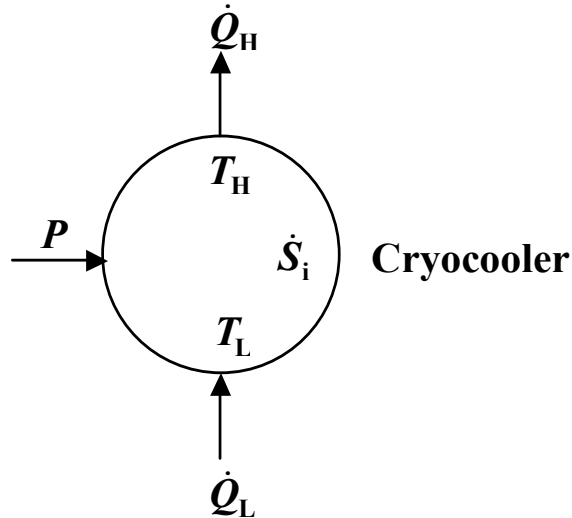


Figure 2. 5. Schematic representation of a cryocooler. A heat \dot{Q}_L is extracted from a cooling object at a temperature T_L ; and a heat \dot{Q}_H is rejected to the surroundings at a temperature T_H . The cooler requires an input power P . There is a certain amount of irreversible entropy, \dot{S}_i , produced in the cooler.

Chapter 2

consumes a power P and rejects a heating power \dot{Q}_H at a temperature T_H . Irreversible processes create entropy \dot{S}_i . The first law of thermodynamics reads

$$\dot{U} = \sum \dot{Q} + \sum \dot{n}H_m - \sum p\dot{V} + P. \quad (2.18)$$

The internal energy U of an open system will change due to heat flows \dot{Q} , enthalpy flows $\dot{n}H_m$, work, done by the system, or by external work, applied to the system. The heat and molar flows are positive, when they enter the system. For a fixed volume V $p\dot{V}=0$.

For the cryocooler, represented on FIG. 2.5, equation 2.18 reads

$$0 = \dot{Q}_L - \dot{Q}_H + P. \quad (2.19)$$

The 2nd law of thermodynamics expresses the rate of the change of entropy of a control volume

$$\dot{S} = \sum \frac{\dot{Q}}{T} + \sum \dot{n}S_m + \dot{S}_i. \quad (2.20)$$

The entropy S of an open system will change due to heat flows, entropy flows, and irreversible entropy production \dot{S}_i . It is a requirement of the 2nd law, that for any process

$$\dot{S}_i \geq 0. \quad (2.21)$$

If $\dot{S}_i = 0$, a process is called reversible. Applying the 2nd law to the cryocooler in the steady state, we get

$$0 = \frac{\dot{Q}_L}{T_L} - \frac{\dot{Q}_H}{T_H} + \dot{S}_i. \quad (2.22)$$

Eliminating \dot{Q}_H from equations 2.19 and 2.22 gives a general expression for the relation between the cooling power and the work, applied to the system

$$P = \left(\frac{T_H}{T_L} - 1 \right) \dot{Q}_L + T_H \dot{S}_i. \quad (2.23)$$

If we rewrite equation 2.23 as follows

$$P - T_H \dot{S}_i = \left(\frac{T_H}{T_L} - 1 \right) \dot{Q}_L, \quad (2.24)$$

we can easily see that, the smaller the power loss due to irreversible processes, $T_H \bar{S}_i$, the higher is the cooling power of the system.

With equation 2.23 it is seen, that the best performance is reached, if the process is reversible. It means, that the COP is equal to the Carnot coefficient of performance

$$COP_{\text{Carnot}} = \frac{T_L}{T_H - T_L}. \quad (2.25)$$

If there is any irreversible entropy production, the COP will be smaller, than COP_{Carnot} .

From another side, if there is no heat, supplied to the cooler ($\bar{Q}_L = 0$), all the work is used to compensate the irreversible entropy production.

Because of irreversible processes or losses in the PTR, the COP of the PTR is always smaller than the COP_{Carnot} . The irreversible entropy production in the PTR has two main sources:

- Heat transport over a finite temperature difference (e.g. heat conduction and imperfect heat exchange in the regenerator and the heat exchangers, etc.)
- Gas flow over a certain pressure difference (pressure drop in the orifices, regenerator, heat exchangers and the rotating valve)

If we consider an ideal PTR, most of the losses are neglected. Although the entropy production in the orifices cannot be avoided. As it has already been mentioned above, the efficient operation of the cooler is not possible in the absence of the orifice O_1 . That means, that even the COP of the ideal PTR will still be smaller than COP_{Carnot} .

To demonstrate that, we split the pulse tube system into subsystems (see FIG.2.6) and apply the 1st and the 2nd laws of thermodynamics to the subsystems. In this way we can determine the COP of the ideal PTR. In our approximation entropy is produced only in the orifice. In all other subsystems $\bar{S}_i = 0$. The heat flows \bar{Q} are only non-zero in the heat exchangers. If we assume that the working gas in the pulse tube is ideal, we can write for the molar entropy

$$S_m(p, T) = S_m(p_0, T_0) + \frac{C_p}{T} \ln \frac{T}{T_0} - R \ln \frac{p}{p_0}, \quad (2.26)$$

and for the molar enthalpy

$$H_m(p, T) = C_p T. \quad (2.27)$$

At the buffer side of the orifice p and T are constant. Thus, $\overline{\dot{n}H_m} = 0$ and $\overline{\dot{n}S_m} = 0$. Between the orifice and the hot heat exchanger the temperature is constant, so $\overline{\dot{n}H_m} = 0$, but $\overline{\dot{n}S_m} \neq 0$. The second law for the subsystem, consisting of the orifice and the heat exchanger, gives

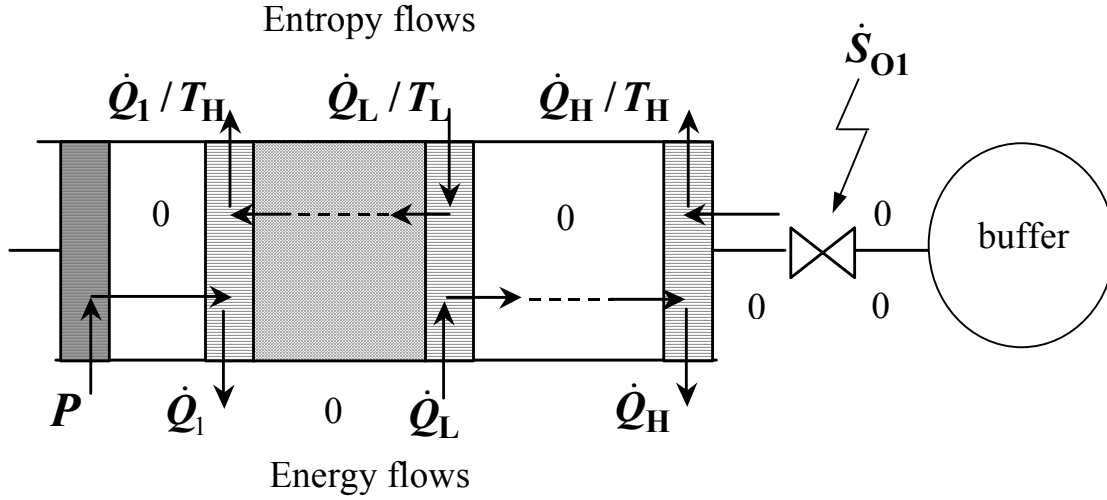


Figure 2. 6. The energy (lower half) and the entropy (the upper half) flows in the PTR. The only source of the entropy production is the orifice. In all other parts of the PTR the irreversible entropy production is considered to be negligible. The heat flows are only non-zero in the heat exchangers.

$$\bar{\dot{Q}}_H = T_H \bar{\dot{S}}_{O1}, \quad (2.28)$$

where $\bar{\dot{S}}_{O1}$ is the irreversible entropy production rate in the 1st orifice.

In the subsystem, containing the pulse tube and its two heat exchangers, the temperature of the gas in the tube is high, when it moves to the right, and low, when it moves to the left. Thus the enthalpy flows internally from the cold heat exchanger to the hot heat exchanger. The 1st law for this subsystem gives

$$\bar{\dot{Q}}_L = \bar{\dot{Q}}_H. \quad (2.29)$$

Now we consider the subsystem, consisting of the cold heat exchanger. If the heat capacity of the regenerator material is much larger, than that of the gas $c_r \gg C_p$, and that the heat exchange between the gas and the regenerator material is perfect, the temperature in the regenerator is constant in time. Therefore, there is no enthalpy flow in the regenerator ($\overline{\dot{n}H_m} = 0$). However, the entropy flow in the regenerator is nonzero. It is directed from the cold to the warm end of the regenerator, since the gas moves to the right, when the pressure is high (low entropy, see equation 2.26), and to the left, when the pressure is low (entropy is high). In the ideal case the entropy flow is constant. The 2nd law for the cold heat exchanger gives:

$$\bar{\dot{Q}}_L = \bar{\dot{S}}_L T_L, \quad (2.30)$$

where $\bar{\dot{S}}_L$ is the average entropy flow at the cold end of the regenerator, which is expressed as

$$\bar{\dot{S}}_L = \overline{\dot{n}_L S_m} . \quad (2.31)$$

The gas in the adiabatic compressor moves back and forth isentropically, so $\overline{\dot{n} S_m} = 0$ here. As the gas temperature is high, when it flows to the right, and low, when it moves to the left, the enthalpy flow directed from the compressor to the after-cooler (X_1 in FIG. 2.1). In X_1 the heat is removed ($\bar{\dot{Q}}_1 < 0$). The 2nd law for the after-cooler reads:

$$\bar{\dot{Q}}_1 = \bar{\dot{S}}_H T_H , \quad (2.32)$$

where $\bar{\dot{S}}_H$ is the entropy flow of the gas at the hot end of the regenerator, which is

$$\bar{\dot{S}}_H = \overline{\dot{n}_H S_m} . \quad (2.33)$$

The 1st law for the subsystem, containing the compressor and the after-cooler X_1 gives:

$$\bar{\dot{Q}}_1 = P . \quad (2.34)$$

In the regenerator with zero irreversible entropy production the entropy flow at the hot end is equal to the entropy flow at the cold end of it. Hence,

$$\bar{\dot{S}}_H = \bar{\dot{S}}_L . \quad (2.35)$$

Combining the equations 2.30, 2.32, and 2.34, we obtain the expression for the ideal COP of the PTR:

$$COP_{id} = \frac{T_L}{T_H} . \quad (2.36)$$

If $T_L = T_H$, then $COP_{id} = 1$, while COP_{Carnot} becomes infinite. But if $T_L \ll T_H$, the difference between COP_{id} and COP_{Carnot} becomes so small, that it can be neglected.

However, in reality $\bar{\dot{S}}_i^r > 0$. This results in the additional term in the COP

$$COP = \xi_r COP_{id} , \quad (2.37)$$

where ξ_r is the efficiency of the regenerator [4], which can be defined as

$$\xi_r = \frac{\bar{\dot{S}}_L}{\bar{\dot{S}}_H} . \quad (2.38)$$

2.5. MULTISTAGE PULSE TUBE REFRIGERATORS

In multistage PTRs one pulse tube pre-cools the other one. For the best performance of the system the hot end of all the pulse tubes are connected to room temperature and not to the cold end of the pre-cooling stage. In this way large heat loads on the cold end of the pre-cooling stage, resulting from the heat release in the hot heat exchanger of the following pulse tube, are avoided. The disadvantage of multistage pulse tubes is that the pre-cooling stage reduces the flow to the final stage, thus reducing the cooling power of the final stage.

The subject of the advantages and the disadvantages of multistaging has not been extensively treated in the literature. In [5] we have tried to answer the questions at what temperature range it is useful to have multistage PTRs, and how the next stage should be attached to the pre-cooling stage for the best performance. We have considered a single-stage OPTR with a cooling power \dot{Q}_L at a temperature T_2 and have added an extra stage with the cold end temperature T_1 to it, as shown in FIG. 2.7. In order to simplify the

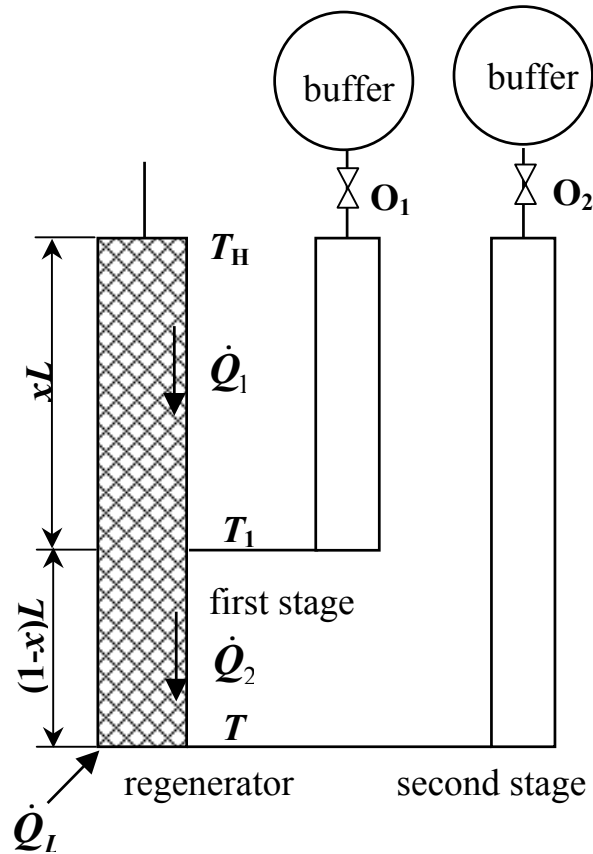


Figure 2. 7. A schematic diagram of a two-stage single-orifice PTR. The PTR has a cooling power \dot{Q}_L at a temperature T_2 . The heat flows \dot{Q}_1 and \dot{Q}_2 are caused by the heat conduction.

derivations we have assumed, that the only irreversible process in the regenerator is the heat conduction. Hence, there is a zero pressure drop in the regenerator; and the heat exchange between the regenerator material and the gas is perfect. If the heat capacity of the regenerator material is much larger than the heat capacity of the gas, and the gas is considered to be ideal, then in the steady state the average enthalpy flow in the regenerator is zero.

With all the assumptions described above the optimum COP of a two-stage PTR is

$$COP = \frac{T_2}{T_H} - \kappa + \kappa\psi. \quad (2.39)$$

The parameter κ in equation 2.39 is the loss term due to the heat conduction, given by

$$\kappa = \frac{kA_r T_H}{L_r P}, \quad (2.40)$$

where k and A_r are the thermal conductivity and the cross-sectional area of the regenerator respectively, which are assumed to be constant, L_r is the total length of the regenerator, and P is the compressor power.

Function ψ in equation 2.39 is derived in [5] and is expressed as follows

$$\psi(x, t_2) = 1 - 2\sqrt{\frac{t_2}{x(1-x)} + \left(\frac{t_2}{1-x}\right)^2} + \frac{t_2}{x} + \frac{2t_2}{1-x}, \quad (2.41)$$

where

$$t_2 = T_2/T_H. \quad (2.42)$$

The value of x determines a position of the first stage attachment to the regenerator (FIG. 2.7).

From equation 2.39 it is seen that the PTR will have the maximum efficiency, when the function ψ is at its maximum. Several ψ - x dependences for various values of T_2 and $T_H=300$ K are plotted in FIG. 8. For a fixed t_2 the function ψ has its maximum at

$$x_0 = \frac{4 - t_2 + \sqrt{t_2^2 + 4t_2}}{8 - 6t_2}. \quad (2.43)$$

Equation 2.43 determines a position, at which the first stage should be attached to the regenerator for the most efficient performance of the PTR for given t_2 . The value of x_0 ranges from 0.5 for $t_2=0$ to 1 for $t_2=0.5$. For very low T_2 values the first stage should be connected in the middle of the regenerator ($x \approx 0.5$). The higher the value of T_2 , the closer to the cold end of the regenerator ($x=1$) moves the position of the first stage attachment. For temperatures above 150 K ($T_2 > 0.5T_H$) the attachment of the second stage has no positive effect.

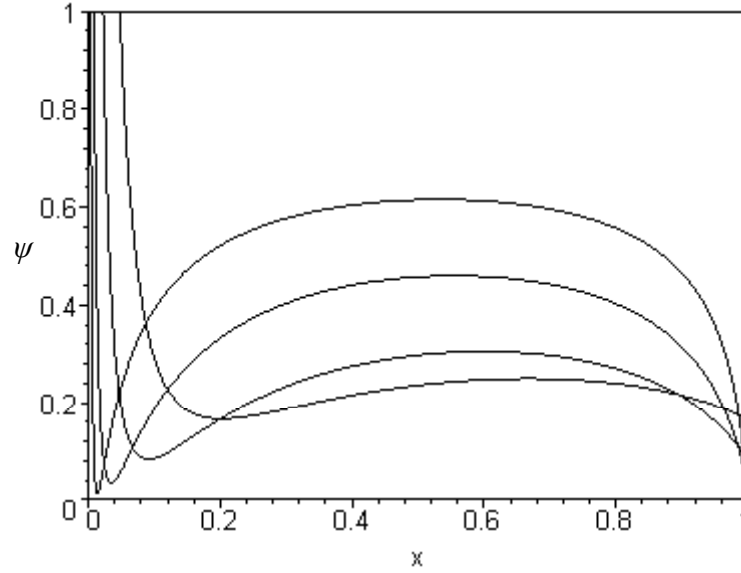


Figure 2. 8. ψ -function, given by equation 2.41 versus the position of the 1st stage attachment in the two-stage PTR. $T_H=300$ K.

2.6. THE MAIN COMPONENTS OF THE PTR AND THEIR FUNCTIONS

In this section we will discuss various components of the PTR in more detail with emphasis on the thermodynamical analysis.

2.6.1. Compressor

In case of G-M type PTRs, treated in this thesis, the compressor produces continuous high and low pressures and is usually water-cooled. A schematic drawing of a compressor is shown in FIG. 2.9. It consumes a certain amount of electric power P . A molar flow of gas \dot{n} enters the compressor at a low-pressure, p_L , and room temperature, T_H . It is compressed; and the heat of the compression, \dot{Q} , is released to the cooling water. The gas, which goes out of the compressor, is at a high pressure, p_H , and at room temperature. There is an irreversible entropy production in the compressor, \dot{S}_{com} .

The efficiency of the compressor can be defined as

$$\xi_{\text{com}} = \frac{P - T_H \dot{S}_{\text{com}}}{P}. \quad (2.44)$$

The first law of thermodynamics for the compressor system in the steady state reads

$$0 = P - \dot{Q} + \dot{n}_0 (H_m(T_H, p_L) - H_m(T_H, p_H)). \quad (2.45)$$

The second law gives

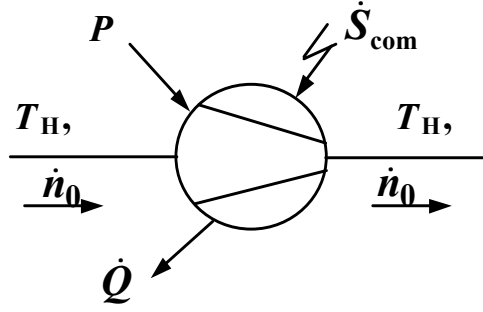


Figure 2. 9. A schematic drawing of a compressor.

$$0 = -\frac{\dot{Q}}{T_H} + \dot{n}_0 (S_m(T_H, p_L) - S_m(T_H, p_H)) + \dot{S}_{\text{com}}. \quad (2.46)$$

At room temperature helium usually can be treated as an ideal gas. Therefore,

$$H_m(T_H, p_L) = H_m(T_H, p_H). \quad (2.47)$$

Combining equations 2.45 and 2.46 and using equations 2.26 and 2.47, we can write the following expression for the power loss in the compressor

$$T_H \dot{S}_{\text{com}} = P - \dot{n}_0 R T_H \ln \frac{p_H}{p_L}. \quad (2.48)$$

With equation 2.48 the minimum input power of the compressor is

$$P_{\min} = \dot{n}_0 R T_H \ln \frac{p_H}{p_L}. \quad (2.49)$$

The pressure oscillations in the pulse tube are described by equation 2.2. We assume, that

$$p_H = p_0 + p_1 \quad (2.50)$$

and

$$p_L = p_0 - p_1. \quad (2.51)$$

With equations 2.50 and 2.51 and for $p_1 \ll p_0$ the minimum power of the compressor, given by equation 2.49 is

$$P_{\min} \cong 2\dot{n}_0 R T_H \frac{p_1}{p_0}. \quad (2.52)$$

2.6.2. Rotary valve

The function of the rotary valve is to connect the pulse-tube system periodically to the high- or to the low-pressure side of the compressor. In this way pressure oscillations in the PTR are generated. The flow of gas over a pressure difference in the rotary valve creates entropy, \dot{S}_{rv} . A schematic drawing of the rotary valve is represented in FIG. 2.10. Half of the cycle a molar flow of the gas \dot{n}_0 enters the PTR from the compressor with the high pressure, p_H . During the other half of the cycle the PTR is connected to the low-pressure side of the compressor. Therefore, \dot{n}_0 flows from the PTR to the compressor at the low-pressure, p_L . At the regenerator side of the rotating valve we have an oscillating flow \dot{n}_r at a pressure p_r . All the parts of the system in FIG. 2.10 are at room temperature, T_H . The second law of thermodynamics for the rotary valve system in the steady state gives

$$0 = \dot{n}_0 [S_m(T_H, p_H) - S_m(T_H, p_L)] - \overline{\dot{n}_r S_m(T_H, p_r)} + \dot{S}_{rv}. \quad (2.53)$$

With equation 2.26 equation the average entropy production in the rotary valve is

$$\bar{\dot{S}}_{rv} = \dot{n}_0 R \ln \frac{p_H}{p_L} - \overline{R \dot{n}_r \ln \frac{p_r}{p_0}}. \quad (2.54)$$

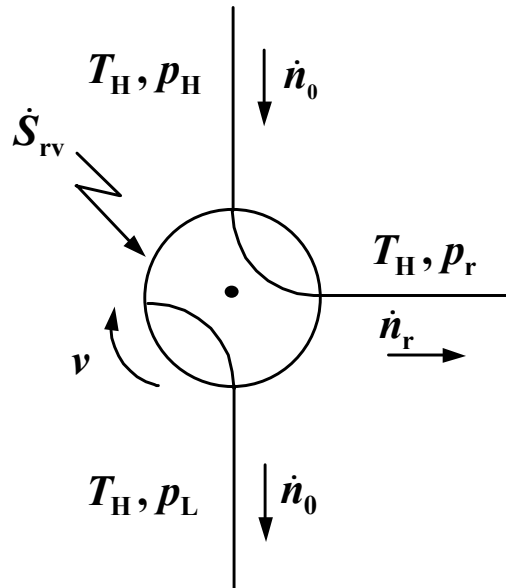


Figure 2. 10. A schematic drawing of a rotary valve.

In the harmonic approximation the molar flow at the regenerator side of the rotating valve can be written as

$$\dot{n}_r = n_{rA} \cos(\omega t + \varphi_r), \quad (2.55)$$

where n_{rA} is the amplitude of the molar flow, and φ_r is the phase angle between the flow and the pressure. The average flow of the gas, passing the compressor, is equal to the average gas flow in the regenerator for $\dot{n}_r \geq 0$. Thus,

$$\dot{n}_0 = \frac{1}{\pi} n_{rA}. \quad (2.56)$$

Substituting equations 2.2, 2.50, 2.51, and 2.55 in equation 2.54 and for small pressure changes, we obtain the following expression

$$\dot{S}_{rv} = \dot{n}_0 R \frac{2p_1}{p_0} - R n_{rA} \cos(\omega t + \varphi_r) \frac{p_1 \cos \omega t}{p_0}. \quad (2.57)$$

With equation 2.56

$$\dot{S}_{rv} = R n_{rA} \frac{p_1}{p_0} \left(\frac{2}{\pi} - \frac{1}{2} \cos \varphi_r \right). \quad (2.58)$$

The power loss in the rotary valve is

$$T_H \bar{\dot{S}}_{rv} = R T_H n_{rA} \frac{p_1}{p_0} \left(\frac{2}{\pi} - \frac{1}{2} \cos \varphi_r \right). \quad (2.59)$$

With equations 2.52 and 2.59 it is seen, that the power loss in the rotary valve is a significant fraction of the compressor power.

The design of the rotary valve and additional losses, resulting from its mechanical construction, will be discussed in Chapter 3.

2.6.3. Heat exchangers

There are three heat exchangers in the single stage PTR (X_1 , X_2 , and X_3 in FIG. 2.1). The heat exchangers should provide efficient heat exchange between the gas and the surroundings in case of X_1 and X_3 , and the gas and the cooling object in case of X_2 . Practically most of the heat exchangers are made of copper, which has a high heat conductivity. The main requirements to the construction of the heat exchangers are a large heat exchange surface and a low pressure drop. For heat exchangers consisting of N parallel channels with a length L_{ch} and a diameter d_{ch} the total pressure drop consists of two contributions. First of all, the pressure drop due to the flow resistance of N channels, Δp_1 , which can be determined as follows

$$\Delta p_1 = \frac{\rho v^2}{2} \frac{f_{ch} L_{ch}}{d_{ch}}, \quad (2.60)$$

where ρ is the density and v is the velocity of the fluid in the heat exchanger respectively, and f_{ch} is the friction factor, which can be found in [6]. Secondly, the pressure drop due to the change of flow channel diameter (entrance/exit effect due to the split of flow from a big channel into a number of parallel channels), Δp_2 , which equals to

$$\Delta p_2 = \frac{\rho v^2}{2} \left(1 - \left(\frac{N A_{ch}}{A_t} \right)^2 + K + \frac{f_{ch} L_{ch}}{d_{ch}} + \frac{f_t L_t}{d_t} \right), \quad (2.61)$$

where A_t , L_t , and d_t are the cross-sectional area, the length, and the diameter of a tube before the heat exchanger, and f_t is the friction factor in the tube [6].

The average heat exchange rate between the fluid and the heat exchanger is given by

$$\bar{\dot{Q}}_e = N A_{ch} L_{ch} \alpha_e F \Delta T, \quad (2.62)$$

where α_e is a heat exchange parameter, and F is heat exchanging surface area per unit volume. The parameter

$$\alpha_e = \frac{k_f Nu}{d_{ch}}, \quad (2.63)$$

where k_f is a heat conductivity of the fluid, and Nu is the Nusselt number. For a circular channel F is equal to

$$F = \frac{4}{d_{ch}}. \quad (2.64)$$

In the steady state \dot{Q}_e is equal to the amount of heat, \dot{Q}_f , transported by the fluid into the heat exchanger

$$\bar{\dot{Q}}_e = \bar{\dot{Q}}_f \quad (2.65)$$

with

$$\bar{\dot{Q}}_f = \dot{n} C_p \Delta T, \quad (2.66)$$

where C_p is the molar heat capacity of the gas. From equation 2.65 the length of the heat exchanger can be determined as

$$L_{ch} = \frac{\dot{n} C_p}{N \pi d_{ch} \alpha_e}. \quad (2.67)$$

The entropy production rate in the heat exchanger can be described by the following equation [7]

$$\dot{S}_X = \dot{n} \int_{T_1}^{T_2} C_p \left(\frac{1}{T} - \frac{1}{T_X} \right) dT. \quad (2.68)$$

Here, T_X is the temperature of the heat exchanger, which is assumed to be constant, T_1 and T_2 are the temperatures at the entrance and the exit of the heat exchanger respectively. For an ideal gas C_p is constant, so equation 2.68 can be rewritten as

$$\dot{S}_X = \dot{n} C_p \left(\ln \frac{T_2}{T_1} - \frac{T_2 - T_1}{T_X} \right). \quad (2.69)$$

In case of a perfect heat exchanger $T_2 = T_X$.

2.6.4. Regenerator

2.6.4.1. Regenerator and its function

The regenerator is one of the most important components of the PTR. An ideal regenerator fulfils the following conditions:

- Maximum heat-exchange area. This means a high filling factor, which is the ratio of the regenerator volume occupied by the material and the total volume of the regenerator. It also means, that the configuration of a unit of the regenerator material should be optimum to provide the maximum possible contact area between the gas and the regenerator material. The size of the regenerator material unit should be smaller or equal to the thermal penetration depth (eq.2.1).
- Minimum axial conduction.
- Minimum pressure drop. The regenerator material is a flow resistance, which causes a pressure drop. That means, that the pressure amplitude in the inlet of the regenerator is larger than in the pulse tube. According to the expression for the cooling power (eq.2.16), it has a negative effect on the performance of the PTR.
- High heat capacity of the regenerator material.

Some of these criteria are conflicting. For example, by increasing the filling factor (the 1st condition) the pressure drop becomes higher (the 3rd condition). Therefore, the optimisation of the regenerator is one of the main problems in pulse-tube cooling nowadays. Another important issue is the fixation of the regenerator material inside the regenerator. The movement of the regenerator material inside the regenerator during the operation of the system causes large heat dissipation and, thus, decreases the performance of the cooler significantly.

Practically, the regenerator is a stainless steel tube, filled with different materials. The choice of the regenerator material is based on the thermal properties of the material and the working gas (He). The regenerator material should have a large heat-exchange surface and a much higher heat capacity than the working gas in order to provide good heat storage conditions. At temperatures above 50 K helium has a rather low heat

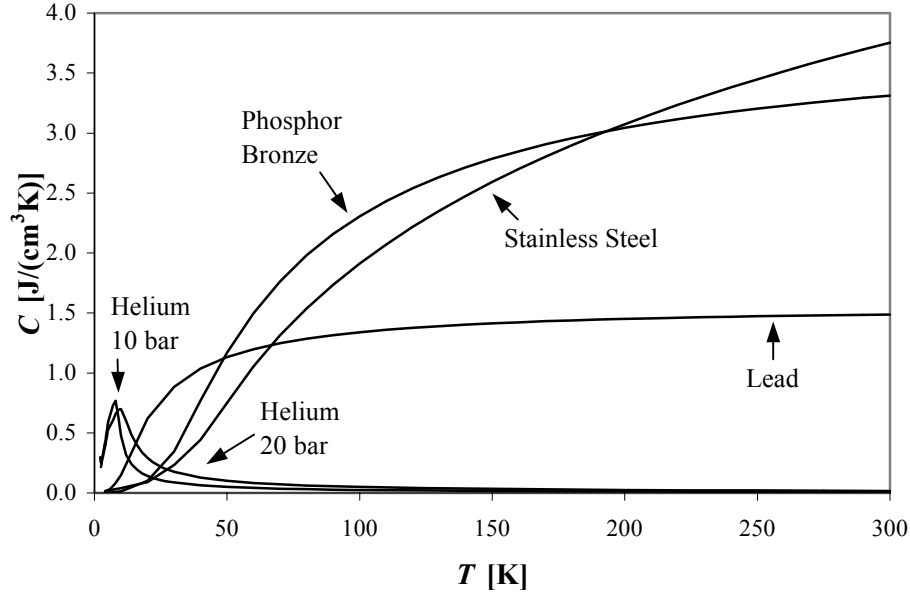


Figure 2. 11. Volumetric heat capacity of helium and several regenerator materials as functions of temperature.

capacity (FIG. 2.11). Therefore, it is not difficult to find a good and cheap regenerator material for this temperature range. Usually above 50 K the regenerator is filled with metal mesh screens (stainless steel, phosphor bronze or copper). In the temperature range 15 to 50 K lead is usually used. Below 15 – 20 K the heat capacity of helium increases significantly, while the heat capacity of most of the conventional regenerator materials rapidly decreases. This barrier on the way to reach low temperatures is overcome by using rare-earth magnetic materials in the coldest part of the regenerator (see Chapter 5). These materials have a magnetic phase transitions below 15 K accompanied by a considerable rise in their heat capacities.

2.6.4.2. Temperature profile in the regenerator with an ideal gas

The energy conservation for the gas in the regenerator can be expressed as follows [7]

$$\frac{(1-f)C_p}{V_m} \frac{\partial T_g}{\partial t} = -jC_p \frac{\partial T_g}{\partial l} - jV_m(1-T_g\alpha_v) \frac{\partial p}{\partial l} + (1-f)T_g\alpha_v \frac{\partial p}{\partial t} + \beta(T_r - T_g) + \frac{\partial q_g}{\partial l} \quad (2.70)$$

Here the lower index “g” stands for the gas, and “r” - for the regenerator material. The physical meaning of the terms from left to right is the following:

- the rate of the change of the gas temperature;

- the convective term due to the flow of gas in presence of a temperature gradient;
- the throttling term due to the flow resistance of the regenerator material;
- the compression term;
- the term, describing the heat exchange between the gas and the regenerator material, where β is a volumetric heat exchange parameter [7];
- the heat conduction term with the heat conduction flux in the gas, q_g , written as

$$q_g = -k_g \frac{\partial T_g}{\partial l} \quad (2.71)$$

where k_g is the heat conductivity of the gas.

The parameter j in the first and the second term on the right hand side of the equation 2.70 expresses the molar flux and is written as

$$j = \frac{\dot{n}}{A_r}, \quad (2.72)$$

where A_r is the cross-sectional area of the regenerator.

The energy conservation for the regenerator material reads

$$C_r \frac{\partial T_r}{\partial t} = \beta(T_g - T_r) - \frac{\partial q_r}{\partial l}, \quad (2.73)$$

where C_r is the heat capacity per unit volume of the regenerator material, and q_r is the heat conduction flux in the regenerator material, equal to

$$q_r = -k_r \frac{\partial T_r}{\partial l}. \quad (2.74)$$

Combining equations 2.70 and 2.73 gives

$$\begin{aligned} & -\frac{(1-f)C_p}{V_m} \frac{\partial T_g}{\partial t} - C_r \frac{\partial T_r}{\partial t} - jC_p \frac{\partial T_g}{\partial l} - jV_m(1-T_g\alpha_v) \frac{\partial p}{\partial l} \\ & + (1-f)T_g\alpha_v \frac{\partial p}{\partial t} + \frac{\partial q_g}{\partial l} + \frac{\partial q_r}{\partial l} = 0 \end{aligned} \quad (2.75)$$

To simplify this expression 2.75, we will assume that the regenerator is ideal. Therefore, the heat exchange area is maximum (neglect the 1st and the 5th terms), the axial conduction is absent (neglect last two terms), the pressure drop in the regenerator is equal to zero (neglect the 4th term), and, finally, the heat exchange is perfect, so $T_g=T_r=T$. In this way only the 2nd and the 3rd terms in equation 2.75 remain. It can be further simplified with the minus-one rule to

$$\left(\frac{\partial l}{\partial t}\right)_T = j \frac{C_p}{C_r} = v_T(T), \quad (2.76)$$

where v_T is a velocity, with which a temperature T moves through the regenerator. The value of the velocity is proportional to the molar flow rate density and the ratio of the specific heats of the gas and the regenerator material, which is a function of T only. If j is constant in the regenerator, all points with the same temperature move through the regenerator with the same speed. As v_T and j have the same sign, the temperature profile moves in the same direction as the flow. Half of the period the gas moves from the compressor towards the pulse tube, half of the period it moves back. The net mass flow in the cooler in case of single orifice mode is close to zero even during cool-down. So

$$\int_0^{t_c} j dt \approx 0. \quad (2.77)$$

It means, that the temperature profile only moves back and forth. At the hot end the temperature of the gas entering the regenerator is T_H during half of the cycle. The temperature T_H penetrates the regenerator over certain distance. The next half of the cycle it is pushed out of the regenerator again. At the cold end the same happens with T_L . As the heat capacity of the regenerator material at high temperatures is much larger than it is at the low temperatures, the distance, travelled by a certain temperature inside the regenerator will be larger at the cold end than at the hot end. As a result the temperature profile in the regenerator moves back and forth as it is shown in FIG 2.12. The dotted

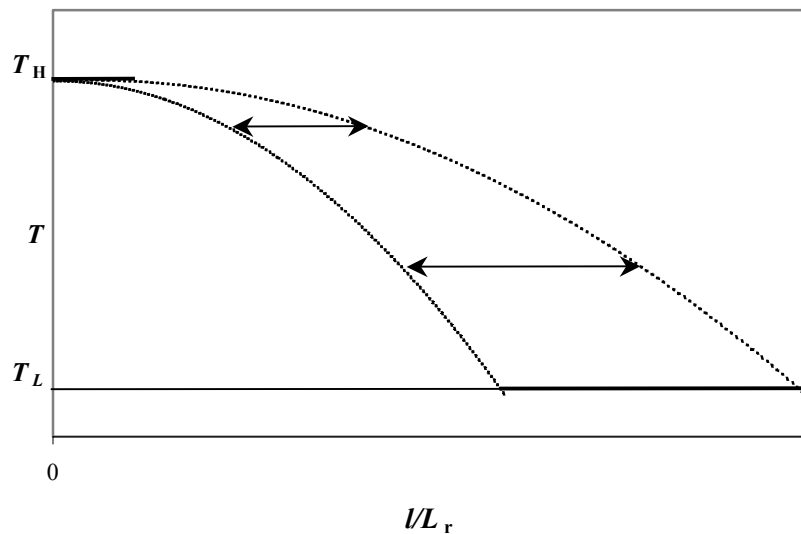


Figure 2. 12. Schematic representation of the motion of the temperature profile in the regenerator. At the hot end a temperature T_H penetrates the regenerator for a certain distance. A temperature T_L penetrates the regenerator for a certain distance from the cold end as well. The dotted curve is a qualitative continuous connection between the cold and the hot ends.

curve is a qualitative continuous connection between the hot and the cold end of the regenerator.

2.6.4.3. Nonideal-gas effects in the regenerator

The energy flow in the regenerator can be described by the following equation

$$E_r = \dot{Q}_{cr} + \bar{\dot{H}}_r, \quad (2.78)$$

where \dot{Q}_{cr} is the flow due to the heat conduction, and $\bar{\dot{H}}_r$ is the average enthalpy flow in the regenerator. As it has been shown in [8], the heat conduction plays an important role in determining the temperature profile in the regenerator.

The heat flow due to the thermal conduction in the regenerator is given by

$$\dot{Q}_{cr} = -k_r A_r \frac{dT}{dl}. \quad (2.79)$$

The enthalpy flow in the regenerator can be expressed as

$$\dot{H}_r = \dot{n}_r H_m, \quad (2.80)$$

where \dot{n}_r is the molar flow rate in the regenerator. The change of the molar enthalpy of the gas for the small pressure variations δp is written as

$$\delta H_m = C_p \delta T + H_p \delta p \quad (2.81)$$

with

$$H_p = (1 - T\alpha_V) V_m. \quad (2.82)$$

If the heat exchange between the gas and the regenerator material is perfect, and the heat capacity of the regenerator material is much larger than the heat capacity of the gas, in the steady state the temperature in the regenerator is constant in time (see eq. 2.76): $\delta T=0$. Hence, the first term in equation 2.81 is equal to zero.

We will write the molar enthalpy as the sum of the time average and a varying part

$$H_m = \bar{H}_m + \delta H_m; \quad (2.83)$$

and use the fact, that the average molar flow rate in the regenerator is zero

$$\bar{\dot{n}}_r = 0. \quad (2.84)$$

In this case with equations 2.83 and 2.84 we can express the average enthalpy flow in the regenerator as

$$\overline{\dot{H}}_r = \overline{(1 - T\alpha_v)V_m \dot{n}_r \delta p}. \quad (2.85)$$

With equation 2.83 equation 2.85 can be written as

$$\overline{\dot{H}}_r = n_p H_p, \quad (2.86)$$

with

$$n_p = \overline{\dot{n}_r \delta p}. \quad (2.87)$$

With equations 2.79 and 2.86 equation 2.78 can be rewritten as follows

$$E_r = -kA_r \frac{dT}{dl} + n_p H_p. \quad (2.88)$$

For an ideal gas $H_p=0$. However, in reality H_p is non-zero even at room temperature [9]. An example of H_p at a pressure of 15 bar is plotted versus temperature in FIG. 2.13. From FIG. 2.13 it is seen that in the high-temperature limit at $T > 6.4$ K $H_p=12$ cm³/mol has and in the low-temperature limit at $T < 6.4$ K $H_p=24$ cm³/mol. H_p at an average pressure of 15 bar can be described by the following analytical expression

$$\frac{H_p}{\text{cm}^3/\text{mol}} = 24 \frac{1 - \left(\frac{T}{8\text{K}}\right)^4}{1 + \exp((0.9/\text{K})(T - 8\text{K}))} + 12 \frac{1 - \frac{38\text{K}}{T}}{1 + \exp((0.9/\text{K})(10.6\text{K} - T))}. \quad (2.89)$$

The first term on the right-hand side of equation 2.89 gives the low-temperature part of H_p , and the second term – the high-temperature part.

For a given molar flow rate and a given pressure amplitude the enthalpy flow in the regenerator is a function of H_p , and therefore, a function of temperature. Here we assume, that the flow resistance of the regenerator is zero.

With equation 2.88 the temperature profile in the regenerator can be determined as

$$\int_T^{T_H} \frac{kA_r dT}{E_r - n_p H_p} = l. \quad (2.90)$$

The value of E_r can be obtained from the boundary conditions $T=T_L$ for $l=L_r$

$$\int_{T_L}^{T_H} \frac{kA_r dT}{E_r - n_p H_p} = L_r. \quad (2.91)$$

Due to the shape of H_p , represented in FIG. 2.13, the solutions of equation 2.90 for $T_L > 6.4$ K and for $T_L < 6.4$ K will have totally different behavior. In [9] the temperature profiles in the regenerator of a single-stage PTR, operating between 2.2 and 300 K, are

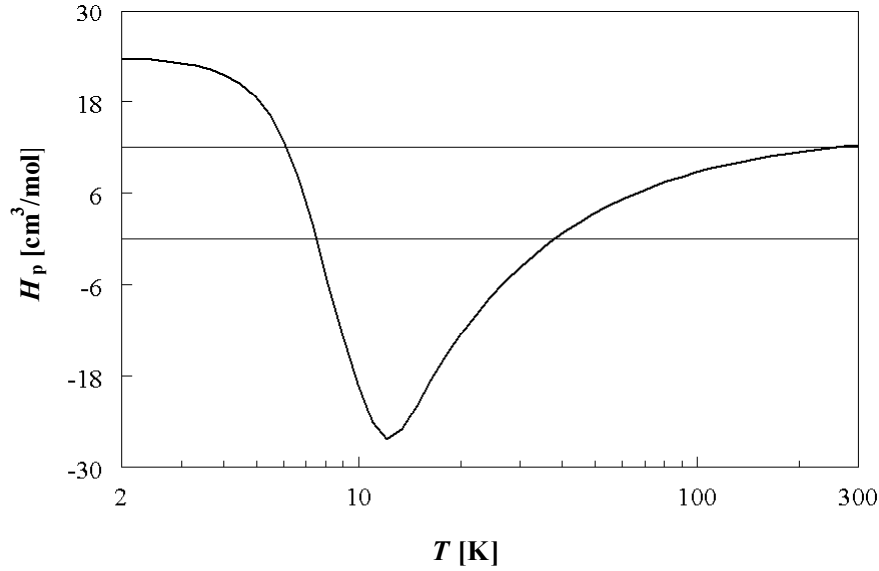


Figure 2.13. H_p - T dependence of ^4He at 15 bar. The horizontal line is drawn at $H_p=12 \text{ cm}^3/\text{mol}$. If $T < 6.4 \text{ K}$, $H_p > 12 \text{ cm}^3/\text{mol}$.

illustrated. However, in practice the lowest temperature, reached by a single-stage PTR so far, is equal to 13 K [10]. In multistage PTRs it is difficult to determine regenerator temperature profiles with equation 2.90 due to the changing from stage to stage flow. Therefore, we have concentrated on the final stage of a multistage PTR in order to calculate temperature profiles. The thermal conductivity, k , is considered to be constant, and the heat capacity of the regenerator material is considered to be much higher than the heat capacity of the gas.

In the calculations the hot end temperature of the regenerator varies between 30 K and 40 K. The temperature profiles have been calculated for $T_L=4 \text{ K}$ (the case of $2.2 \text{ K} \leq T_L \leq 6.4 \text{ K}$) and for $T_L=13 \text{ K}$ (the case of $T_L \geq 6.4 \text{ K}$). In the calculations first E_r is determined with equation 2.91 for a certain value of n_p . Knowing E_r the temperature profile is calculated with equation 2.90.

The calculated temperature profiles for $T_L=4 \text{ K}$ are plotted in FIG. 2.14 for different values of n_p . If n_p is equal to zero, the energy flow is just the heat conduction (see equation 2.88). Therefore, the temperature profile is linear. The temperature profiles for $n_p > 0$ are flat near the low-temperature side of the regenerator. This is due to the fact that H_p for $T < 6.4 \text{ K}$ has its maximum at T_L in the interval $[T_L; T_H]$. In this situation according to equation 2.88 the heat flow at T_L is small, and the temperature gradient is close to zero. The maximum temperature gradient, corresponding with the maximum heat flow, appears at around 12 K, where H_p has its minimum (see FIG. 2.13). With the increase of n_p the part of the temperature profile with the minimum temperature gradient becomes larger. According to [9], for large flow rates, the energy flow is equal to the enthalpy flow, corresponding to the maximum H_p . So the influence of the heat

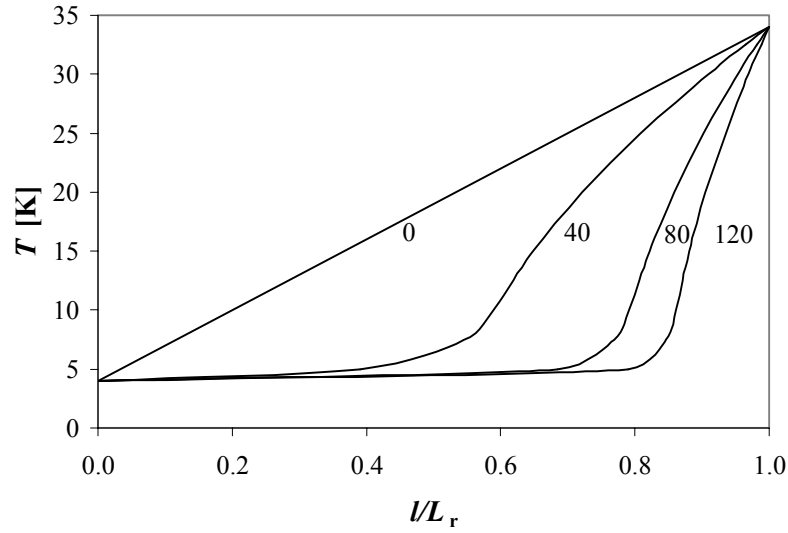


Figure 2. 14. Calculated temperature profiles in the regenerator for $T_L=4$ K and $T_H=34$ K for various values of n_p (indicated in the graph in kPa mol/s).

conduction, or in other words the influence of the thermal conductivity of regenerator material, is negligible.

The calculated temperature profiles for $T_L=13$ K for various n_p are shown in FIG. 2.15. Here we can see that the difference between the temperature profiles for $n_p < 800$ kPa mol/s is not big. The temperature profiles are almost linear. In this temperature region

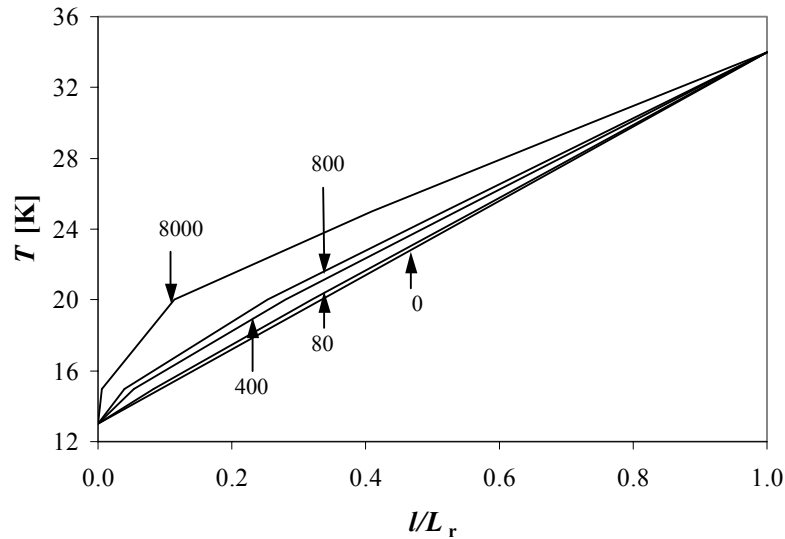


Figure 2. 15. Calculated temperature profiles in the regenerator for $T_L=13$ K and $T_H=34$ K for various values of n_p (indicated in the graph in kPa mol/s).

(between 13 and 34 K) H_p is close to its minimum, and the heat flow is maximal. At very high n_p values, in the order of a few thousands kPa mol/s, the gradient of the temperature at the cold end is much larger than the gradient at the hot end.

2.6.4.4. Regenerator losses

The total entropy production rate in the regenerator consists of four contributions: entropy production due to the heat exchange between the gas and the regenerator material, \dot{S}_e , entropy production due to the thermal conduction in the gas, \dot{S}_{cg} , and in the regenerator material, \dot{S}_{cr} , and entropy production due to the flow resistance of the regenerator, \dot{S}_z [7]

$$\dot{S}_r = \dot{S}_e + \dot{S}_{cg} + \dot{S}_{cr} + \dot{S}_z. \quad (2.92)$$

The expressions for each of the terms are given below:

$$\dot{S}_e = A_r \int_0^{L_r} \frac{\beta(T_r - T_g)^2}{T_r T_g} dl, \quad (2.93)$$

$$\dot{S}_{cg,r} = A_r \int_0^{L_r} \left[\frac{k}{T^2} \left(\frac{\partial T}{\partial l} \right)^2 \right]_{g,r} dl, \quad (2.94)$$

$$\dot{S}_z = A_r \int_0^{L_r} \frac{\eta z_r (jV_m)^2}{T_g} dl. \quad (2.95)$$

In equation 2.95 z_r is the characteristic flow impedance of the regenerator. The flow impedance of the regenerator, Z_r , is then determined as

$$Z_r = \frac{z_r L_r}{A_r}. \quad (2.96)$$

Knowing a value of Z_r , we can determine the pressure drop in the regenerator, which is defined as follows

$$\Delta p = \eta Z_r \dot{V}_r, \quad (2.97)$$

where \dot{V}_r is the volume flow in the regenerator.

In case of the regenerator, filled with screens, the flow impedance of one screen can be defined as follows

$$z_s = \frac{Z_r}{N_r} = \frac{z_r L_s}{A_r}, \quad (2.98)$$

where L_s is the height of one screen. With equation 2.98 the characteristic flow impedance of one screen with an area of 1 m^2 is equal to

$$z_1 = z_r L_s. \quad (2.99)$$

With equation 2.99 equation 2.97 can be rewritten for the pressure drop over N screens as follows

$$\Delta p_N = \frac{\eta z_1}{A_r} N \dot{V}_r. \quad (2.100)$$

For the resistance of the regenerator we write

$$R_r = \eta Z_r. \quad (2.101)$$

The resistance of the regenerator can be determined in the DC-flow measurements at room temperature (see Chapter 3) and calculated with the following expression

$$R_r = \frac{p_r^2 - p_t^2}{2RT_H \dot{n}_r}. \quad (2.102)$$

Here, p_r is the pressure at the inlet to the regenerator, and p_t is the pressure in the pulse tube.

2.6.5. Pulse tube

2.6.5.1. Velocities of the gas at the hot and at the cold ends.

The expressions for the temperature and the flow of the gas at the cold and hot ends of the pulse tube have been derived above. Here, we will discuss the velocities of the gas at the hot and at the cold end of the pulse tube. The velocity of the gas at the hot end of the pulse tube is given by

$$v_H = \frac{V_{HA}}{A_t} \cos \omega t, \quad (2.103)$$

where A_t is the cross-sectional area of the tube, and V_{HA} is the amplitude of the volume flow at the hot end, written as

$$V_{HA} = \frac{p_1}{R_1}. \quad (2.104)$$

With equation 2.12 the velocity amplitude of the gas at the hot end of the pulse tube is

$$v_{HA} = \frac{\omega}{\alpha} \frac{C_V}{C_p} \frac{p_1}{p_0} L_t, \quad (2.105)$$

where L_t is the length of the pulse tube. The velocity v_H is in phase with the pressure oscillations. We consider v_H positive during the ωt interval $[-\pi/2, +\pi/2]$, so the gas moves from the tube to the buffer. When gas flows from the buffer into the tube, v_H is negative. This takes place during the ωt interval $[\pi/2, 3\pi/2]$. The maximum distance, travelled by the gas into the tube from the hot end, is

$$x_H = - \int_{\pi/2\omega}^{3\pi/2\omega} v_{HA} \cos \omega t dt = \frac{2v_{HA}}{\omega}. \quad (2.106)$$

With equation 2.105 equation 2.106 becomes

$$x_H = C_H L_t, \quad (2.107)$$

where

$$C_H = \frac{2}{\alpha} \frac{C_V}{C_p} \frac{p_1}{p_0}. \quad (2.108)$$

The velocity of the gas at the cold end of the pulse tube is equal to [3]

$$v_L = \frac{V_{HA}}{A_t} \sqrt{1 + \alpha^2} \cos(\omega t + \varphi_L), \quad (2.109)$$

where $\tan(\varphi_L) = \alpha$. The velocity amplitude at the cold end is

$$v_{LA} = \frac{V_{HA}}{A_t} \sqrt{1 + \alpha^2}. \quad (2.110)$$

So the maximum distance, travelled by the gas at the cold end of the pulse tube is equal to

$$x_L = \frac{2v_{LA}}{\omega} = C_L L_t, \quad (2.111)$$

where

$$C_L = 2 \sqrt{\frac{1 + \alpha^2}{\alpha^2}} \frac{C_V}{C_p} \frac{p_1}{p_0}. \quad (2.112)$$

With equations 2.107 and 2.108 equation 2.111 can be written as

$$x_L = \sqrt{1 + \alpha^2} x_H. \quad (113)$$

Typically C_L varies between 1/3 and 1/2 (see Chapter 4). The total volume, moving in and out of the pulse tube at the cold end during one cycle is

$$V_L = \frac{2V_{LA}}{\omega}. \quad (2.114)$$

With equations 2.111 and 2.3

$$V_{LA} = \frac{\omega V_t}{2C_L} = \frac{\pi v V_t}{C_L}, \quad (2.115)$$

where V_t is the volume of the tube, and v is the frequency.

2.6.5.2. Pulse tube losses

The total entropy production rate in the pulse tube consists of four terms: entropy production due to the heat exchange of the gas with the tube walls, entropy production due to the heat conductivity in the gas and in the tube walls, and finally, entropy production due to the turbulence of gas, which can appear in the pulse tube [7]. The first three terms are determined in the same way as for the regenerator. The only difference is, that instead of the regenerator material we have a pulse tube wall. The entropy production due to turbulence, \dot{S}_{tb} , occurs due to cross-sectional area changes (*e.g.* from the connection tube into the pulse tube) or large Reynolds numbers of the gas flow. As a result cold and hot gases get mixed, and entropy is produced. We consider two gas elements with N_1 and N_2 amount of moles at temperatures T_1 and T_2 respectively mix with each other. The uniform gas, obtained from the mixing, has the temperature T_e . Formally, \dot{S}_{tb} is given by the following expression

$$\dot{S}_{tb} = N_1 \int_{T_1}^{T_e} \frac{C_p}{T} dT + N_2 \int_{T_2}^{T_e} \frac{C_p}{T} dT. \quad (2.116)$$

Due to the complex flow pattern and temperature distribution, it is rather difficult to determine the value of \dot{S}_{tb} . In practice \dot{S}_{tb} can be greatly reduced by the use of good flow straighteners at both ends of the tube.

2.6.6. Flow straighteners

Most of multistage PTRs are of U-shape type. In this case it is very often, that the cold end of the regenerator is connected to the cold end of the pulse tube by means of a narrow connection tube. Therefore, the gas, entering the pulse tube from the regenerator side, expands from the connection tube with a small cross-sectional area into the pulse tube with a larger cross-sectional area as shown in FIG. 2.16. The turbulent eddies are formed on the sides of the main flow jet. This results in the irreversible loss, described by

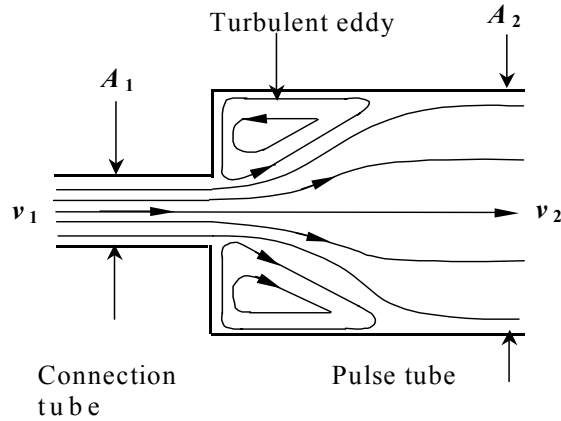


Figure 2. 16. The gas flow through an abrupt expansion from the connection tube with the cross sectional area A_1 into the pulse tube with the cross-sectional area A_2 .

equation 2.116. The turbulence also occurs, when the gas leaves the pulse tube, contracting into the connection tube. A similar situation happens at the warm end of the pulse tube, when the gas enters from and goes into the buffer, connected to the pulse tube by a narrow connection tube as well. Using flow-straighteners greatly helps to reduce the irreversible entropy production due to the turbulence. The flow-straighteners usually consist of a number of fine-meshed screens, placed close to the entrance into the pulse tube (FIG. 2.17). The number of the screens in a flow-straightener can be calculated in the following way. The difference in Bernoulli pressure due to the flow in a connection tube with a cross-sectional area A_1 to a pulse tube with a cross-sectional area A_2 is

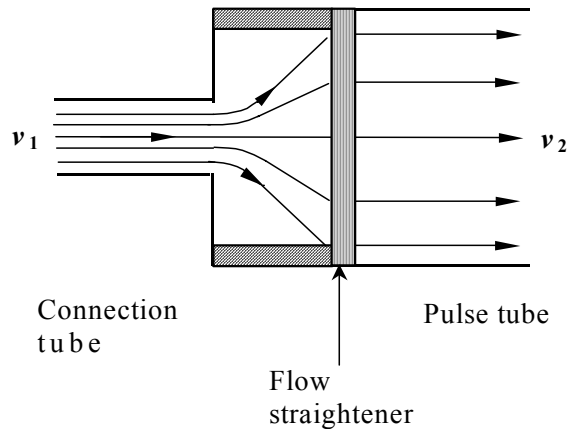


Figure 2. 17. The gas flow through an abrupt expansion from the connection tube into the pulse tube with a flow straightener in it.

$$\Delta p_B = \frac{1}{2} \rho (v_1^2 - v_2^2) = \frac{1}{2} \rho \dot{V}^2 \left[\left(\frac{1}{A_1} \right)^2 - \left(\frac{1}{A_2} \right)^2 \right], \quad (2.117)$$

where \dot{V} is the volume flow.

For the flow-straightener we require the pressure drop over N screens to be larger than Δp_B . With equation 2.100

$$N > \Delta p_B \frac{A_2}{\eta z_1 \dot{V}}, \quad (2.118)$$

2.6.7. 1st orifice

The 1st orifice in combination with the buffer provides the gas flow at the hot end of the pulse tube. The flow at the hot end of the pulse tube is not in phase with the flow at the cold end of the pulse tube. The phase shift between the flow of the gas at the hot and the cold end of the pulse tube is expressed via the phase angle φ_L . In case of the ideal PTR (ideal regenerator with the filling factor $f=1$, adiabatic pulse tube, ideal working gas), the maximum performance is reached when $\varphi_L=45^\circ$ [3, 8]. In practice the optimum for the single stage PTR is shifted from 45° to somewhat lower values. The typical parameters for φ_L of our three-stage PTR are 25° for the 1st stage, 35° for the 2nd stage, and 45° for the 3rd stage.

A schematic drawing of the orifice is shown in FIG. 2.18. All the orifices are at room temperature. Hence, helium, flowing through the orifices, can be considered as an ideal gas. In the ideal case, there is no heat exchange between the gas and the environment. In reality there is a certain amount of heat produced due to the throttling in the orifices. However, the rate of this heat exchange is so small, that it can be neglected. Therefore, the 2nd law of thermodynamics for the system in the steady state, consisting of the orifice, gives

$$0 = \dot{n}(S_m(T_H, p_H) - S_m(T_H, p_L)) + \dot{S}_O, \quad (2.120)$$

where \dot{S}_O is the irreversible entropy production in the orifice, which is for the ideal gas equals to

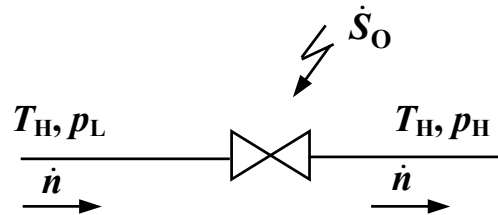


Figure 2. 18. A schematic diagram of an orifice.

$$\dot{S}_O = \dot{n}R \ln \frac{p_H}{p_L}. \quad (2.121)$$

2.6.8. Double-inlet orifice

In the double-inlet pulse tube refrigerator (DPTR) the hot end of the pulse tube is connected with the hot end of the regenerator by a tube with an orifice (FIG. 2.1). In this case the gas can move in and out of the pulse tube not only via regenerator, but also via the 2nd orifice. That explains the name double-inlet. Since the gas can enter the pulse tube from the hot end via the double-inlet, bypassing the regenerator, the cooling power of the PTR reduces, as it depends on the amount of the gas, passing the cold heat exchanger of the pulse tube (eq.2.16). In addition, the pressure drop over the double-inlet orifice is a source of the irreversible entropy production, which also leads to losses. However, both disadvantages are overcome by the fact, that the double-inlet reduces the entropy production in the regenerator. As a result the overall performance of the system improves significantly.

2.6.9. Minor orifice

The presence of the double-inlet opens an internal closed circuit. Any asymmetrical flow resistance in this circuit leads to an internal circulation of the gas through the loop of the regenerator, the pulse tube and the double-inlet. This is the so-called DC-flow. The DC-flow can exist even in a perfectly symmetrical system with the double-inlet due to the fact, that the mass flow through the double-inlet, when the system is connected to the low-pressure side (low density of He), is different from the mass flow through it, when the system is connected to the high-pressure side of the compressor (high density of He). In any case the DC-flow runs from hot to cold, thus giving a heat load on the coldest parts of the cooler. And that can lead to a severe degradation in the performance of the cooler.

The DC-flow can be suppressed by installing a so-called minor orifice. The minor orifice is a flow resistance on the line between the hot end of the pulse tube and the high- or low-pressure side of the compressor.

2.7. CONCLUSIONS

In this chapter we have discussed the general features of the PTR and its main components. The operation principle of the PTR has been explained and the expressions for the cooling power of the PTR and for its coefficient of performance have been derived. Furthermore, the loss mechanisms in the PTR have been treated. A schematic diagram, showing the sources of various important losses in a PTR, is given in FIG. 2.19. The total irreversible entropy production in the PTR can be described by the following expression

$$\dot{S}_{\text{PTR}} = \dot{S}_c + \dot{S}_{\text{rv}} + \sum \dot{S}_{\text{Xi}} + \dot{S}_r + \sum \dot{S}_{\text{Oi}} + \dot{S}_t. \quad (2.122)$$

Equation 2.122 can be used in the design and analysis of PTRs.

We have also discussed the effect of the multistaging on the performance of the PTR (note, that a highly idealized situation has been considered). Multistaging has a positive effect only below 150 K. The position of the attachment of the following stage depends on the required lowest temperature. In case of the two-stage PTR the lower the required temperature, the closer to the middle of the regenerator the first-stage pulse tube should be attached.

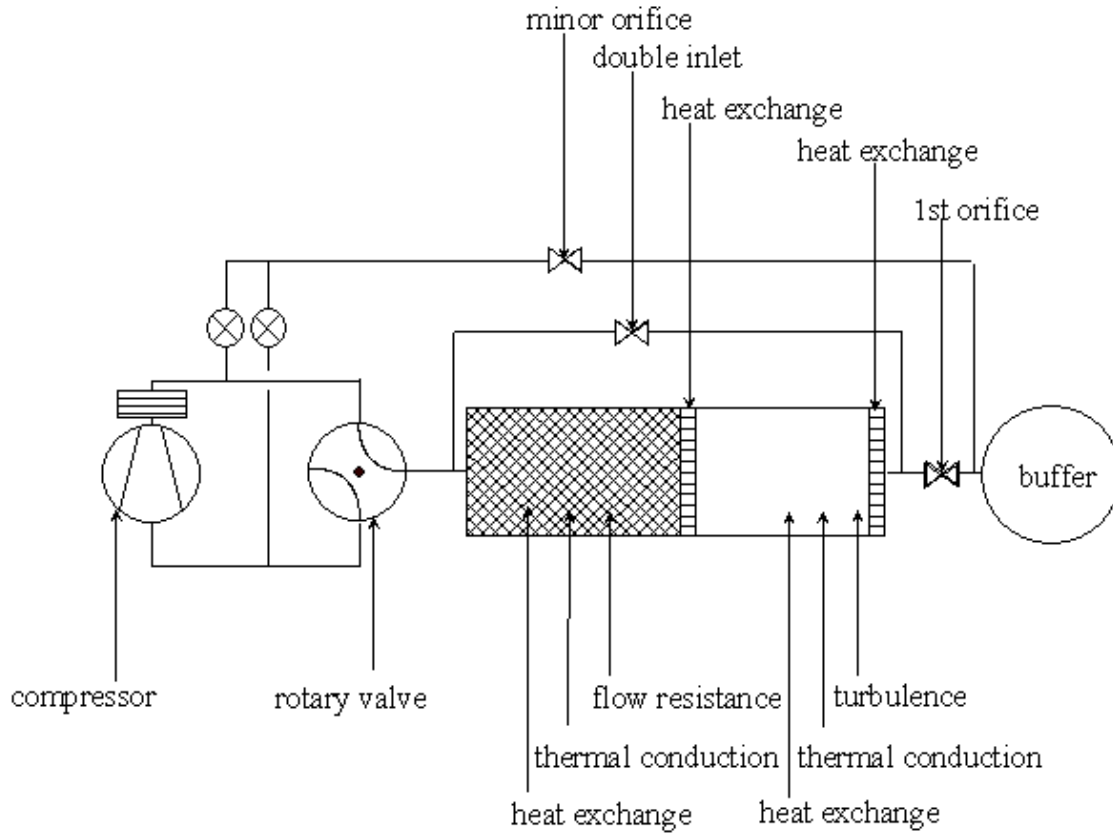


Figure 2. 19. A schematic diagram of the sources of various important losses in the PTR.

REFERENCES

1. Corey, J., James, E., Kashani, A., Helvensteijn, B., Rhoads, G., "Development of a Linear Compressor for Use in G-M Cryocoolers", to be published in Cryocoolers **13**, 2004.

2. Olson, J., Champagne, P., Roth, E., Evtimov, B., Clappier, R., Nast, T., Renna, T., Martin, B., "Lockheed Martin 6K/18K Cryocooler", to be published in *Cryocoolers* **13**, 2004.
3. Waele, A. T. A. M. de, Steijaert, P. P., and Koning, J. J., "Thermodynamical aspects of pulse tubes II", *Cryogenics* **38**, 1998, pp. 329-335.
4. Waele, A. T. A. M. de, "Optimization of pulse tubes", *Cryogenics* **39**, 1999, pp. 13-15.
5. Waele, A. T. A. M. de, Tanaeva, I. A., and Ju, Y. L., "Multistage pulse tubes", *Cryogenics* **40**, 2000, pp. 459-464.
6. Blevins, R. D., "Applied fluid dynamics handbook", Krieger Publishing Company, USA, 1984.
7. Waele, A. T. A. M. de, Steijaert, P. P., and Gijzen, J., "Thermodynamical aspects of pulse tubes", *Cryogenics* **37**, 1997, pp. 313-324.
8. Waele, A. T. A. M. de, Hooijkaas, H. W. G., Steijaert, P. P., and Benschop, A. A. J., "Regenerator dynamics in the harmonic approximation", *Cryogenics* **38**, 1998, pp. 995-1006.
9. Waele, A. T. A. M. de, Xu, M., Y., Ju, Y., L., "Nonideal-gas effect in the regenerator", *Cryogenics* **39**, 1999, pp. 847-851.
10. Giebeler, F., Thummes, G., Siegel, A., and Hafner, H., U., "High-capacity single-stage pulse tube cooler for 25 K operation", presented on the 12th International Cryocooler Conference in Cambridge, USA, 2002.

CHAPTER 3.

PRACTICAL ASPECTS OF PULSE-TUBE REFRIGERATORS, PART I

In this chapter the development of a three-stage pulse tube refrigerator (PTR1) and a two-stage PTR (PTR 2) is discussed. The difference of using ^4He and ^3He as a working fluid in a PTR is treated. A big part of this chapter is dedicated to the optimization of the rotary valve. The rotary valve is one of the most important components of a GM-type PTR. About 25% of the total power loss originates from the rotary valve. Therefore, an improvement of the rotary valve can increase the performance of the PTR considerably.

3.1. ^4He AND ^3He AS WORKING FLUIDS IN THE PTR

The cooling power of a PTR (equation 2.16) is proportional to the volumetric thermal expansion coefficient, α_v . If $\alpha_v=0$, the PTR has no cooling power. If α_v is negative, adiabatic expansion results in heating instead of cooling. Therefore, the PTR operates only if $\alpha_v > 0$. For ^4He $\alpha_v > 0$ at temperatures above the λ -line, which runs from 2.17 K at the saturated vapour pressure to 1.76 K at the melting curve (FIG. 3.1). Hence, the lowest temperature, attainable with a ^4He PTR, is a value just above the λ -line. In order to cool below 2 K, ^3He should be used as the working fluid. As can be seen from FIG. 3.1 at pressures of 10-20 bar $\alpha_v=0$ at around 1 K. So, by using ^3He , the temperature range of PTRs can be extended down to temperatures close to 1 K.

3.2. THREE-STAGE PTR (PTR1)

The three-stage PTR (PTR1) had been built before this research started [1]. However, many experiments have been performed with this system as a part of this work. The schematic diagram of the PTR1 is shown in FIG. 3.2. The system is operated by a 4 kW compressor and a rotary valve. The tubes and the regenerator are fabricated from stainless steel. The dimensions of them are given in Table 3.1. The first-stage regenerator is filled with phosphor-bronze screens (mesh # 200¹), the second stage with lead spherical particles (0.2-0.3 mm), and the third stage with a combination of Er_3Ni , ErNi , and $\text{ErNi}_{0.9}\text{Co}_{0.1}$. Copper thermal radiation shields are attached to the first- and the second-

¹ Mesh size means a number of openings in a screen per linear inch.

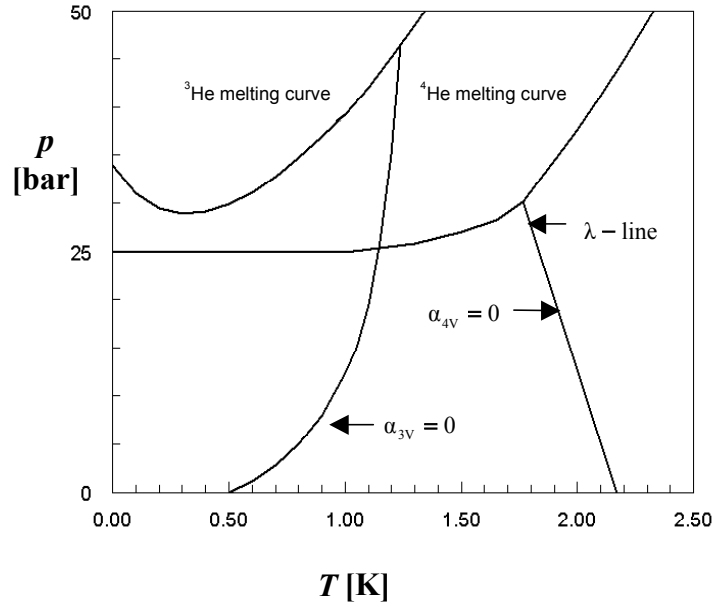


Figure 3.1. ^4He and ^3He phase diagrams. The λ -line and the line $\alpha_{4V} = 0$ practically coincide. The lines $\alpha_{4V} = 0$ and $\alpha_{3V} = 0$ give the limiting temperatures of most of cryocoolers, using ^4He and ^3He respectively.

stage cold heat exchangers. Each stage has three adjustable needle valves: the first orifice, the double-inlet, and the minor orifice.

The temperature at the cold end of the 1st stage is measured by a platinum resistor. The temperatures of the second and the third stages are measured by calibrated diode thermometers.

The lowest temperature, reached with this system with ^4He as the working fluid, is 2.19 K with an operating frequency of 1.2 Hz, an average pressure of 16.1 bar, and a pressure amplitude at the inlet to the system of 3.76 bar. The cooling power at 4.2 K is 40 mW.

Table 3.1. Dimensions of the main components of the three-stage PTR.

Stage		1	2	3
Pulse tube	Inner diameter [mm]	25	18	9
	Wall thickness [mm]	0.5	0.5	0.25
	Length [mm]	183	203.5	430
	Volume [cm ³]	89.8	51.75	27.3
Regenerator	Inner diameter [mm]	50	29.7	19
	Wall thickness [mm]	0.7	0.6	0.5
	Length [mm]	141	130	155
	Volume [cm ³]	276.7	90	43.9

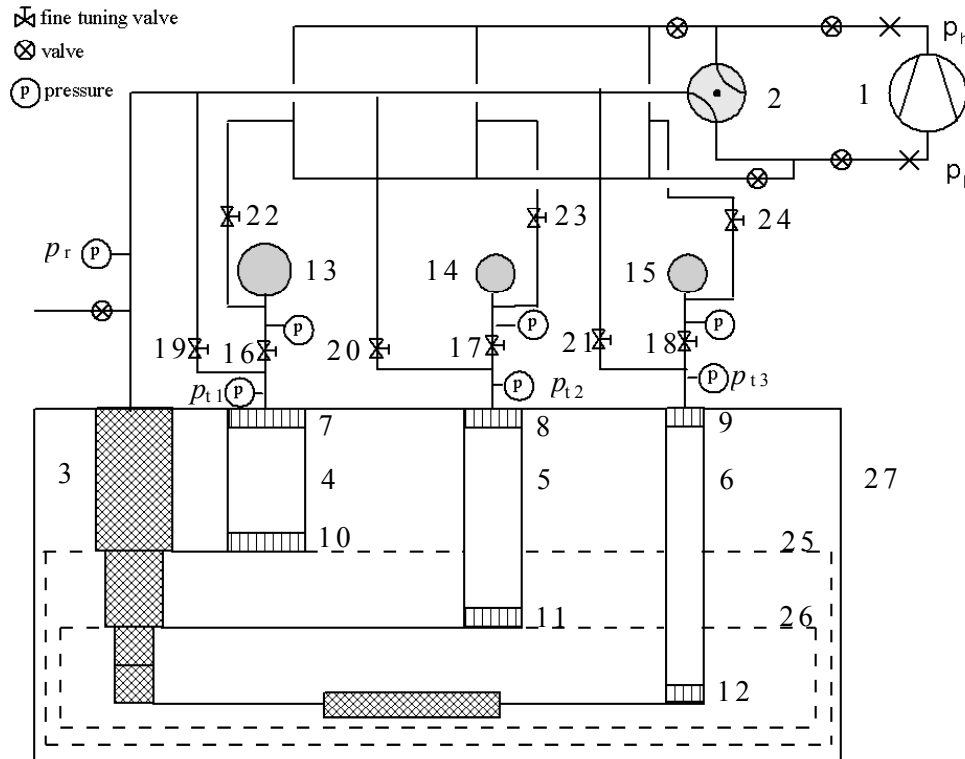


Figure 3. 2. Schematic diagram of the PTR1. 1 - compressor; 2 - rotating valve; 3 - regenerator; 4-6 – pulse tubes; 7-9 – hot heat exchangers; 10-12 – cold heat exchangers; 13-15 – buffers; 16-18 – first orifices; 19-21 – double-inlet valves; 22-24 – minor orifices; 25 – 1st heat shield; 26 – 2nd heat shield; 27 – cryostat.

Usually the optimum setting of the orifices in case of a lowest temperature with no heating, supplied to the cold end of a PTR (“no-load” temperature), is different from the optimum setting for a maximum cooling power at a certain temperature. In particular the setting of the orifices of the final stage is different. The resistance of the 1st orifice of the final stage should be smaller for a minimum temperature with applied heat load than for a “no-load” temperature. At higher temperatures the molar volume of the gas is smaller, and, therefore, the molar flow through the cold heat exchanger is higher. Hence, in order to keep the optimum phase difference between the flow at the cold and at the hot end of the pulse tube, the first orifice should be opened more. As a consequence, the DC-flow in the system should be adjusted as well, by opening the DC-flow valves.

After adjusting the valves for optimum cooling power and filling more gas in the PTR, so that the average pressure increased with 0.5 bar and the pressure amplitude increased from 3.76 to 4.37 bar, the cooling power with ^4He increased to 114 mW at 4.2 K.

Simply by replacing ^4He with ^3He the lowest temperature decreased to 1.87 K. The valve settings as well as the average pressure, the pressure amplitude, and the

frequency were kept the same. After fine tuning of the valves the temperature reduced to 1.78 K. The cooling power with ^3He was 80 mW at 4.2 K. The amount of ^3He , used in the PTR, is 220 liters NTP. In order to use less helium the charcoal filters, which have a volume of 12.4 liters, have been removed from the compressor.

The next step was to change the stainless steel tube of the 3rd stage for a titanium one. Titanium has a much lower thermal conductivity than stainless steel (see FIG. 3.3). This results in a reduction of the heat leak to the cold end of the PTR. In this arrangement the cooling power at 4.2 K was 160 mW with ^4He . Therefore, the efficiency of the system with the titanium 3rd stage pulse tube increased by 60 %.

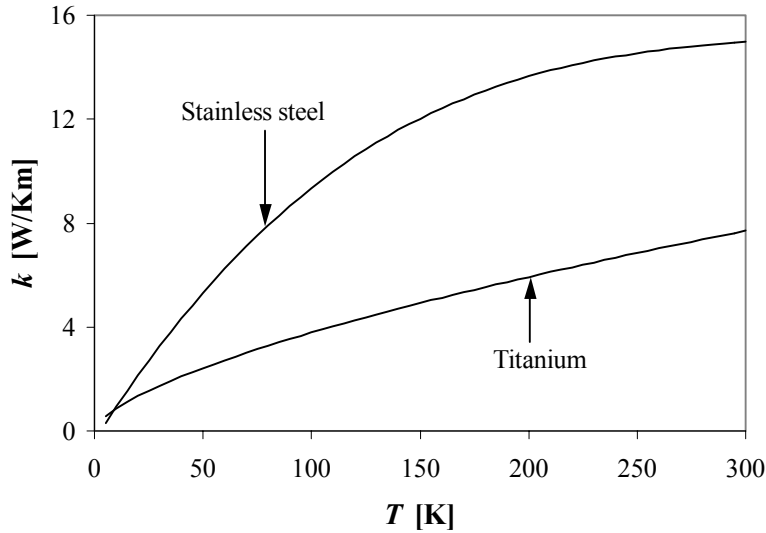


Figure 3. 3. Thermal conductivities of stainless steel and titanium as functions of temperature.

3.3. TWO-STAGE PTR (PTR2)

3.3.1. Experimental set-up

Simply by removing the 2nd stage pulse tube from PTR1, it has been transformed into a two-stage PTR (PTR2). In the new arrangement the 1st stage pulse tube is attached to the cold end of the 2nd stage regenerator of PTR1. The advantage of eliminating one stage is the reduction of the volume of the system. This results in an increase of the pressure amplitude with the same input power and a reduction of the amount of ^3He . In addition to that the pressure drop in the first-stage regenerator decreases. A negative aspect of eliminating a stage is the increase of the losses in the regenerator, which can be illustrated by a significant change in the temperature profile² in the regenerator (FIG. 3.4). The temperature of the 1st stage regenerator cold end has increased from 88 to 219 K due to the absence of the cooling power, provided by the 1st stage pulse tube of the PTR1

² All temperature profiles are measured by thermometers, placed on copper strips, wrapped around the tube walls.

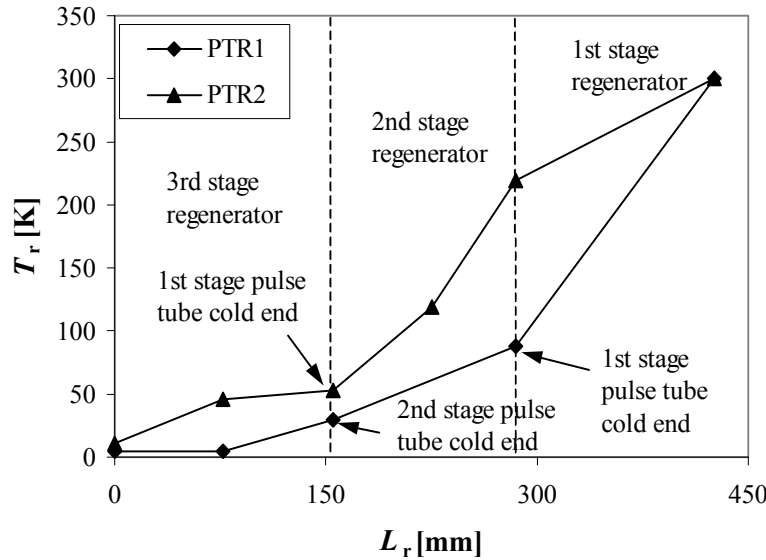


Figure 3. 4. Regenerator temperature profiles in case of PTR1 and PTR2. The PTR2 is obtained by eliminating of the 2nd stage pulse tube of the PTR1 and attaching the 1st stage pulse tube to the cold end of the 2nd stage regenerator. The regenerator is the same in both cases.

to the cold end of the 1st stage regenerator. Therefore, the gas enters the 2nd stage regenerator, which is filled with lead (see Table 3.3), with a higher temperature. At this temperature the heat capacity of lead is significantly smaller than the heat capacity of the stainless steel and phosphor bronze used in the 1st stage regenerator (see FIG. 2.11). For PTR2 this results in a higher irreversible entropy production due to the heat exchange (equation 2.89). The same holds for the 3rd stage regenerator. The relation between the heat conduction loss and a stage adding/removing has been discussed in section 2.7 of Chapter 2. There we have concluded, that below 150 K the attachment of an extra stage has a positive effect on the performance of the cooler.

With the two-stage PTR (PTR2) a lowest temperature of 2.43 K has been reached with ⁴He. This temperature has been obtained with an operating frequency of 1 Hz, an average pressure in the system of 17.4 bar, and a pressure amplitude at the inlet to the system of 6.3 bar. The highest cooling power at 4.2 K has been 163 mW with a 4 kW compressor (FIG. 3.5).

In order to increase the cooling power of PTR2 the regenerator has been changed for a larger one. The dimensions and the composition of the new two-stage regenerator are given in Tables 3.2 and 3.3. Occasionally an extra regenerator part (see FIG. 3.2), filled with ErNi_{0.9}Co_{0.1} particles (particle size 0.2-0.5 mm, $m=102$ g), has been added between the cold end of the 2nd stage regenerator and the cold end of the 2nd stage pulse tube. The volume of the extra regenerator part is 18 cm³. Further in the text the regenerator with the extra regenerator part will be indicated with a superscript “asterisk” as regenerator*.

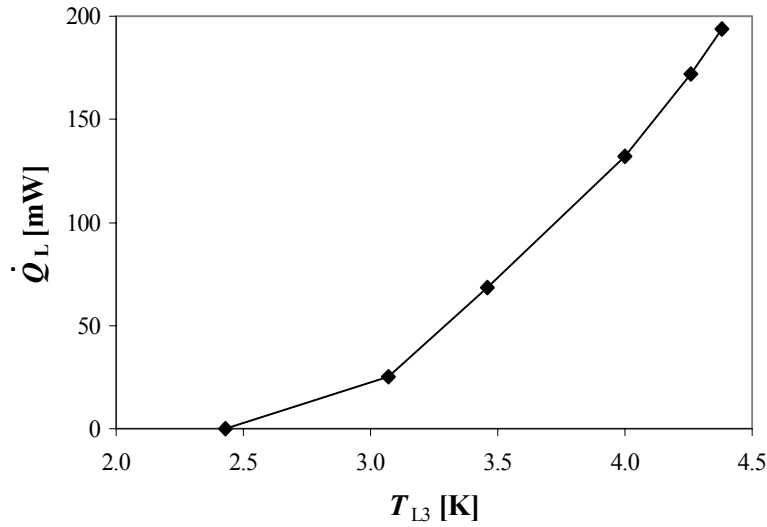


Figure 3. 5. Cooling power of the PTR2 with the ‘small’ regenerator as a function of temperature.

Table 3.2. Dimensions of the two-stage regenerator.

	1 st stage	2 nd stage
Inner diameter [mm]	50	29.7
Length [mm]	223	252
Wall thickness [mm]	0.6	0.4
Volume [cm ³]	438	177

Table 3.3. Composition of the two-stage regenerator (from the warm end).

Stage	Material	Size	Number of screens or mass	Fraction [%]	Filling factor
1	Stainless steel	Mesh # 60	41	5	0.31
	Stainless steel	Mesh # 200	250	14	
	Phosphor bronze	Mesh # 200	1350	77	
2	Lead	0.2-0.24 mm	548 g	47	0.58
	HoCu ₂	0.18-0.45 mm	423 g	46	0.56

3.3.2. Material fixation in the regenerator

Good fixation of the regenerator material is very important. A movement of the material inside the regenerator causes a large heat production, resulting in a significant degradation of the cooler performance. Lead, which in our PTR is used in the 2nd stage regenerator, is a very difficult material for packing. It is rather soft. Therefore, it often

happens, that the whole lead column begins to move after a few hours of running an experiment with a newly packed regenerator.

The separation between various materials should be accurately considered. Originally, for the separation of the two materials in the second stage regenerator, as well as at the warm and the cold end of the 2nd stage, we used a construction, consisting of two layers of felt with 5 stainless steel screens (mesh # 325) in between the felt layers, and a spring to keep the construction in place (FIG. 3.6). However, a beating sound appeared in the system after several experiments. After opening the regenerator we found, that HoCu₂ and lead were mixed completely and the separator was tilted. It is amazing that with such a material mixture in the 2nd stage regenerator a lowest temperature of 4.9 K has been reached.

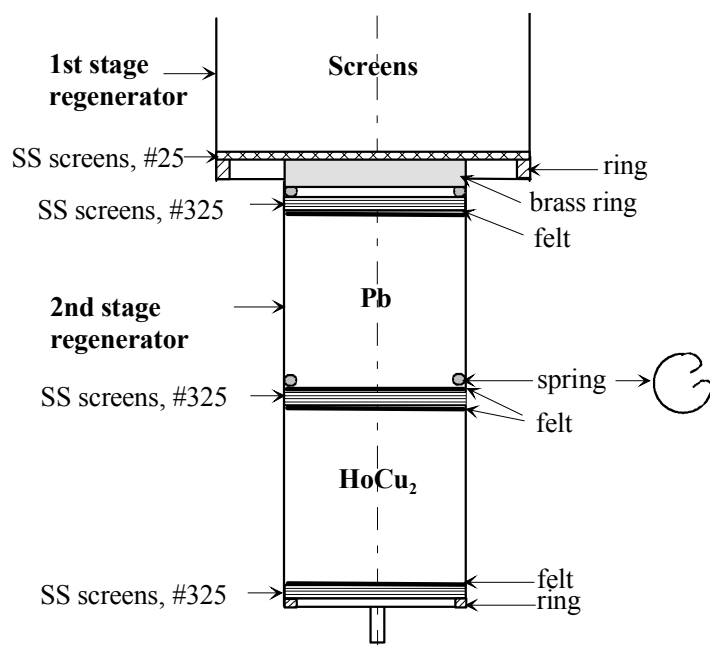


Figure 3. 6. Construction of the 2nd stage regenerator, described in Tables 3.2 and 3.3.

The new design of a separator is shown in FIG. 3.7. Here, the screens are spot-welded to a stainless steel ring of 1 cm high. In this way there is no risk of tilting of the new separator, and therefore, mixing of various regenerator materials.

The composition of the regenerator has been changed as well. The new composition of the 2nd stage regenerator is given in Table 3.4.

Table 3.4. New composition of the 2nd stage regenerator.

Composition (from the warm end)	Lead	ErNi	ErNi _{0.9} Co _{0.1}
Granule size [mm]	0.2-0.24	0.2-0.5	0.2-0.5
Mass [g]	667	209	128
% of the 2 nd stage regenerator volume	55 %	22 %	14 %
Filling factor	0.60	0.56	0.53

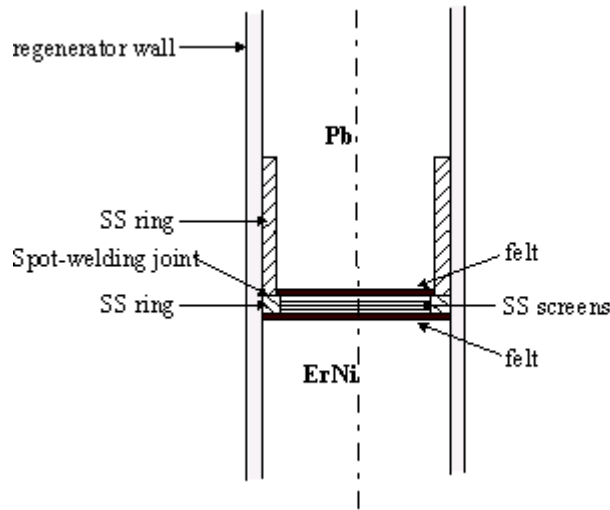


Figure 3. 7. New construction of the separator between materials in the 2nd stage regenerator. The ring with a typical height of 1 cm high disables the separating screens and the felt from tilting.

3.3.3. Regenerator flow resistance

The composition of the regenerator* in these measurements is given in Table 3.3. The flow resistance of the regenerator* has been measured in a DC-flow experiment at room temperature, T_H . For this the rotary valve has been stopped in a position that the system is connected to the high-pressure side of the compressor. The valves 1, 2, 3, 15, 25, and 26 have been open (FIG. 3.8). All the other valves have been closed. In this way we create a closed circuit for the gas flow from the high- to the low-pressure side of the compressor (thick line in FIG. 3.8). The gas molar flow, \dot{n} , is measured by a flow meter. The flow is varied by regulating the bypass valve 3. The pressures are measured at the inlet to the regenerator (p_r), at the hot end of the 1st stage pulse tube (p_{t1}), and at the hot end of the 2nd stage pulse tube (p_{t2}). The resistance of the first stage regenerator, R_{r1} , can be determined according to equation 2.102 as follows

$$p_r^2 - p_{t1}^2 = 2R_{r1}RT_H\dot{n}. \quad (3.1)$$

A similar expression is used for the resistance of the 2nd stage regenerator, R_{r2}

$$p_{t1}^2 - p_{t2}^2 = 2R_{r2}RT_H\dot{n}. \quad (3.2)$$

The results of the measurements are shown in Table 3.5. The resistance of the 1st stage regenerator, R_{r1} , is practically constant and equal to

$$R_{r1}=25 \text{ MPas/m}^3. \quad (3.3)$$

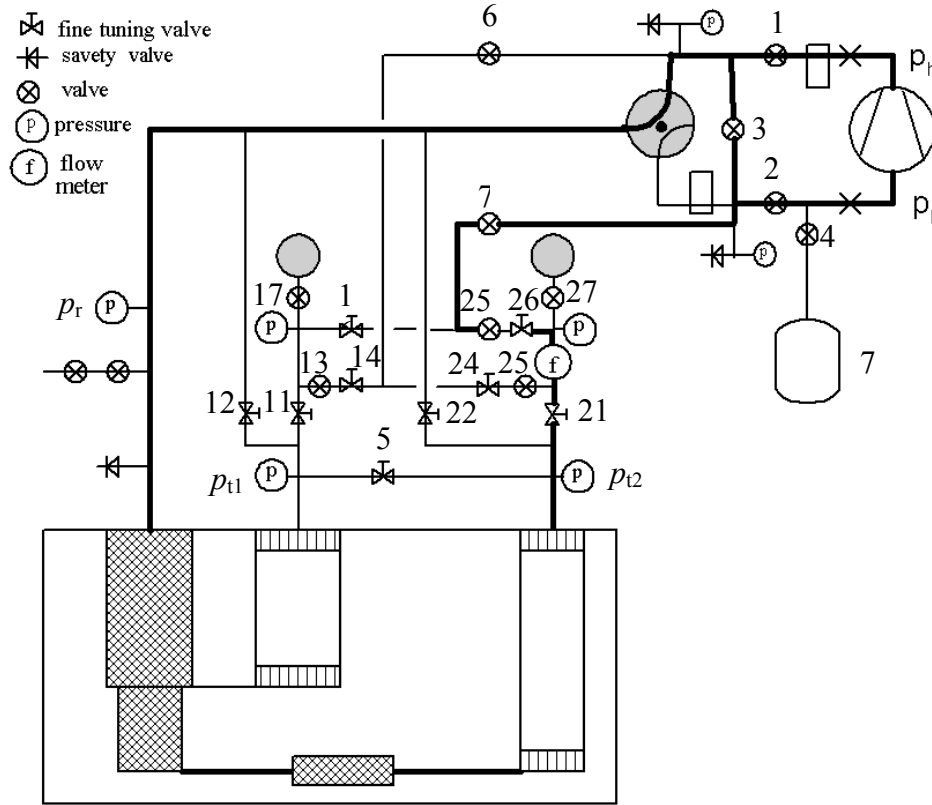


Figure 3. 8. Schematic diagram of the gas flow in the PTR2 in the DC-measurement of the regenerator* flow resistance. Gas flow is indicated by a thick line. The flow is measured by a flow meter, f . The pressure is measured by three pressure meters: p_r , p_{t1} , and p_{t2} .

The main source of the resistance in the 1st stage regenerator is the column of screens with a fine mesh size (# 200). The total amount of these screens $N_r=1600$. So, the flow resistance of one screen, R_s , is

$$R_s = \frac{R_{r1}}{N_r} = 15 \text{ kPas/m}^3. \quad (3.4)$$

Table 5. The results of the regenerator resistance measurements in a DC-flow experiment.

\dot{n} [mol/s]	p_r [bar]	p_{t1} [bar]	p_{t2} [bar]	R_{r1} [MPas/m ³]	R_{r2} [MPas/m ³]
0.100	20.795	20.770	20.330	21.5	375
0.110	21.286	21.258	20.753	22.5	401
0.120	21.850	21.812	21.262	28.6	408
0.136	22.799	22.769	22.128	20.8	438
0.169	24.907	24.870	24.060	22.6	486
0.183	25.919	25.872	25.015	27.5	494
0.201	27.425	27.385	26.450	22.6	519

The flow impedance of the 1st stage regenerator with equation 2.101 is equal to

$$Z_{r1} = 1.2 \times 10^{12} \text{ 1/m}^3. \quad (3.5)$$

Thus, with equation 2.96 the characteristic flow impedance of the material in the 1st stage regenerator is

$$z_{r1} = 14.3 \times 10^9 \text{ 1/m}^2. \quad (3.6)$$

From the measurements we can also determine the characteristic flow impedance of one screen with the mesh size 200 with an area of 1 m², z_1 ,

$$z_1 = 1.5 \times 10^6 \text{ 1/m}. \quad (3.7)$$

The Reynolds number for helium flow in the regenerator is

$$Re = \frac{\rho v^2 d_h}{\eta}, \quad (3.8)$$

where ρ and η are the density and the viscosity of helium respectively, d_h is a hydraulic diameter, and v is a velocity of the gas, calculated by

$$v = \frac{\dot{n} V_m}{(1-f) A_r}. \quad (3.9)$$

Here, V_m is a molar volume of helium, f is a filling factor, and A_r is a cross-sectional area of the regenerator.

The value of d_h for the regenerator, filled with screens, is equal to the diameter of the wires of a screen. In our case $d_h = 50 \text{ }\mu\text{m}$. With equation 3.8 the Reynolds number in the 1st stage regenerator is in the order of 1.

The resistance of the 2nd stage regenerator* is shown in FIG. 3.9. It increases visibly with the molar flow. The empirical expression for the resistance of the 2nd stage regenerator*, deduced from the experiments, is

$$R_{r2} = B \dot{n} + C, \quad (3.10)$$

where B and C are the constants, given in Table 3.6.

The value of d_h for spherical particles, is equal to the diameter of a particle (see Table 3.3). So, with equation 3.8 the Reynolds number of helium in the 2nd stage regenerator is approximately equal to 25. The Reynolds number in the 2nd stage regenerator is an order of magnitude higher than Re in the 1st stage regenerator. This is the reason for a strong flow rate dependence of R_{r2} compared to R_{r1} .

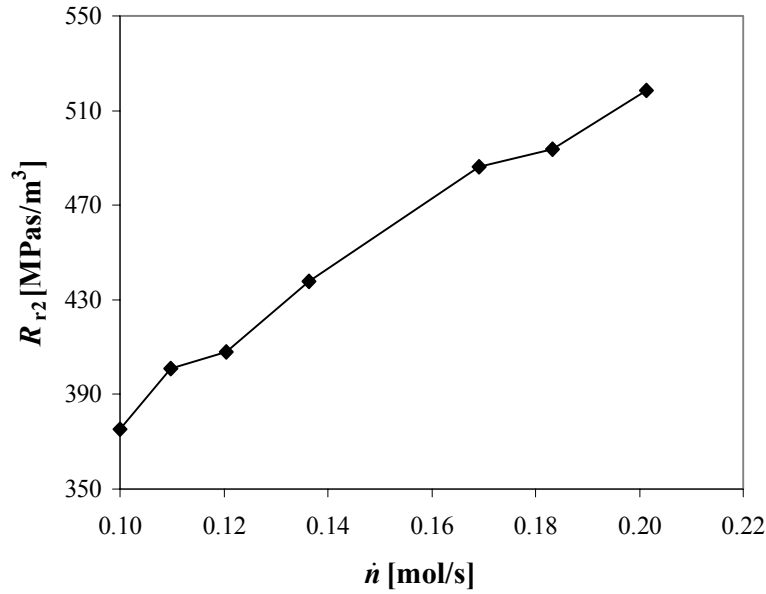


Figure 3. 9. The resistance of the 2nd stage regenerator as a function of the molar flow.

Table 3.6. Empirical constants for the flow resistance, given by equation 3.10, and characteristic flow impedances.

	B [MPas ² /m ³ mol]	C [MPas/m ³]	$z \times 10^{10}$ [1/m ²]
2 nd stage regenerator*	1381	245	$9.5[\text{s}/(\text{m}^2 \text{mol})] \times \dot{n} + 1.7[1/\text{m}^2]$
2 nd stage regenerator	916	198	$12.7[\text{s}/(\text{m}^2 \text{mol})] \times \dot{n} + 2.8[1/\text{m}^2]$
Extra regenerator part (ErNi _{0.9} Co _{0.1})	465	47	$10[\text{s}/(\text{m}^2 \text{mol})] \times \dot{n} + 1[1/\text{m}^2]$

3.3.4. Orifices optimum

The PTR2 has 6 orifices in total. Each stage has a 1st orifice, a double-inlet, and a minor orifice. There is a possibility to connect the minor orifice to the high- or the low-pressure side of the compressor, depending on the direction of the DC-flow. All ‘orifices’ are needle valves, which have to be adjusted for optimum performance of the system. Tuning of the needle valves is a long and complicated procedure. Usually the adjustment of the valves of one stage has a great effect on the performance of the other stage.

In a single-orifice PTR the setting of the orifice defines the phase angle between the pressure and the flow at the cold end of the pulse tube

$$\varphi_L = \arctan \alpha, \quad (3.11)$$

where α is given by equation 2.1. If the pressure amplitude in the pulse tube, p_{tA} , is much larger than the pressure amplitude in the buffer, p_{bA} , and for $p_{tA} \ll p_0$ we can write for the molar flow at the hot end of the pulse tube [2]

$$\dot{n}_1 = \frac{p_0}{RT_H} \frac{p_{tA}}{R_{O1}} \cos \omega t, \quad (3.12)$$

where R_{O1} is the flow resistance of the 1st orifice. If we consider adiabatic expansion and compression in the buffer we can also write

$$\dot{n}_1 = \frac{C_V}{C_p} \frac{V_b}{RT_H} \dot{p}_b, \quad (3.13)$$

where V_b is the volume of the buffer, and \dot{p}_b is the pressure variations in the buffer. Combining equations 3.12 and 3.13 we can write for the pressure in the buffer

$$p_b = p_0 + p_0 \frac{C_p}{C_V} \frac{p_{tA}}{R_{O1} \omega V_b} \sin \omega t. \quad (3.14)$$

The amplitude of the pressure oscillations in the buffer is

$$p_{bA} = p_0 \frac{C_p}{C_V} \frac{p_{tA}}{R_{O1} \omega V_b}. \quad (3.15)$$

With equation 2.12 we can write for α

$$\alpha = \frac{p_{tA} V_t}{p_{bA} V_b}, \quad (3.16)$$

where V_t the volume of the pulse tube. The theoretical optimum value for α in case of an ideal single-orifice PTR (an adiabatic pulse tube, an ideal regenerator with the filling factor equal to 1) is 1 [3].

For a double-inlet PTR the optimum value for α will be slightly different due to the fact that the flow at the hot end of the PTR in this case consists of two components: the flow through the 1st orifice, \dot{n}_1 , and the flow through the double-inlet valve, \dot{n}_{di} ,

$$\dot{n}_H = \dot{n}_1 - \dot{n}_{di}. \quad (3.17)$$

The flow through the double-inlet valve has a certain phase difference with the flow through the 1st orifice [3], and, in practice, is of the order of \dot{n}_1 . We can still define α according to equation 3.17. But the value of α , obtained in this way, α_{di} , cannot be simply related to the phase difference at the cold end as given by equation 3.11. However, α_{di} is still useful for characterizing the optimum situation in a double-inlet configuration.

The practical optimum values for α_{di} for our two-stage PTR are shown in FIGs. 3.10 and 3.11. The optimum values are $\alpha_{di1}=0.55$ and $\alpha_{di2}=1.8$ for the first and the second stage respectively.

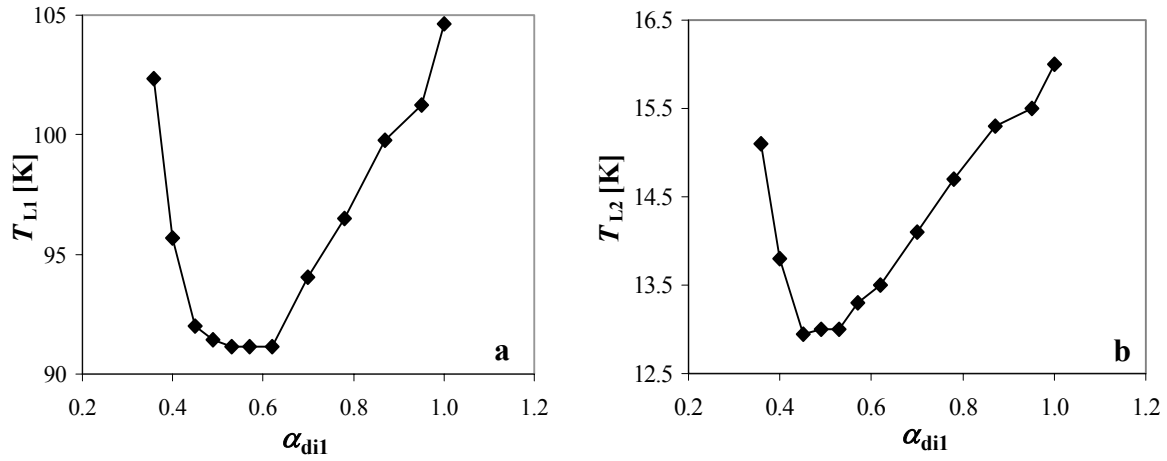


Figure 3. 10. Dependence of T_{L1} (a) and T_{L2} (b) on α_{di1} . The value of α_{di2} is about 1.8.

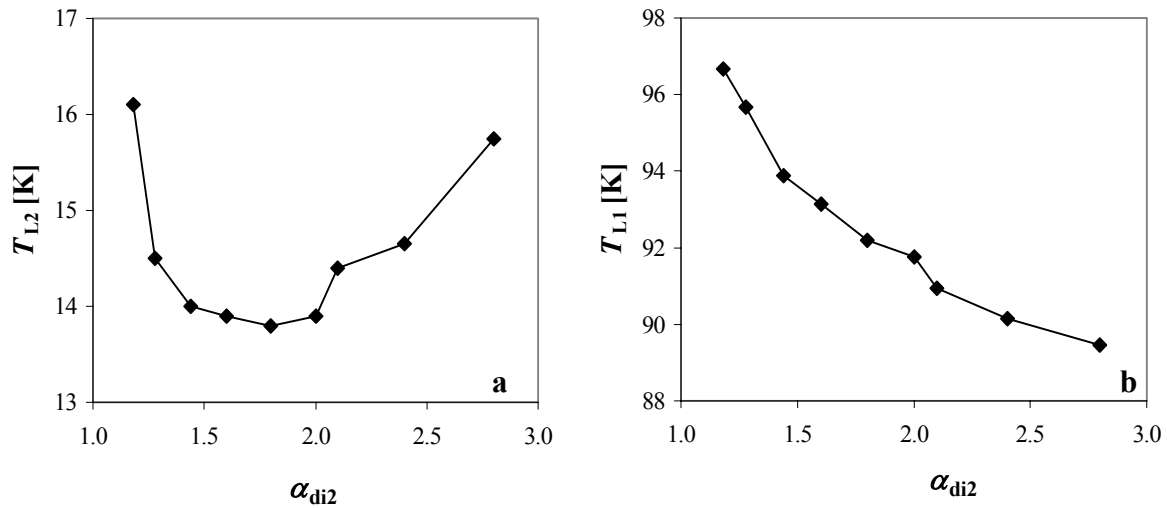


Figure 3. 11. Dependence of T_{L1} (a) and T_{L2} (b) on α_{di2} . The value of α_{di1} is about 0.6.

FIG. 3.12a shows the influence of the opening of the double-inlet valve of the 2nd stage³ on T_{L2} . It decreases from 41 K, when the double-inlet valve is closed, to 13 K at 12.3 turns of the valve. A possibility of multiple optimums for the double-inlet settings has been investigated in a later experiment (see FIG. 3.12b). The optimum of the double-inlet setting in FIG. 3.12b is at 16.7 turns. When the valve has been opened further, T_{L2} has started to increase rapidly, which later on caused the warming up of the whole

³ “Brooks” needle valve with the needle size 5.

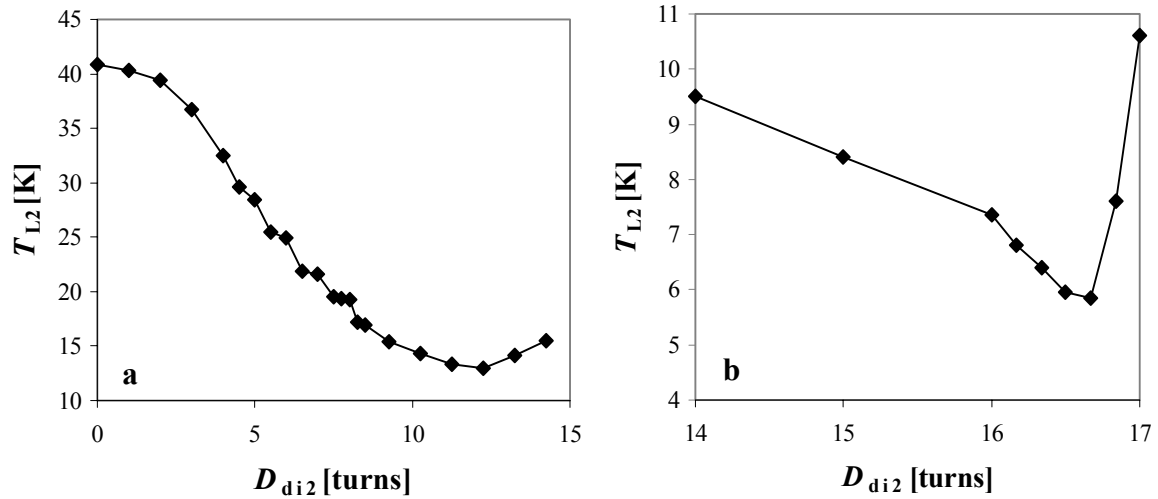


Figure 3.12. (a) T_{L2} as a function of the setting of the double-inlet valve of the 2nd stage. (b) T_{L2} as a function of the setting of the double-inlet valve of the 2nd stage close to its maximum opening. Note, that T_{L2} starts to increase rapidly after passing the optimum setting.

system. Based on our experiments we have no evidence of multiple optimums in the system.

For fine-tuning of the DC-flow we use a combination of the double-inlet and the minor orifice. In our case the DC-flow is directed from the cold end of the pulse tube to its warm end. Therefore, the minor orifice is connected to the high-pressure side of the compressor to suppress the DC-flow. The effect of opening of the minor orifice on T_{L2} and T_{L1} (the lowest temperature of the 1st stage) is shown in FIG. 3.13. There is a very clear optimum at 2.7 turns of the minor orifice, after which the system starts to warm up. Regulating of the DC-flow is a very delicate work. Before the optimum is reached, the

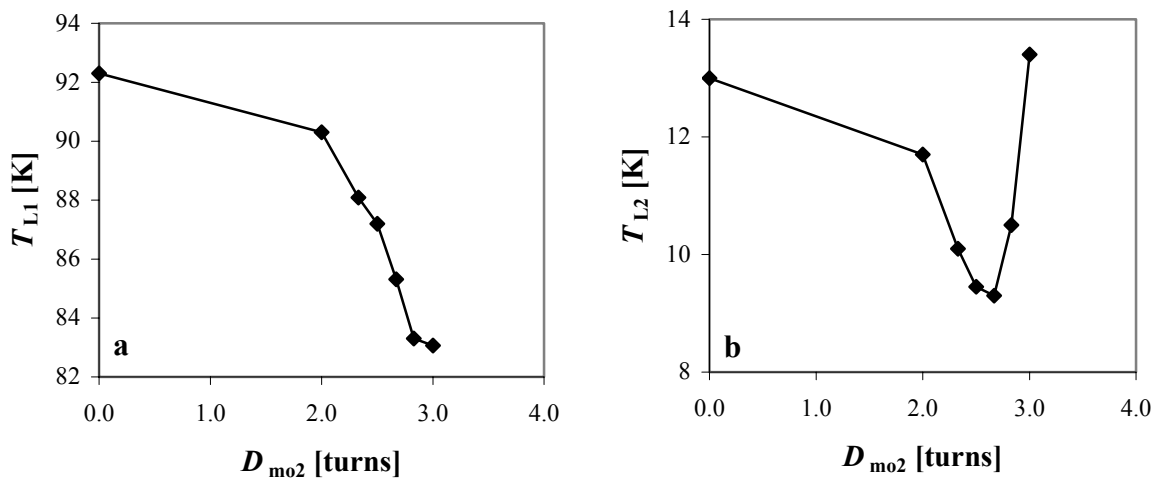


Figure 3.13. The influence of the setting of the minor orifice of the 2nd stage on T_{L2} (a) and on T_{L1} (b).

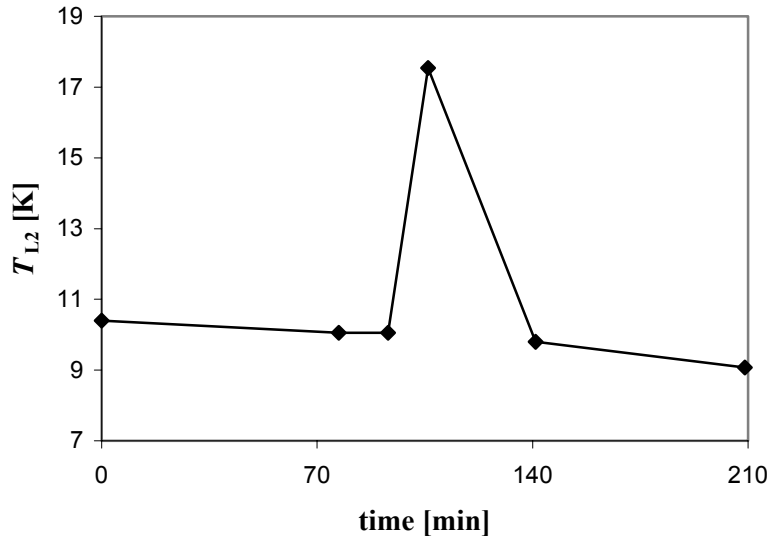


Figure 3.14. T_{L2} as a function of time during an adjustment of the double-inlet valve of the 2nd stage. T_{L2} increases rapidly after the optimum setting has been passed. However, it returns to its original value after the optimum setting of the double-inlet valve has been reinstalled.

system behaves very stable: the temperature decreases with the opening of the DC-flow valves and reaches the stable state rather fast. However, directly after passing the optimum value the system starts to warm up rapidly and stabilizes after a rather long period of time. The advantage of controlling the DC-flow by a combination of a double-inlet valve and a minor orifice, is that the system always returns to its optimum performance, when the optimum setting of the valves is arranged, even after passing the optimum setting and the corresponding rapid warming up (see FIG. 3.14).

3.3.5. Cooling power

The lowest temperature, reached with PTR2 with a regenerator, the composition of which is given in Table 3.4, is 3.5 K. The cooling power versus the cold-end temperature of the 2nd stage, T_{L2} , is plotted in FIG. 3.15. The maximum cooling power at 4.2 K is 160 mW. This value is basically the same as the cooling power of PTR2 with the smaller regenerator (see FIG. 3.5). The fact, that the cooling power of the PTR2 remained the same with the increase of the regenerator volume, means that the system is close to its optimum. If a higher cooling power is desired, one should increase the sizes of the pulse tubes in correspondence with a larger size of the regenerator. This would also imply larger heat exchangers, larger buffers, a compressor with a higher input power, etc.

3.4. ROTARY VALVE

The rotary valve is a very important component of a G-M type PTR. It provides pressure oscillations in the PTR by connecting it alternately to the high- or the low-

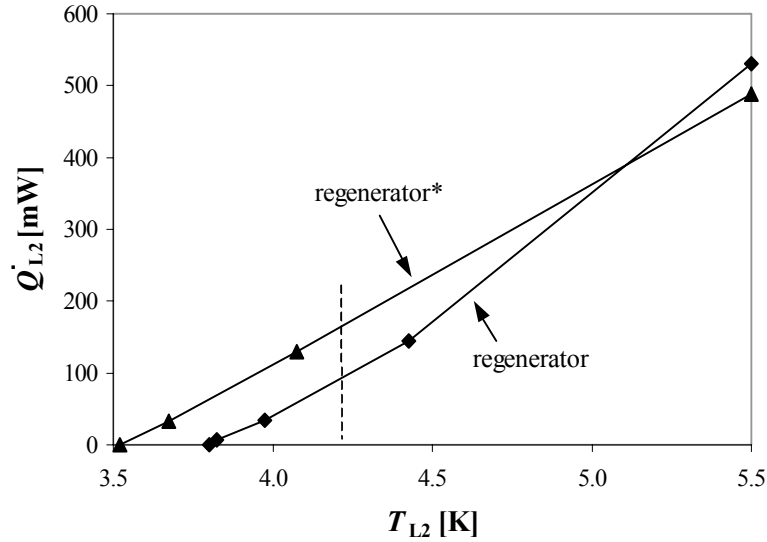


Figure 3. 15. Cooling powers of PTR2 with the ‘big’ regenerator (see Tables 3.2 and 3.3) with and without an additional part as functions of temperature. The regenerator with the added part, filled with $\text{ErNi}_{0.9}\text{Co}_{0.1}$, is indicated as “regenerator*”.

pressure side of the compressor. The rotary valve is also a large source of entropy production. There are two mechanisms of entropy production in a rotary valve: the entropy production due to the limitations in the flow channels in the valve (bends, change of channels sizes, abrupt expansions and contractions, etc.) and intrinsic entropy production. The intrinsic entropy production is related to the change of the flow from the DC flow at the compressor side of the rotary valve to the AC flow at the pulse tube side. It is described in section 2.8.2 in Chapter 2. It can never be avoided and has a certain value even in the ideal case.

In this section we will discuss two types of a rotary valve: the conventional rotary valve and the so-called ‘no-contact’ rotary valve. The mechanical constructions of the valves as well as the losses in them will be treated.

3.4.1. Conventional rotary valve (valve 1)

The construction of the original rotary valve (valve 1) is shown in FIG. 3.16. It consists of a rotor and a stator, placed in a housing, and is driven by a high-powered motor (the input voltage of the motor is 80 V). A spring keeps the rotor in the position. Channel 1 in the stator leads to the low-pressure side of the compressor, p_L ; and two channels 2, combining into one, provide the connection to the regenerator (p_r). The housing is connected to the high-pressure side of the compressor, p_H . The rotor is made of vespel⁴. The stator is made of aluminum. The surface area of the stator, which has to be in contact with the rotor, undergoes the anodizing process, transforming aluminum into aluminum oxide. This is done to harden the surface in order to provide good wear

⁴ Vespel[®]S, produced by DuPont.

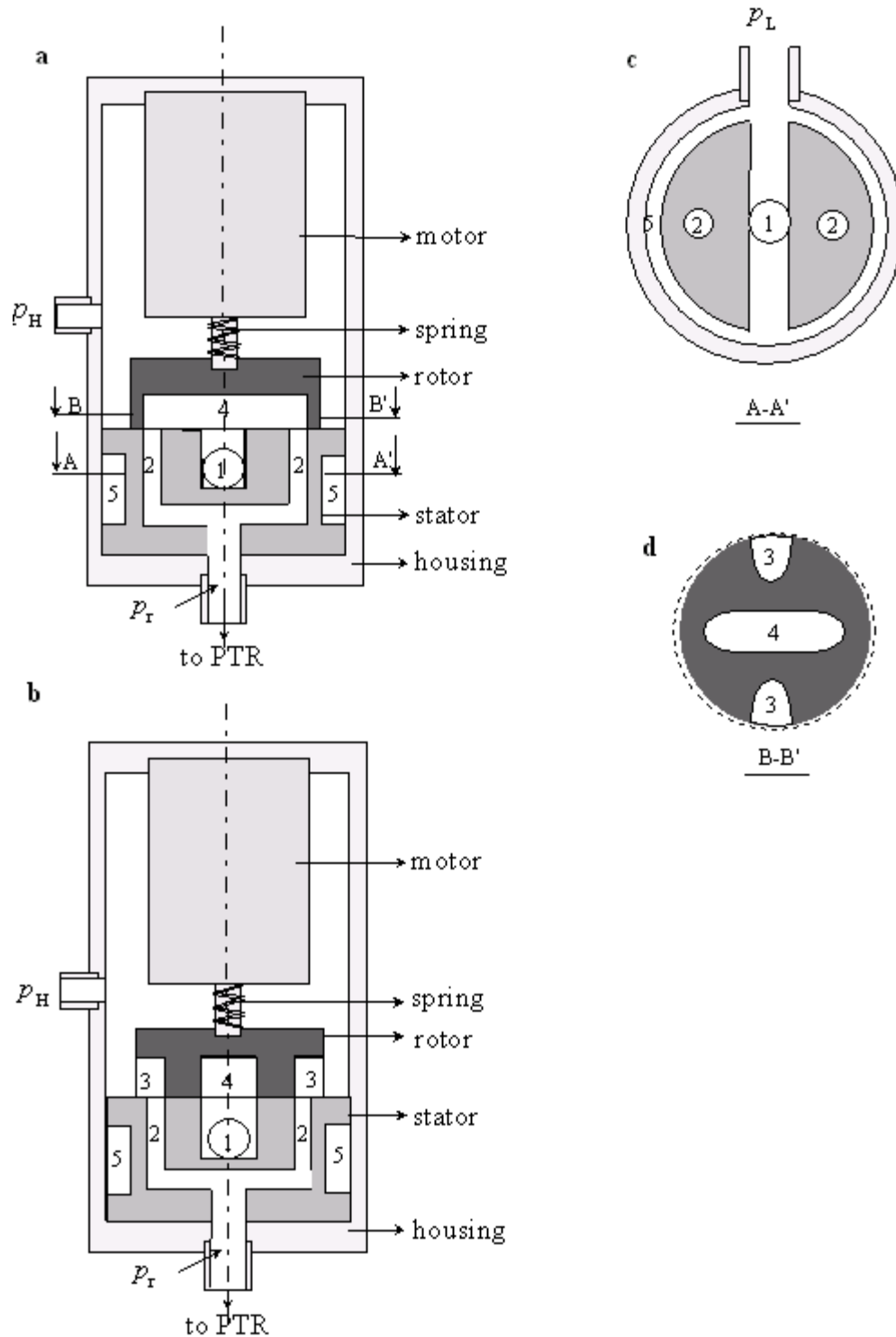


Figure 3.16. Schematic drawing of the conventional rotary valve, consisting of the rotor, the stator, the housing, and the motor. The numbers in the figures correspond with the various flow channels. **(a)** The PTR is connected to the low-pressure side of the compressor. **(b)** The PTR is connected to the high-pressure side of the compressor. **(c)** The cross-section of the stator. **(d)** The cross section of the rotor.

resistance of the stator. In FIG. 3.16 (cross-section A-A') it is shown that a part of the stator has a reduced radius, which provides a flow channel, 5, from the regenerator to the low-pressure side of the compressor. The rotor has a slit 4 and two openings 3. As the rotor turns, the slit 4 connects channels 1 and 2 for a part of the cycle, as shown in FIG. 3.16a. So the PTR is connected to the low-pressure side of the compressor. In FIG. 3.16b the rotor is turned 90° . Now the PTR is connected to the inside of the housing, which is under high pressure, p_H , via 2 and 3. So, during a cycle, the channels 2 are periodically connected to the high- and the low-pressure side of the compressor. For a part of the cycle the rotor is in such a position, that the channels 2 are connected neither to the low- nor to the high-pressure side of the compressor. These periods of the cycle are called the waiting time, t_w . The influence of the waiting time on the performance of the PTR can be described as follows. During t_w the gas flows from the buffer into the pulse tube or vice versa. Hence, the value of the pressure in the pulse tube becomes closer to the value of the average pressure in the system. Therefore, longer t_w means lower dissipation in the first orifice. According to equations 2.28 and 2.29 the cooling power is proportional to the dissipation rate in the 1st orifice. Hence, a lower dissipation in the orifice leads to a lower cooling power. In this respect it is better to have short waiting times. However, short t_w brings higher dissipation in the rotary valve. During t_w the pressure at the entrance to the regenerator, p_r , approaches the average pressure due to the flow from/to the buffer. The closer to the average pressure p_r is, the smaller the pressure drop over the valve will be, when the rotary valve opens to p_L or p_H . This will result in the lower power loss. Therefore, there exists an optimum for t_w . It will be experimentally determined below. The waiting time of the present rotary valve is equal to $0.13t_c$.

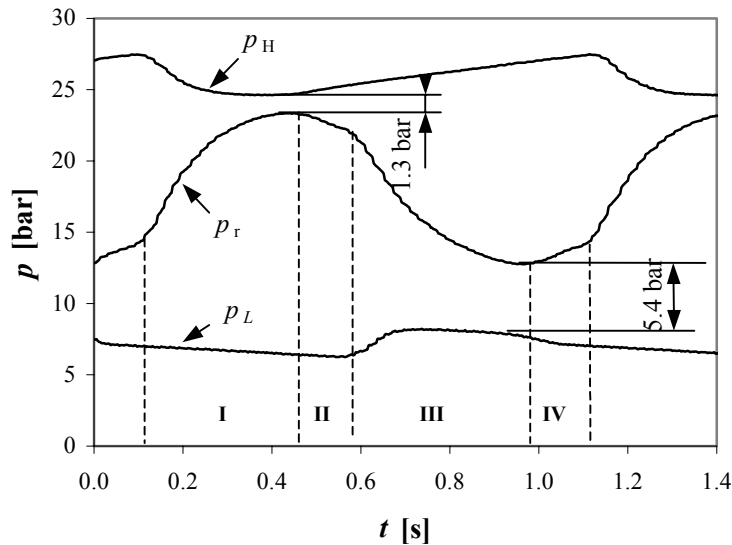


Figure 3. 17. Pressure variations in the PTR2 with the conventional rotary valve versus time. Here, p_H is the pressure at the high-pressure side of the compressor, p_r is a pressure at the inlet to the regenerator, and p_L is a pressure at the low-pressure side of the compressor. The difference between p_H and p_r and between p_L and p_r is due to the resistance of the rotary valve, gas lines, and the filter. Four steps of the cycle are shown as well. I is a compression step (the PTR is connected to the high-pressure side of the compressor), III is an expansion step (the PTR is connected to the low-pressure side of the compressor). During steps II and IV the system is connected neither to the high- nor to the low-pressure side of the compressor.

The pressure variations in PTR2 with a flow of 1 mol/s are given in FIG. 3.17. It also illustrates the pressure loss in the rotating valve. There is a 5.4 bar of the pressure drop, when the system is connected to the low-pressure side of the compressor; and 1.3 bar, when the system is connected to the high-pressure side. This pressure loss originates from the mechanical construction of the rotary valve (bends, curves, contractions, expansions, etc.) as well as from the tubing and the filter, placed between the two pressure meters (FIG. 3.18).

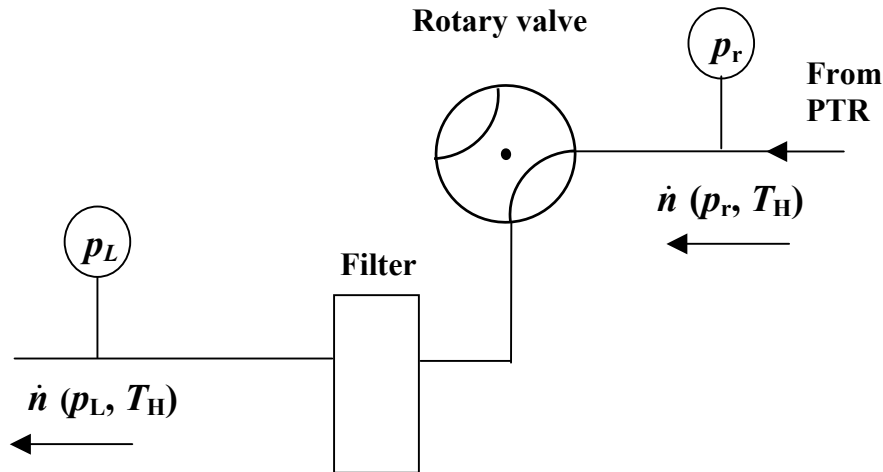


Figure 3. 18. Schematic diagram of the measurements of the pressure drop in the rotary valve, when the system is connected to the low-pressure side of the compressor. The pressure is measured at the low-pressure side of the compressor, p_L , and at the inlet to the regenerator. The pressure drop is caused by the rotary valve, the filter, and the gas lines.

The calculations of the pressure drop in the rotary valve due to its mechanical construction are given in Appendix. The pressure drop, when the valve is connected to the low-pressure side, is equal to 2.24 bar. The entropy production due to the pressure drop can be calculated with equation 2.121. When the rotary valve is connected to the high-pressure side, the entropy production is equal to 0.45 W/K. This corresponds to the power loss of 136 W. When the rotary valve is connected to the low-pressure side of the compressor, the entropy production is as high as 4.46 W/K, which corresponds to 1338 W of the power loss.

The intrinsic entropy can be calculated with equation 2.58. It is equal to 0.71 W/K. This entropy production rate results in the power loss of 212 W. Therefore, the total power loss in the rotating valve is equal to

$$\dot{Q}_{rv}^{tot} = 212 + 136 + 1338 = 1686 \text{ W.} \quad (3.18)$$

This is 28% of the input power of the compressor (see FIG. 3.19).

The flow resistance of the rotary valve has been measured in a DC-flow measurement, when the valve has been connected to the high-pressure side of the compressor. It can be described as a function of the molar flow rate

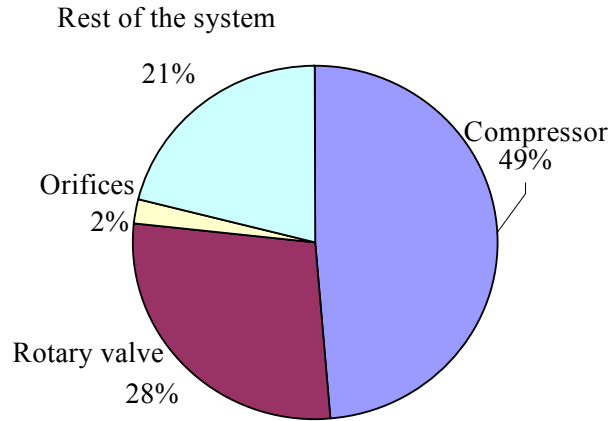


Figure 3. 19. Power losses in PTR2 with the conventional rotary valve.

$$R_{rv} = D\dot{n} + E, \quad (3.19)$$

where D and E are the empirical constants, equal to $63.6 \text{ MPas}^2/\text{m}^3\text{mol}$ and $14.1 \text{ MPas}/\text{m}^3$ respectively. At a typical molar flow through the rotary valve in PTR2 of 1 mol/s , $R_{rv}=51 \text{ MPas}/\text{m}^3$. The calculations of the pressure drop due to the mechanical construction of the rotary valve, when it is connected to the high-pressure side of the compressor, are given in Appendix. The pressure drop is equal to 0.51 bar . The corresponding flow resistance is then about $78 \text{ MPas}/\text{m}^3$. This value is 30% higher than the measured value due to the assumptions, made when calculating the pressure drop. For example, all the expressions for calculating the pressure drop are based on the assumption, that the diameter of a circular channel, d , is much smaller than the length of the channel, L , which is not the case for some of the flow channels in our rotary valve.

The improvement of the mechanical construction of the rotary valve can reduce the pressure loss, and therefore, the power loss significantly.

3.4.2. Modified conventional rotary valve (valve 2)

The rotor and the stator of the rotary valve have been modified. The valve housing has been kept the same. The schematic representation of the new construction of the rotary valve (valve 2) is shown in FIG. 3.20. The diameters of channels 1 and 2 have been increased, and the stator has been made shorter. Channel 5 between the housing and the stator has been eliminated. The diameter of the rotor has been increased. The scheme of the gas flow in the modified rotary valve, when the PTR is connected to the low-pressure side of the compressor, is shown in FIG. 3.21. The new construction includes two bends (1), combining flow (2), and a bend (3). With equations A.1-8 from Appendix and for the same conditions as for the old construction of the valve the calculated

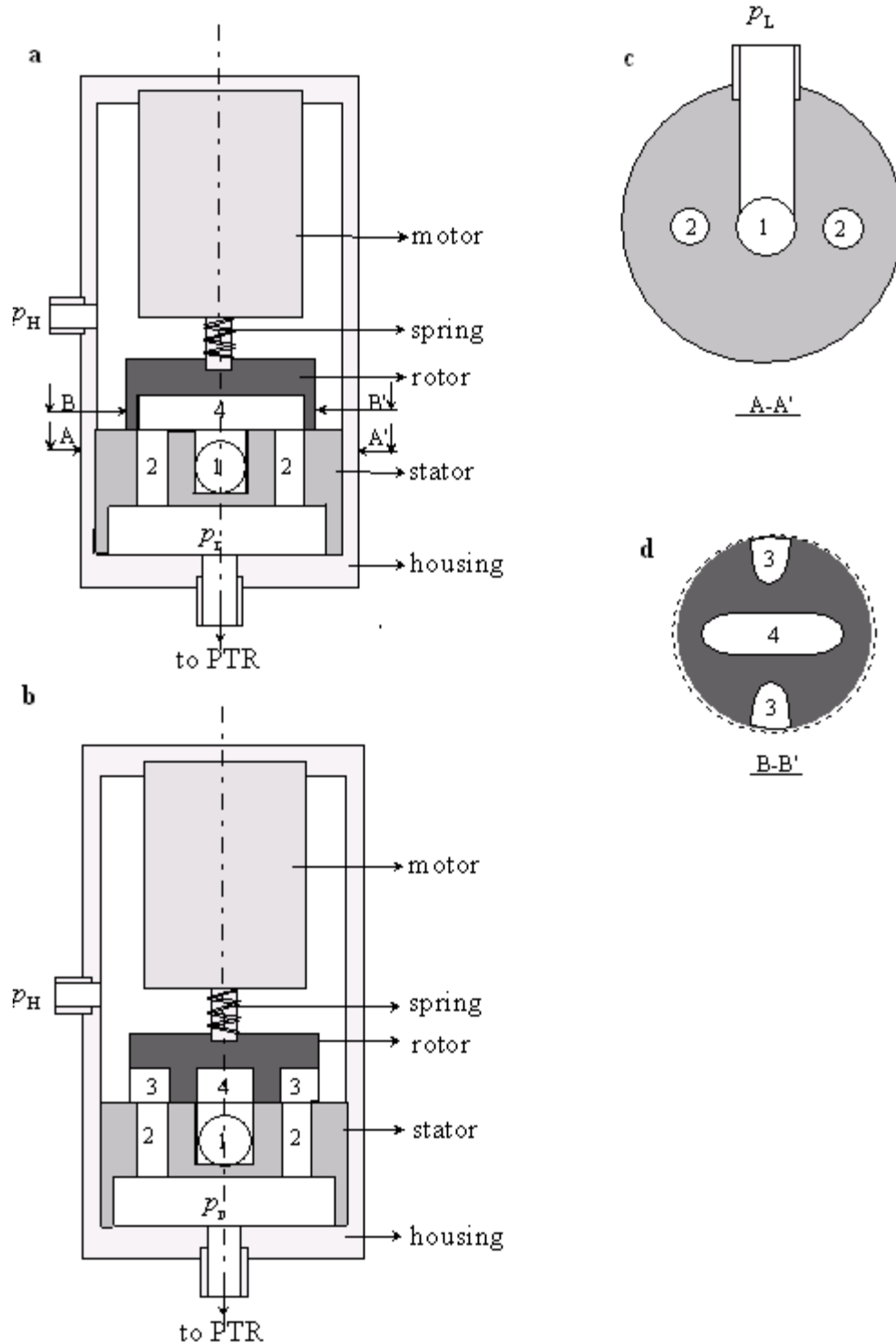


Figure 3. 20. Schematic drawing of the modified conventional rotary valve. The numbers in the figures correspond with the various flow channels. **(a)** The PTR is connected to the low-pressure side of the compressor. **(b)** The PTR is connected to the high-pressure side of the compressor. **(c)** The cross-section of the stator. **(d)** The cross section of the rotor.

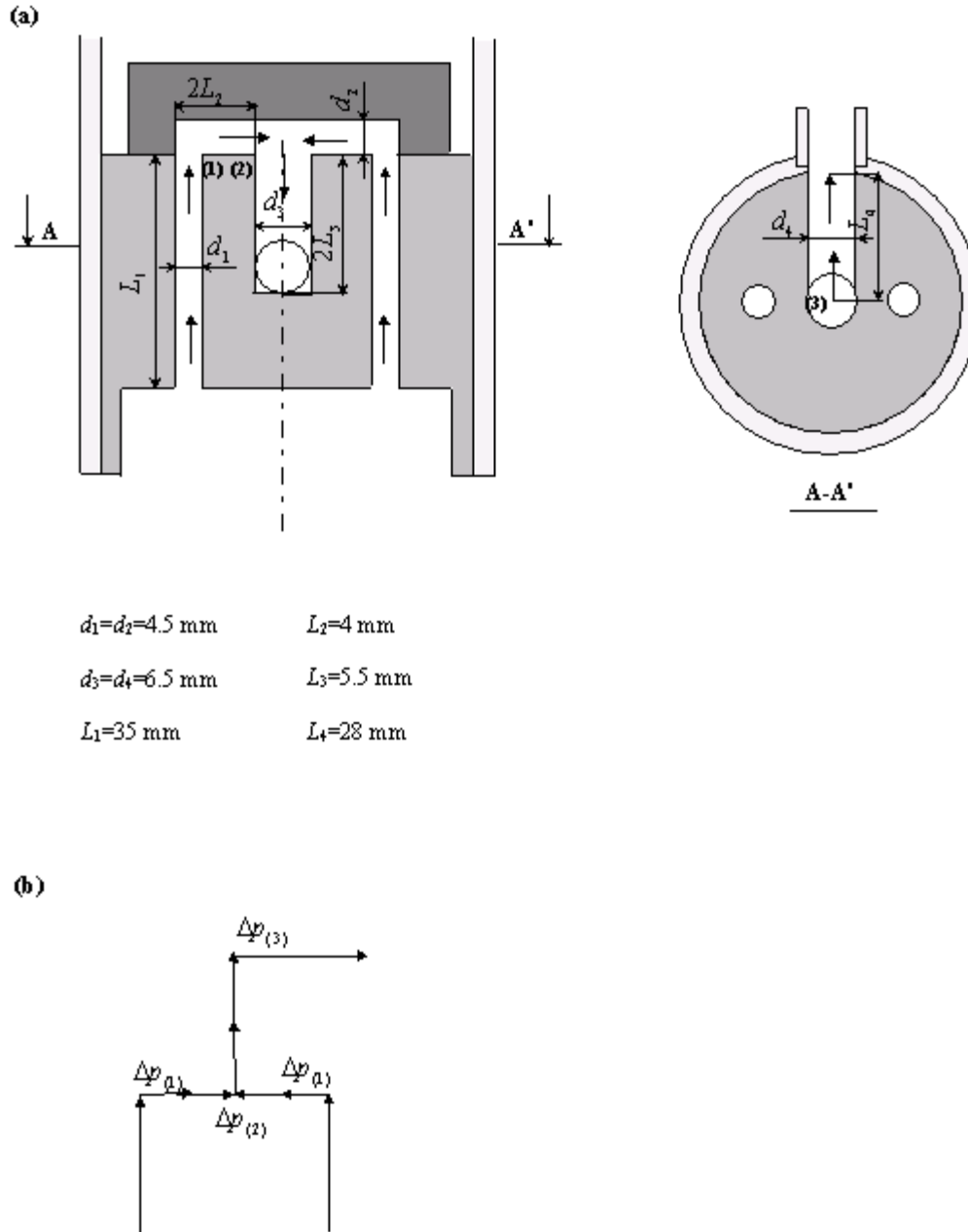


Figure 3. 21. (a) Schematic diagram of the gas flows in the modified conventional rotary valve, when the system is connected to the low-pressure side of the compressor. **(b)** Equivalent diagram of the gas flows in the modified rotary valve.

pressure drop is 0.19 bar. This value is an order of magnitude lower than the value for the pressure loss in the old rotary valve.

The pressure profiles in the system with the valve 2 are shown in FIG. 3.22. The pressure drop at the low-pressure side of the compressor decreased from 5.4 to 2.16 bar. With the new construction of the rotary valve the contribution of the pressure drop due to

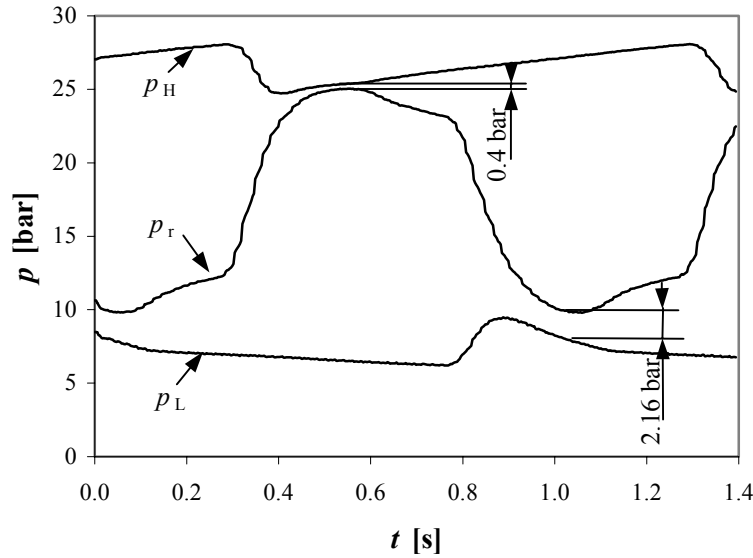


Figure 3.22. Pressure variations in the PTR2 with the modified conventional rotary valve versus time.

the flow resistance in the valve of 0.19 bar to the value of 2.16 bar is almost negligible. The remaining pressure drop is due to the flow resistance of the tubing and the filter, placed between the two pressure meters (see FIG. 3.18).

The energy dissipation in the rotary valve has significantly decreased. The entropy production, calculated with equation 2.121, is equal to 0.17 W/K, when the rotary valve is connected to the high-pressure side of the compressor, and 2.06 W/K, when the rotary valve is connected to the low-pressure side. However, the intrinsic entropy production in the rotary valve has increased due to an increase of the pressure amplitude in the PTR. The pressure amplitude at the inlet to the regenerator, p_r , increased from 5.3 bar with the valve 1 to 7.6 bar with the valve 2. Therefore, with equation 2.58 the intrinsic entropy production in the valve 2 is equal to 1.71 W/K.

The total energy dissipation in the valve 2 equals to

$$\dot{Q}_{rv}^{tot} = 513 + 52 + 619 = 1184 \text{ W.} \quad (3.20)$$

This value is 30% lower than the entropy production in the valve 1, and is now 20 % of the input compressor power, compared to 28 % with the valve 1.

A negative aspect of the increase of the size of the rotor and the stator is the increase of the contact area between them, A_c . The force, F , pressing the rotor against the stator, is proportional the contact area between the rotor and the stator. So, more power is needed to drive the new rotary valve. In the new arrangement the input power to the rotary valve has become almost 3 times larger.

3.4.3. ‘No-contact’ rotary valve (valve 3)

3.4.3.1. The construction of a ‘no-contact’ rotary valve.

The conventional type of the rotary valve, described above, is large and heavy. It requires a high-power motor and is usually used in the systems with large gas flows ($\dot{n} > 1$ mol/s). Large driving torques are needed to operate the valve. A typical value for the torque in the conventional rotary valve is 1.2 Nm [4]. In addition to that the rotor makes a heavy mechanical contact with the stator, which means rather short lifetime of the rotary valve. Therefore, a new type of the rotary valve (valve 3) has been developed⁵. The valve consists of a rotor, placed in a housing. The rotor makes no mechanical contact with the housing. Therefore, the valve is called the “no-contact” valve. The schematic drawing of the ‘no-contact’ rotary valve is shown in FIG. 3.23. The forces in the valve 3 are very

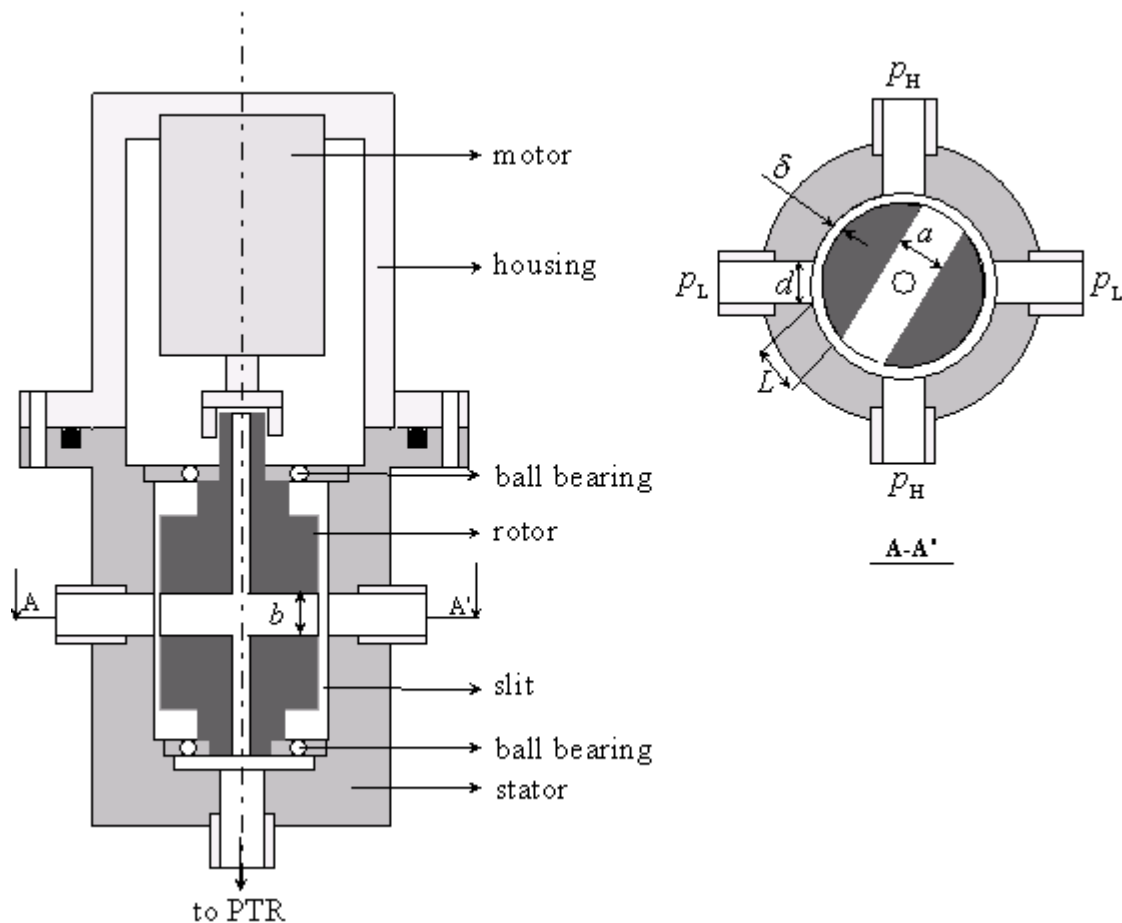


Figure 3. 23. Schematic drawing of the ‘no-contact’ rotary valve, consisting of the rotor, placed in the housing, and the DC motor. A gap, δ , prevents mechanical contact between the rotor and the housing. In the housing the opposing connections to the high- and the low-pressure side of the compressor are made. The rotor contains two channels: the radial channel with the height b and the width a , and the axial channel. The channels provide a balance of the forces on the valve both in the radial and the axial direction

⁵ The ‘no-contact’ rotary valve has been designed in collaboration with Sumitomo Heavy Industries, Japan [5].

well balanced. There are four connections to the compressor in the housing of the rotary valve: two of them, situated opposite each other, are the connections to the low-pressure side of the compressor; and the other two connect the valve to the high-pressure side. In this way the forces on the rotor are balanced in the radial direction. In the axial direction the forces are balanced by an axial channel in the rotor. In the radial direction the rotor contains another channel with the width a and the height b . The value of b is usually equal to a diameter of the connections to the high- or the low-pressure side of the compressor, d . When the rotor turns, it connects the PTR to the low- or the high-pressure side of the compressor via the radial and the axial channels. The value of a determines the timing of the pressure wave. There is a gap, δ , between the rotor and the housing, preventing contact between the housing and the rotor. The rotor is held in the position by two stainless steel ball bearings. It is driven by a small DC-motor, with a maximum torque of 1 Nm. The rotary valve requires only about 1.4 W of motor power ($i \approx 0.1$ A, $U = 14$ V) to provide a frequency of 1 Hz.

Although the construction of the valve 3 in principle provides a balance of all the forces, there is still a torque on the rotor, resulting from the change of momentum in the gas flow. It is illustrated in FIG. 3.24. At the moment, when the PTR is at the point of being connected to the high-pressure side of the compressor, the gas flows through the gap between the housing and the rotor with velocities close to the speed of sound. The gas collides with the wall of the rotor. Thus, the direction of the gas velocity changes towards the center of the rotor. The magnitude of the reaction force can be estimated as

$$F = \dot{m}c, \quad (3.21)$$

where \dot{m} is the mass flow of the gas, and c is the velocity of sound. For valve 3 the value of F is typically 2 N [4]. The total torque, corresponding to this reaction force, is around 0.06 Nm. This value is an order of a magnitude lower than the value of the torque of the conventional rotary valve.

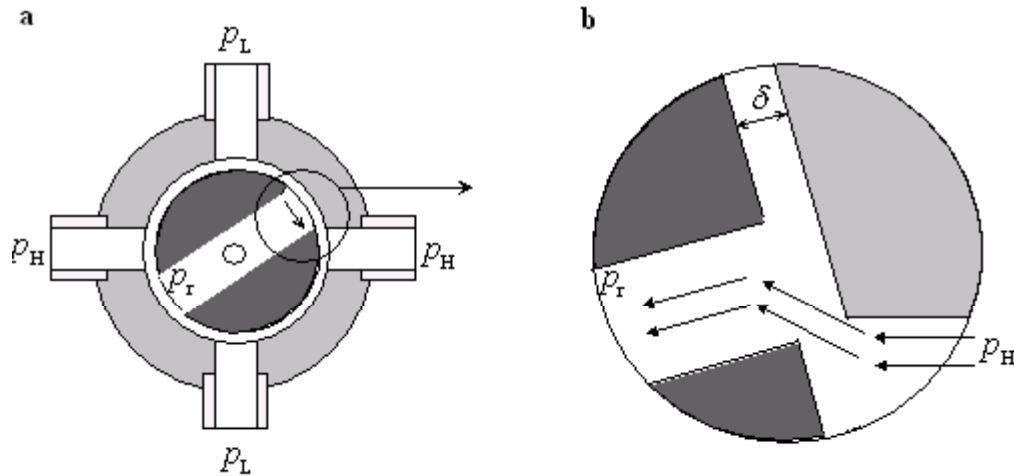


Figure 3. 24. Schematic drawing of the gas flow through the radial channel in the rotor at the moment, when the PTR is at the point of being connected to the high-pressure side of the compressor. The gas flows from the high-pressure side of the compressor with the pressure, p_H , to the PTR at a pressure, p_r , with velocities close to the speed of sound.

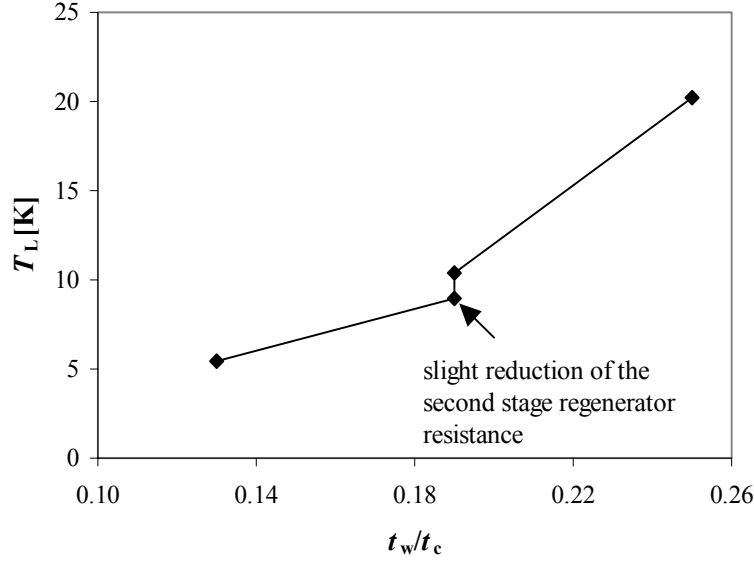


Figure 3. 25. The cold-end temperature of PTR2 with the ‘no-contact’ rotary valve as a function of the waiting time, t_w .

The rotor of valve 3 has a diameter $D_r=25$ mm. The gap between the housing and the rotor $\delta=20$ μm . The connections to the high- and the low-pressure side of the compressor have a diameter $d=4$ mm. The width of the radial channel, a , has been varied, while its height, b , has been kept constant and equal to 4 mm. The value of a also defines the waiting time of a cycle, t_w . The influence of a on the lowest temperature of the PTR2 is shown in FIG. 3.25. As it is seen from the figure the lowest temperature is reached in the system with the shortest waiting time. Further decrease of t_w is not possible because of the increased short-circuiting the high- and the low-pressure side of the compressor through the gap between the housing and the rotor. Hence, the leak rate from the high- to the low-pressure side of the compressor increases with enlarging of a .

3.4.3.2. The maximum leak rate

Assuming Poiseuille flow the leak rate in the gap between the housing and the rotor can be estimated by the following expression

$$\dot{n}_{\text{leak}} = \frac{\pi b \delta^3}{24 \eta R T L} (p_H^2 - p_L^2), \quad (3.22)$$

where L is a distance between the radial channel in the rotor and one of the connections to the compressor, as shown in FIG. 3.23b. The value of L is equal to

$$L = \frac{\pi D_r}{4} - a - d. \quad (3.23)$$

The maximum leak from the high- to the low-pressure side of the compressor via the gap, δ , occurs at the moment, when the radial channel has almost passed the connection to the high-pressure side of the compressor (see FIG. 3.23b). For $a=11.6$ mm the maximum leak rate, calculated with equation 3.22, is equal to 0.28 mol/s with the total flow amplitude of the PTR of 1 mol/s. If a is increased to 13 mm, the maximum leak rate is 0.30 mol/s. The small difference between the maximum leak rate for $a=11.6$ mm, $L=4$ mm and $a=13$ mm, $L=2.6$ mm is due to the change of the pressure amplitudes for different values of a and L . Although the value of the maximum leak rate seems to be rather large compared to the total molar flow amplitude, it should be noted, that it takes place during a small fraction of the total cycle time.

The minimum leak from the high- to the low-pressure side via the gap between the rotor and the housing for $a=13$ mm, $L=2.6$ mm is about 0.04 mol/s.

3.4.3.3. The power loss

The pressure drop in the valve 3 can be derived from FIG. 3.26. It is equal to 0.95 bar at the low-pressure side and 0.25 bar at the high-pressure side. This pressure drop is more than 50% less than the pressure drop in the valve 2 (see FIG. 3.22). The entropy production due to the pressure drop in the valve 3 is equal to 0.11 W/K, when the rotary valve is connected to the high-pressure side of the compressor, and is 1.1 W/K, when the valve is connected to the low-pressure side. The corresponding energy dissipation is equal to 32 W and 330 W respectively.

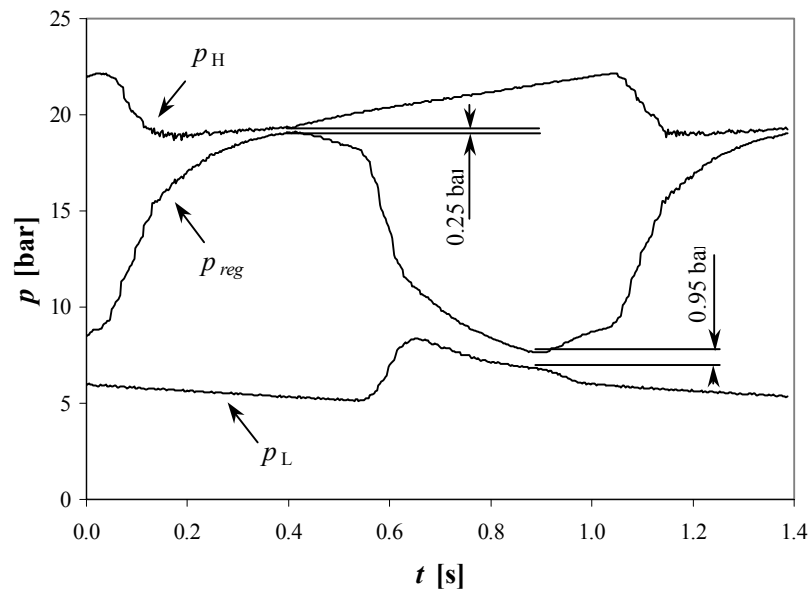


Figure 3. 26. Pressure variations in the PTR2 with the ‘no-contact’ rotary valve versus time.

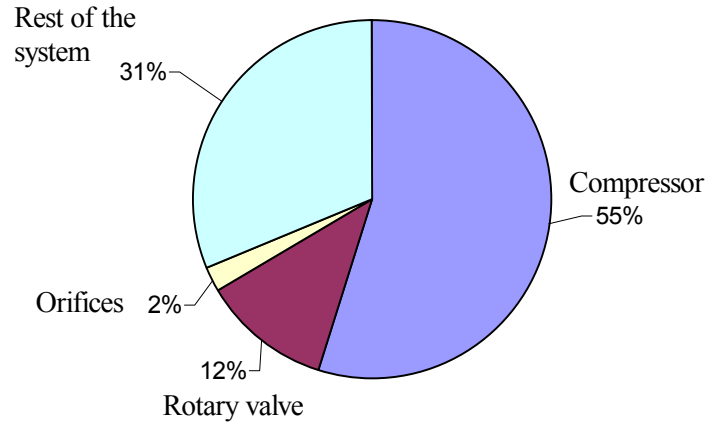


Figure 3. 27. Power losses in PTR2 with the ‘no-contact’ rotary valve.

The intrinsic entropy production rate is 1.1 W/K. Thus, the total energy dissipation in the valve 3 is

$$\dot{Q}_{rv} = 330 + 32 + 330 = 690 \text{ W.} \quad (3.24)$$

This is 12 % from the input compressor power (FIG.3.27). Therefore, the rotary valve loss is reduced by 40 % by using the “no-contact” type of the valve.

3.4.3.4. The influence of the shape of the radial channel in the rotor on the shape of the pressure wave in the PTR.

The shape of the radial channel in the rotor determines the shape of the pressure wave in the PTR. The mass flow through the channel, when the system is connected to the high- or the low-pressure side, is expressed as

$$\dot{m} = \rho v A, \quad (3.25)$$

where v is the velocity of the gas in the channel, and A is the cross-sectional area, through which the gas flows. The maximum mass flow of the gas expanding from the high pressure, p_H , (22-25 bar in our case) to a lower pressure (to the vacuum in the limit) is called the “choked” mass flow and can be determined from the relation [6]

$$\dot{m}_{\max} = \frac{A p_H}{\sqrt{RT}} \sqrt{\gamma} \left(\frac{2}{\gamma + 1} \right)^{\frac{\gamma+1}{2(\gamma-1)}}, \quad (3.26)$$

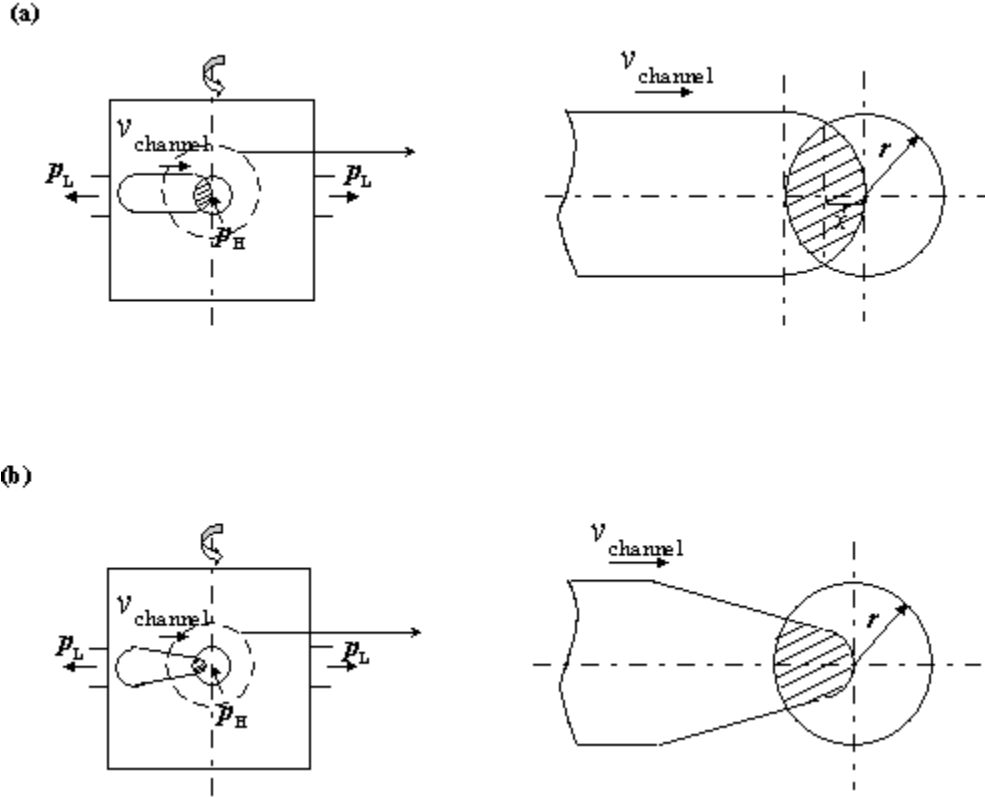


Figure 3. 28. Movement of the radial channel of the rotor during a connection of the PTR to the high-pressure side of the compressor. The common area of the gas supply tube and the channel is filled with a diagonal pattern in the figure. **(a)** Oval shape of the radial channel. **(b)** Droplet shape of the radial channel.

where $\gamma = C_p/C_v$ is the heat capacity ratio. From equation 3.26 it is seen, that the “choked” mass flow is proportional to the area A .

We consider a part of the cycle, when the system is about to be connected to the high-pressure side of the compressor. FIG. 3.28a illustrates the movement of the radial channel with the oval shape towards the high-pressure side connection. The height of the channel, b , is equal to the diameter of the gas supply tube, d . The common surface of the gas supply tube in the housing and the radial channel in the rotor is given by

$$A = 2 \left[r^2 \arccos\left(\frac{r-x}{r}\right) - (r-x)\sqrt{2rx-x^2} \right], \quad (3.27)$$

where $r = d/2$ is the radius of the gas supply tube in the housing, and the parameter x is defined in FIG. 3.28a. After A reaches its maximum value, equal to the area of the connection channel, it remains constant for some time and then decreases as the radial channel moves away from the gas supply tube. The typical time of the cycle of PTR2 is 1 s. The waiting time of the cycle with $a = 13$ mm is 13% of the total cycle time. Hence, the PTR is connected to the high- or the low-pressure of the compressor during 0.37 s. The area A is shown in FIG. 3.29 as a function of time. The area reaches its maximum value

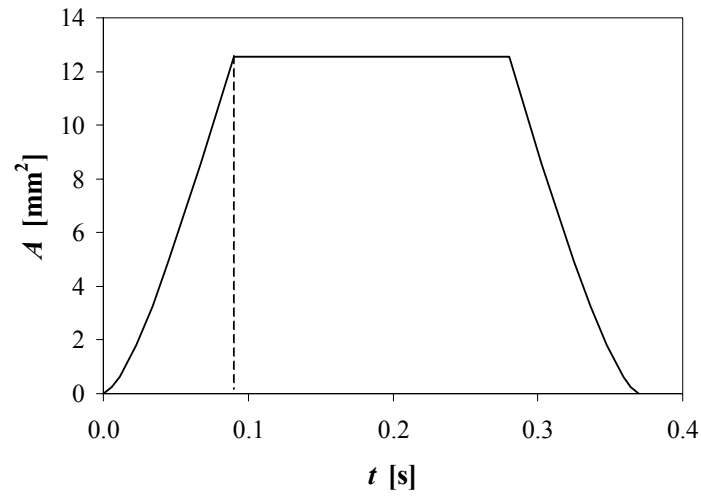


Figure 3. 29. The change of the common area of the gas supply tube and the radial channel in the rotor (indicated in FIG. 3.28a), when the system is connected to the high-pressure side of the compressor, as a function of time. The total time of the cycle, t_c , is equal to 1 s. The vertical dashed line indicates the moment of the maximum flow in the PTR at $t=0.09$ s from the beginning of the cycle.

0.09 s after the beginning of the connection of the slit to the high-pressure side. During this time the difference between the high pressure, p_H and the pressure at the inlet to the regenerator, p_r , is high (see FIG. 3.26). So there is a “choked” flow condition in the

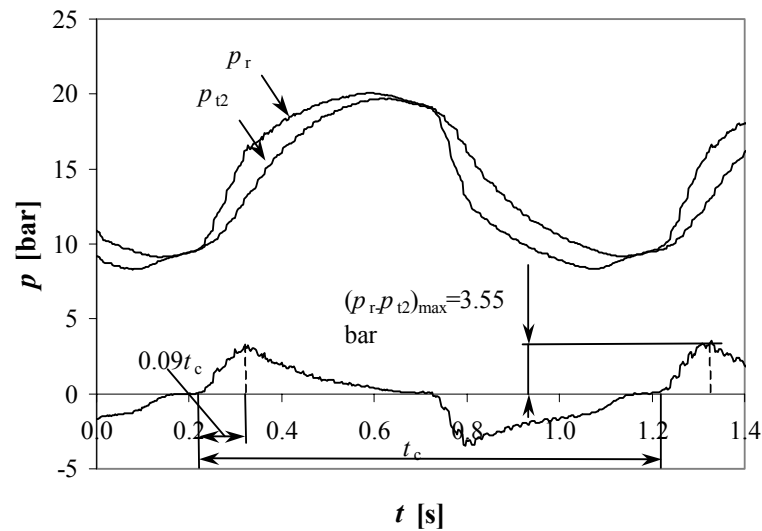


Figure 3. 30. Pressure variations at the inlet to the regenerator, p_r , and in the 2nd stage pulse tube, p_{t2} , of the PTR2 with the ‘no-contact’ valve with the oval shape of the radial channel versus time. The lowest curve gives the difference between p_r and p_{t2} or, in other words, the pressure drop in the regenerator. The total cycle time, t_c , is 1 s. The dashed lines indicate the moment, when the common area, A , reaches its maximum value.

system. The “choked” mass flow at the beginning of the cycle results in a steep increase of the pressure drop over the regenerator. FIG. 3.30 shows the pressure wave in the PTR2 at room temperature. In the beginning of the cycle the pressure at the high-pressure side of the compressor, p_H , steeply decreases, while the pressure drop in the regenerator (the bottom line on the graph) increases and reaches its maximum value of 3.55 bar 0.09 s after the beginning of the cycle. As A remains constant, p_r approaches p_H . Hence, the mass flow of the gas is no longer close to the value of m_{\max} . At this time of the cycle the mass flow is just a function of the velocity of the gas, which rapidly decreases. Thus, the pressure drop in the regenerator decreases too as shown in FIG. 3.30. From all said above we can conclude that by varying the shape of the axial slit we can influence the pressure drop in the regenerator of the PTR.

One more negative effect, resulting from the high-speed mass flow through the rotary valve, is an annoying whistling sound.

In order to reduce the pressure drop in the regenerator and to decrease the whistling sound, the shape of the radial channel in the rotor has been modified from oval to droplet. The rotor with the droplet-shape channel is shown in FIG. 3.31. Now when the channel moves towards a gas supply tube with the narrow end forward, A increases slower than in case of the oval shape of the channel (see FIG. 3.28b). This means a lower increase rate of the mass flow and a lower pressure drop over the regenerator (see FIG. 3.32). With the droplet shaped channel the maximum value of the pressure drop has decreased to 2.75 bar, and the pressure wave became smoother. The time derivative of the pressure has decreased almost 50%. The whistling noise has been reduced as well.

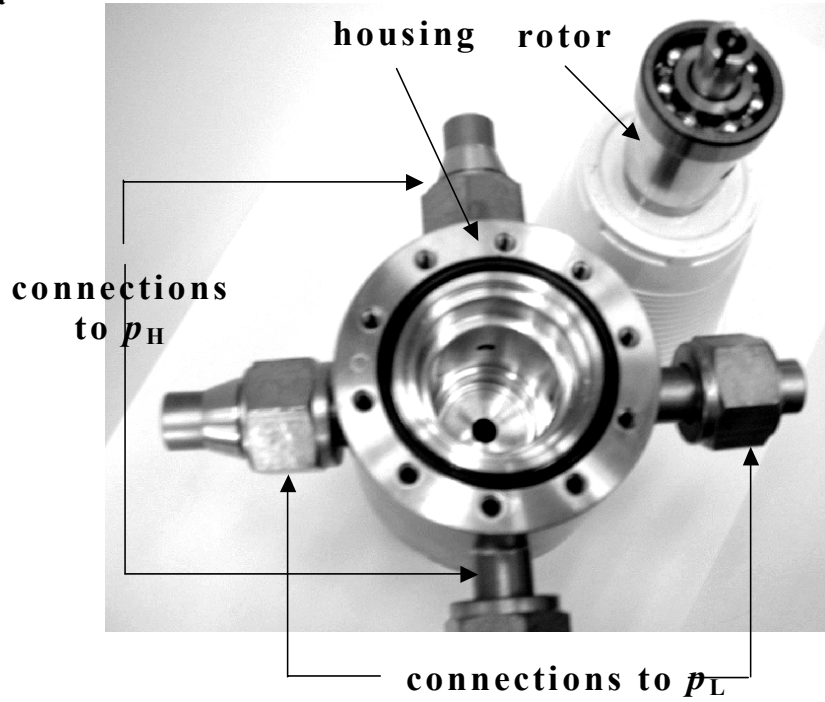
3.5. CONCLUSIONS

In this chapter we have described a three-stage PTR (PTR1) and a two-stage PTR (PTR2). The latter has been obtained simply by eliminating one stage in PTR1. A lowest temperature of 1.78 K has been achieved with PTR1 with ^3He as a working fluid. At that time (1999) this was the lowest temperature, ever achieved by a PTR. A cooling power of 160 mW at 4.2 K has been reached with ^4He as a working fluid.

A number of experiments has been carried out with PTR2. The resistance of the regenerator material at room temperature has been measured. As the regenerator material in the first stage regenerator we use stainless steel screens with a mesh size #200, which is one of the most commonly used regenerator materials for temperatures above 50 K. The characteristic flow impedance of the screens has been measured to be $14 \times 10^9 \text{ 1/m}^2$. This value can be used for calculating the regenerator loss due to the pressure drop as well as for the design of the flow straighteners.

The influence of the 1st orifice, the double-inlet orifice, and the minor orifice on the performance of the system has been investigated. Tuning of the orifices is quite a complicated job, considering that the PTR2 contains 6 orifices in total. From our experiments we have no indication that the system has multiple optimums. Both the PTR1 and the PTR2 are very stable. The systems always return to the optimum performance after passing a certain value of the DC-flow control valves and rapid warming. In our case the DC-flow control is provided by a combination of the double-inlet and the minor orifices.

a



b



Figure 3. 31. (a) A photograph of a part of the housing of the ‘no-contact’ rotary valve with the connections to the high- and the low-pressure side of the compressor, and a rotor. **(b)** A photograph of the rotor with the droplet-shaped radial channel.

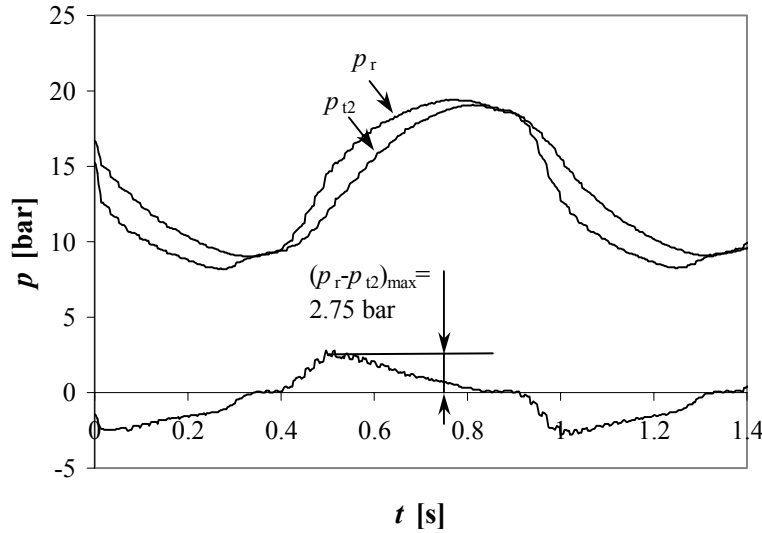


Figure 3. 32. Pressure variations at the inlet to the regenerator, p_r , and in the 2nd stage pulse tube, p_{t2} , of PTR2 with the ‘no-contact’ valve with the droplet shape of the radial channel versus time. The lowest curve gives the pressure drop in the regenerator.

A lot of work has been done on improving the rotary valve. The rotary valve is the second biggest source of the losses in GM-type PTRs. The power loss in the rotary valve can approach 1/3 of the total input power to a PTR. Two types of rotary valves are described in this chapter: the conventional rotary valve (the old and the modified construction) and the ‘no-contact’ rotary valve. In the conventional type of rotary valve the rotor and the stator are in a heavy mechanical contact with each other. The resulting wear makes the lifetime of the valve rather short. In addition to that dust particles of the rotor and the stator, released due to the wear of the valve, are taken by the gas flow into the pulse tube, and can severely degrade the performance of the system by blocking the orifices. The construction of the ‘no-contact’ valve differs significantly from the conventional valve. The rotor is placed into the housing and makes no mechanical contact with it. The ‘no-contact’ rotary valve is much smaller and lighter than the conventional valve and requires only 1.4 W of input power to provide a frequency of 1 Hz. The disadvantage of the ‘no-contact’ valve is that the high- and the low-pressure side of the compressor are short-circuited via a gap between the housing and the rotor. However, due to a very small size of the gap (the width of it is typically 10-20 μm) the leak from the high- to the low-pressure side is acceptable. By using the ‘no-contact’ rotary valve the power loss in the PTR reduces to 12 % of the total input power from 28 % with the conventional valve.

By eliminating a stage of the PTR1 we made the system simpler. However, due to the increased regenerator losses the lowest temperature with ^4He increased from 2.19 K for PTR1 to 2.43 K for PTR2. The cooling power remained unchanged and equal to 160 mW at 4.2 K. After increasing the regenerator volume of the PTR2 the lowest temperature increased even more to a value of 3.5 K. The cooling power at 4.2 K was still at the same value. The fact that the cooling power of the PTR did not change with the change of the regenerator volume meant, that the system was close to its optimum for the

cooling power. However, the negative effect of eliminating a stage at first, and then the increase of the regenerator volume disproportionally to the pulse tubes volumes on the lowest temperature of the PTR was clear.

It was decided to go back to a three-stage PTR and to design a new system, the volume of which will be much smaller than the volume of the PTR1. The new system should be flexible and has a performance, which is at least comparable to the performance of the PTR1. The development of the new PTR will be discussed in Chapter 4.

REFERENCES

1. Xu, M. Y., Waele, A. T. A. M. de, and Ju, Y. L., "A Pulse Tube Refrigerator Below 2 K", *Cryogenics* **39**, 1999, pp. 865-869.
2. Waele, A. T. A. M. de, Hooijkaas, H. W. G., Steijaert, P. P., and Benschop, A. A. J., "Regenerator dynamics in the harmonic approximation", *Cryogenics* **38**, 1998, pp. 995-1006.
3. Waele, A. T. A. M. de, Steijaert, P. P., and Koning, J. J., "Thermodynamical aspects of pulse tubes II", *Cryogenics* **38**, 1998, pp. 329-335.
4. Will, M. E., Tanaeva, I. A., Li, R., Waele, A. T. A. M. de, "New rotary valves for pulse-tube refrigerators", *Cryogenics* **44**, 2004, pp. 793-800.
5. The "no-contact" valve has been designed in collaboration with Sumitomo Heavy Industries, "High-low pressure gas directional control valve of refrigerator", Japanese patent, application number 2001-90627, filed on March 27 2001.

CHAPTER 4.

PRACTICAL ASPECTS OF PULSE-TUBE REFRIGERATORS, PART II

In this chapter a new three-stage PTR (PTR3) is discussed. It is designed by scaling down PTR1, the volume of which has been decreased by 50 %. The results of the measurements with PTR3 are described and compared with the performance of PTR1.

4.1. DESIGN OF THE NEW TREE-STAGE PTR (PTR3)

One of the main goals of this research is to investigate the physics and technology of PTRs, operating near their lowest temperature region. As shown in Chapter 3, the lowest temperature of 1.78 K has been reached with the PTR1. In this chapter we will discuss a new three-stage PTR (PTR3), which has been designed with the following requirements:

- Small size and weight.
- Flexible and convenient for modifications. This is especially important for laboratory PTRs. In order to test various components and different regenerator materials, it should be easy to access all parts of the PTR.
- Reduction of the amount of ^3He and the amount of regenerator material. The price of 1 liter NTP of ^3He is typically 125 \$. The PTR1 requires 220 liter NTP of ^3He . Hence, the reduction of the amount of ^3He will significantly decrease the total cost of the system. Similar things can be said about the regenerator materials. As it has been shown in Chapter 2, in order to reach low temperatures special rare-earth magnetic materials, which are usually rather expensive (typically 15-25 \$ per gram), have to be used.
- Reduction of power consumption.

The PTR3 has been designed by scaling down the volume of PTR1 by 50%. This has been done by decreasing the diameters of the tubes, while keeping the same lengths.

Here, we will show the influence of the reduction of the tubes diameters on the losses, the cooling power, and the lowest temperature of a PTR. The cooling power of a PTR can be described as

$$\dot{Q}_L = \bar{E}_t - \bar{E}_r, \quad (4.1)$$

where $\bar{\dot{E}}_t$ is the average energy flow in the pulse tube, and $\bar{\dot{E}}_r$ is the average energy flow in the regenerator. The energy flow is a sum of the enthalpy flow, \dot{H} , and the heat flow, \dot{Q} . Here, we assume, that the energy flows are one-dimensional and directed along the axes of the regenerator and the pulse tube (FIG. 4.1). The pulse tube is assumed to operate in the adiabatic mode. The enthalpy flow and the heat flow due to the thermal conduction in the regenerator are given by equations 2.85 and 2.79 respectively.

The enthalpy flow in the pulse tube can be expressed as

$$\dot{H}_t = \dot{n}_r H_m, \quad (4.2)$$

where \dot{n}_r is the molar flow rate of the gas through the cold heat exchanger of the pulse tube. The molar enthalpy is given by equation 2.83, and the change of the molar enthalpy for small pressure variations – by equation 2.81. For an adiabatic pulse tube $\delta S_m = 0$. So

$$\delta H_m = V_m \delta p. \quad (4.3)$$

Using the fact that the average molar flow through the cold heat exchanger $\dot{n}_r = 0$, the average enthalpy flow in the pulse tube can be expressed as follows

$$\bar{\dot{H}}_t = \overline{V_m \dot{n}_r \delta p}. \quad (4.4)$$

The cooling power of the PTR is given by equation 2.16. With equations 2.85 and 4.4 the energy balance for the 3rd stage of the PTR can be written as:

$$\dot{Q}_L + \dot{Q}_c = \overline{T \alpha_v V_m \dot{n}_r \delta p}. \quad (4.5)$$

If we decrease the cross-sectional area of the regenerator and the pulse tubes with a certain factor, keep their lengths the same, and make sure, that the average pressure and the pressure variations in the pulse tube remain the same, all the terms in equation 4.5 will decrease by the same factor. Thus, the losses reduce proportionally with the cooling power.

Now the question is, will the lowest temperature remain the same in this case? We will write the following expression for the cooling power of the pulse tube (eq. 2.30)

$$\bar{\dot{Q}}_L = T_L \bar{\dot{S}}_r. \quad (4.6)$$

The entropy flow in the regenerator is

$$\dot{S}_r = \dot{n}_r S_m. \quad (4.7)$$

The change in the molar entropy of the gas for small temperature and pressure variations is

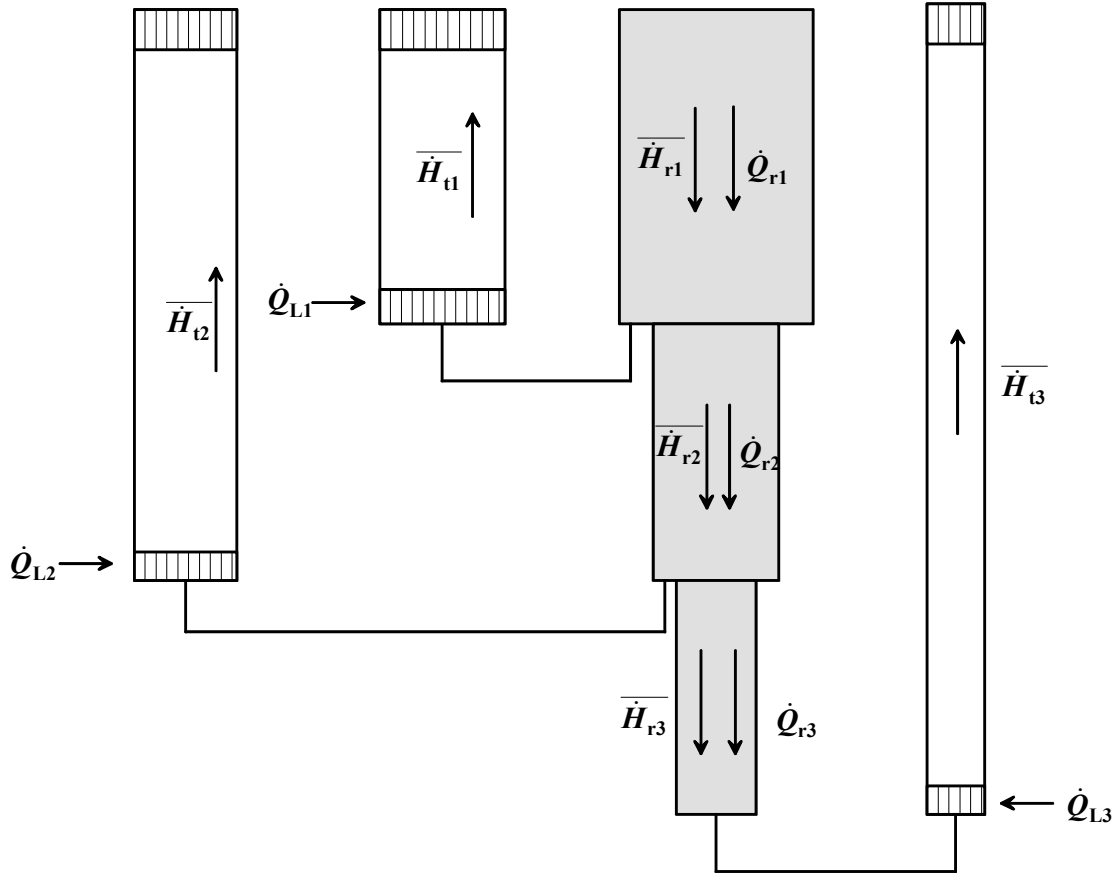


Figure 4. 1. Energy flows in a three-stage PTR.

$$\delta S_m = \frac{C_p}{T} \delta T - \frac{R}{p} \delta p. \quad (4.8)$$

If we split the molar entropy into a time average part and a varying part, we can write the following expression for the entropy flow in the regenerator with the perfect heat exchange conditions

$$\dot{S}_r = -\dot{n}_r \frac{R}{p} \delta p. \quad (4.9)$$

With equations 4.6 and 4.9 we get

$$T_L = \frac{\overline{\dot{Q}_L}}{\dot{n}_r \frac{R}{p} \delta p}. \quad (4.10)$$

From this expression we can see, that in the first order, reducing the cross-section with a certain factor and at the same time reducing the flow rate with the same factor, should

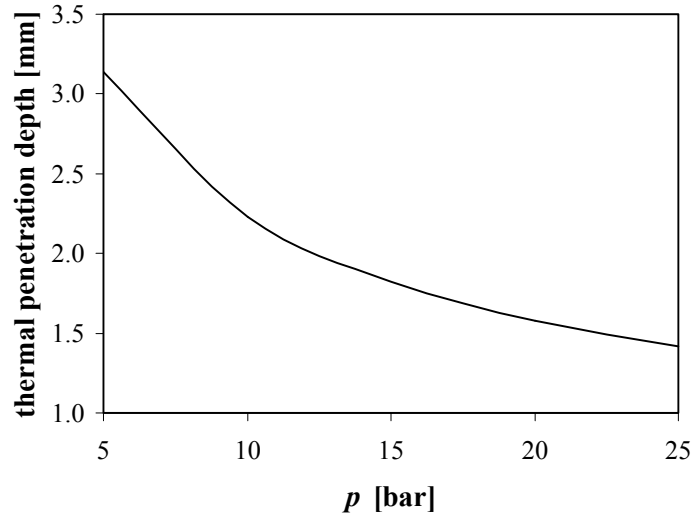


Figure 4. 2. Thermal penetration depth in helium at a frequency of 1.2 Hz and at room temperature as a function of pressure.

keep the lowest temperature the same. However, parameters, which do not scale with the surface area, such as external heat leaks and the heat-shuttle effect, complicate this simple picture.

The volume of the PTR1 is not reduced by more than 50% since the surface heat-pumping effect negatively influences the performance of the PTR (see Chapter 2, paragraph 2.2, [1]). Therefore, the diameters of the tubes should be significantly larger than the thermal penetration depth in helium (equation 2.1), so that the tubes could operate close to the adiabatic mode. The thermal penetration depth in helium at room temperature at the optimum frequency of the PTR1 as a function of pressure is shown on FIG. 4.2.

4.2. NEW THREE-STAGE PTR (PTR 3)

Figure 4.3 shows the schematic diagram of PTR3. The dimensions of the regenerator and the pulse tubes of the PTR3 are given in Table 4.1. The volumes of the

Table 4.1. Dimensions of the main components of PTR3.

Stage		1	2	3
Pulse tube	Inner diameter [mm]	20	12.1	7.65
	Wall thickness [mm]	0.5	0.3	0.15
	Length [mm]	141	204	430
	Volume [cm ³]	45.2	23.5	19.8
Regenerator	Inner diameter [mm]	34	20	14
	Wall thickness [mm]	0.6	0.5	0.4
	Length [mm]	141	130	155
	Volume [cm ³]	128	40.8	23.8

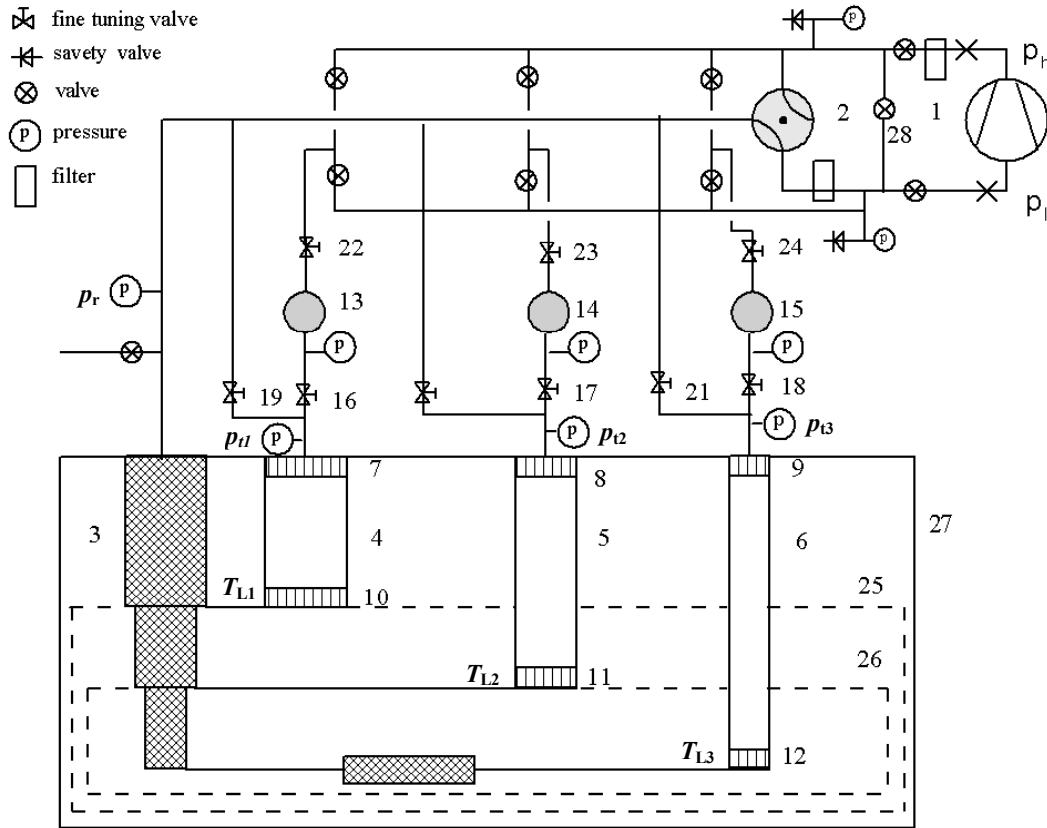


Figure 4. 3. Schematic diagram of PTR3. 1 - compressor; 2 - rotary valve; 3 - regenerator; 4-6 – pulse tubes; 7-9 – hot heat exchangers; 10-12 – cold heat exchangers; 13-15 – buffers; 16-18 – first orifices; 19-21 – double-inlet valves; 22-24 – minor orifices; 25 – 1st heat shield; 26 – 2nd heat shield; 27 – cryostat; 28 – bypass valve.

regenerator and all the pulse tubes of the new system are 50% smaller than the corresponding volumes of PTR1 (see Table 3.1). The exception is the 3rd stage pulse tube, the volume of which is around 70% of the volume of the 3rd stage pulse tube of PTR1. The choice of such dimensions for the 3rd stage tube is a compromise between decreasing the diameter to a value as close as possible to the desired value (50% of PTR1) and keeping it at a value larger than the thermal penetration depth in helium (see FIG. 4.2).

Each stage of the PTR has three adjustable needle valves: the first orifice, the double-inlet and the minor orifice. Therefore, the system contains nine needle valves in total.

The cooler is driven by a 4 kW compressor. In order to reduce the volume of the compressor two charcoal/zeolite filters with a volume of 6.2 liters are substituted by one filter, the volume of which is only 0.24 liters. Such a small filter is sufficient to provide a protection of the system from the oil vapour from the compressor, since the compressor always operates at almost maximum pressure difference. In addition to the charcoal/zeolite filter, there are two microfibre filters on the high- and the low- pressure line of the compressor as a protection from oil droplets entering the system. Under this

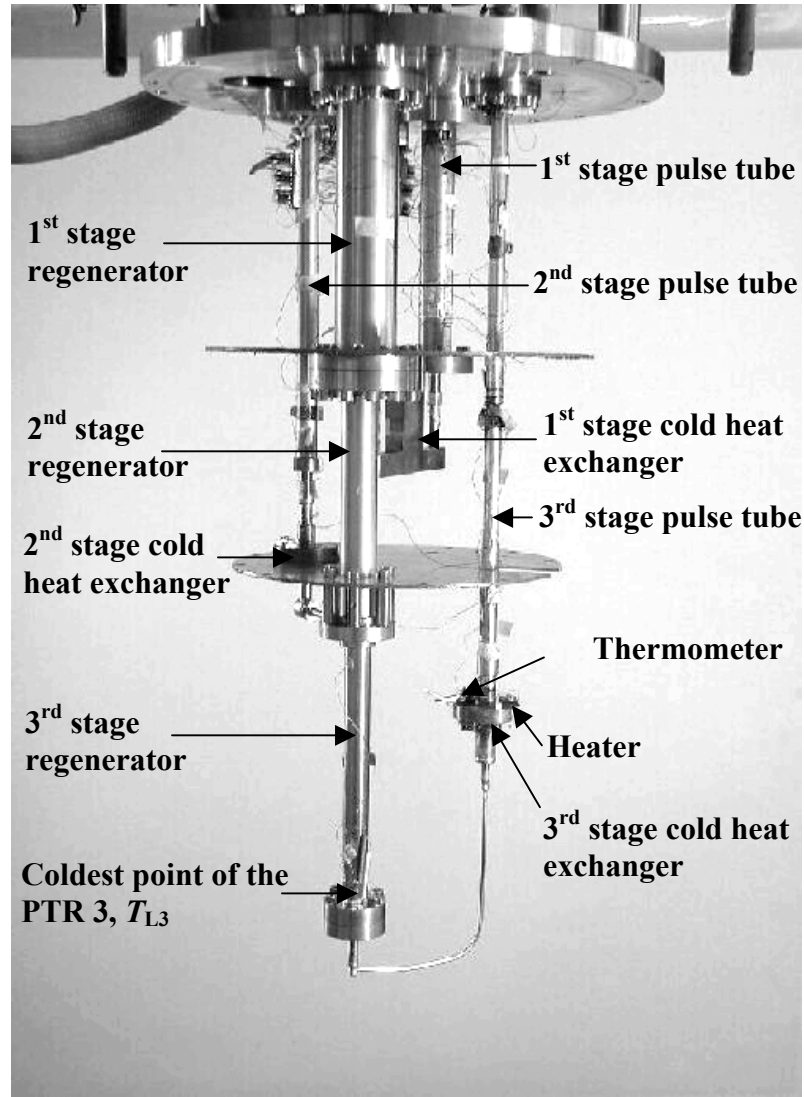


Figure 4. 4. A photograph of the low-temperature part (pulse tubes + regenerator) of PTR3. The total volume of the low-temperature part is 0.28 liters.

circumstances the risk of oil contamination is minimal.

The “no-contact” type of the rotary valve is used to create pressure oscillations in the PTR. There are two copper heat shields in the set-up. One of them is precooled by the first stage (1st heat shield). The other one is attached to the second stage cold heat exchanger (2nd heat shield).

The system contains two overpressure safety valves, adjusted for 28 bar and connected to a large volume (not shown in FIG. 4.3) in order to avoid losing ^3He , in case of overpressure in the system.

The photo of PTR3 is shown in FIG. 4.4. All tubes are fabricated from stainless steel. The regenerator is designed to be flexible to provide easy access to each stage. In this way the regenerator material can be fixed easily. The regenerator material of any stage can be changed without opening the rest of the regenerator and disturbing its fixation. The composition of the regenerator is given in Table 4.2. In order to decrease

Table 4.2. The composition of the three-stage regenerator.

	Material	Size	Number of screens or mass	Fraction [%]	Filling factor
1st stage	Stainless steel	Mesh # 200	1480, 335 g	96	0.35
2nd stage	Lead	0.4-0.48 mm	251 g	95	0.54
3rd stage	ErNi	0.2-0.5 mm	71 g	52	0.61
	ErNi _{0.9} Co _{0.1}	0.2-0.5 mm	52 g	39	0.59

the flow resistance of the 1st stage regenerator several screens with a larger mesh size (# 50) are placed at both ends of the 1st regenerator. A bended tinned copper wire is put between these screens as shown in FIG.4.5. This is done in order to create some space between the screens for better distribution of the gas flow at the entrance to the regenerator.

Copper blocks with a few parallel channels are used as the cold heat exchangers for the 1st and the 2nd stage. The heat exchanger of the 1st stage contains three parallel channels with a diameter of 2 mm. The length of the channels, calculated with equation 2.64 and corrected for minimizing a pressure drop, is 20 mm. The heat exchanger of the 2nd stage includes 7 parallel channels with a diameter of 1 mm and a length of 10 mm.

The cold heat exchanger of the third stage (FIG. 4.6) is made of copper powder with 0.2 mm particle size, sintered at 900°C. The heat exchanger is directly attached to the 3rd stage pulse tube and has an inner diameter of 9 mm, which is slightly larger than

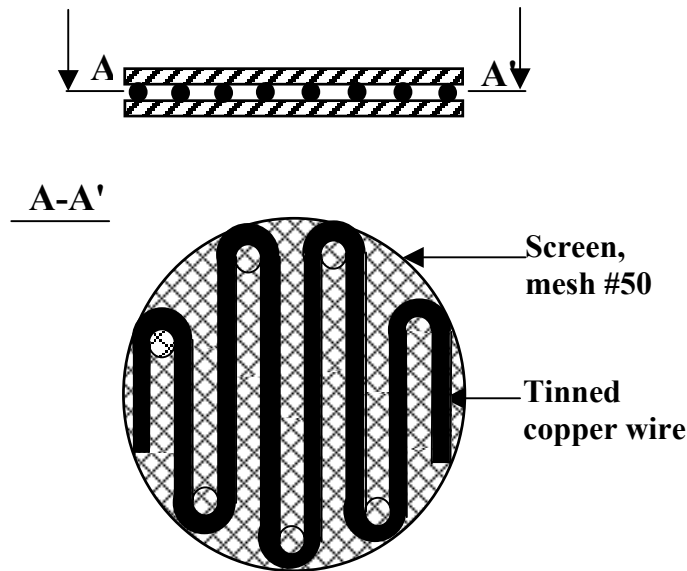


Figure 4. 5. Schematic drawing of a construction, consisting of two screens with a mesh size #50 and a tinned copper wire, placed between the screens. A number of such constructions is placed at both ends of the 1st stage regenerator in order to decrease the flow resistance of it

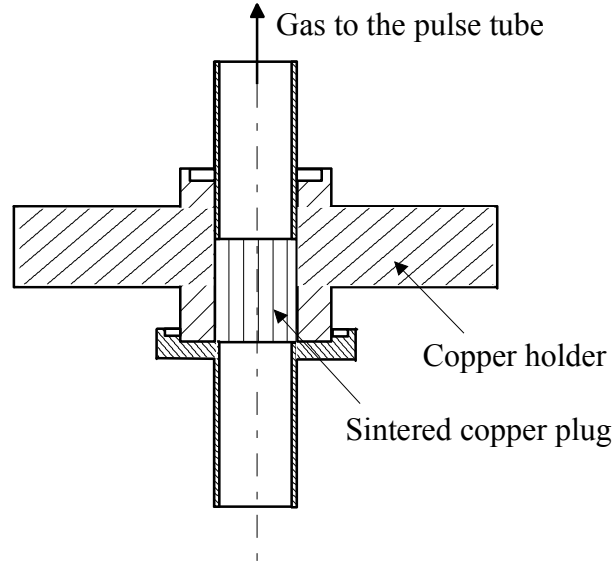


Figure 4. 6. Schematic drawing of a 3rd stage cold heat exchanger, consisting of a sintered copper powder, filled in a copper holder. The heat exchanger is attached directly to the pulse tube by soft soldering.

the inner diameter of the 3rd pulse tube. Therefore, it acts as a flow straightener as well. The characteristic flow impedance of the copper used in our heat exchanger for typical flow at the cold end of the 3rd stage pulse tube ($\approx 34 \text{ cm}^3/\text{s}$) is $3 \times 10^{10} \text{ 1/m}^2$ [2]. The length of the sintered plug is 13 mm. With these values and with equations 2.79 and 2.80 the pressure drop in the 3rd stage cold heat exchanger at an average pressure of 15 bar has a typical value of 1400 Pa. With equation 2.78 at a temperature of 2.2 K this pressure drop results in a power loss of around 24 mW.

As flow straighteners at the cold ends of the 1st and the 2nd pulse tubes, as well as at the hot ends of all the pulse tubes, stainless steel screens with a mesh number #200 are used. The number of screens at the cold end of the 1st stage, calculated with equations 2.89 and 2.90 for an average pressure of 15 bar and a temperature of the cold end of the 1st stage of 80 K, should be larger than 10. For the cold end of the 2nd stage pulse tube the number of screens increases to 16 screens. However, from our observations, we have the impression that the amount of screens should be larger than the amount of screens deduced from equations 2.89 and 2.90. In order to decrease the amount of screens in the flow straighteners at the cold ends of the 1st and the 2nd stage pulse tubes we have designed a two-stage flow straightener. A schematic drawing of the two-stage flow straightener is shown in FIG. 4.7. Each stage consists of a ring of 3-5 mm height with several screens (typically 5-7) attached to it. Both stages are connected with each other. There is a space between two layers of screens. Hence, the flow straightening takes place in two steps. The flow straighteners are welded at the ends of the pulse tubes.

At the hot end of the pulse tubes only a few screens are sufficient to provide a good flow straightening. Therefore, only one stage of the two-stage flow straightener is used there.

The hot heat exchangers are water-cooled. A spiraled copper tube for the gas flow is inserted into a volume, through which the cooling water flows.

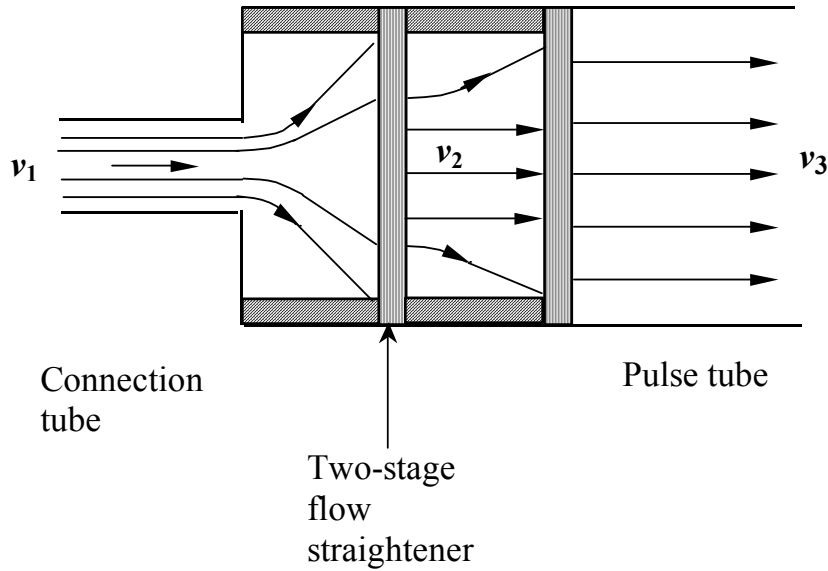


Figure 4. 7. Schematic drawing of a two-stage flow straightener at the cold end of a pulse tube.

For measurements of temperature above 70 K platinum resistors are used. Temperatures below 70 K are measured by diode thermometers and Carbon Ceramic resistors, calibrated down to 1.5 K. For pressure measurements differential pressure sensors are used.

4.3. EXPERIMENTAL RESULTS WITH ^4He

In the first run after assembling PTR3, it has reached 14.9 K. After that, during a number of runs, the performance of the PTR3 has been improved from run to run by modifying the system. Some of the most important steps will be discussed in this section, and the intermediate results will be given. The final step has been a change of the regenerator material of the 3rd stage, which has resulted in a system, reaching 1.73 K.

4.3.1. Optimum frequency

First the optimum frequency of the new PTR has been determined. The cold-end temperatures of the three stages of the PTR are plotted versus frequency in FIG. 4.8. The system has demonstrated its best performance at a frequency of 1.86 Hz with the tendency to become even better at a higher frequency. However, it has been rather difficult to increase the frequency much more due to practical reasons. To provide the frequency of 1.86 Hz the motor of the rotary valve requires about 4 W of the input power ($i \approx 0.15$ A, $U = 26.5$ V). This value for the voltage is the maximum possible for this type of the motor. More powerful motors exist only in larger sizes. If a larger motor is used, the size of the housing of the rotary valve has to be increased as well. In this case it will be difficult to set the rotary valve in position on top of the regenerator, as it is tightly

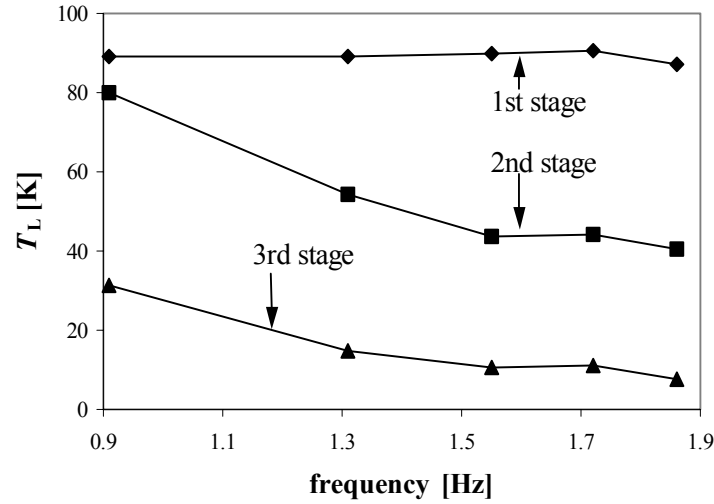


Figure 4. 8. The cold-end temperatures of the three stages of PTR3 as functions of frequency.

surrounded by tubes with the needle valves. In a later experiment we have increased the frequency to 2.11 Hz, using the same motor. But at this frequency the temperature showed a tendency to increase.

The higher operating frequency of PTR3 of 1.86 Hz, compared to 1.2 Hz of PTR1, can be explained by the small size of the new system. The ratio of the thermal penetration depth and the radius of the tubes in case of the PTR3 is larger than in the PTR1. This results in a higher surface heat pumping in the PTR3 (see Chapter 2, paragraph 2.2, [1]). The thermal penetration depth decreases with frequency, which leads to a decrease of the surface heat pumping.

In addition to that, the phase shift between the flow of the gas at the cold end and the pressure is proportional to the frequency (see equations 2.12 and 2.3). In order to keep the phase shift at its optimum value, the frequency should be increased for a PTR with a smaller volume.

In a later experiment the 3rd stage pulse tube has been changed for a tube with a larger diameter, $d=9$ mm. The system has been tested for an optimum frequency again. The frequency of 1.86 Hz has still remained the optimum frequency. The temperature profiles in the pulse tubes with two different diameters are shown in FIG. 4.9. In both cases the system has been adjusted for the lowest temperature. The difference between the temperature profiles is caused by a combination of the DC-flow change and a decreased surface heat pumping. The temperature in the larger tube decreases steeply from the hot end. However, the lowest temperature in case of the larger tube is slightly higher. This is caused by the fact that the increased volume of the 3rd stage tube has resulted in the increased flow through the regenerator, producing more irreversible entropy. In addition to that the size of the 3rd pulse tube is now misbalanced with the size of the 3rd regenerator. Therefore, an extra regenerator part, filled with $\text{ErNi}_{0.9}\text{Co}_{0.1}$, has been added between the cold end of the 3rd pulse tube and the 3rd regenerator (the dimensions and the composition of the extra regenerator part are given in Chapter 3). The

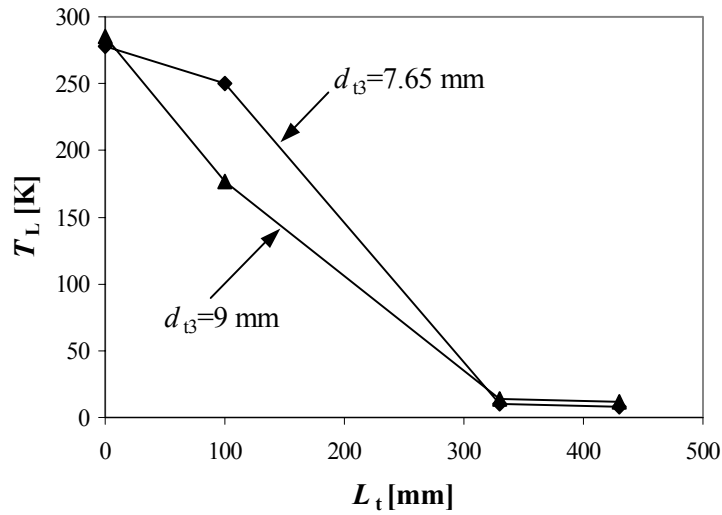


Figure 4. 9. Temperature profiles for two different diameters of the 3rd stage pulse tube. In both cases the system is adjusted for a minimum temperature.

second heat shield has been removed to reduce the time constant. In this arrangement the lowest temperature of the PTR3 decreased from 11.84 K to 4.03 K.

4.3.2. 2nd stage improvement

In Table 4.3 the lowest temperatures of the 2nd, T_{L2} , and the 3rd, T_{L3} , stage cold ends under different conditions are given. As we can see from the 1st row of Table 4.3 T_{L2} is high compared to $T_{L2}=25-30$ K of the PTR1. The gas enters the part of the regenerator, filled with ErNi having the temperature of 43 K. The heat capacity of ErNi is much lower than the heat capacity of lead in this temperature region (FIG. 4.10). Therefore, the efficiency of a big part of the 3rd stage regenerator is not at the optimum. In the same arrangement the 2nd stage regenerator operates between 84 and 43 K. Hence, the temperature difference in the 2nd stage regenerator is not very large. That means, that

Table 4.3. Improvement of the 2nd stage of the PTR.

	T_{L2} [K]	T_{L3} [K]
2 nd stage regenerator with 0.4-0.48 mm lead particles	43.2	4.03
2 nd stage regenerator with 0.2-0.24 mm lead particles	35.5	3.04
2 nd heat shield is attached to the cold heat exchanger of the 2 nd stage	34.5	2.31

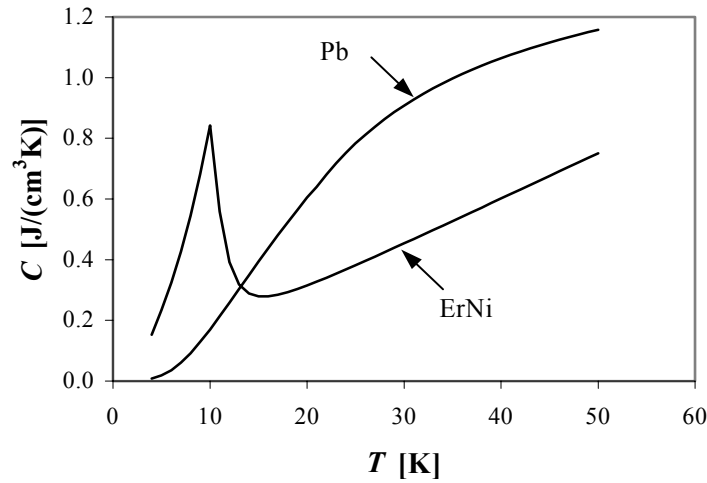


Figure 4. 10. Heat capacities of lead and ErNi as functions of temperature.

the heat storage in the second stage regenerator can be improved. To examine this matter more carefully, the third stage has been removed from the PTR3, and the temperature profile in the regenerator of the remaining two stages has been measured (see FIG. 4.11). In this arrangement the temperature of the 1st stage regenerator changes from 292 K to 61 K, whereas the temperature of the 2nd stage regenerator changes from 61 K to only 35 K. The reasons for such a small temperature difference in the 2nd stage regenerator are the following. The thermal penetration depth (see equation 2.1) in lead and in helium at an average pressure of 15 bar and a frequency of 1.8 Hz is shown in FIG. 4.12. For a lead with a diameter of particles of 0.4-0.48 mm, a typical size of pores is 0.1-0.15 mm. From

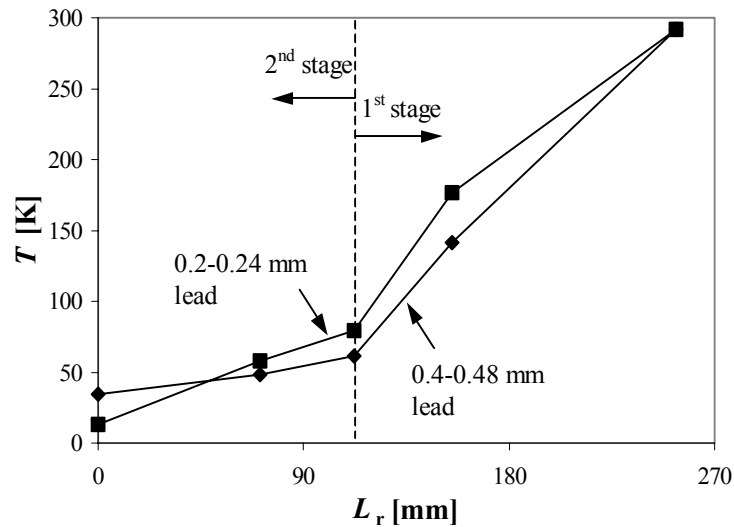


Figure 4. 11. Temperature profiles in the 1st and the 2nd stages of the regenerator for two different sizes of lead in the 2nd stage regenerator. In these experiments the 3rd stage is disconnected from the system.

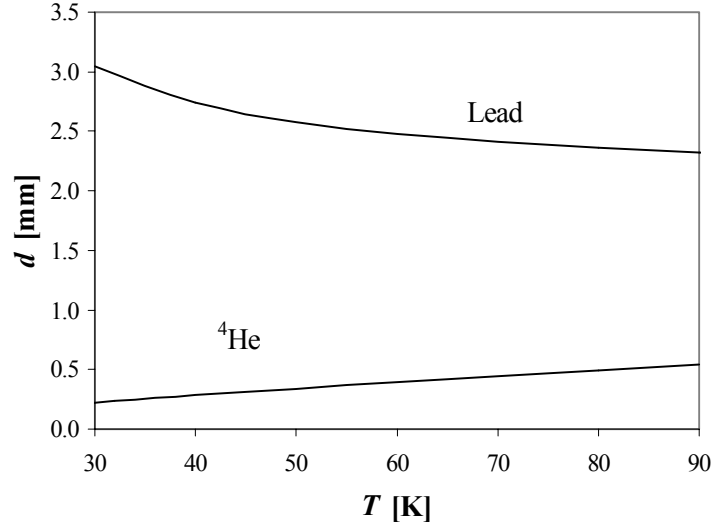


Figure 4. 12. Thermal penetration depths in lead and in helium at a pressure of 15 bar and a frequency of 1.8 Hz.

FIG. 4.12 it is seen that the thermal penetration depth in lead is larger than the radius of particles, and that the thermal penetration depth in ^4He is larger than the size of pores. Therefore, the problem of the bad heat storage results from an insufficient heat exchange area between the gas and the material. For the heat exchange rate due to the heat flow from the gas to the regenerator material per m^3 we can write

$$\dot{Q}_e = \alpha_e F (T_g - T_r), \quad (4.11)$$

where α_e is a heat exchange parameter, given by equation 2.63, T_g and T_r are the temperatures of the gas and the regenerator material respectively, and F is the heat exchanging surface per unit volume, which for spherical particles with a diameter, d_s , equals to

$$F = \frac{6}{d_s}. \quad (4.12)$$

In order to increase the heat exchanging area, the lead with a diameter of spherical particles 0.4-0.48 mm has been changed for lead with a diameter of 0.2-0.24 mm. The new temperature profile of the regenerator is shown in FIG. 4.11. In the new arrangement the T_{L2} decreased to 13.3 K, and the temperature difference in the 2nd stage regenerator increased from 26 K to 66 K.

After reattaching the 3rd stage, the change of lead in the 2nd stage regenerator resulted in the reduction of T_{L3} to 3.04 K (see Table 4.3). However, the pressure drop in the 2nd stage regenerator (the lowest line in FIG. 4.13) greatly increased.

As the next step a second heat shield has been attached to the second stage to reduce radiation heat leak on the coldest parts of the cooler. With both heat shields a lowest temperature of 2.31 K has been achieved.

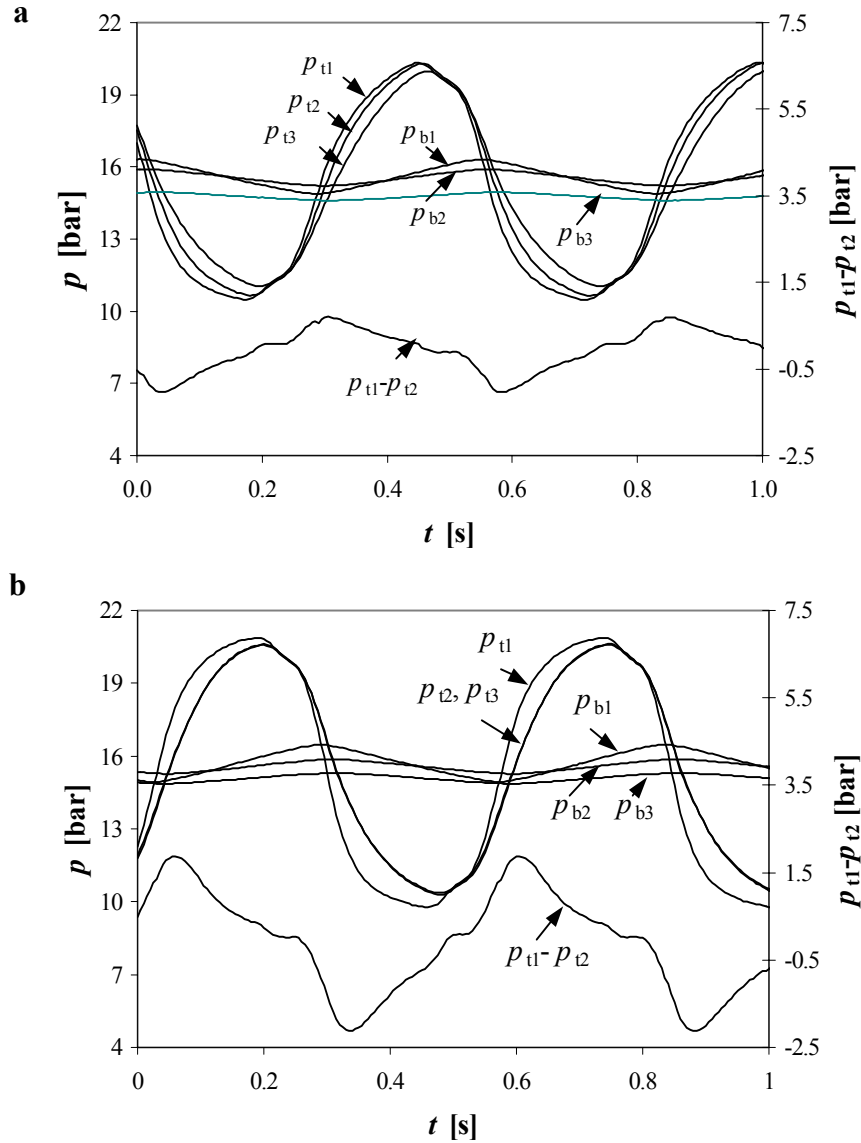


Figure 4. 13. (a) Pressure variations at the inlet to the regenerator, p_{t1} , in the pulse tubes, p_{t2} , p_{t3} , and in the buffers, p_{b1} , p_{b2} , p_{b3} , in case of 0.4 – 0.48 mm lead particles in the 2nd stage regenerator of PTR3. The lower line, the values of which are indicated on the secondary axis, is the pressure drop in the 2nd stage regenerator. **(b)** Pressure variations in PTR3 with 0.2 – 0.24 mm lead particles in the 2nd stage regenerator. The lower line is the pressure drop in the 2nd stage regenerator (the values of it are again indicated on the secondary axis).

4.3.3. Improvement of the 3rd stage

4.3.3.1. The length of the pulse tube.

In section 4.2.1 we have described the change of the 3rd stage pulse tube with an inner diameter of 7.65 mm for a larger one with the inner diameter of 9 mm and at the

same time the enlarging the regenerator by adding an extra part filled with $\text{ErNi}_{0.9}\text{Co}_{0.1}$. However, in this arrangement the volume of the 3rd stage tube is equal the volume of the 3rd stage pulse tube of PTR1, whereas the volumes of all other components are 50% of the volumes of PTR1. In order to decrease the volume of the 3rd stage pulse tube, we have replaced it by a shorter tube with the same inner diameter. The extra regenerator part has been removed as well. The length of the new 3rd stage tube is 342 mm, and the

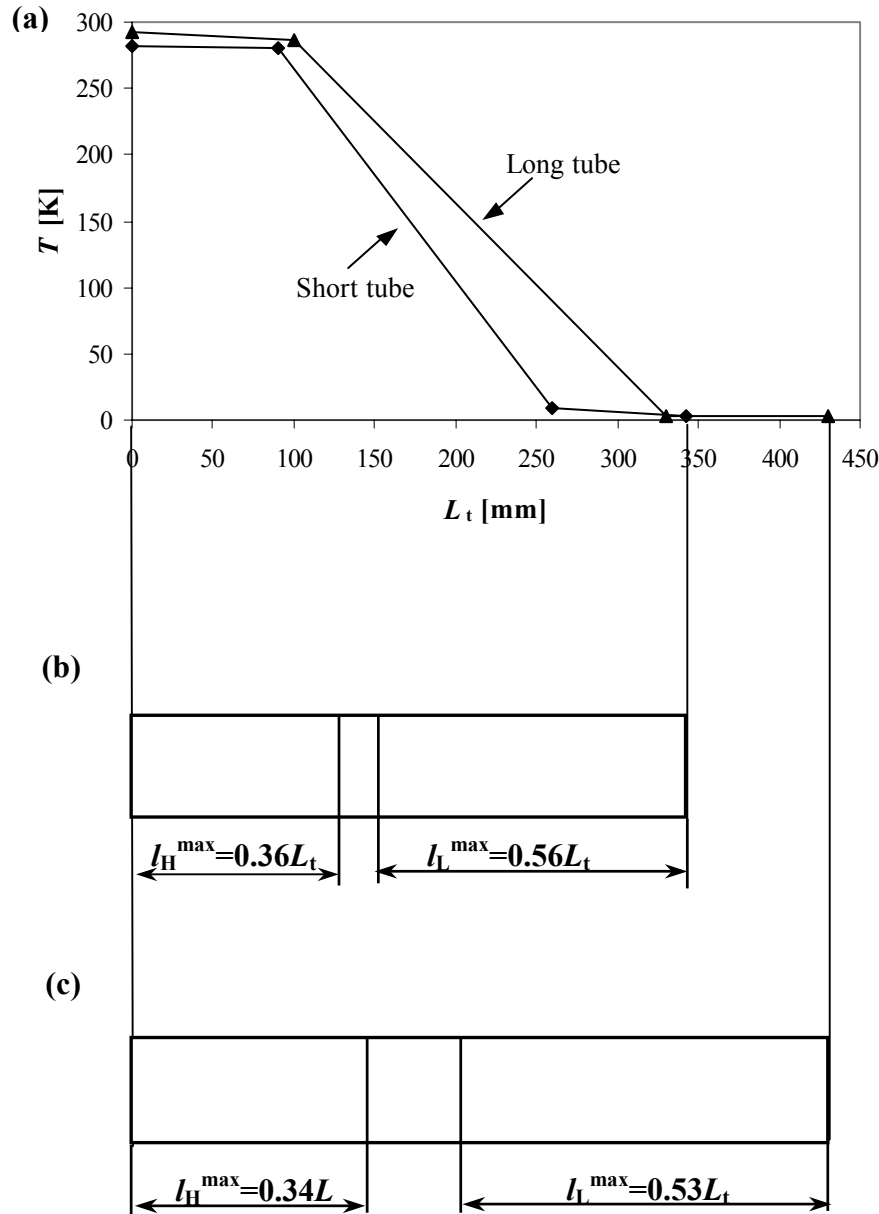


Figure 4. 14. (a) Temperature profiles in the 3rd stage pulse tube of two different lengths. (b) The calculated maximum travelling lengths of the gas at the cold and at the hot ends of the short 3rd stage pulse tube. (c) The calculated maximum travelling lengths of the gas at the cold and at the hot ends of the long 3rd stage pulse tube.

volume is 21.8 cm^3 . This is 80% of the volume of the 3rd stage pulse tube of PTR1. Such a length of the tube has been chosen for practical reasons. In addition to that further reduction of the 3rd stage tube length would increase the risk of a dramatical change in the temperature profile in the tube, resulting in the increase of the cold-end temperature.

The temperature profiles in the long and in the short pulse tubes are given in FIG. 4.14a. In FIG. 4.14b and 4.14c the maximum lengths, traveled by the gas at the cold, l_L^{\max} , and the hot, l_H^{\max} , ends of the short and the long pulse tubes, calculated with equations 2.107 and 2.111, are shown. Although equations 2.107 and 2.111 are derived for a single orifice pulse tube with an ideal gas, they give a good estimation of the traveling lengths. From FIGs. 4.14b and 4.14c we can see that the relative traveling lengths l_L^{\max}/L_t and l_H^{\max}/L_t are rather high. In fact, the warm gas “plug” almost overlaps with the cold gas “plug”. Therefore, there is a high risk of a big heat-pumping effect. However, this does not seem to affect the performance of the PTR3 as a lowest temperature of 2.24 K is reached. In this experiment 1/3 of $\text{ErNi}_{0.9}\text{Co}_{0.1}$ is substituted by GdAlO_3 (for details see Chapter 5). In all other experiments the composition of the regenerator is according to Table 4.2.

The reduction of the pulse tube length also results in the increase of the thermal conduction loss in it (see equation 3.62). The thermal conduction loss through the walls of the pulse tube has increased from 49 mW in the long tube to 58 mW in the short tube. The cooling power of the PTR at 2.5 K, calculated with equation 2.16, is 330 mW. So the thermal conduction loss through the walls of the tube is considerable. On the other hand the velocity of the gas in a shorter tube decreases (see equations 2.105 and 2.109), thus, reducing the turbulence loss in the tube. The amplitude of the velocity of the gas at the cold end of the 3rd pulse tube decreased from 0.79 m/s to 0.63 m/s.

After certain adjustments of the system (fine tuning of the needle valves, improving the thermal isolation of the 2nd heat shield) a lowest temperature of 2.18 K has been reached.

4.3.3.2. Two different types of ErNi in the 3rd stage regenerator.

More than a half of the 3rd stage regenerator is filled with ErNi. We have purchased ErNi from two different sources. The first type, which we will call ErNi-A, has particles of an irregular shape with a size of 0.2–0.5 mm. The shape of the particles of the other type of ErNi, which we will call ErNi-B, is spherical with a diameter of 0.2–0.24 mm. In most of the experiments with PTR3, including the ones, described above, ErNi-A has been used. In the final experiments it has been substituted by ErNi-B. The change of the regenerator temperature profile, resulting from this substitution, is shown in FIG. 4.15. The temperature in the middle of the ErNi part has dropped from 14.3 to 3.3 K! It is hard to believe that this change has been caused only by the change of the shape of the particles. In fact the irregular shape of the particles should provide a larger heat exchange area than the spherical shape. It is very likely, that such a difference in the performance of the ErNi part of the regenerator has been caused by different fabrication methods of the material, which has resulted in the significant difference in its heat capacity.

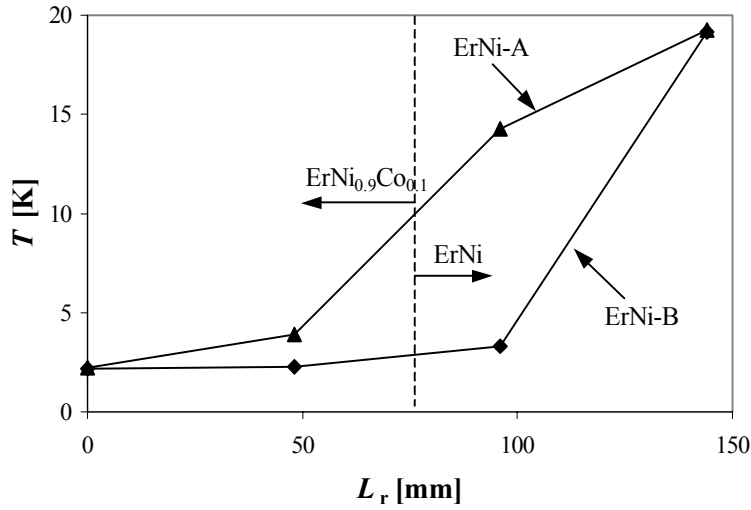


Figure 4. 15. Temperature profiles in the 3rd stage regenerator, filled with $\text{ErNi}_{0.9}\text{Co}_{0.1}$ and two different types of ErNi (so-called ErNi-A and ErNi-B).

With ErNi-B the cold-end temperature of PTR3 has decreased to the average value of 2.128 K. During a cycle the temperature oscillated between 2.120 and 2.136 K. These are the oscillations of helium, which can be observed at such low temperatures due to a low heat capacity of regenerator material in this temperature region. The value of 2.128 K is basically the lowest value, achievable with ^4He at an average pressure of 15 bar and a pressure amplitude in the 3rd stage tube of 4.66 bar.

The temperature profile in the 3rd stage regenerator with ErNi-B can be compared to the temperature profile, calculated with equation 2.90 (see FIG. 2.15). The expression for n_p value, given by equation 2.87, can be rewritten as

$$n_p = \frac{1}{2} n_{t3A} p_{t3A}, \quad (4.13)$$

where n_{t3A} and p_{t3A} are the molar flow and the pressure amplitudes at the cold end of the 3rd stage pulse tube. With $n_{t3A}=0.7$ mol/s and $p_{t3A}=4.66$ bar $n_p=330$ kPa mol/s. From FIG.15 it is seen that the temperature gradient close to the cold end of the regenerator is much smaller than in the rest of the regenerator, as expected.

4.3.4. Cooling power of PTR3. Comparison of PTR3 with PTR1.

The lowest temperature of PTR3 has been measured at the cold end of the regenerator. The temperature at the cold end of our 3rd stage pulse tube is typically 0.3 K higher than the temperature at the cold end of the regenerator at an average temperature of 2.2 K. The heater for the cooling power measurements has been installed at the cold heat exchanger of the 3rd stage pulse tube (see FIG. 4.4). In general, two types of cooling power can be defined: the technical cooling power and the intrinsic cooling power. The

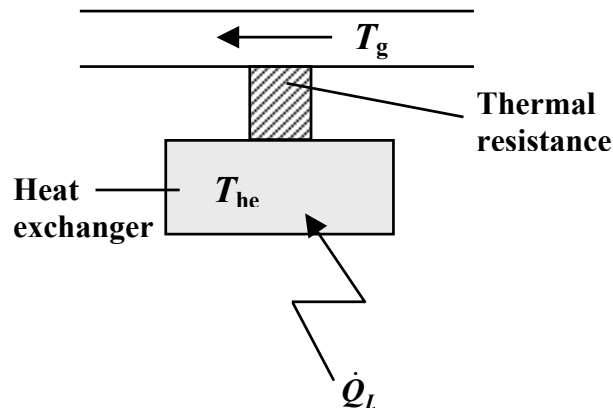


Figure 4. 16. Illustration to the explanation of the difference between the intrinsic and the technical cooling powers of a PTR. A certain amount of heat, \dot{Q}_L , is supplied to the heat exchanger at a temperature T_{he} . This heat causes an increase of the temperature of the gas, passing the heat exchanger, T_g . Due to a thermal resistance between the gas flow and the heat exchanger $T_g < T_{he}$ at the same \dot{Q}_L .

technical cooling power is determined by heating and measuring the temperature at the same place (in our case at the cold heat exchanger of the 3rd stage pulse tube). When supplying heat, \dot{Q}_L , to a cold heat exchanger, the temperature of it, T_{he} , is rising (see FIG. 4.16). The temperature of the gas, T_g , passing the cold heat exchanger is rising as well, but with a smaller rate due to a thermal resistance between the gas and the heat exchanger. The intrinsic cooling power is the cooling power, carried by the gas, passing the cold heat exchanger. This cooling power is the one, calculated with equation 2.16. Due to the thermal resistance between the gas and the heat exchanger the intrinsic cooling power is always higher than the technical cooling power at the same temperature. In our case the intrinsic cooling power is determined by heating at the cold heat exchanger, but measuring at the cold end of the regenerator.

The technical cooling power of the PTR3 versus temperature is plotted in FIG. 4.17. It is equal to 80 mW at 4.2 K. The average pressure in the system is 14.6 bar, and the pressure amplitude in the 3rd stage is 4.56 bar. The cooling power of the PTR1 at 4.2 K is 114 mW (FIG. 4.17). It is measured at an average pressure of 16.7 bar and a pressure amplitude of 4.37 bar. The difference of 43 % between the cooling powers of PTR1 and PTR3 instead of the expected difference of around 100 % can be explained by the fact, that the pressure amplitude in PTR3 is higher than that in PTR1 (see Table 4.4).

It is rather difficult to compare two complicated systems with a large number of variables, such as the volume, the frequency, the pressure amplitude, the shape of the pressure variations, the composition of a regenerator, etc. We have summarized the main parameters of PTR1 and PTR3, both adjusted for a lowest temperature, in Table 4.4. The lowest temperature of the PTR3 is slightly lower than that of the PTR1. However, the pressure amplitudes in the PTR3 are higher than those in the PTR1.

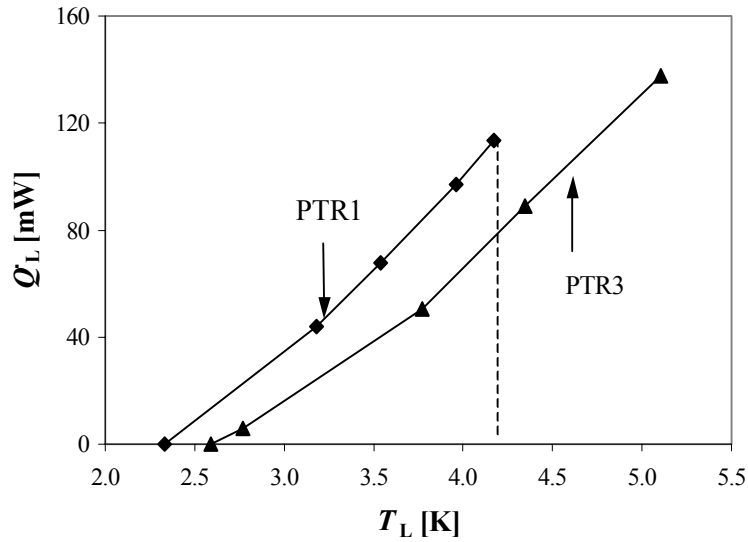


Figure 4.17. The technical cooling powers of PTR1 and PTR3 as functions of the cold-end temperature. The dashed line is drawn at $T_L=4.2$ K.

Table 4.4. Comparison of PTR 1, adjusted for a lowest temperature, and the PTR 3.

	PTR 1	PTR 3
Total volume of the low-temperature part (regenerator + tubes) [cm ³]	580	283
Input power [kW]	4	4
Frequency [Hz]	1.20	1.84
p_0 [bar]	16.40	15.26
p_{inA} [bar]	3.77	5.58
p_{t1A} [bar]	3.67	5.18
p_{t2A} [bar]	3.57	4.67
p_{t3A} [bar]	3.55	4.67
T_{L1} [K]	79.5	89.5
T_{L2} [K]	26.1	18.8
T_{L3} [K]	2.19	2.13

4.3.5. The performance of PTR3, driven by 4 kW and 2 kW compressors

We have investigated the dependence of the lowest temperature of the PTR on the inlet pressure amplitude in the system, p_{tA} . The pressure amplitude has been reduced simply by opening the bypass valve connecting the high- and the low-pressure sides of the compressor (number 28 in FIG. 4.3). We have found a broad optimum (see FIG.

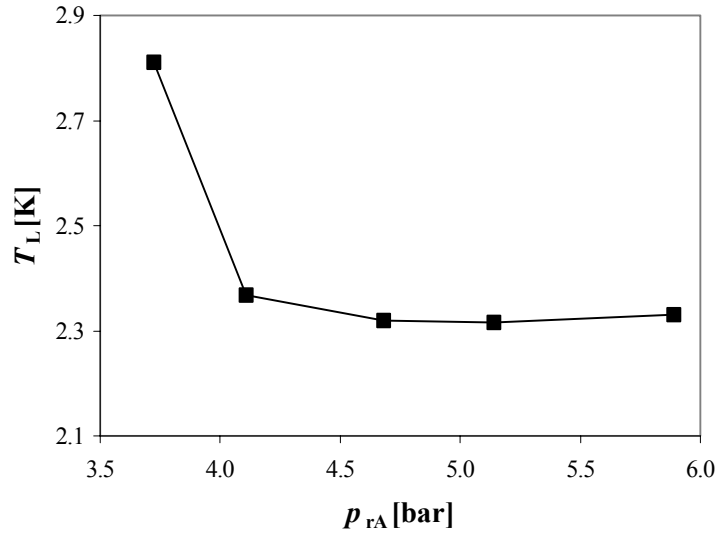


Figure 4. 18. The influence of the pressure amplitude at the inlet to the regenerator, p_{rA} , on the cold-end temperature of PTR3.

4.18). Hence, the system is not very sensitive to the change in the inlet pressure amplitude.

Based on scaling a 2 kW compressor should be sufficient to operate PTR3 and to keep its performance at the same level as the performance of PTR1. Therefore, the 4 kW compressor was replaced by a 2 kW compressor. The results of the change are summarized in Table 4.5. The average pressure in the 2 kW PTR increased from 13.3 to 18.1 bar. On the other hand the pressure amplitude in the system decreased. Therefore, as expected from the results, illustrated in FIG. 4.18, the minimum temperature went up

Table 4.5. Comparison of the performances of the new PTR, operated by 4 kW and 2 kW compressor (* T_{L3} in this case is measured at the cold heat exchanger of the 3rd stage pulse tube).

	4 kW compressor	2 kW compressor	
Frequency [Hz]	1.84	1.84	1.22
Average pressure [bar]	13.3	18.1	18.1
p_{inA} [bar]	5.41	2.96	3.76
p_{t1A} [bar]	5.04	2.82	3.64
p_{t2A} [bar]	4.73	2.70	3.60
p_{t3A} [bar]	4.65	2.70	3.53
T_{L1} [K]	98	110	120
T_{L2} [K]	24.4	37.8	43.3
T_{L3} [K]	2.59*	3.95	3.94
\dot{Q}_L at 4.2 K [mW]	80	5.86	6.18

from 2.59 K to 3.95 K. There was no possibility to increase the pressure amplitude by adding some extra gas into the system due to compressor limitations. However, the pressure amplitude in the PTR can be increased by decreasing the frequency. With the frequency of 1.22 Hz (the optimum frequency of the PTR1) the pressure amplitude in the PTR3 increased from 2.96 to 3.76 bar, and the average pressure remained the same. In spite of the increased pressure amplitude, the minimum temperature remained the same due to the negative influence of the lower frequency on the performance of the PTR3 (see FIG. 4.8). Therefore, the optimum parameters combination for the frequency and the pressure amplitude in case of the 2 kW compressor could not be provided.

4.4. ^3He EXPERIMENTS

Due to the small volume of PTR3 the amount of ^3He has reduced from 220 liters NTP to 165 liters NTP. A number of experiments, in which ^4He was replaced by ^3He , was carried out with PTR3 with ErNi-A in the 3rd stage regenerator. However, the system did not cool below 2 K.

After changing ErNi-A for ErNi-B a lowest temperature of 1.73 K has been reached. The average pressure in the PTR has been 16.55 bar, and the pressure amplitude in the 3rd stage has been 5.1 bar (FIG. 4.19). The technical cooling powers of the PTR3 with ^3He and with ^4He are shown in FIG. 4.20 as functions of temperature. In both cases the system has been adjusted for the lowest temperature. The cooling power of PTR3 with ^3He is 124 mW at 4.2 K. Therefore, the substitution of ^4He by ^3He has improved the performance of the system by 55 %. The cooling power of PTR1 at 4.2 K is 80 mW. The higher cooling power of PTR3 at 4.2 K is due to the fact, that the pressure amplitudes in

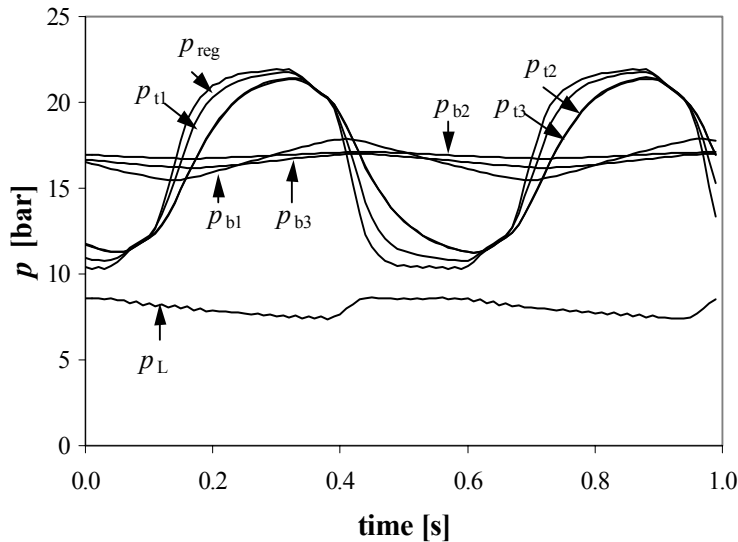


Figure 4. 19. Pressure variations in PTR3 with ^3He as the working fluid and $T_{L3}=1.73$ K. Here, p_r is the pressure at the inlet to the regenerator, p_{t1} , p_{t2} , p_{t3} are the pressures in the pulse tubes, p_{b1} , p_{b2} , p_{b3} are the pressures in the buffers, and p_L is the pressure at the low-pressure side of the compressor. The noise in the p_L curve results from the 50 Hz pick-up.

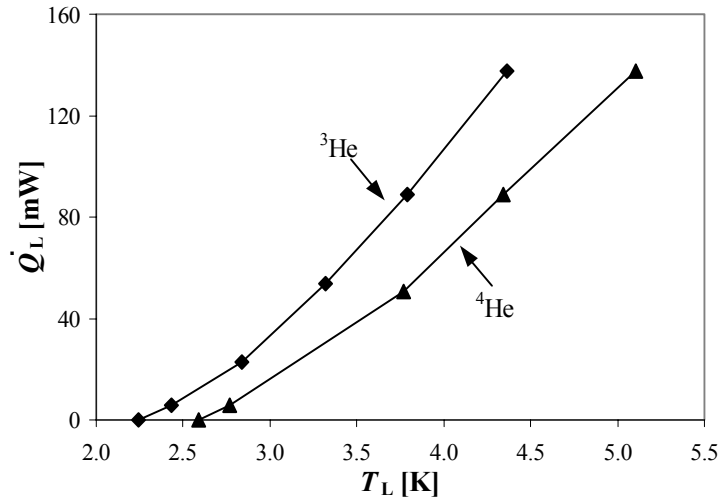


Figure 4. 20. Technical cooling powers of PTR3 with ^4He and with ^3He as functions of the cold-end temperature.

PTR3 are considerably higher than in PTR1. The comparison of PTR1 and PTR3, both using ^3He , is shown in Table 4.6.

The intrinsic cooling power of the PTR3 versus temperature is plotted in FIG. 4.21. It is as high as 225 mW at 4.2 K. The difference between the technical and the intrinsic cooling powers, discussed in paragraph 4.2.4, is illustrated in FIG. 4.22. Different values of the technical and the intrinsic cooling powers at the same temperature is caused by the thermal resistance between the heat exchanger and the gas flow.

The temperature profiles in the regenerator with ^4He and with ^3He are shown in FIG. 4.23. The settings of the orifices, the frequencies, the average pressures, and the pressure amplitudes are the same in both cases. The temperature profiles in the 2nd stage

Table 4.6. Comparison of PTR 1 and PTR 3, both using ^3He as a working fluid.

	PTR 1	PTR 3
Total volume of ^3He [liters NTP]	220	165
Input power [kW]	4	4
Frequency [Hz]	1.20	1.84
p_0 [bar]	16.46	16.55
p_{inA} [bar]	4.06	5.83
p_{t1A} [bar]	3.96	5.50
p_{t2A} [bar]	3.87	5.10
p_{t3A} [bar]	3.85	5.10
T_{L1} [K]	80.2	92.6
T_{L2} [K]	28.8	20.9
T_{L3} [K]	1.78	1.73
$\bar{\dot{Q}}_L$ at 4.2 K [mW]	80	124

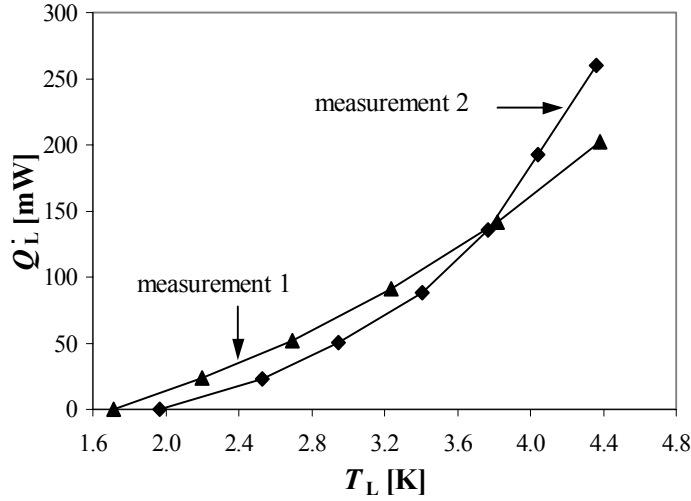


Figure 4. 21. Intrinsic cooling powers of PTR3 with ^3He versus temperature in two different measurements. In measurement 1 the PTR is adjusted for the minimum temperature. In measurement 2 the PTR is adjusted for the maximum cooling power at 4.2 K.

are almost linear and are slightly higher for ^3He than ^4He . The thermodynamical properties of ^4He and ^3He far above their critical temperatures (5.2 K for ^4He , and 3.32 K for ^3He) do not differ much. However, even a small difference can affect the DC flow, and therefore, the shape of a temperature profile. The temperature in the 3rd stage regenerator is rather flat in 2/3 of the regenerator from the cold end both for ^3He and for ^4He . Such a shape of a temperature profile matches nicely with a shape predicted in subsection 2.8.4.3 (see FIG. 2.14).

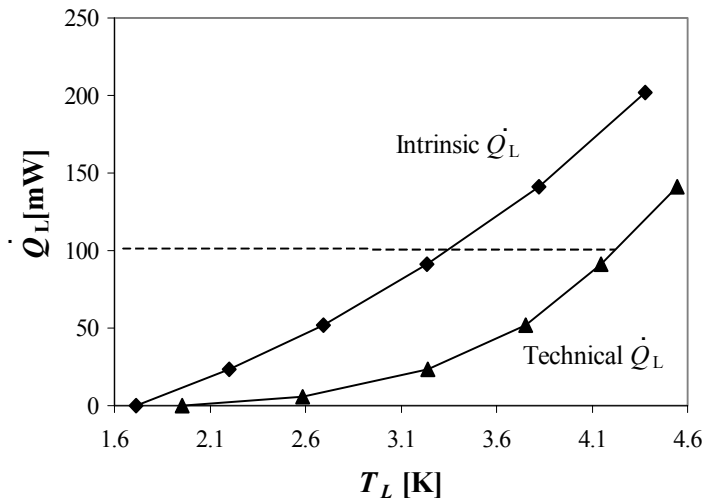


Figure 4. 22. The intrinsic and the technical cooling powers of PTR3 with ^3He as functions of temperature. The dashed line is drawn at an arbitrary value of 100 mW. The temperature of the heat exchanger, corresponding to the technical cooling power curve, is higher than the temperature of the gas (on the intrinsic cooling power curve) at the same amount of applied heat.

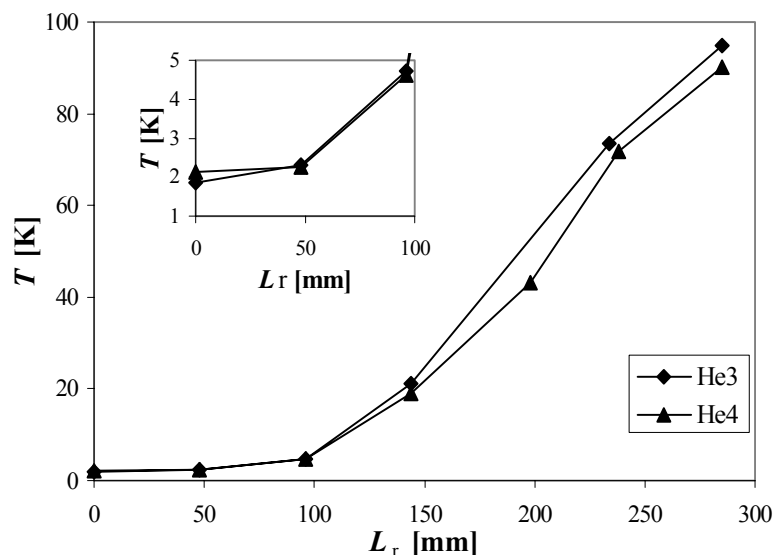


Figure 4.23. The temperature profiles in the 2nd and the 3rd stage of the regenerator with ^4He and with ^3He in PTR3.

4.5. CONCLUSIONS AND DISCUSSIONS

In this chapter we have described the performance of the three-stage PTR (PTR3), designed by scaling down of PTR1 by 50 %. The volume of the low-temperature part of the PTR3 (pulse tubes + regenerator) is as small as 0.28 liter. By scaling down the PTR1, we have reduced the necessary amount of ^3He from 220 to 160 liter NTP. Considering the liter price of ^3He , this is a great improvement. The PTR3 is very flexible and convenient for modifications. A number of experiments have been carried out with PTR3. A lowest temperature of 2.13 K has been reached with ^4He . This temperature is basically the lowest temperature, achievable by a ^4He PTR at an average pressure of 15 bar.

PTR3 is driven by 4 kW compressor. However, based on scaling, a 2 kW compressor should be sufficient for a good performance of the system. Therefore, we substituted the 4 kW compressor by a 2 kW compressor. But it turned out that the optimum combination of a frequency and a pressure amplitude could not be provided by the 2 kW compressor.

In several experiments ^4He was substituted by ^3He . However, PTR3 did not cool below 2 K. In one of the final experiments ErNi-A in the 3rd stage regenerator was replaced by ErNi-B (the difference between the materials is described in subsection 4.2.3.2.). With this change the lowest temperature of 1.73 K has been achieved. The lowest temperatures, reached with PTR3 with ^4He and with ^3He , are about the same as the temperatures, reached with PTR1. Therefore, generally speaking, scaling the system, based on one-dimensional model for the PTR, worked out very well.

From the optimization point of view one should keep in mind that the system has a very large number of variables (the frequency, the pressure amplitude, the shape of pressure variations, the composition of the regenerator, nine adjustable needle valves, construction of various components, etc.), and a rather long time is needed for each of the measurements. Therefore, the time limit for this research has not allowed us to explore

the full potential of the system. Several suggestions of improving the performance of PTR3 are given below.

As a lowest temperature of 1.73 K has been reached in one of the final experiments, there is still a possibility of bringing the lowest temperature further down simply by further adjusting the needle valves. The influence of the average pressure on the performance of PTR3 with ^3He should be studied as well together with the modification of the system geometry.

The big improvement of the performance of the PTR3 by replacing ErNi-A by ErNi-B has demonstrated how great is the importance of the thermal properties of the regenerator materials. Therefore, it would be very interesting to test various regenerator materials in PTR3. For example, GdAlO_3 , which has a high heat capacity below 4 K (see Chapter 5 for details), is very suitable for the coldest part of the 3rd stage regenerator.

In the 2nd stage regenerator we have used lead, which is rather soft material, and therefore, is difficult to pack. Once it is very well packed, it gives a high flow resistance, which results in a power loss. A substitution of lead by ErPr [3] could improve the performance of the PTR3. ErPr is easy to pack and has a higher heat capacity than lead. Therefore, if using ErPr, less material would be needed to provide the same cold-end temperature of the 2nd stage. Preliminary ^4He experiments¹, in which lead in the 2nd stage regenerator of PTR3 has been replaced by ErPr (1:1 replacement), have been carried out. The cold-end temperature of the 2nd stage remained the same, and the temperature in the 3rd stage regenerator showed a tendency to decrease (See FIG. 4.24). As the next step the amount of ErPr could be decreased up to 50%, and ^3He experiments with the new arrangement of the regenerator should be carried out.

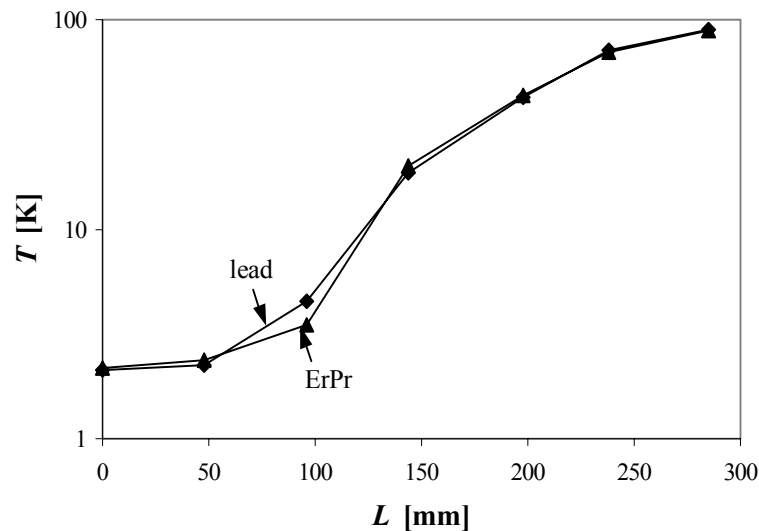


Figure 4. 24. The temperature profiles in the 2nd and the 3rd stage of the regenerator with lead and with ErPr in the 2nd stage.

¹ These experiments have been done in collaboration with Atlas Scientific, NASA-ARC, USA.

REFERENCES

1. Gifford, W.E., and Longworth, R. C., "Surface heat pumping", *Advances in Cryogenic Engineering* **11**, 1966, pp.171-179.
2. Vermeulen, K., "A helium-helium heat exchanger and an introductory investigation of a 20 K pulse tube refrigerator", Master thesis, Eindhoven University of Technology, 2000.
3. Gschneidner, K. A., Pecharsky, A. O., and Pecharsky, V. K., "Ductile, high heat capacity, magnetic regenerator alloys for the 10 to 80 K temperature range", *Cryocoolers* **11**, 2001, pp/ 985-991.

CHAPTER 5.

HEAT CAPACITIES AND MAGNETIC MOMENTS OF POTENTIAL REGENERATOR MATERIALS AT LOW TEMPERATURES¹

As it has been shown in the previous chapters, the regenerator is one of the most important components of a PTR. The regenerator material should have a high heat capacity in order to provide an efficient operation of a PTR. Up till recent times one of the main obstacles for reaching low temperatures has been the inefficiency of most of the regenerator materials below 15 K. This barrier can be overcome by using rare-earth magnetic materials in the coldest part of the regenerator. These materials have magnetic transitions below 15 K, accompanied by a significant rise in the heat capacity. There are no existing theories or computer methods, which predict the transition temperature and the heat capacity of an alloy or intermetallic compound. To some extent finding a new regenerator material is still a matter of intuition and trial and error. Therefore, a large variety of materials has to be investigated on the way to discover a better material for regenerators.

In this chapter, we will discuss the measurement results of the magnetic moments and heat capacities of a group of rare-earth oxide magnetic materials with the magnetic transitions below 4 K. We also give the estimation of an optimum quantity of a regenerator material for the best performance of the regenerator and the results of a preliminary experiment with GdAlO_3 in the coldest part of the 3rd stage regenerator.

5.1. SELECTION OF MAGNETIC MATERIALS

In 2000, T. Numazawa proposed GdAlO_3 as a potential regenerator material and named it GAP [1]. This material is a perovskite with an orthorhombic structure of the unit cell (see FIG. 5.1). It has a high peak in the heat capacity around 3.8 K, originating from a magnetic phase transition to the anti-ferromagnetic state.

In parallel with the work of Numazawa GdAlO_3 has been developed at the Institute of Material Science of the University of Tsukuba, Japan. In collaboration with this Institute, as well as with the Atomic Energy Research Institute of Nihon University, Japan, we have investigated the heat capacities and the magnetic moments of GdAlO_3 and a group of GdAlO_3 related materials. For this purpose several samples of rare-earth magnetic materials were developed by consistently varying A- and B-sites in the general

¹ This chapter is based on the article [1], published in Cryogenics.

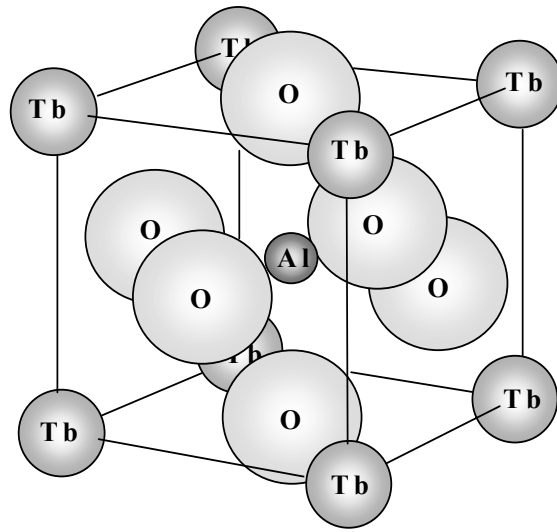


Figure 5. 1. An ideal perovskite structure (on the example of TbAlO_3). The general formula is ABO_3 , where A is a rare-earth ion, B is a metal ion.

formula of a perovskite ABO_3 (FIG. 5.1). In this formula A is a rare-earth ion and B is a metal ion. The magnetic heat capacity of a rare-earth element is a function of the entropy change due to the order-disorder magnetic phase transition. According to the magnetic entropy data for the rare earth elements [2], a number of the heavy lanthanides, such as Gd, Tb, Dy, Ho, Er, and Yb, are expected to have a rather high heat capacity (FIG. 5.2). The total heat capacity is the sum of the magnetic and lattice heat capacities. The lattice contribution to the heat capacity depends on the chemical composition of a material as

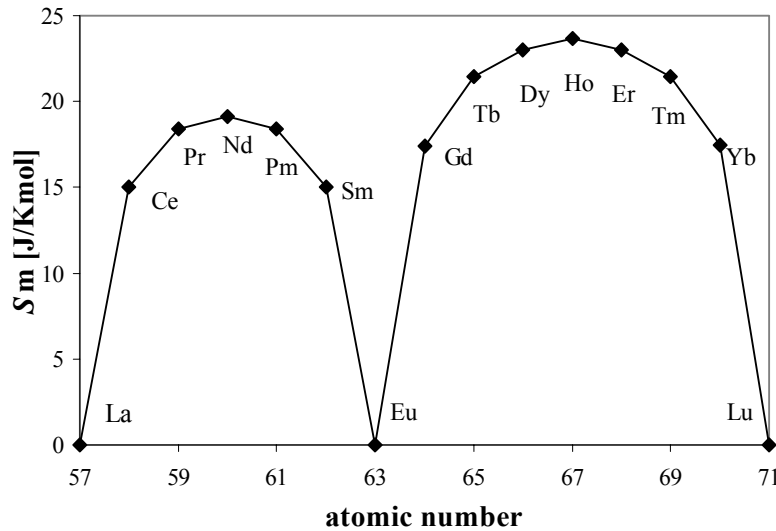


Figure 5. 2. The molar magnetic entropies of the lanthanide elements as a function of the atomic number.

well as on the temperature and the crystal structure. Therefore, the correct choice of an alloying metal can improve the heat capacity significantly. In our research we investigated Al, Fe, and Ga as the B components.

5.2. THE SAMPLES PREPARATION AND THEIR MAGNETIC MOMENTS

All samples were prepared at the University of Tsukuba. Their magnetic moments were measured there as well. Here, we will shortly describe the preparation procedure and give the results of the measurements of the magnetic moments.

5.2.1. Preparation procedure

As a first step fine powders of A- and B-site component oxides were mixed. The A- and B-site materials had 99.99 wt. % purity. After that, the mixture was placed into a tube furnace of the three-zone type. The homogeneity of the furnace was about ± 0.2 K per 100 mm. The mixed powder was calcined at 800°C for 12 hours in air. Pellets were formed by applying 500 MPa pressure. The second sintering was performed at a temperature between 1200 and 1300°C for 12 hours in air. The samples were then analyzed, using X-ray diffraction and electron-probe-microscope analysis. All the samples were confirmed to be single phase with a perovskite unit-cell structure.

5.2.2. Magnetic moments measurements

The magnetic properties were measured using a SQUID magnetometer [3]. The results of the measurements are presented in Figures 5.3-5.6. Figure 5.3 represents the

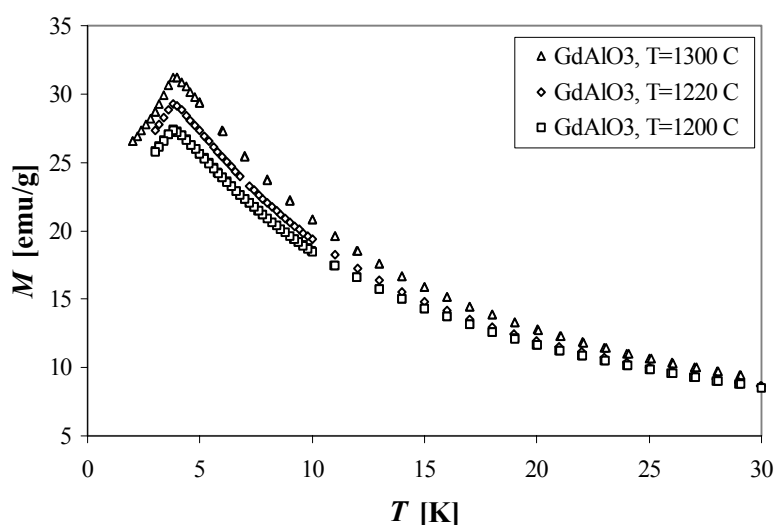


Figure 5. 3. Magnetic moments of three samples of GdAlO_3 , prepared at different sintering temperatures.

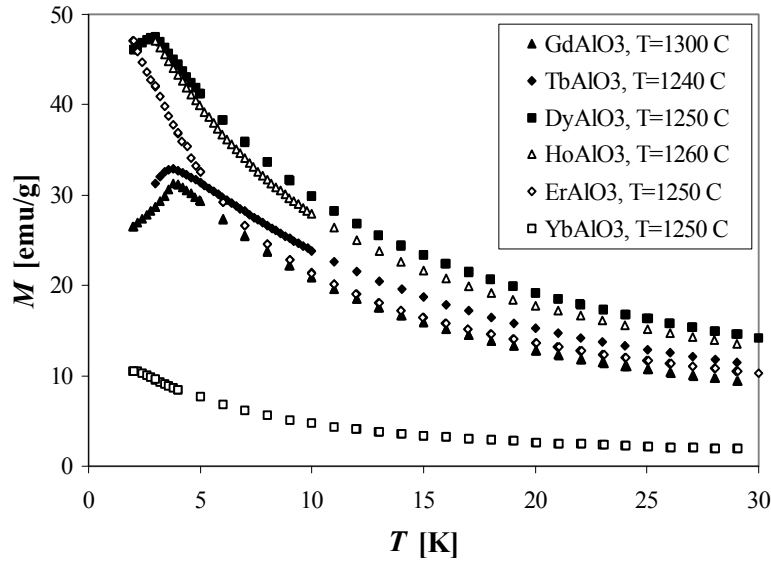


Figure 5. 4. Magnetic moments of several samples of rare-earth orthoaluminates, obtained by consistently changing the A component.

magnetic moments of three samples of GdAlO_3 sintered at different temperatures. The peaks of the magnetic moments increase with the increasing of the sintering temperature.

Figure 5.4 demonstrates the A-site substitution in the rare-earth orthoaluminates. As aluminum is non-magnetic, the magnetic behavior of the magnetic moments of rare-earth aluminates is due to the lanthanide elements. The magnetic entropy of heavy lanthanides increases from Gd to Ho, where it is at the maximum, and then it decreases again (see FIG. 5.2). As we can see from FIG. 5.4, the magnetic moments increase from GdAlO_3 to

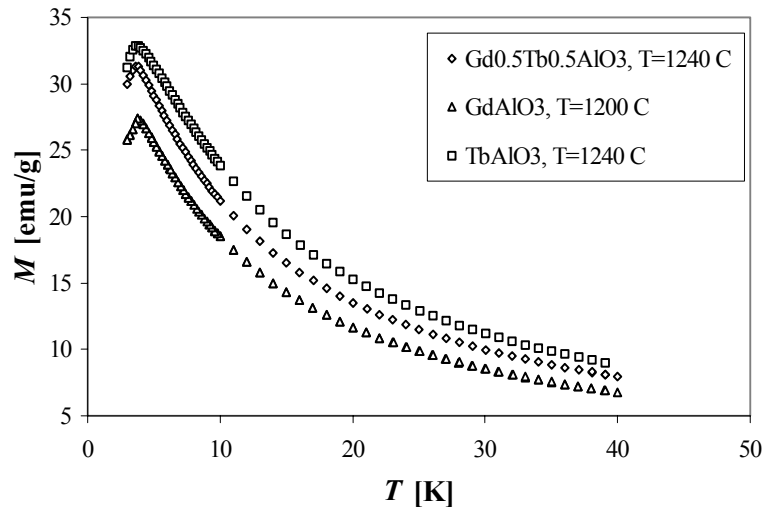


Figure 5. 5. Magnetic moments of materials, prepared by partial substitution of Gd with Tb according to the general formula $\text{Gd}_{1-x}\text{Tb}_x\text{AlO}_3$.

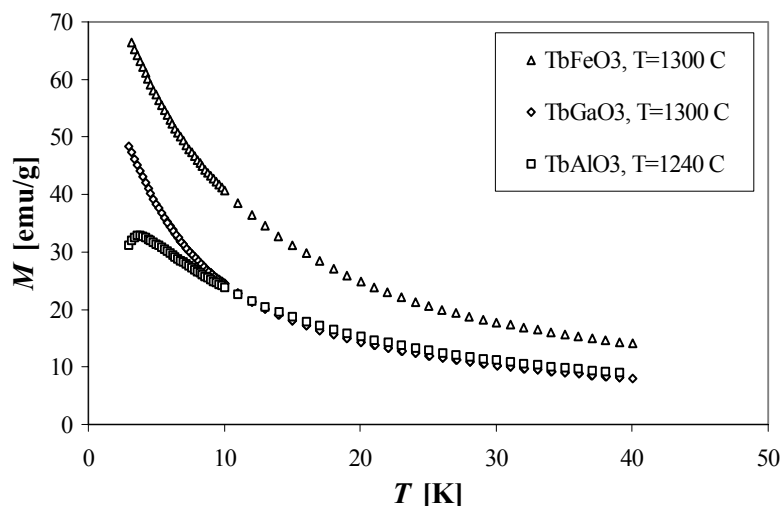


Figure 5. 6. B-site substitution in perovskites with Tb as a rare-earth component.

DyAlO₃. These three orthoaluminates exhibit magnetic transitions around 4 K. However, HoAlO₃ does not go through the magnetic transition above 3 K. Its magnetic moment has almost the same values as DyAlO₃ below 10 K. From HoAlO₃ to YbAlO₃ the magnetic moments decrease. ErAlO₃ does not show a transition above 2 K. YbAlO₃ shows a tendency for a transition around 2 K.

Figure 5.5 shows the results of the partial substitution of Gd by Tb in GdAlO₃. The magnetic moment increases with the increase of the concentration of Tb.

The substitution of the B site was realized on the example of a rare-earth perovskite with Tb as the rare-earth ion (see FIG. 5.6). There were no magnetic transitions in TbFeO₃ and in TbGaO₃ above 3.2 K.

5.3. HEAT CAPACITY MEASUREMENTS

5.3.1. The experimental set-up and technique

The heat-capacity measurements are carried out using an adiabatic calorimeter². The schematic drawing of the low-temperature part of the set-up is shown in FIG. 5.7. The sample is attached to a copper sample holder by means of vacuum grease. A carbon-glass resistance thermometer and a heater are attached to the sample holder as well. The heater is made of 50-μm manganine wire of 120 cm long, wrapped around a copper holder. The heater holder is soldered to the sample holder with woods metal. The heating power is measured by the four-wire method. To prevent uncontrolled dissipation, we used superconducting wires for the electrical connections. The sample holder is suspended on a frame with nylon threads in order to minimize heat leaks. The sample and the sample holder are cooled by means of a mechanical heat switch, which provides thermal contact

² The insert of the calorimeter has been developed by K. Kopinga and co-workers.

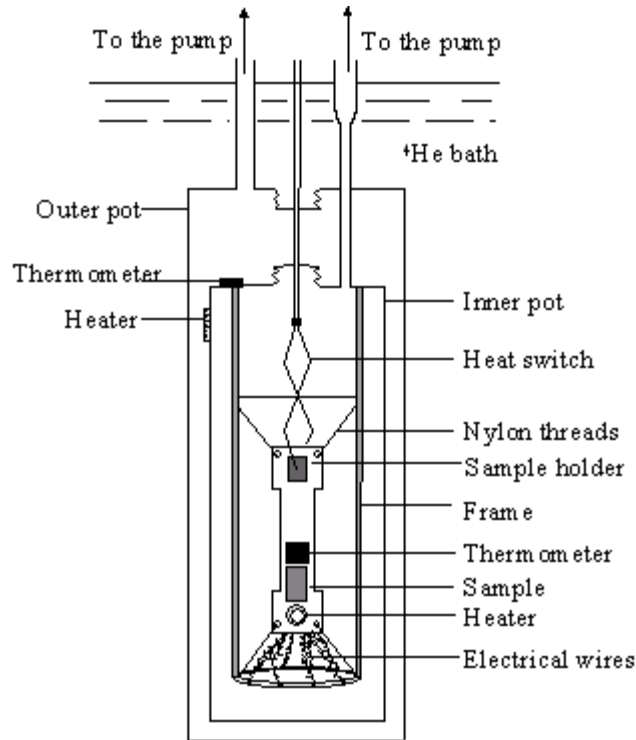


Figure 5. 7. The low-temperature part of the experimental set-up. A sample, a thermometer, and a heater are attached to a copper sample holder. The sample is cooled by means of the mechanical heat switch, providing an indirect contact of the sample with the helium bath. The sample holder is suspended on a frame with nylon threads and placed into the inner pot. A thermometer and a heater are placed on the surface of the inner pot, creating a thermal shield. The inner pot is surrounded by the outer pot, which is immersed in the helium bath.

with the helium bath. In this way we avoid using helium contact gas for cooling the sample, which can cause errors. The heat switch is operated from room temperature by compressed air.

The sample holder, with the attached elements, is placed in an inner vacuum pot, which is pumped down to 10^{-4} Pa while the system is at room temperature. A thermometer and another heater are glued on the surface of the inner pot, thus creating a thermal shield. The temperature of the inner pot is regulated to a value close to the sample temperature, thus reducing the heat leak significantly. The inner pot is surrounded by an outer pot, which is immersed in liquid helium. The temperature of the helium bath is lowered down to 1 K by pumping. The space between the inner and the outer pots is filled with helium contact gas during the cool-down of the system. After the system is cooled to a desired value, the contact gas is pumped out.

The heat capacity measurements are performed by the adiabatic heat-pulse method. During a certain time interval Δt , typically 20 seconds, a well-defined amount of heating power Q is supplied to the system, consisting of the sample holder, the sample, the thermometer, the heater, and the connecting wires. The heat causes a rise of the temperature of the system ΔT , which in our case results in a decrease of the resistance of

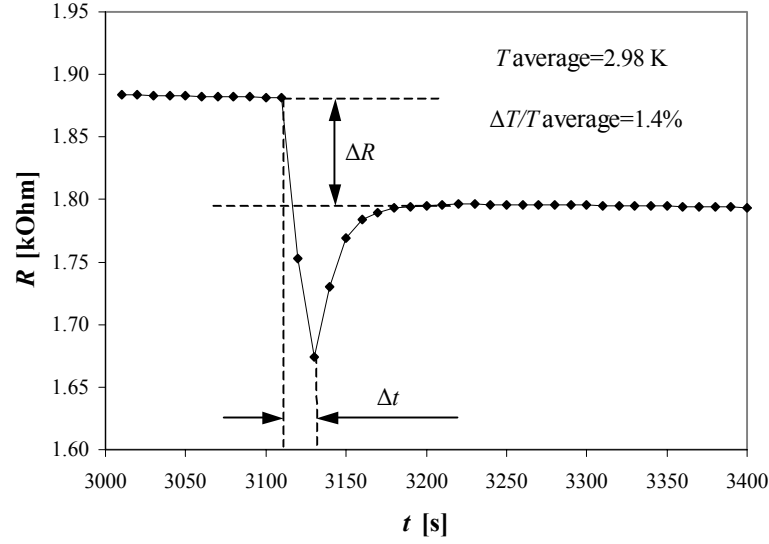


Figure 5. 8. A typical measurement curve of the thermometer resistance versus time at the average temperature of a measurement T_{ave} . The resistance variation ΔR corresponds to the temperature difference ΔT , caused by a heat pulse. The value of $\Delta T / T_{\text{ave}}$ varies between 1 and 5%. Around the peak in the heat capacity $\Delta T / T_{\text{ave}}$ is less than 1%. The duration of a heat pulse Δt is typically 20 seconds.

the thermometer (see FIG. 5.8). For small temperature changes ΔT the heat capacity of the system, C_{sys} , follows from the definition of the heat capacity

$$C_{\text{sys}}(T) = \frac{Q}{\Delta T} . \quad (5.1)$$

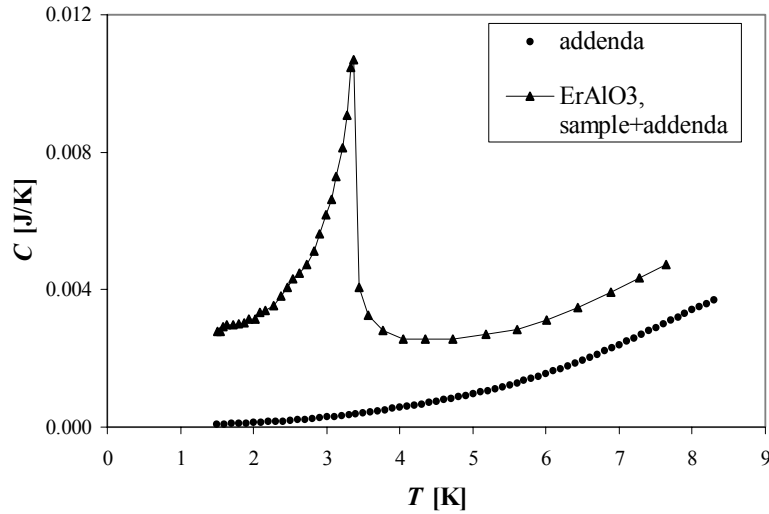


Figure 5. 9. The addenda heat capacity C_{ad} and the heat capacity of the system C_{sys} , including the heat capacity of a sample, C_{sam} , and C_{ad} . In this example ErAlO_3 is chosen for the demonstration of the contribution of C_{ad} . Note, that ErAlO_3 has a small heat capacity, compared to other samples.

The heat capacity of the addenda (the sample holder, the thermometer, the heater, and the connecting wires) C_{ad} was measured in a separate experiment (see FIG. 5.9). In FIG. 5.9 the heat capacity of the addenda is compared with the heat capacity of ErAlO_3 , which has a relatively small heat capacity, compared to other samples.

The heat capacity of the sample follows from

$$C_{\text{sam}} = C_{\text{sys}} - C_{\text{ad}}. \quad (5.2)$$

The estimated accuracy of C_{sam} ranges from 2% at the peak to 7% in the temperature regions, where C_{sam} is small.

5.3.2. Results

First, we measured three samples of GdAlO_3 , prepared at different sintering temperatures (see FIG. 5.10 and compare to FIG. 5.3). The three curves coincide over most of the temperature range. The specific heat peak of the sample, sintered at 1300°C , is 13 % higher than the peak of the sample, sintered at 1200°C , and 11 % higher than the peak of the sample, sintered at 1220°C . Therefore, the peak in the specific heat increases with increasing the sintering temperature. This agrees with the magnetic moments measurements (FIG. 5.3).

The A-site substitution results are shown in FIG. 5.11 (compare FIG. 5.4). All samples went through transitions within the investigated temperature region. Note, that the magnetic moment of ErAlO_3 does not show a transition above 2 K. The shapes of the curves, except for HoAlO_3 , which has a rather broad maximum (see FIG. 5.12), are similar. In contrast to the magnetic moments measurements, the peaks of the specific

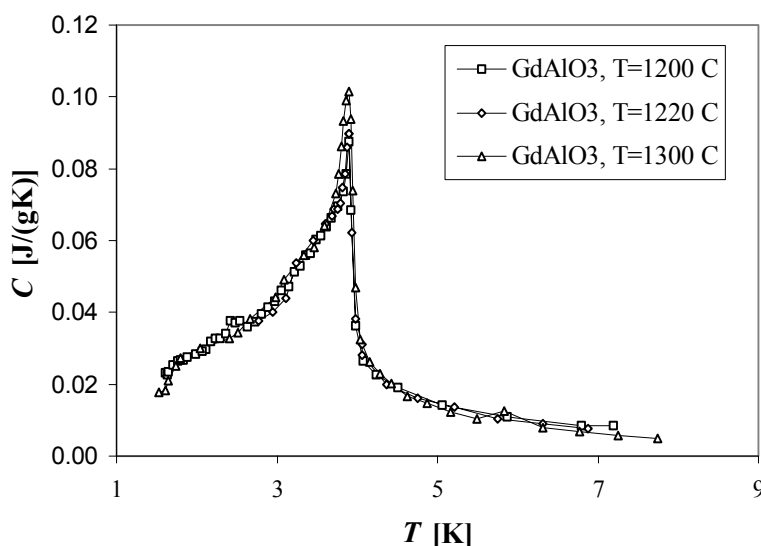


Figure 5. 10. Specific heats of three samples of GdAlO_3 prepared at different sintering temperatures. At the peak value the specific heat of the sample, sintered at 1300°C is 13% higher than the specific heat of the sample, prepared at 1200°C , and 11% higher than the sample, prepared at 1220°C .

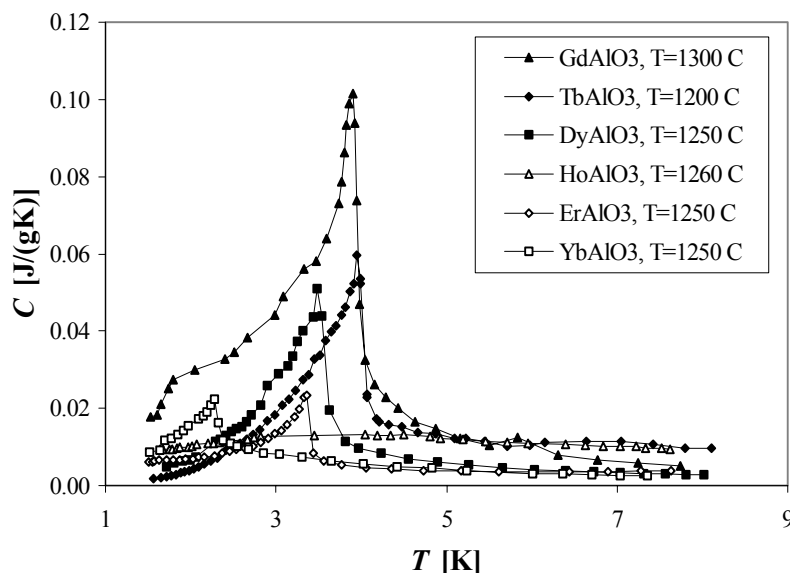


Figure 5. 11. Specific heats of several samples of rare-earth orthoaluminates, obtained by consistently changing the A component. The peaks of the specific heats decrease from GdAlO_3 to HoAlO_3 , after which they start increasing again. The peaks of ErAlO_3 and YbAlO_3 have nearly the same value, but at different transition temperatures. Note, that specific heat of GdAlO_3 , prepared at 1200°C , is used in the figure. (There is only 2% difference between the specific heats of the samples of GdAlO_3 , prepared at 1200°C and 1220°C (see FIG. 5.8).)

heats of the rare-earth orthoaluminates decrease from GdAlO_3 to HoAlO_3 , after which they increase again. The peaks of ErAlO_3 and YbAlO_3 have nearly the same value, but at different transition temperatures.

Figure 5.13 (compare to FIG. 5.5) demonstrates the partial substitution of Gd in GdAlO_3 with Tb. In this case the specific heat maxima decrease with increasing of x in

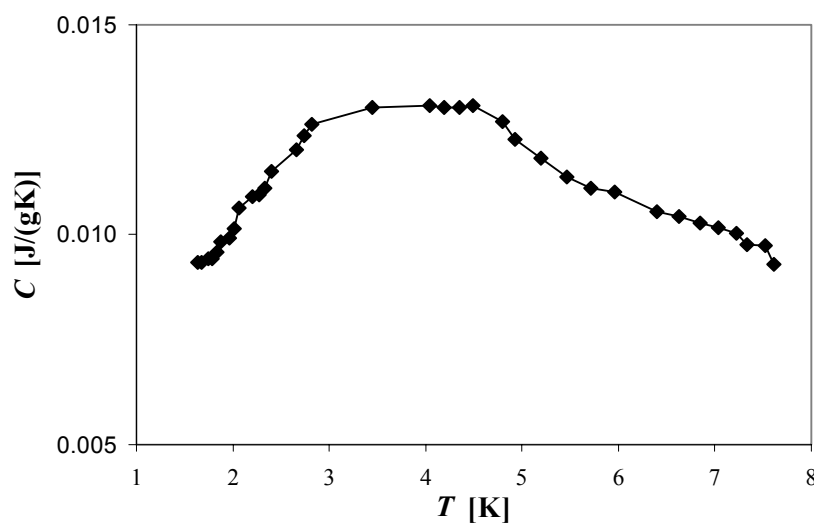


Figure 5. 12. Specific heat of HoAlO_3 , prepared at 1260°C .

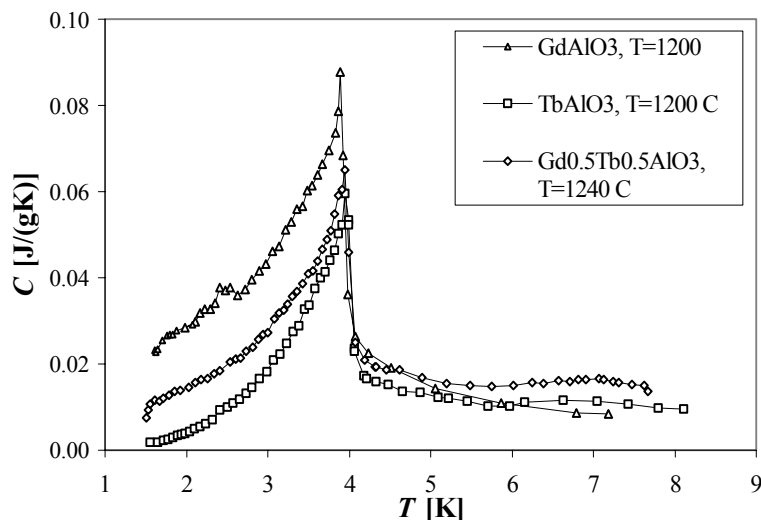


Figure 5. 13. Specific heats of materials, prepared by partial substitution of Gd with Tb according to the general formula $\text{Gd}_{1-x}\text{Tb}_x\text{AlO}_3$. The specific heat below the transition temperature decrease with the increase of Tb concentration.

the general formula $\text{Gd}_{1-x}\text{Tb}_x\text{AlO}_3$. In the magnetic moments measurements the maxima increase with increasing of Tb concentration.

The results of the specific heat measurements of rare-earth perovskites with Tb as the rare-earth ion and Al, Ga, and Fe as the B-site are represented in FIG. 5.14 (compare to FIG. 5.6). We found, that TbFeO_3 exhibited a high peak in the specific heat at 3.32 K. The peak is rather sharp, compared to TbAlO_3 . This can be explained by the fact, that both A and B ions in TbFeO_3 are magnetic, while Al in TbAlO_3 is non-magnetic. So in

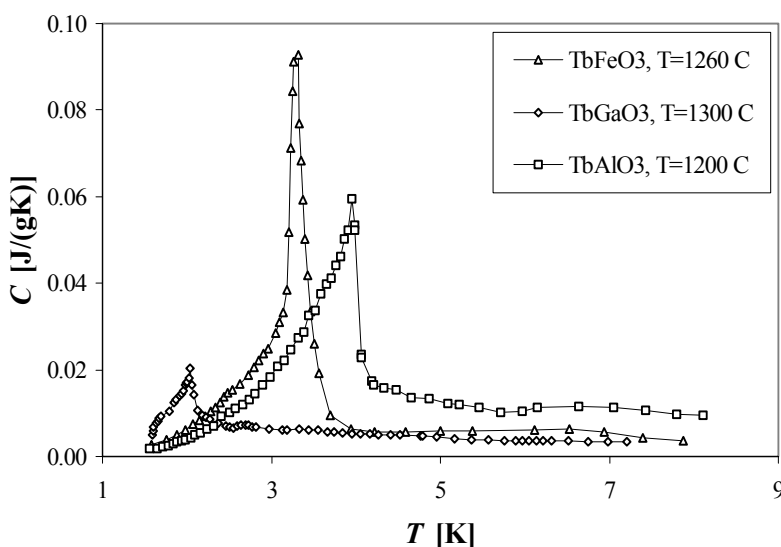


Figure 5. 14. B-site substitution in perovskites with Tb as a rare-earth component. Note the high peak of TbFeO_3 at 3.32 K.

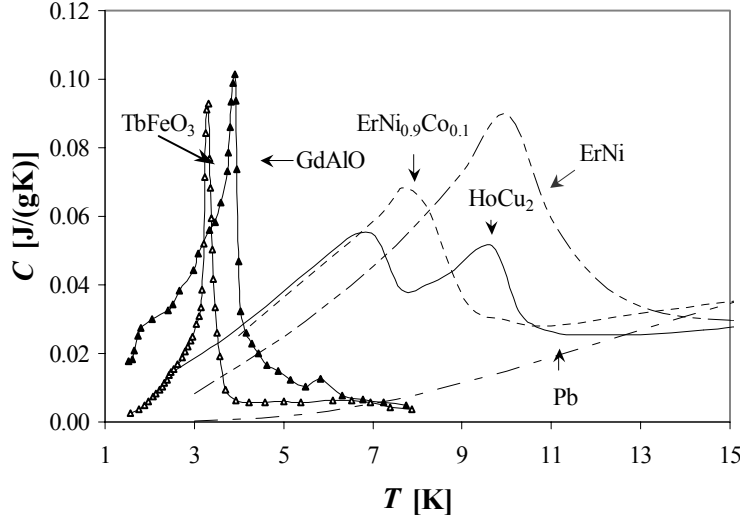


Figure 5. 15. Specific heats of TbFeO₃, GdAlO₃ and several commonly used regenerator materials. Note, that the samples of GdAlO₃ and TbFeO₃ with the highest measured specific heats are used (GdAlO₃, T=1300°C, and TbFeO₃, T=1260°C).

TbAlO₃ the only magnetic contribution comes from the rare-earth ion.

Figure 5.15 shows the specific heats of TbFeO₃, GdAlO₃ and several commonly used regenerator materials. So far GdAlO₃ remains the best material for temperatures below 4 K. However, at the peak value the specific heat of TbFeO₃ is 1.7 times larger, than the specific heat of GdAlO₃ at the same temperature. Thus, TbFeO₃-related materials could be considered as good candidates for further investigations as potential regenerator materials.

5.4. THE OPTIMUM QUANTITY OF REGENERATOR MATERIAL

A quantity of a regenerator material, needed to provide the best heat storage in the regenerator, can be determined from the expression for the regenerator dynamics, given by equation 2.70. For an ideal regenerator (zero pressure drop, large filling factor, perfect heat exchange between the gas and the regenerator material), we can rewrite equation 2.70 as

$$C_r \frac{\partial T}{\partial t} = -j C_p \frac{\partial T}{\partial l} - \frac{\partial q}{\partial l}. \quad (5.3)$$

It can be further simplified with the minus-one rule to

$$\left(\frac{\partial l}{\partial t} \right)_T = v_T(T) = j \frac{C_p}{C_r} + \frac{1}{C_r} \frac{\partial q}{\partial l} \bigg/ \frac{\partial T}{\partial l}, \quad (5.4)$$

where $v_T(T)$ is a velocity of the temperature profile in the regenerator. The first term on the right hand side describes the velocity of the temperature profile due to the heat

exchange between the gas and the matrix and the second term is a contribution due to the thermal conduction.

The molar flow density is

$$j = \frac{\dot{n}}{A_r}, \quad (5.5)$$

where \dot{n} is the molar flow rate and A_r is the cross-sectional area of the regenerator. With the molar flow rate $\dot{n} = \dot{V} / V_m$, where \dot{V} is the volume flow rate, the velocity of the gas can be written as

$$v_g = j V_m. \quad (5.6)$$

Now we can describe the velocity of the temperature profile in the regenerator as follows

$$v_T = v_g \frac{C_g}{C_r} + \frac{1}{C_r} \frac{\partial q}{\partial l} \bigg/ \frac{\partial T}{\partial l}, \quad (5.7)$$

where $C_g = C_p / V_m$ is the volumetric heat capacity of the gas. If we neglect the thermal conduction in Equation 5.7, it reduces to

$$v_T = v_g \frac{C_g}{C_r}. \quad (5.8)$$

The volume of a regenerator material, needed to provide the best heat-storage condition, can be determined by multiplying equation 5.8 with A_r and by integrating it over half a cycle

$$V_r = \frac{C_g}{C_r} V_{t/2}, \quad (5.9)$$

where $V_{t/2}$ is the volume of the gas, passing V_r during half a cycle, equal to

$$V_{t/2} = A_t \int_0^{tc/2} v_g dt, \quad (5.10)$$

where A_t is the cross-sectional area of the tube.

The calculations above can be illustrated if we consider a part the regenerator with the length L to be completely filled with GdAlO_3 (see FIG. 5.16). We assume the gas to enter the GdAlO_3 part of the regenerator with a temperature higher than the peak temperature of GdAlO_3 ($T_H > 3.9$ K), at which the heat capacity of GdAlO_3 is much smaller than the heat capacity of helium, and to go out of the GdAlO_3 regenerator with the temperature lower than T_{peak} . In order to avoid mathematical complications in calculating the temperature profile we will concentrate on a section of the GdAlO_3 regenerator with a certain length l , so that $l < L$. We will assume, that helium enters this regenerator part with $T = 6$ K and goes out with a temperature close to the lambda-

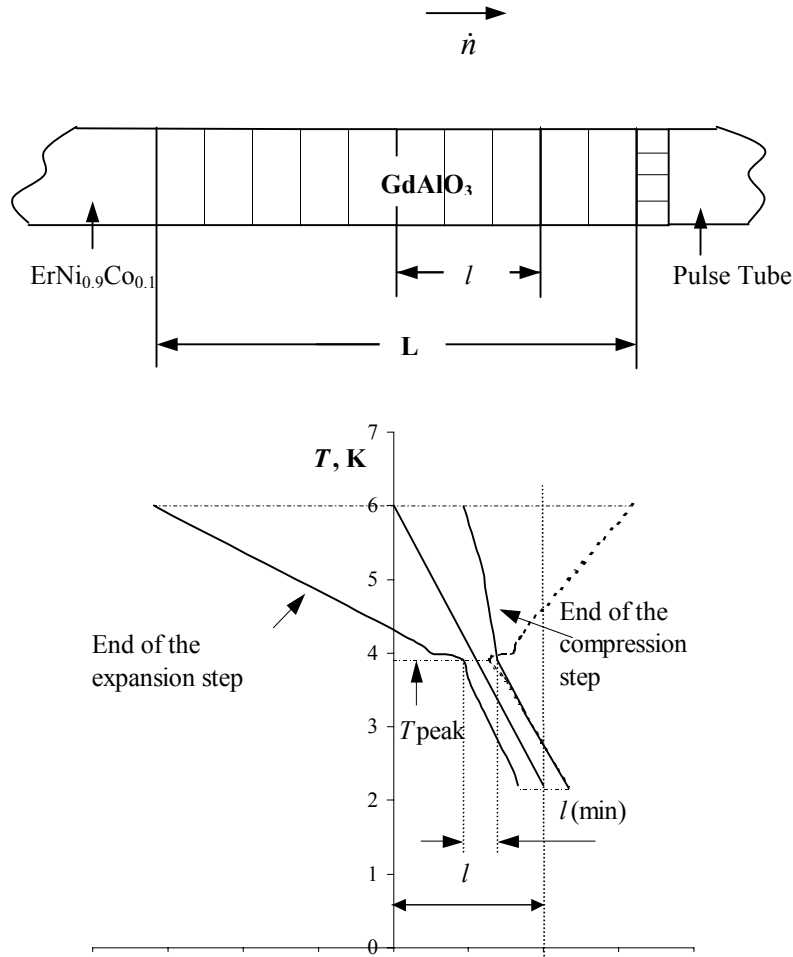


Figure 5. 16. Schematic representation of the temperature profile in a part of the regenerator, filled with GdAlO_3 . The temperature versus position graph shows how far a certain temperature travels inside the regenerator. The middle solid line represents a hypothetical temperature profile in the middle of half a cycle inside a section of the GdAlO_3 regenerator with the length l . Here the temperature varies between 2.2 and 6 K. Note, that the choice of the temperatures is arbitrary. The left and the right solid curves represent respectively the end of the expansion step and the end of the compression step. The dotted line shows the end of the compression step according to the mathematical model. l_{min} is the displacement of the peak temperature during a cycle.

temperature. The choice of the entering temperature of the gas is rather arbitrary. Any other temperature above T_{peak} could be used as well.

A schematic representation of the temperature profile in the regenerator is plotted in FIG. 5.16. The middle solid line represents the assumed temperature profile in the GdAlO_3 regenerator section in the middle of half a cycle. According to equation 5.8 the velocity of $T=6$ K will be rather large. That means, that this temperature will travel a long distance inside the regenerator during half a cycle. At the peak temperature the situation is different. The heat capacity of GdAlO_3 is considerably larger than the heat capacity of helium. So the point with the peak temperature will be nearly fixed in the regenerator;

and the motion of this temperature during the cycle will be very small. It is equal to the minimum length of the layer of GdAlO_3 in the regenerator, l_{\min} .

The left curve in FIG. 16 represents the end of the expansion step. The right curve is the end of the compression step. The dotted line is the result of the calculation of the end of the compression step with equation 5.8. The positive temperature gradient, appearing in the curve, shows, that in this part of the cycle the mathematical model is not valid, as a result of it has no physical meaning. It is due to the fact, that the thermal conduction term in equation 5.7 has been neglected.

Figure 5.16 is an alternative representation of the comparison of heat capacities of a gas and a regenerator material. This form of representation of heat capacities also gives us an idea about the amount of the material, needed for good efficiency of the regenerator. From FIG. 5.16 we can see that above the peak temperature one needs a very large quantity of GdAlO_3 for sufficient heat storage. And that would mean the increase of the regenerator volume and the increase of the pressure drop in the regenerator. For GdAlO_3 the best heat storage condition will take place at the peak of the heat capacity at 3.9 K.

5.5. PRELIMINARY ^4He TEST WITH GdAlO_3 IN THE 3rd STAGE REGENERATOR OF PTR3

The 3rd stage regenerator of PTR3, described in Chapter 4, consists of two layers. Half of it is filled with ErNi at the warm end; and the other half is filled with $\text{ErNi}_{0.9}\text{Co}_{0.1}$. We have replaced a part of $\text{ErNi}_{0.9}\text{Co}_{0.1}$ by GdAlO_3 . The minimum volume of GdAlO_3 for the best heat storage condition can be calculated by equation 5.9. For the cross-sectional area of the 3rd stage regenerator of PTR3 of 1.5 cm^2 , the amplitude of the molar flow of 0.5 mol/s , and the average pressure of 15 bar the minimum volume of GdAlO_3 is typically 7 cm^3 . The results of the test have been promising. The lowest temperature of PTR3 has decreased from 2.31 K to 2.24 K.

5.6. CONCLUSIONS

In this chapter, we have presented the results of the research, aimed on finding new regenerator materials for sub-4 K cryocoolers. A group of rare-earth oxides has been studied in the temperature region between 1.5 and 10 K. The magnetic moments and the specific heats of several samples of rare-earth oxides have been measured. All the samples have exhibited rather high magnetic moments; and most of them have gone through the magnetic transitions within the investigated temperature region. Therefore, the materials are interesting for further investigations as potential regenerator materials. The specific heat measurements have shown that all the investigated materials exhibited maxima in their specific heats between 2 and 4 K. Nevertheless, the specific heats of most of the materials are rather low, even at the peak values. Thus, most of the investigated materials cannot be used in the regenerator effectively. However, two of them, GdAlO_3 and TbFeO_3 , have demonstrated interesting results. Both materials have fairly large specific heats below 4 K, compared to other conventional regenerator

materials. The peak of TbFeO_3 is rather sharp. Therefore, GdAlO_3 , with its higher and broader peak, is still the best choice for sub-4 K regenerators. However, TbFeO_3 -related materials can be considered as good candidates for further research as potential regenerator materials.

We have also treated the subject of the optimum quantity of regenerator material for the best performance of the regenerator. In case of an ideal regenerator this optimum quantity is proportional to the ratio of the volumetric heat capacities of the gas and the material and the amount of gas, passing a certain section of the regenerator during a half a cycle.

We have performed a preliminary ^4He test with PTR3, substituting a part of $\text{ErNi}_{0.9}\text{Co}_{0.1}$ with GdAlO_3 in the coldest part of the third-stage regenerator. The lowest temperature of PTR3 has decreased from 2.31 K to 2.24 K.

REFERENCES

1. Tanaeva, I. A., Ikeda, H., Bokhoven, L. J. A. van, Matsubara, Y., and Waele, A. T. A. M. de, "Heat capacities and magnetic moments of potential regenerator materials at low temperatures", *Cryogenics* **43**, 2003, pp. 441-448.
2. Numazawa, T., Arai, O., Sato, A., Fujimoto, S., Oodo, T., Kang, Y.M., Yanagitani, T., "New regenerator material for sub-4 K cryocoolers", *Cryocoolers* **11**, 2001, pp. 465-473.
3. Gschneidner, Jr., K.A., Pecharsky, A.O., Pecharsky, V.K., "Low temperature cryocooler regenerator materials", *Cryocoolers* **12**, 2003, pp. 457-465.
4. Ikeda, H. et al, Magnetic property of oxide magnetic materials for regenerator, Proceedings of the 66th Meeting on Cryogenics and Superconductivity, Japan, 2002, to be published.

CHAPTER 6.

SUPERFLUID VORTEX COOLER

A superfluid vortex cooler (SVC) is a combination of a fountain pump and a vortex cooler. A pressure difference is created in the fountain pump. This pressure difference is then used in the vortex part to activate the cooling process. At saturated vapor pressure the vortex cooler is capable of reaching temperatures as low as 0.75 K [1, 2]. At pressures close to the melting pressure the temperature can be brought down to 0.65 K [3]. As the SVC operates only below the lambda temperature (2.17 K), it has to be precooled e.g. by a liquid-helium bath or a cryocooler. The SVC is a closed-cycle cooler. To cause the flow circulation in the SVC, a certain amount of heat has to be supplied to the fountain pump. This heat has to be removed by a cryocooler or by a helium bath. In the case of a cryocooler the heat, supplied to the SVC, increases the precooling temperature, which has a negative effect on the coldest temperature of the SVC. If a liquid-helium bath is used as a precooler, the precooling temperature of the SVC can be fixed.

In these experiments the SVC has been precooled by pumped liquid helium to temperatures between 1.2 and 1.7 K. The SVC is designed to be convenient for modifications. In the first measurements we have optimized the SVC for the lowest temperature. Later on we concentrated on reducing the input heating power. This is very useful for future integration of the SVC with a cryocooler, e.g. a pulse-tube refrigerator. We have investigated the influence of the base temperature and overall pressure on the cooler performance.

The goal of this research is to prepare the SVC for the integration with the PTR in order to prove the principle. This work should not be considered as a systematic research of superfluid vortex coolers in general.

6.1. OPERATION PRINCIPLE OF THE SVC

6.1.1. Fountain effect

HeII can be considered as a mixture of two components: a superfluid component, with the density ρ_s , and a normal component, with the density ρ_n (FIG. 6.1). So we can write

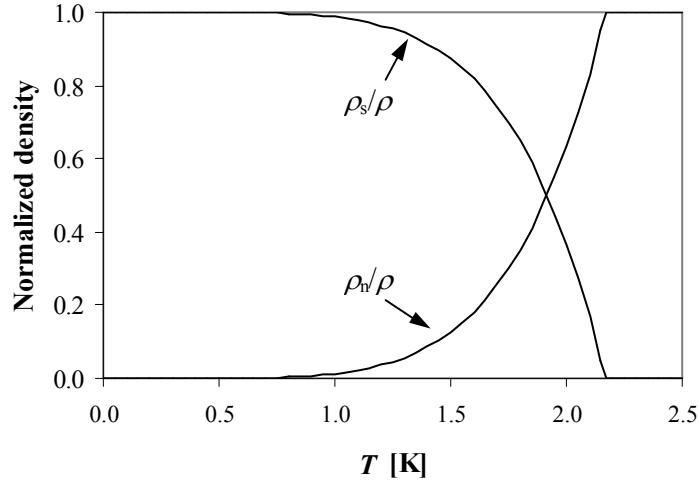


Figure 6. 1. Normalized normal and superfluid densities in HeII as functions of temperature.

$$\rho = \rho_n + \rho_s. \quad (6.1)$$

The empirical expression for ρ_n is

$$\rho_n = \rho_0 T^{\alpha_1}, \quad (6.2)$$

where ρ_0 and α_1 are the empirical constants. At saturated vapour pressure (SVP) $\rho_0=1.58 \text{ kg}/(\text{m}^3 \text{ K}^{\alpha_1})$, and $\alpha_1=5.72$. With the increase of the pressure ρ_0 slightly increases, while α_1 goes down.

The superfluid carries no entropy and has no viscosity, whereas the normal component carries all the entropy of the fluid and behaves as an ordinary viscous fluid. Therefore, the flow of the normal component is driven by a pressure difference and is given by

$$\Delta p = \eta_n Z \dot{V}_n, \quad (6.3)$$

where η_n is the viscosity of normal helium, Z is a geometrical factor, and \dot{V}_n is the volume flow of the normal component. The equation for motion of the superfluid component is

$$M \frac{d\vec{v}_s}{dt} = -\vec{\nabla}\mu, \quad (6.4)$$

where $\vec{\nabla}\mu$ is the gradient of the chemical potential of ^4He per mol, M is the molar mass of ^4He , and \vec{v}_s is the velocity of the superfluid component. Equation 6.4 is valid only in a certain region of the (v_n, v_s) plane, when v_n and v_s are below certain critical values [4, p.77].

We will give a short explanation of the fountain effect. Figure 6.2 illustrates two reservoirs filled with helium and connected by the superleak. The superleak is just a tube, filled tightly with fine powder. The superfluid component has the ability to flow through

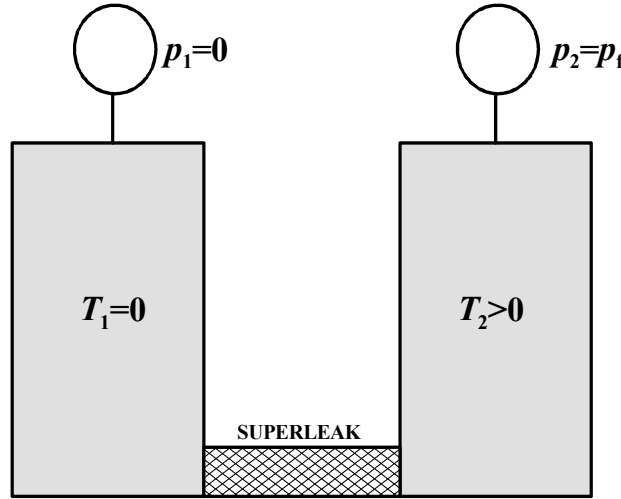


Figure 6. 2. The fountain effect. Two reservoirs are filled with HeII and connected by a superleak. The pressure and the temperature in the left reservoir are equal to 0. The temperature in the right reservoir has a finite value T . In the steady state the pressure in the right reservoir is equal to the fountain pressure.

narrow channels without friction. However, the normal component is blocked by its viscosity. Therefore, in the ideal case only the superfluid component will be able to flow through the superleak. In our explanation the temperature in the left reservoir T_1 and the pressure p_1 are assumed to be equal to zero. We create a temperature difference between the two reservoirs by applying a certain amount of heat to the right reservoir. The concentration of the superfluid component in the warm reservoir will become smaller than in the cold reservoir. The superfluid component from the cold reservoir will flow through the superleak to the warm reservoir to establish the equilibrium. The change of chemical potential is

$$d\mu = -S_m dT + V_m dp, \quad (6.5)$$

where S_m and V_m are the molar entropy and the molar volume, respectively. When the system reaches the steady state, v_s is equal to zero. From equation 6.4 it follows, that in this case the chemical potentials on both sides of the superleak are equal

$$\mu_1 = \mu_2. \quad (6.6)$$

Hence,

$$\Delta\mu = 0. \quad (6.7)$$

With equation 6.7 equation 6.5 is written as follows

$$dp = \frac{S_m}{V_m} dT. \quad (6.8)$$

Integrating equation 6.8 gives us

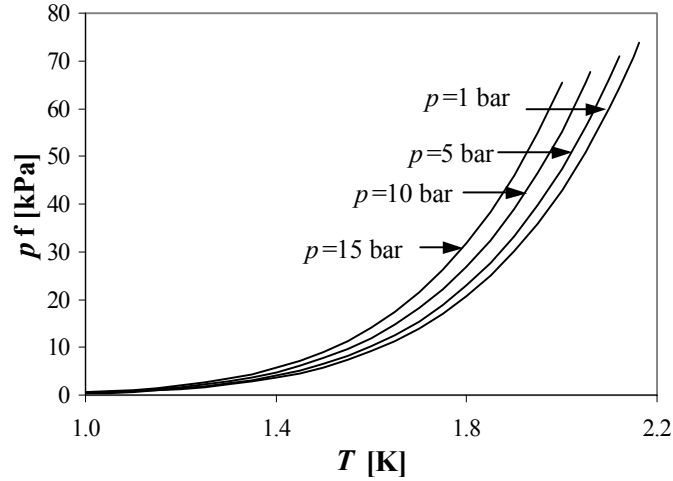


Figure 6. 3. The fountain pressure in HeII at different average pressures as a function of temperature.

$$p_2 - p_1 = \int_{T_1}^{T_2} \frac{S_m}{V_m} dT. \quad (6.9)$$

For $V_m = \text{const}$, $p_1 = 0$, and $T_1 = 0$

$$p_2 = p_f, \quad (6.10)$$

where p_f is the fountain pressure, which is given as

$$p_f(T, p) = \frac{1}{V_m(p)} \int_0^T S_m(T', p) dT'. \quad (6.11)$$

The essence of the fountain effect is, that the superfluid helium flows through the superleak in the direction of high temperature and maintains a pressure difference over it. The fountain pressure of HeII at the lambda temperature is as high as 70 kPa (see FIG. 6.3).

6.1.2. Vortex-cooling effect

The vortex cooler consists of a superleak, followed by a chamber and a capillary (FIG. 6.4). In the absence of flow all parts of the system have the same temperature and pressure. If superfluid helium is forced to flow through the superleak, the fluid, leaving the superleak, carries no entropy. The helium in the capillary is a combination of the normal and the superfluid components. If superfluid helium flows through the capillary with supercritical velocity, quantum vortices are created there [5]. These vortices interact with the normal component, dragging it along in the direction of the superfluid flow. So

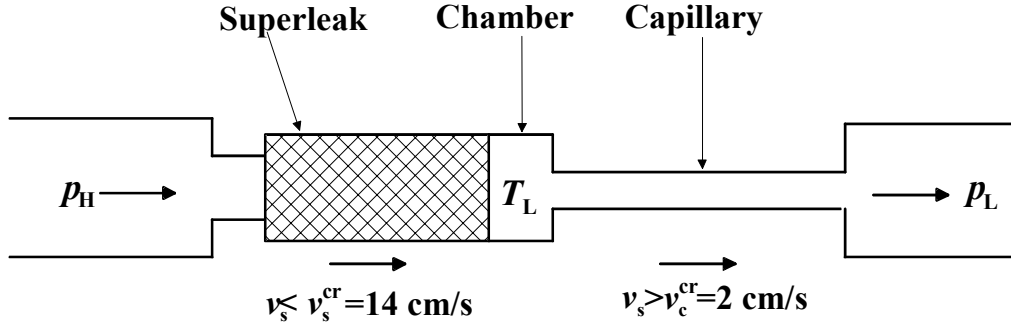


Figure 6. 4. Vortex cooling effect. Superfluid helium flows through the superleak with a velocity lower than the critical velocity in the superleak. The velocity of the superfluid helium in the capillary is supercritical. Normal helium is pushed out of the chamber by the quantum vortices. Cooling occurs in the chamber. The values for the critical velocities are discussed in section 6.2.1.

the normal component is forced out of the chamber. The reduced concentration of the normal component corresponds with a reduction of temperature (see FIG. 6.1). Hence, cooling takes place.

6.1.3. Superfluid vortex cooler *

A schematic diagram of the SVC is shown in FIG. 6.5. It consists of a main heat exchanger, a fountain part (a superleak S_1 , fountain heat exchanger H_1 , and a capillary C_1), and a vortex part (a superleak S_2 , vortex heat exchanger H_2 , and a capillary C_2). The main heat exchanger of the SVC is attached to a precooling stage at a temperature T_b . At the beginning all parts of the system have a temperature T_b . By supplying heat to the heater H_1 we activate the fountain pump, which generates a high pressure in H_1 . The pressure difference causes a flow of helium in the SVC from the low-pressure part of the main heat exchanger through S_1 and C_1 . Helium arrives to the high-pressure part of the main heat exchanger with a temperature higher than T_b . It cools down in the heat exchanger and is then forced through S_2 . Through C_2 the fluid returns back to the main heat exchanger. The coldest point of the SVC is at the exit of S_2 .

6.2. CONCEPTUAL DESIGN OF THE SVC

6.2.1. Diameters of superleaks and capillaries

When designing the SVC, certain conditions have to be fulfilled. The velocity of helium in the superleaks, v_s , has to be lower than the superleak critical velocity, v_s^{cr} . The average velocity of helium in a superleak is given by

* Not to be confused with the Ranque-Hilsch Vortex-Tube, which is a cooling device near room temperature [6].

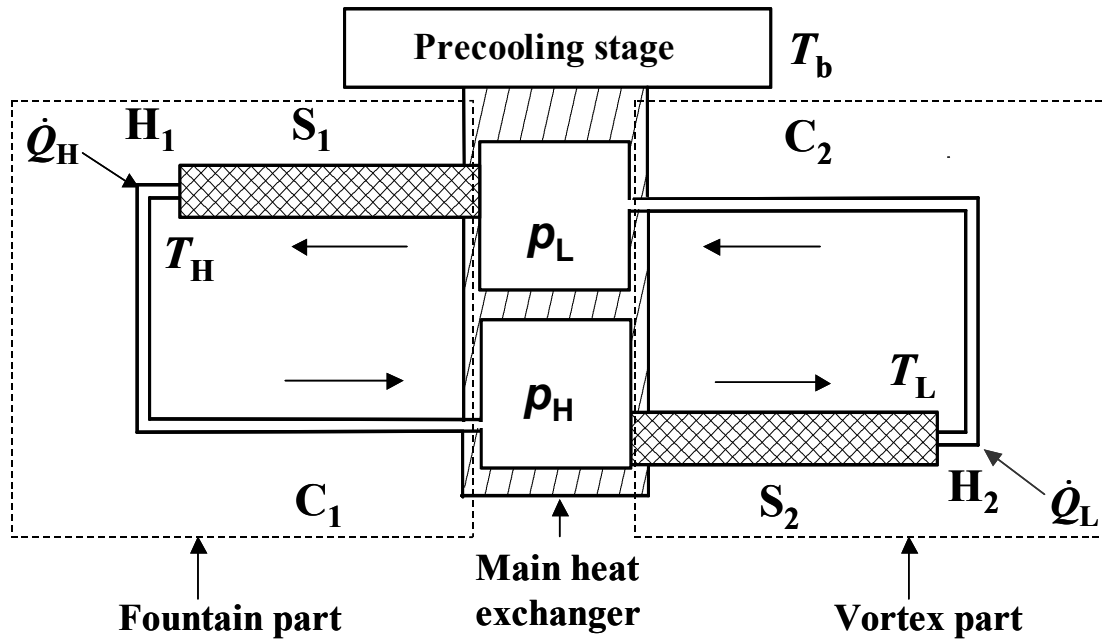


Figure 6. 5. The schematic diagram of the superfluid vortex cooler.

$$v_s = \frac{\dot{m}}{\rho_s(1-f)A_s}, \quad (6.12)$$

where \dot{m} is a mass flow of the superfluid helium flowing through a superleak, f is the filling factor, ρ_s is the density of the superfluid helium, and A_s is the cross-sectional area of the tube, filled with the superleak material, given by

$$A_s = \frac{\pi d_s^2}{4}, \quad (6.13)$$

where d_s is the diameter of the superleak container. When a certain amount of heat \dot{Q}_H is supplied at one end of a superleak, the mass flow of helium in it in the direction of high temperature T_H can be expressed as

$$\dot{m} = \frac{\dot{Q}_H}{T_H s_H}, \quad (6.14)$$

where s_H is the specific entropy of helium at temperature T_H . With equations 6.13 and 6.14 equation 6.12 can be written as

$$v_s = \frac{4\dot{Q}_H}{T_{H\rho_s} s \pi (1-f) d_s^2}. \quad (6.15)$$

We require

$$v_s < v_s^{\text{cr}}. \quad (6.16)$$

Therefore, the diameter of a superleak should fulfil the following condition:

$$d_s^2 > \frac{4\dot{Q}_H}{T_H \rho_s s \pi (1-f) v_s^{\text{cr}}}. \quad (6.17)$$

In contrast to the superleak, the velocity of helium in the capillary, v_c , should significantly exceed the critical velocity there, v_c^{cr} . In the capillary a quite complicated situation occurs. The velocity of the superfluid and the normal components can differ in magnitude and sign. At very high velocities, however, the coupling between the two components is so strong that the two velocities are equal; and HeII flows as any normal fluid. In this case we can write for the velocity of helium in the capillaries:

$$v_c = \frac{\dot{m}}{\rho A_c}, \quad (6.18)$$

where \dot{m} is the mass flow of helium in the capillary, ρ is the density of helium, and A_c is the cross-sectional area of the capillary, which can be expressed as

$$A_c = \frac{\pi d_c^2}{4}, \quad (6.19)$$

where d_c is the diameter of the capillary. With equation 6.14 and requiring that

$$v_c \gg v_c^{\text{cr}}, \quad (6.20)$$

we can write for capillaries

$$d_c^2 \ll \frac{4\dot{Q}_H}{T_H \rho s \pi v_c^{\text{cr}}}. \quad (6.21)$$

It has been found empirically [7], that the critical velocity is temperature independent and varies with a forth root of the channel diameter d according to the relation:

$$v^{\text{cr}} = C/d^{1/4}, \quad (6.22)$$

where $C \approx 1 \text{ cm}^{5/4} \text{ s}^{-1}$. Equation 6.22 is valid for d , ranging from a few Å up to a few cm. The critical velocity of helium in the superleaks, filled with jeweler's rouge powder, is typically 14 – 20 cm/s. For capillaries with diameters of a few tenth of a mm it is in the range of 2-5 cm/s.

6.2.2. Thermal losses in the SVC

Now we will discuss various loss mechanisms in the cooler, such as the heat conduction through the superleaks and the walls of the capillaries, the heat transport via the flow of normal helium through S_2 , and the dissipation in the capillaries.

6.2.2.1. Heat conduction

The heat flow due to heat conduction via the material and the walls of the superleaks and the walls of the capillaries is determined as

$$\dot{Q}_c = -kA \frac{dT}{dl}, \quad (6.23)$$

where k is the thermal conductivity, and A is a cross-sectional area. For the superleaks A is given by equation 6.13. For the tube walls

$$A = \pi \delta d, \quad (6.24)$$

where δ and d are the wall thickness and the outer diameter of a tube, respectively. The calculated values of the heat conduction through the superleaks and the walls of the capillaries in our SVC are all less than $3 \mu\text{W}$, and, therefore, can be neglected.

6.2.2.2. Heat transport with the normal flow

The heat, transported by the flow of normal helium through S_2 , can be explained as follows. Ideally the normal component cannot pass the superleak. However, in practice a superleak is just a flow resistance. Although the resistance of the superleak is very high, a pressure difference across S_2 causes a certain amount of the normal component to flow through it, transporting heat from the main heat exchanger to the coldest point of the SVC. We describe the superleak as a system, consisting of N parallel circular channels. A section of the channel with the diameter d_{ch} and the length dl is drawn in FIG. 6.6. A certain volume of the normal component \dot{V}_n flows through the channel from the high temperature T_H to the low temperature T_L . Applying the 2nd law of thermodynamics to the section of the channel gives us the following expression

$$d\dot{S} = d\dot{S}_i. \quad (6.25)$$

The change of the entropy flow $d\dot{S}$ in the channel is equal to the irreversible entropy production $d\dot{S}_i$ in it. The entropy production rate is expressed as

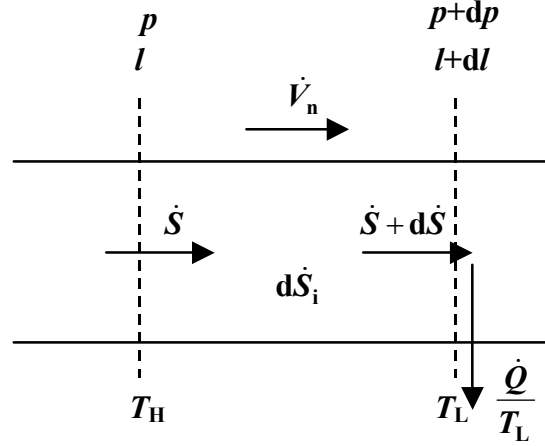


Figure 6. 6. Entropy, produced by a flow of normal helium in a channel. Normal helium flows from a high temperature and a high pressure to a low temperature and a low pressure. A certain amount of irreversible entropy is produced in the channel. The heat is removed at the low temperature, T_L .

$$d\dot{S}_i = -\dot{V}_n \frac{dp}{T}, \quad (6.26)$$

where \dot{V}_n is the volume flow of the normal component in the superleak. With equation 6.26 equation 6.25 can be written as follows

$$\frac{d\dot{S}}{dT} = -\frac{\dot{V}_n}{T} \frac{dp}{dT}. \quad (6.27)$$

It is assumed that the chemical potential μ in the superleak is constant. So the velocity of helium in the superleak is lower than the critical velocity there. In this case the change in the pressure is equal to the change in the fountain pressure. Hence, using equation 6.8,

$$\frac{dp}{dT} = \frac{dp_f}{dT} = \rho s. \quad (6.28)$$

With equation 6.28 equation 6.27 becomes

$$\frac{d\dot{S}}{dT} = -\frac{\dot{S}}{T}. \quad (6.29)$$

Simplifying equation 6.29, we get the expression

$$\dot{S}T = C_1, \quad (6.30)$$

Chapter 6

where C_1 is a constant and has a meaning of a heat flow. The entropy flow \dot{S} is directed the same way as \dot{V}_n and is equal to

$$\dot{S} = \dot{V}_n \rho s . \quad (6.31)$$

With equations 6.30 and 6.31 we can write

$$\dot{V}_n \rho s T = C_1 . \quad (6.32)$$

The pressure difference, causing \dot{V}_n , is given by equation 6.3. Introducing the geometrical factor g_z , which is

$$g_z = \frac{Z}{L} , \quad (6.33)$$

we can rewrite equation 6.3 as follows

$$\frac{dp}{dl} = \eta g_z \dot{V}_n . \quad (6.34)$$

Applying the chain rule and equation 6.28 to equation 6.34, we obtain the following expression

$$\frac{dT}{dl} = \eta g_z \frac{C_1}{\rho^2 s^2 T} . \quad (6.35)$$

We rewrite equation 6.35 as follows

$$g_z C_1 dl = \frac{\rho^2 s^2 T}{\eta} dT . \quad (6.36)$$

Integrating equation 6.36, assuming constant ρ , and with equation 6.33 we obtain the expression for C_1

$$C_1 = \frac{\rho^2}{Z} \int_{T_1}^{T_2} \frac{s^2}{\eta} T dT . \quad (6.37)$$

Using HeII data from [8], the empirical equation for s can be obtained

$$s = s_0 T^{\alpha_2} , \quad (6.38)$$

where s_0 and α_2 are the empirical constants, given in Table 6.1.

Table 6.1. Empirical constants s_0 and α .

p [bar]	s_0 [J/(kgK $^{\alpha+1}$)]	α
SVP	17.5	5.84
1	17.5	5.85
5	17.5	5.98
10	20.4	5.86
15	23.5	5.85
20	35.72	5.32

The viscosity of helium below the lambda line is not constant [9]. However, the temperature dependence of the viscosity has a rather flat plateau between 1.3 and 2 K. Therefore, in our calculations we considered it to be constant and equal to 1.5×10^{-6} Pas.

We can determine the effective conductivity of normal helium, κ_{ef} , in the superleak as follows

$$\kappa_{\text{ef}} = \frac{C_1}{A_{\text{ch}}} \frac{dl}{dT}, \quad (6.39)$$

where A_{ch} is the cross-sectional area of a superleak channel, given by

$$A_{\text{ch}} = \frac{\pi d_{\text{ch}}^2}{4}. \quad (6.40)$$

The impedance of a circular channel of length L with Poiseuille flow is [9]

$$Z_{\text{ch}} = 128 \frac{L}{\pi d_{\text{ch}}^4}. \quad (6.41)$$

With equations 6.35, 6.38, 6.40, and 6.41 equation 6.39 becomes

$$\kappa_{\text{ef}} = \kappa_0 T^{\alpha_3}, \quad (6.42)$$

where

$$\kappa_0 = \frac{\rho^2 d_{\text{ch}}^2 s_0^2}{32\eta}, \quad (6.43)$$

and

$$\alpha_3 = 2\alpha_2 + 1 = 12.7. \quad (6.44)$$

For our superleak with the average size of pores of $0.15 \mu\text{m}$ ($d_{\text{ch}}=0.15 \mu\text{m}$) $\kappa_0=0.0031 \text{ W}/(\text{K}^{\alpha_2+1} \text{ m})$. The effective conductivity of helium in the superleak at an average pressure of 1 bar is plotted versus temperature in FIG. 6.7.

G. van der Heijden measured the heat conduction through a superleak as a function of temperature [4]. As the superleaks he used stainless steel tubes filled with jeweller's rouge powder with the particle size of $0.7 \mu\text{m}$. In our experiments we use the

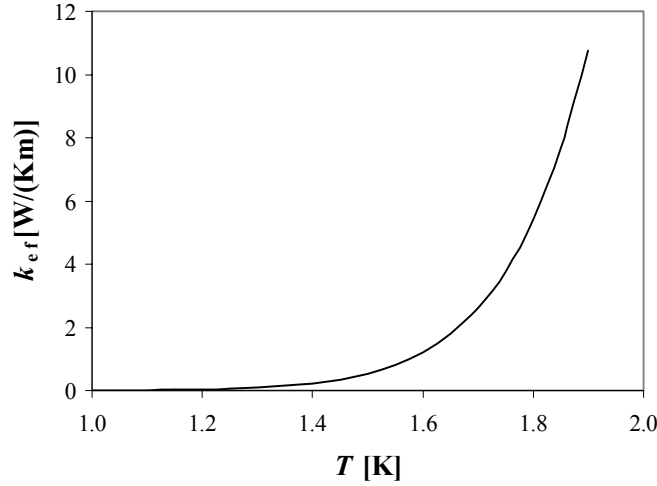


Figure 6. 7. The effective conductivity of helium at an average pressure of 1 bar as a function of temperature.

same material. Therefore, we can compare our calculated κ_{ef} with the experimental one. For the temperature interval 0 – 1.7 K, the experimental κ_{ef} can be described by the following empirical expression

$$\kappa_{\text{ef}}^{\text{exp}} = \kappa_0^{\text{exp}} T^{\alpha_4}, \quad (6.45)$$

with $\alpha_4=12.6$ and $\kappa_0^{\text{exp}}=0.0039 \text{ W}/(\text{K}^{\alpha_4+1} \text{ m})$. Comparing the calculated and the experimental value of effective conductivity, we can conclude that they match within 14% difference.

For our SVC the value of the heat, transported in S_2 by the normal component is only a few tenth of a μW , and, therefore, can be neglected.

6.2.2.3. Dissipation in the capillaries

To estimate the amount of energy, transported by helium flow in the capillaries, we will make several assumptions. The equation, describing the heat flow in the capillaries, is limited to the steady state situation and is based on the energy conservation law. We consider the uniform turbulent mass flow in the capillaries with a velocity significantly higher than the critical velocity of helium in a capillary. Hence, there is no heat flux due to the fountain effect. The energy, caused by vortices formation, is neglected. Therefore, we can write, that

$$\dot{H} + \dot{Q}_{\text{He}} = \text{Const}. \quad (6.46)$$

In equation 6.46 the enthalpy flow \dot{H} is a function of temperature and pressure. \dot{Q}_{He} can be described by the Gorter Mellink equation for the heat conduction in the flow of helium

$$\dot{Q}_{\text{He}} = -A_c \left(\frac{1}{f(T)} \frac{dT}{dl} \right)^{1/3}, \quad (6.47)$$

where

$$f(T) = \frac{A \rho_n}{\rho_s^3 s^4 T^3}, \quad (6.48)$$

with A – the Gorter Mellink parameter [5, 10, 11].

After differentiating and with the use of equation 6.47 equation 6.46 takes the form:

$$\dot{m} \left(\frac{\partial h}{\partial T} \right)_p \frac{dT}{dl} + \dot{m} \left(\frac{\partial h}{\partial p} \right)_T \frac{dp}{dl} - A_c \frac{d}{dl} \left(\frac{1}{f(T)} \frac{dT}{dl} \right)^{1/3} = 0. \quad (6.49)$$

The term dp/dl in equation 6.49 is the pressure change due to the flow of turbulent HeII. Previous investigations [12, 13] have shown, that the friction factor in a flow of turbulent HeII f_d is similar to the friction factor of classical fluids. Therefore, the pressure change in the capillary can be written as

$$\frac{dp}{dl} = 2 f_d \rho v^2 \frac{1}{d_c}. \quad (6.50)$$

With equations 6.18 and 6.19 equation 6.50 becomes

$$\frac{dp}{dl} = 32 \dot{m}^2 \frac{f_d}{\rho \pi^2 d_c^5}. \quad (6.51)$$

Simplifying equation 6.49 with the use of thermodynamical relations and equation 6.51, we can write

$$\dot{m} c_p \frac{dT}{dl} - 32 \dot{m}^3 \frac{f_d}{\rho^2 \pi^2 d_c^5} - A_c \frac{d}{dl} \left(\frac{1}{f(T)} \frac{dT}{dl} \right)^{1/3} = 0. \quad (6.52)$$

From this equation and with well-defined boundary conditions we can determine the amount of heat, transported in SVC capillaries as well as temperature profiles in them.

6.3. THE EXPERIMENTAL SET-UP AND RESULTS

6.3.1. Experimental set-up

A photograph of the SVC is represented in FIG. 6.8. All heat exchangers are simply copper blocks with channels inside. The capillaries are made of stainless steel.

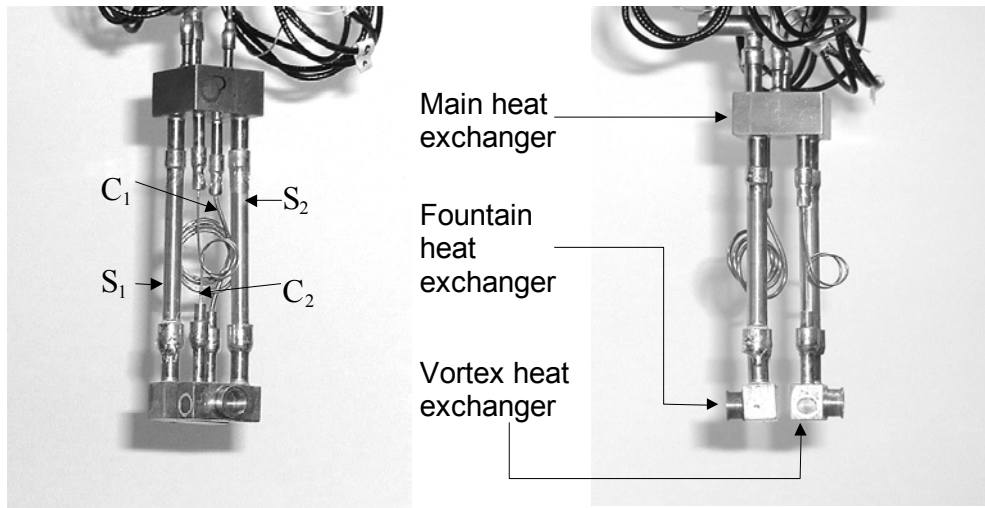


Figure 6.8. The superfluid vortex cooler (for details see section 6.1.3. and FIG. 6.5). The distance between the main heat exchanger and the fountain/vortex heat exchangers is about 6 cm.

The superleaks are German silver tubes, filled with jeweller's rouge powder with a particle size of approximately $0.7\ \mu\text{m}$.

A schematic drawing of the experimental set-up is shown in FIG. 6.9. The SVC is placed in a vacuum chamber, which is pumped down to $10^{-4}\ \text{Pa}$ while the system is at room temperature. The vacuum chamber is immersed in liquid helium. The temperature of the liquid helium bath is lowered by pumping. The main heat exchanger of the SVC contains a little buffer, which is connected with the helium bath by a wide tube. Due to the very large thermal conduction of superfluid ^4He , helium in the buffer has the same temperature as the bath. In this way the precooling of the SVC takes place. The SVC is equipped with two filling capillaries, connecting the SVC with a supply at room temperature. Therefore, it is easy to vary the average pressure in the SVC. The filling capillaries extend from room temperature down to the SVC through the helium bath. Each filling capillary has a pressure meter, so that the pressure in the SVC could be measured. The temperature was measured at three places: at the main heat exchanger (T_b), at the fountain and at the vortex heat exchangers (T_H and T_L respectively). The two thermometers, attached to the fountain and the vortex heat exchangers, are carbon ceramic and are calibrated down to 0.5 K. For measurements of T_b a diode thermometer is used. The accuracy of the thermometers is $\pm 0.01\ \text{K}$ below 4.2 K and $\pm 0.0025T$ above 4.2 K. The heaters are made of $50\ \mu\text{m}$ manganine wire wound around copper holders, which are then soldered on the fountain and the vortex heat exchangers.

6.3.2. Results of the measurements

In total 12 series of measurements (runs) have been made with the set-up. The dimensions of the main components of the SVC, the lowest temperatures, reached in each

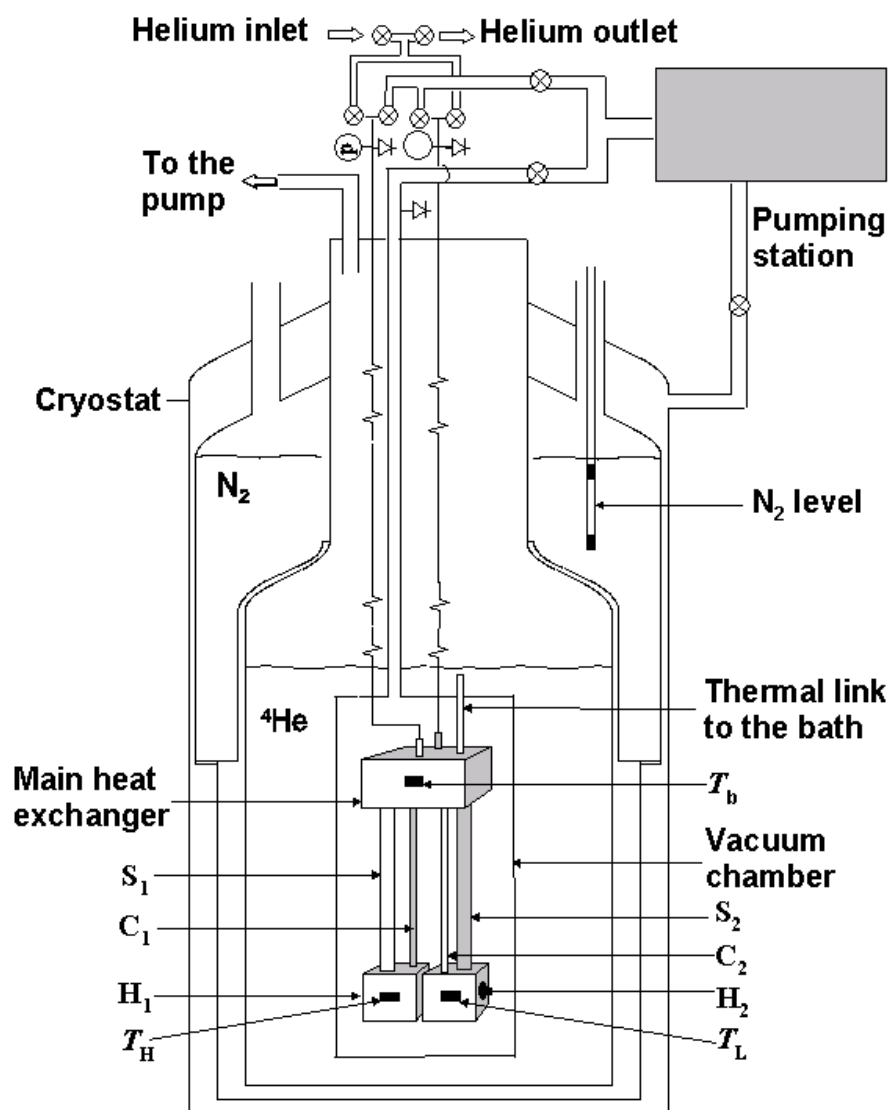


Figure 6. 9. The schematic drawing of the experimental set-up, in which the SVC is precooled by a liquid-helium bath.

run (excluding the trial runs 1 and 2), and the pressures in the SVC, at which the lowest temperatures have been reached, are listed in Table 6.2.

In run 3 we reached the lowest temperature of 0.883 K with an input heating power of 31.6 mW and a base temperature of 1.43 K (see FIG. 6.10). The average pressure in the SVC was around 1 MPa. After that we concentrated on reaching temperatures below 1 K with an input heating power as small as possible. This is important, since precooling by a cryocooler is considered.

Table 6.2. The dimensions of the main component of the SVC, the lowest temperature for each run, and the pressure, at which the lowest temperature is reached (* the number in brackets means the length of the filled part of a superleak). Sizes are in mm.

Run	S ₁		C ₁		S ₂		C ₂		T_L [K]	p [bar]
	d_{S1}	L_{S1}^*	d_{C1}	L_{C1}	d_{S2}	L_{S2}^*	d_{C2}	L_{C2}		
3	2.5	46 (26)	0.3	145	3.5	46 (26)	0.7	281	0.883	9.8
4	3.5	46 (26)	0.7	281	2.5	46 (26)	0.3	145	0.932	10.0
7	3.5	46 (26)	0.2	160	2.5	46 (26)	0.2	80	0.909	10.0
8	1.5	40 (20)	0.2	160	1.5	40 (20)	0.2	80	0.986	10.8
9	1.5	40 (20)	0.1	160	1.5	40 (20)	0.1	80	1.025	10.6
10	1.5	40 (20)	0.1	40	1.5	40 (20)	0.1	80	1.056	10.7
11	3.5	46 (26)	0.1	40	2.5	46 (26)	0.1	80	1.083	10.4
12	3.5	46 (26)	0.2	160	2.5	46 (26)	0.2	80	0.944	13.7

Below we describe the results, demonstrated in FIGs. 6.10-6.13, and give explanations of the observations. However, the time limit for this research didn't not allow us to analyse the results in more detail, and, therefore, to provide better proof of each explanation. The basic idea was to reduce the diameters of the superleaks and the

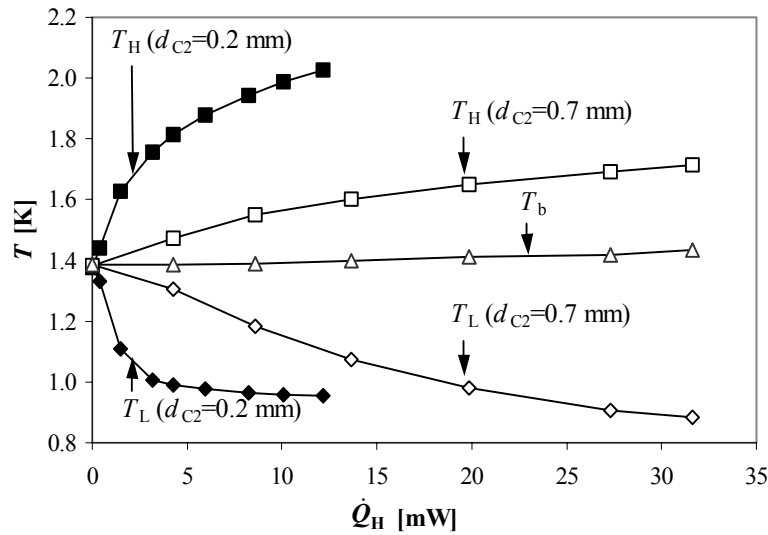


Figure 6. 10. The influence of the diameter of the vortex capillary, d_{C2} on the performance of the SVC. The average pressure in the SVC in both cases is 1 MPa. Note, that for clarity T_b for $d_{C2}=0.2$ mm is not shown in the figure. For details see Table 6.2.

capillaries so that the same velocities could be reached with less mass flow. Hence, our approach is rather phenomenological.

Figure 6.10 shows two $\dot{Q}_H - T$ dependences, illustrating the influence of the diameter of the vortex capillary, d_{C2} , on the performance of the SVC. Each set of measurements results in three curves. The lower curve is the temperature of the vortex heat exchanger (T_L), the middle curve is the base temperature (T_b), and the upper curve is the temperature of the fountain heat exchanger (T_H). At $\dot{Q}_H = 0$ all parts of the SVC are at the same base temperature. When heat is supplied, T_H increases, T_L goes down, while T_b remains almost constant. To reach 1 K with $d_{C2}=0.2$ mm one needs almost six times less heating power than with $d_{C2}=0.7$ mm. This can be explained by the fact, that the critical velocity is achieved faster in a capillary with the smaller diameter. Therefore, less heat input is needed to activate the cooling process with smaller capillaries.

Figures 6.11-6.13 represent T_L as a function of \dot{Q}_H for the runs with different dimensions of the main components of the SVC (Run 7-11 from Table 6.2). The starting temperature in all measurements is 1.38 K. The average pressure in the SVC is around 1 MPa. As it is seen from FIG. 6.11 the change of the superleak diameter (Run 7 compared to Run 8 and Run 10 compared to Run 11) does not affect the steepness of the curves at low \dot{Q}_H , but as \dot{Q}_H increases, the system with a larger superleak diameter reaches a lower temperature. The same mass flow, passing the superleak with a smaller diameter, causes higher velocity in it. Apparently this leads to an increase of the dissipation in the superleak due to the formation of vortices in the channels of it. The diameter of the superleak should satisfy equation 6.17 in order to prevent the formation of the vortices in it. In Run 10 the temperature curve starts levelling off at $\dot{Q}_H=1.5$ mW. At this moment $T_H=1.8$ K. With equation 6.17 this corresponds to

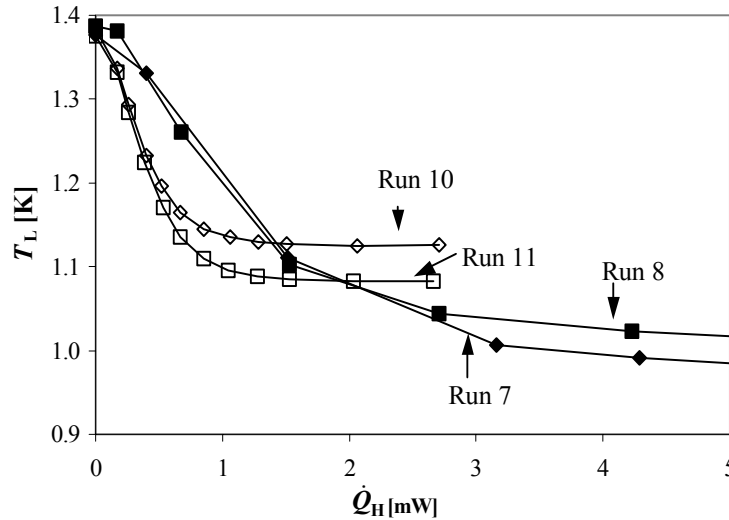


Figure 6. 11. The influence of the diameters of the superleaks on the performance of the SVC. The diameters of the superleaks have been decreased from Run 7 to Run 8. From Run 10 to Run 11 the diameters of the superleaks have been increased. For details see Table 6.2.

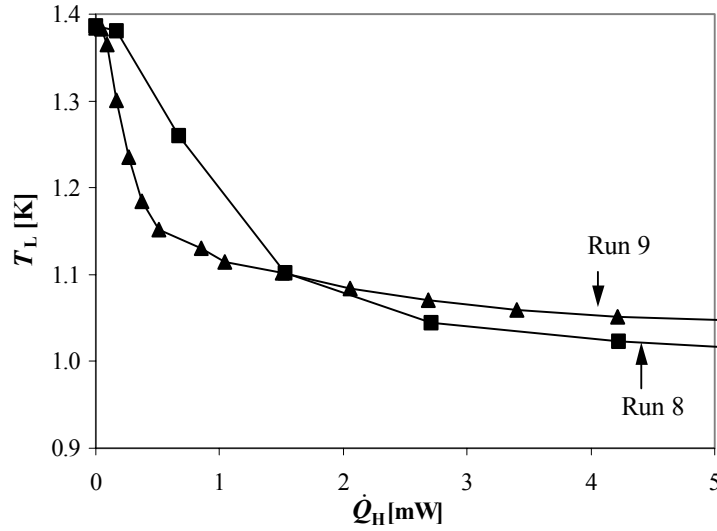


Figure 6. 12. The reduction of the capillaries' diameters in the measurements with a small input heating power. The diameters of the capillaries have been reduced from Run 8 to run 9.

$$d_s > 0.7 \text{ mm.} \quad (6.53)$$

However, d_s in Run 10 is equal to 1.5 mm, which is larger, than the value, given by equation 6.53. It seems that the diameter of the superleak should be heavily oversized in order for the SVC to perform efficiently. This is illustrated by $\dot{Q}_H - T$ curve of Run 11, in which d_s has been increased up to 3.5 mm.

From Run 8 to Run 9 the diameters of both capillaries have been decreased by a factor of two (FIG. 6.12). The result is a steep cool-down at the beginning of the Run 9.

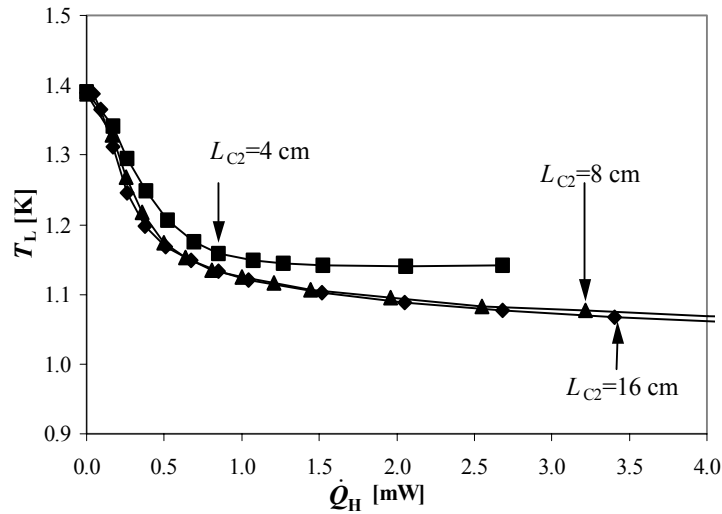


Figure 6. 13. $\dot{Q}_H - T_L$ dependences for three different lengths of the vortex capillary.

However, the minimum temperature in Run 9 is higher than in Run 8. A decrease of the capillary diameter causes an increase of losses in it (second term in equation 6.52). When the mass flow is small (small \dot{Q}_H), this loss is negligible. However, the third power of the mass flow in the second term of equation 6.52 provides a significant increase of the influence of this term on the performance of the cooler with the increase of supplied heat. This might be a reason for the lowest temperature of Run 9 to be higher than the lowest temperature of Run 8.

When decreasing the lengths of the capillaries from Run 9 to Run 10, we may have observed a certain critical value for the length. When passing it, the performance of the cooler changes significantly (see FIG. 6.13). There is no difference in the performance when the length of C_2 is decreased from 16 cm to 8 cm. However, when decreasing the length of C_2 further to 4 cm (Run 10), the cooling curve starts levelling off rather soon. Hence, the lowest temperature of Run10 is higher than the one of Run 9.

Figure 6.14 demonstrates the influence of the pressure in the SVC on the performance of the cooler. At higher pressures T_L is lower. As mentioned above, the cooling in the SVC results from the interactions between the superfluid vortices and excitations of the normal component. There are two kinds of excitations: phonons and rotons. Rayfield and Reif [14] have shown that the rotons are much more scattered by vortices than the phonons. And the roton density in helium increases with the increased pressure. This could be an explanation to the results, presented in FIG. 6.14.

We have also carried out several measurements with different base temperatures (see FIG. 6.15). Higher T_b means that more heating power is needed to achieve the same T_L . In addition to that, the lowest temperature increases with the increase of T_b .

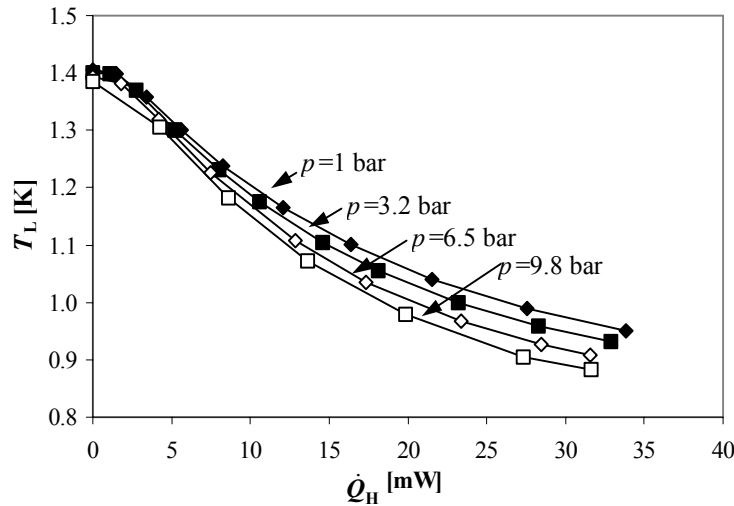


Figure 6. 14. The influence of the pressure in the SVC on the performance of the cooler. The geometry of the SVC for this experiment is given in Table 6.2, Run 3.

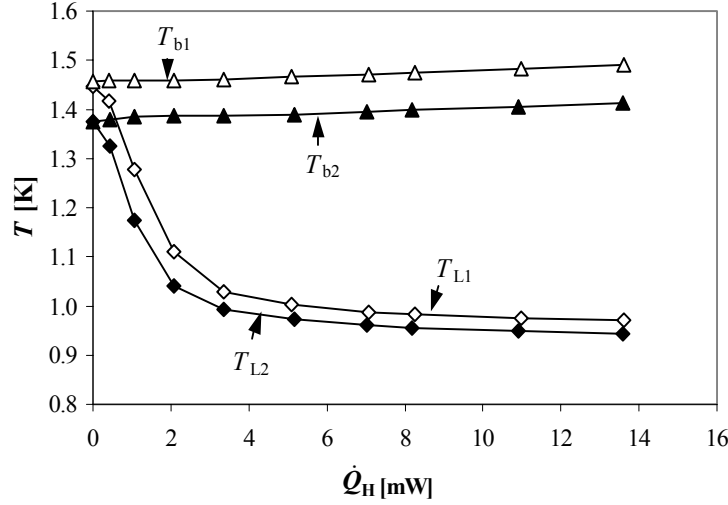


Figure 6. 15. The effect of the base temperature on the lowest temperature of the SVC. The geometry of the SVC for this experiment is given in Table 6.2, Run 7.

6.3.3. Cooling power

The cooling power of the SVC has been measured as well (see FIG. 6.16). At 1 K the cooling power is 0.13 mW with $\dot{Q}_H = 8.75$ mW (Run 3) and 0.36 mW with $\dot{Q}_H = 31.6$ mW (Run 4).

To derive the coefficient of performance (COP) of the SVC, we will describe the cooler as a closed system shown in FIG. 6.17. To activate the cooler, a certain amount of heat \dot{Q}_H is supplied to it at a temperature T_H . Together with the heat \dot{Q}_L , taken from a cooling object at a temperature T_L , \dot{Q}_H is extracted from the system by a precooling stage at a temperature T_b . There is a certain irreversible entropy production in the system, \dot{S}_i . The second law of thermodynamics for such a system is written as

$$\dot{S} = \frac{\dot{Q}_H}{T_H} + \frac{\dot{Q}_L}{T_L} - \frac{\dot{Q}_H + \dot{Q}_L}{T_b} + \dot{S}_i. \quad (6.54)$$

In the steady state and in the ideal case

$$\dot{S} = 0. \quad (6.55)$$

and

$$\dot{S}_i = 0. \quad (6.56)$$

Thus,

$$\dot{Q}_L = \dot{Q}_H \frac{T_H - T_b}{T_H} \frac{T_L}{T_b - T_L}. \quad (6.57)$$

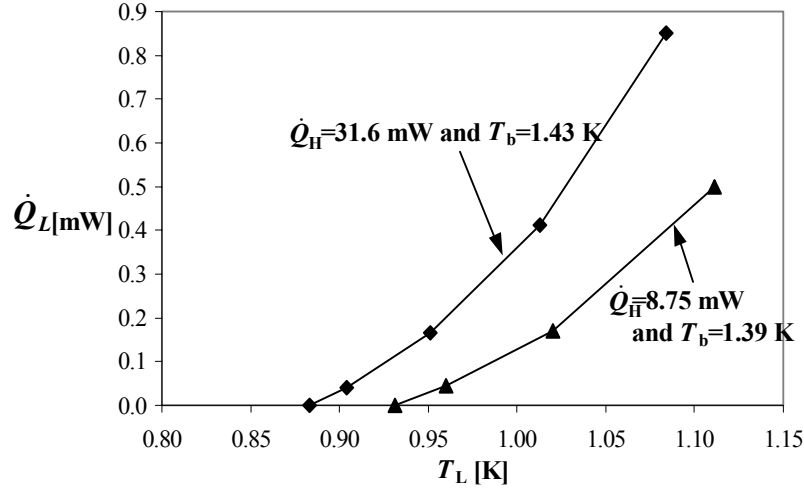


Figure 6. 16. Cooling power of the SVC at two different input heating powers and base temperatures.

The COP of the SVC is

$$\text{COP} = \frac{\dot{Q}_L}{\dot{Q}_H}. \quad (6.58)$$

Hence, the ideal COP is

$$\text{COP}_{\text{id}} = \frac{T_H - T_b}{T_H} \frac{T_L}{T_b - T_L}. \quad (6.59)$$

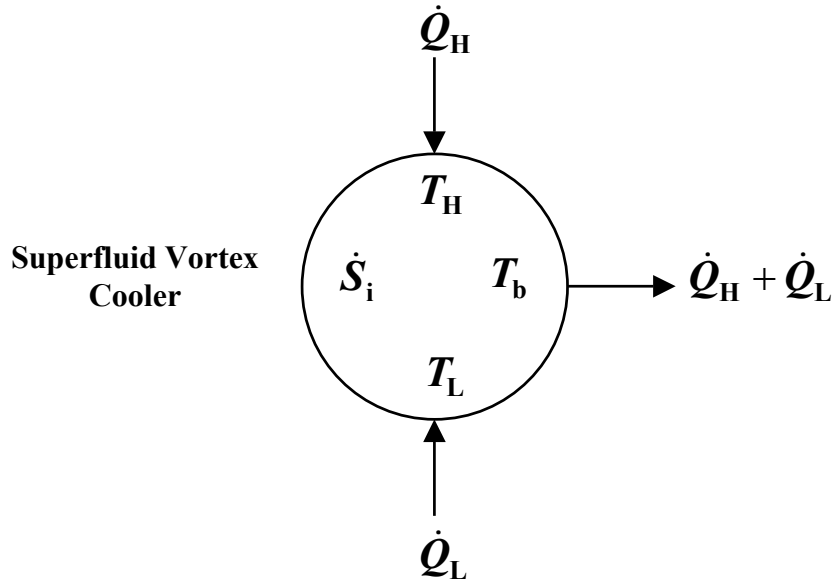


Figure 6. 17. Thermodynamical representation of the SVC. A heat \dot{Q}_H is supplied to the SVC at a temperature T_H ; and a heat \dot{Q}_L is supplied to the SVC at a temperature T_L . \dot{Q}_H and \dot{Q}_L are removed from the cooler at a temperature T_b . There is an irreversible production, \dot{S}_i , in the cooler.

It is interesting to see, that equation 6.59 is a product of the efficiency of the Carnot engine, operating between T_H and T_b , and the efficiency of the Carnot refrigerator, operating between T_L and T_b . The experimental COP of our SVC at 1 K is 1.5 %. It is equal to 7 % of the ideal COP at 1 K. This value can be used as a reference value in further optimisation of the SVC. The main sources of losses, compared to the ideal situation, is the supercritical flow in the vortex capillary, as well as the heat conduction in the helium flow in it.

6.4. CONCLUSIONS

We have designed and built a superfluid vortex cooler. Several experiments have been carried out with a liquid-helium bath as a precooler for the SVC. A minimum temperature of 0.88 K with an input heating power of 31.6 mW has been achieved. After that we have concentrated on reaching temperatures below 1 K with a small input heating power. With certain geometry modifications a temperature of 0.96 K has been reached with only 7 mW input heating power and a base temperature of about 1.4 K.

REFERENCES

1. Olijhoek, J.F., Hoffer, J. K., Beelen, H. van, Bruyn Ouboter, R. de, and Taconis, K. W., "Cooling by convective heat transport in superfluid helium", *Physica* **64**, 1973, pp. 289-305.
2. Olijhoek, J.F., Beelen, H. van, Bruyn Ouboter, R. de, and Taconis, K. W., "Thermal effects in adiabatic flow of He II. II. The temperature distribution along the capillary during stationary flow of He II at saturated-vapour pressure.", *Physica* **72**, 1974, pp. 381-396.
3. Olijhoek, J.F., Beelen, H. van, Bruyn Ouboter, R. de, Taconis, K. W., and Koops, W., "Thermal effects in adiabatic flow of He II. I. The role of mutual friction and the influence of pressure on the limit of cooling.", *Physica* **72**, 1974, pp. 355-380.
4. G. van der Heijden, "Forces in the flow of liquid He II", PhD thesis, Leiden University, 1972.
5. Olijhoek, J.F., "Thermal effects in adiabatic flow of HeII", PhD thesis, Leiden University, 1973.
6. Gao, C., Bosschaart, K.J., Zeegers, J.C. H., Waele, A.T.A.M. de, "Experimental study on a Simple Ranque-Hilsch Vortex tube", submitted to *Cryogenics*, 2004.
7. Alphen, W. M. van, Haasteren, G. J. van, Bruyn Ouboter, R. de, and Taconis, K. W., "The dependence of the critical velocity of the superfluid on channel diameter and film thickness", *Physics Letters* **20**, 1966, pp. 474-475.
8. Sciver, S. W. van, "Helium cryogenics", Plenum Press, New York, 1986.
9. Zeegers, J., "Critical velocities and mutual friction in ^3He - ^4He II mixtures at temperatures below 100 mK", PhD thesis, Eindhoven University of Technology, 1991.
10. Gorter, C. J., and Mellink, J. H., "On the irreversible processes in liquid helium II", *Physica* **15**, 1949, pp. 285-304.
11. Weisend, J. G. II, "Handbook of Cryogenic Engineering", Taylor & Francis, Philadelphia, 1998.

12. Walstrom, P. L., Weisend, J. G. II, Maddocks, J. R., and Sciver, S. W. van, "Turbulent flow pressure drop in various He II transfer system components", *Cryogenics* **28**, 1988, pp. 101-109.
13. Hofmann, A., Khalil, A., and Kramer, H. P., "Operational characteristics in loops with Helium II flow driven by fountain effect pump", *Adv. in Cryog. Eng.* **33**, 1988, pp. 471-478.
14. Rayfield, G. W. and Reif, F., "Quantized Vortex Rings in Superfluid Helium", *Phys. Rev.* **136A**, 1964, p. 1194-1208.

CHAPTER 7.

THE SUPERFLUID VORTEX COOLER, INTEGRATED WITH A PULSE-TUBE REFRIGERATOR

In the previous chapter we have described the design of the superfluid vortex cooler (SVC) and have given the results of the experiments, in which the SVC has been precooled by a pumped liquid-helium bath. In the work, described in this chapter, we have used a two-stage PTR as a precooler for the SVC. The PTR has a lowest temperature of 1.27 K and provides 8 mW of cooling power at 1.45 K [1]. In principle a cryogen-free cooler with no moving parts in the cold area, providing cooling from room temperature to temperatures below 1 K, can be obtained. We will discuss the integration of the SVC with the PTR, present the experimental results, and suggest several ways of improvement of the integrated system.

7.1. THE INTEGRATION OF THE SVC WITH THE PTR

7.1.1. The SVC and the PTR before the integration

The operation principle of the SVC as well as its design are described in Chapter 6. The cooler is very simple and requires little additional infrastructure. Due to the gravity independence of the cooler, there are no specific requirements for its orientation. The cooler, which can be used as a precooler for the SVC, should have sufficient cooling power below the lambda temperature. Such a cooler has been developed in the Giessen University. It is a two-stage G-M type PTR with separate gas circuits. Each stage uses a compressor and a rotary valve. The stages operate at different frequencies. The ^4He stage precools the ^3He stage and the thermal shield around it down to 23 K. The ^3He stage has a no-load temperature of 1.27 K, which is the world record for PTRs at the moment. It provides 8 mW of cooling power at 1.45 K. So the SVC should operate with the input heating power less than 8 mW. In addition to the input heating power, a number of other heat loads, e.g. heat load from the filling capillaries, have to be removed by the PTR.

As it has been described in Chapter 6, a number of experiments, in which the SVC has been precooled by a liquid helium bath, have been made to obtain the required performance. In a certain configuration (see Table 7.1) we have reached 0.95 K with 6 mW of the input heating power and $T_b=1.4$ K (T_{L2} and T_{b2} in FIG. 15, Chapter 6). With a higher base temperature a lowest temperature of 0.98 K with 6.1 mW of the input heat and $T_b=1.47$ K has been achieved (T_{L1} and T_{b1} in FIG. 6.15). The average pressure in the SVC was 17.8 bar.

Table 7.1. The geometry of the main components of the SVC

		S₁	C₁	S₂	C₂
d	mm	3.5	0.2	2.5	0.2
L	mm	46 (26 packed length)	160	46 (26 packed length)	80

7.1.2. Filling capillaries

When the SVC is precooled by a liquid-helium bath, the filling capillaries go all the way from room temperature down to the SVC via the helium bath. Such an arrangement provides a good precooling of helium in the filling capillaries before they enter the SVC. In case of the PTR precooling, the filling capillaries are placed in vacuum and thermally anchored to the regenerator in a few places. The coldest point, at which the filling capillary is attached to the regenerator before entering the SVC, has approximately the lambda temperature. Below the lambda point helium has very high thermal conductivity [2]. A schematic drawing of the SVC with the filling capillary is given in FIG. 7.1. Here, T_r is the temperature of the last thermal anchoring point of the filling capillary before it enters the main heat exchanger of the SVC. The main heat exchanger is attached to the cold end of the PTR and has the temperature T_b . We assume that $T_r=2.17$ K, $T_b=1.4$ K, and that helium in the filling capillary has a pressure of 1 bar. The fountain pressure of helium at 2.17 K is 74 kPa (See FIG. 6.2). At 1.4 K the fountain pressure is only 3.6 kPa. Therefore, there is a pressure difference of about 70 kPa in the last part of the filling capillaries. This pressure difference drives a flow of normal helium from T_r to

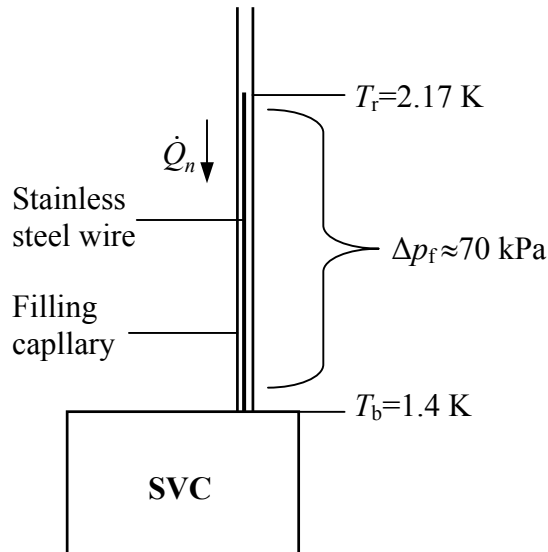


Figure 7. 1. Schematic drawing of the SVC with the filling capillary. The inner diameter of the filling capillary should be rather small to reduce the heat \dot{Q}_n , transported by normal helium with the high thermal conductivity. \dot{Q}_n flows from the capillary last attachment point with a temperature T_r to the main heat exchanger of the SVC with a temperature T_b .

T_b . As a result there will be a heat flow in the direction of the cold end of the PTR. To minimize this heat load, the last part of the filling capillary should be designed carefully.

The heat flow to the SVC can be calculated as

$$\dot{Q} = T_s \rho \dot{V}_n, \quad (7.1)$$

where \dot{V}_n is the volume flow of normal helium. The volume flow in the channel with the impedance factor Z due to the pressure difference Δp is

$$\dot{V}_n = \frac{\Delta p}{Z \eta_n}, \quad (7.2)$$

where η_n is the viscosity of normal helium. The impedance factor Z depends on the shape of the filling capillary. In our case the last 20 cm of the filling capillary with the diameter of 0.3 mm is filled with a stainless steel wire with the diameter of 0.27 mm. The order of magnitude of Z can be estimated with the expression for the laminar flow in an annular tube

$$Z = \frac{12L}{\pi \delta^3 d}, \quad (7.3)$$

where L and d are the length and the inner diameter of a filling capillary, and δ is the thickness of the gap between the walls of the filling capillary and the stainless steel wire, which is assumed to be constant and equal to 0.015 mm. Equation 7.3 is only valid for $\delta \ll d$. According to our estimation the heat leak through our filling capillary for the conditions, given above, should have a value between 1.5 and 18 mW at 1 bar average pressure in the capillary. The exact value of the heat leak depends on the shape of the gap between the walls of the filling capillary and the inserted stainless steel wire. According to the experimental results, which will be described in detail in the following paragraph, the heat leak is around 5 mW, which is within the estimated interval for the heat leak.

7.1.3. The integration of the SVC with the PTR

The SVC is attached to the cold heat exchanger of the ^3He stage by means of a clamp (see FIG. 7.2). A thin layer of indium provides a good thermal contact between the cold heat exchanger of the PTR and the main heat exchanger of the SVC. For convenience the SVC is placed upside down, opposite to the experiments in the liquid helium bath. There are two stainless steel filling capillaries with an inner diameter of 0.6 mm, which extend from room temperature down to the cold end of the ^4He stage. One of the capillaries is used for filling. The other one is the safety capillary, which is used in case of blockages due to possible impurities that might enter the capillary during a filling process. Below the first stage a T-piece connects these two capillaries to another one, with an inner diameter of 0.3 mm, which goes down to the SVC. The design of this

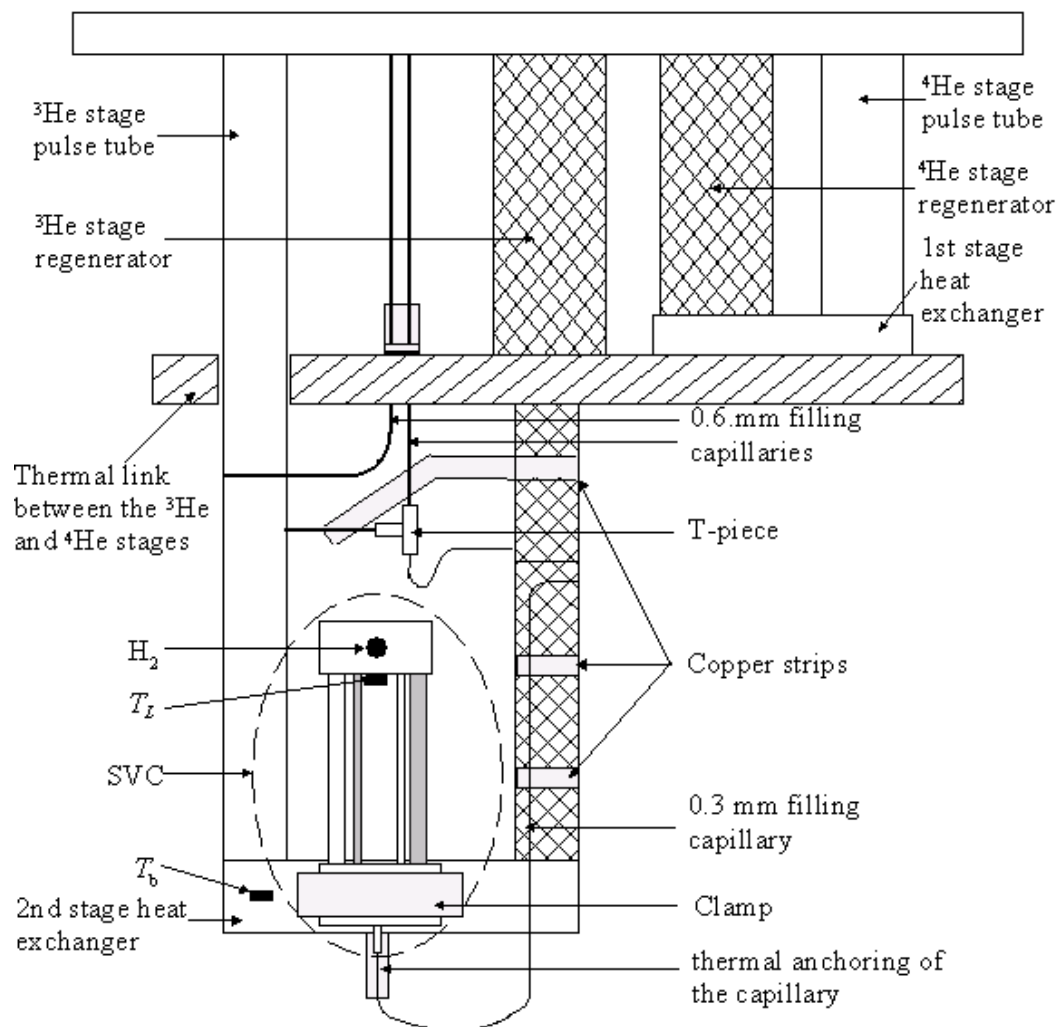


Figure 7. 2. Schematic diagram of the SVC, precooled by the two-stage PTR. For details of the SVC – see FIGs. 6.5 and 6.9.

capillary is described above. The filling capillary runs along the regenerator of the ^3He stage and is soldered in several places to copper strips, which are tightly fixed to the regenerator tube. A photograph of the low-temperature part of the integrated system is shown in FIG. 7.3.

A copper radiation shield (not shown in FIG. 7.2 and FIG. 7.3) is placed around the SVC and attached to the cold head of the second stage of the PTR. Several layers of superisolation are wrapped around the heat shield for the thermal isolation.

For temperature measurements at the fountain and the vortex heat exchangers we use two carbon-ceramic resistors, calibrated down to 0.5 K. The accuracy of these sensors is ± 0.01 K below 4.2 K and $\pm 0.0025T$ above 4.2 K.

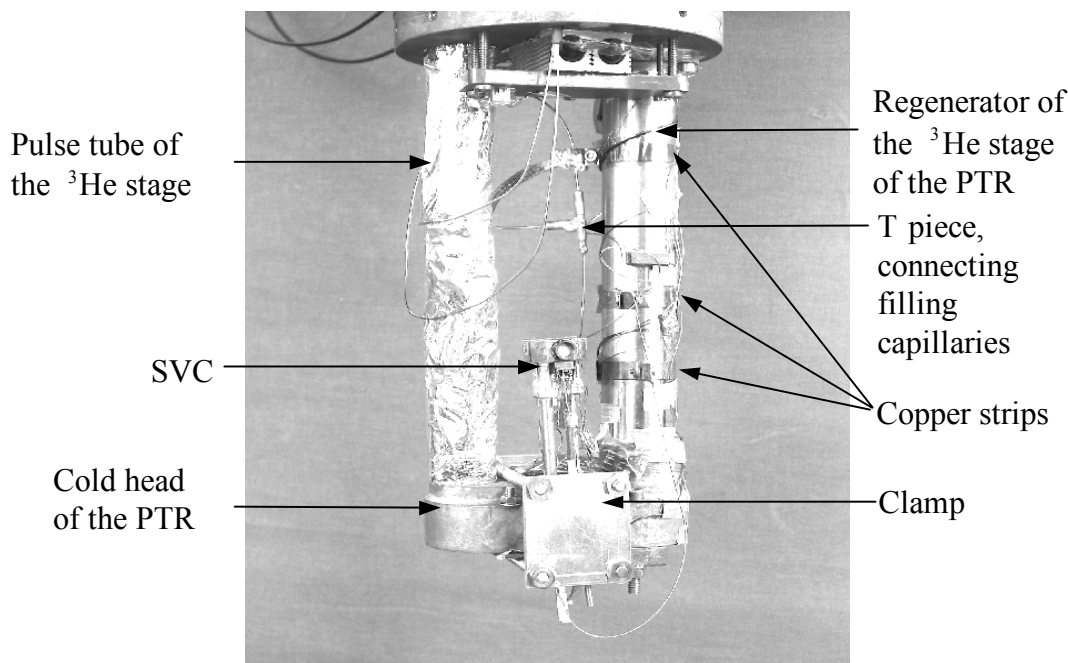


Figure 7. 3. The low-temperature part of the integrated PTR-SVC system.

The temperature of the PTR cold head (T_b) is measured by a Cernox thermometer. The accuracy of the Cernox thermometer is less than 0.01 K below 10 K.

7.2. EXPERIMENTAL RESULTS

In total 9 runs have been performed with the integrated system. The lowest no-load temperature of the PTR, before attaching the SVC, has been 1.27 K. With the SVC attached, the PTR has reached a temperature of 1.48 K. After that the frequency and the valves settings of the PTR have been readjusted and a temperature of 1.39 K has been achieved. The cooling power of the PTR at 1.39 K is around 5 mW. This cooling power deals with all the heat leaks coming from the SVC, mainly from the filling capillary.

When applying heat to the fountain part of the SVC, T_b , increases (see FIG. 7.4). At the same time the temperature of the vortex part, T_L , goes down (see FIG. 7.5). The time interval for each measurement is typically 12 min. With 8.9 mW of input heating power and a PTR cold head temperature of 1.52 K a lowest temperature 1.21 K has been reached (lines with open symbols in FIG. 7.5). The average pressure in the SVC in this case has been 10 bar. When the pressure in the SVC has been increased up to 17.5 bar, the lowest temperature reduced to 1.19 K with 8.4 mW of input heat and T_b of 1.5 K (lines with filled symbols in FIG. 7.5). Note, that the difference between T_H , T_{base} , and T_L at zero applied heat load to the SVC originates from a not identified heat load on the fountain heat exchanger that causes a slight cooling of the SVC, before the external heat is applied to it.

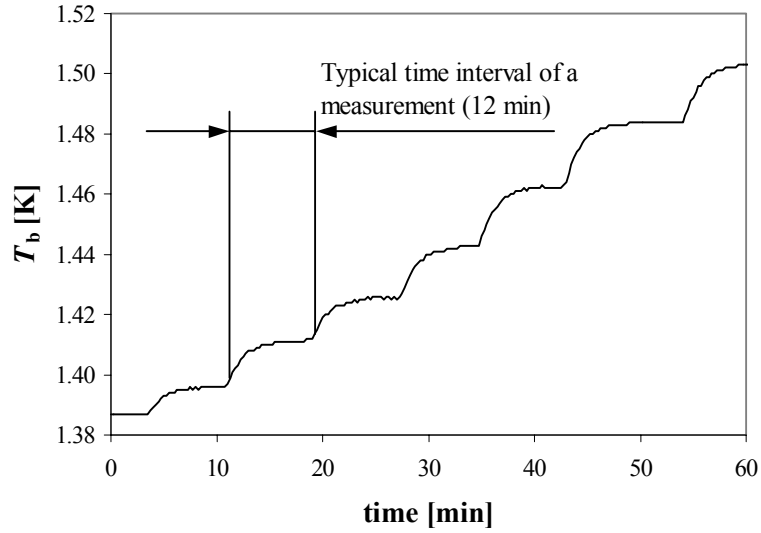


Figure 7. 4. The lowest temperature of the PTR, T_b , as a function of time. T_b increases, when heat is supplied to the SVC.

7.3. CONCLUSIONS AND SUGGESTIONS

The integration of the SVC with the PTR has demonstrated very promising results. The lowest temperature of 1.19 K with the integrated PTR-SVS system is lower than the lowest no-load temperature of the PTR alone. This result is a very good start. With further improvement of the system the lowest temperature can be reduced significantly.

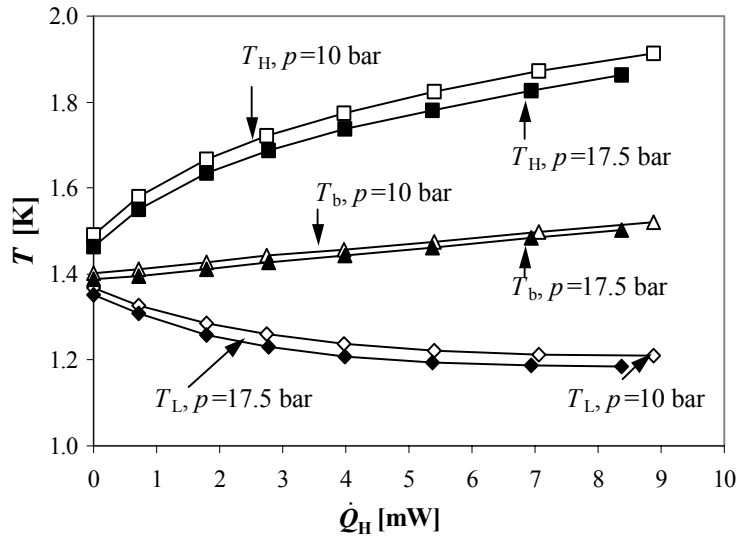


Figure 7. 5. Performance curves of the SVC, precooled by the PTR, at different pressure in the SVC.

In chapter 6 we have seen that the input heating power could only be reduced at the expense of an increase of the low-temperature limit of the SVC. Time was lacking to investigate the full potential of reducing the necessary heating power of the fountain pump without reducing the low-temperature performance.

Hereby, we suggest two possibilities of the optimisation of the integrated system by an improvement of the SVC and the infrastructure, associated with it. As we have seen above, there is about 5 mW of the heat load, brought by the SVC to the PTR. Most of it comes from the filling capillary. In the present system the filling capillary enters the SVC at the main heat exchanger. If this filling capillary is connected to the fountain heat exchanger instead of the main heat exchanger (see FIG. 7.6), the parasitic heat load turns into a positive heat input, needed to activate the fountain pump. The other possibility would be to decrease the heat load to the cold head of the PTR by omitting the filling capillaries at all. In this case the necessary amount of helium is filled into the vortex cooler at high-pressure and at room temperature. Miniaturization of the SVC is another question that has to be answered in the future.

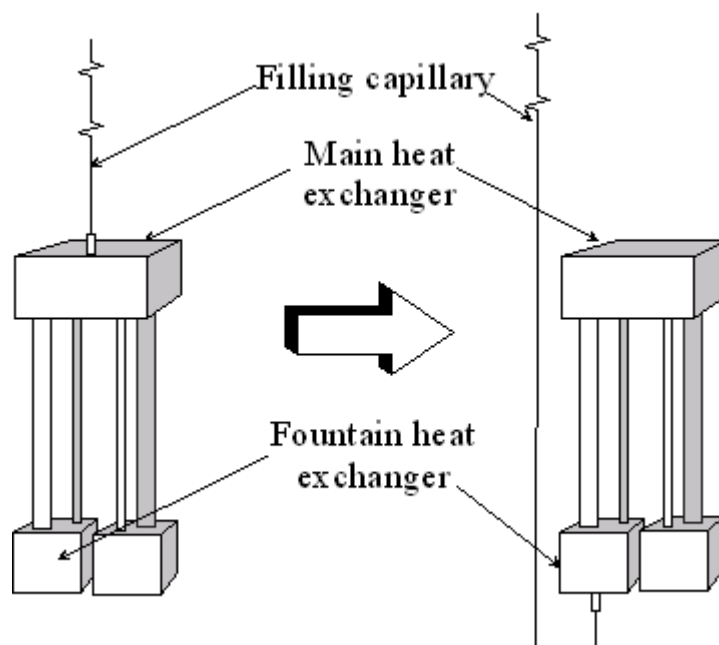


Figure 7. 6. Two different ways of the attachment the filling capillary to the SVC. On the left-hand side the filling capillary is attached to the main heat exchanger of the SVC. On the right-hand side it is attached to the fountain heat exchanger. In this arrangement the conduction heat load turns into the heat input, needed to operate the SVC.

REFERENCES

1. Jiang, N., Lindemann, U., Giebeler, F., and Thummes, G., “A ^3He pulse tube cooler operating down to 1.27 K”, *Cryogenics* **44**, 2004, pp. 809-816.
2. Keesom, W. H., “Helium”, Elsevier, Amsterdam – London – New York, 1942, p. 291.

CHAPTER 8

SUMMARY

In this thesis various aspects of low-temperature cryocooling have been discussed. Special attention has been paid to pulse-tube refrigeration in general, regenerator materials, and the integration of a pulse-tube refrigerator (PTR) with a superfluid vortex cooler (SVC). The main emphasis has been made on pulse-tube refrigerators, which have no moving parts in the low-temperature area, and, therefore, have a long lifetime and a low mechanical and magnetic interference. Both ^4He and ^3He are used as working fluids in a PTR, which is rather unique in this field.

One of the goals of this research has been to explore the physics and technology of PTRs, operating near their lowest temperature region. For that purpose two three-stage PTRs (PTR1 and PTR3) and a two-stage PTR (PTR2) have been developed. A lowest temperature of 2.19 K has been reached with PTR1, using ^4He . A cooling power of 40 mW has been measured at 4.2 K. With certain modifications of the system (increasing the pressure amplitude, using a titanium 3rd stage pulse tube, adjusting the orifices for the maximum cooling power) the cooling power has been increased to 160 mW with ^4He .

The lowest temperature of 2.19 K, reached with PTR1 with ^4He , is very close to the lambda transition temperature of ^4He (1.99 K at an average operating pressure of the PTR of about 15 bar). Just above the lambda point ^4He has a negative volumetric thermal expansion coefficient. This makes it impossible to reach temperatures below the lambda point using ^4He . To overcome this barrier ^3He is used. Using ^3He in PTR1, a lowest temperature of 1.78 K and a cooling power of 65 mW at 4.2 K have been reached.

PTR2 has been obtained by eliminating one stage from PTR1. In this way we have decreased the amount of variables to be adjusted during experiments. A number of experiments, such as determining the flow resistance of the regenerator, finding the optimum settings of the orifices, geometry modifications of the regenerator, etc., have been carried out with PTR2. A lot of work has been done on improving the rotary valve. The rotary valve is the second biggest source of power losses in GM-type PTRs (the biggest loss originates from the compressor). A new type of the rotary valve, 'no-contact' rotary valve, has been developed. By using the 'no-contact' rotary valve the power loss in the PTR has reduced to 12 % of the total input power from 28 % with the conventional valve.

PTR3 has been designed by scaling down PTR1 by 50%. This has been done by decreasing the diameters of the tubes and keeping the same lengths. The performance of PTR3 is required to be at least comparable to the performance of PTR1. In first order, reducing the cross-section with a factor of two and at the same time reducing the flow rate with a factor of two as well, should keep the lowest temperature the same. PTR3 is

small in size and weight, requires little input power, and uses small amount of working gas and regenerator material. In addition to that the system has been designed to be flexible and convenient for modifications. The volume of the low-temperature part of the PTR3 (pulse tubes + regenerator) is as small as 0.28 liter. By scaling down PTR1, we have reduced the necessary amount of ^3He from 220 to 160 liter NTP. The lowest temperature, achieved by PTR3 with ^4He , is 2.13 K. The lowest temperature, reached by PTR3 with ^3He , is 1.73 K. This is the record lowest temperature, reached by a PTR with a single-gas circuit¹. Cooling powers of 80 mW at 4.2 K with ^4He and 124 mW at 4.2 K with ^3He have been reached. The lowest temperatures, reached with PTR3 with ^4He and with ^3He , are almost the same as the temperatures, reached with PTR1. Therefore, generally speaking, the scaling of the system, based on a one-dimensional model for the PTR, worked out very well.

The regenerator is a very important component of a PTR. It consists of porous materials with a high heat capacity. However, at low temperatures the heat capacities of most regenerator materials rapidly decrease, whereas the heat capacity of helium increases. This has been one of the main obstacles for reaching low temperatures. In collaboration with the University of Tsukuba in Japan we have investigated potentially better regenerator materials for the sub-4 K temperature region. Heat capacities of a number of samples of rare-earth magnetic materials have been measured. From these materials GdAlO_3 seems to be the best material for the sub-4 K application. A high and rather sharp peak in the heat capacity of TbFeO_3 makes it a good candidate for further investigations as a potential regenerator material.

In the third part of this research the potential of a PTR to precool other devices for getting even lower temperatures has been studied. A PTR has been used to precool a superfluid vortex cooler. In principle a cryogen-free cooler with no moving parts in the cold area, providing cooling from room temperature to temperatures below 1 K, can be obtained. The working fluid in the SVC is superfluid ^4He . The cooler is gravity independent and hardly requires any additional infrastructure. First, the SVC has been precooled by a pumped liquid-helium bath. Various geometries of the cooler components as well as the influence of the working pressure and the base temperature on the performance of the cooler have been investigated. A lowest temperature of 0.88 K has been reached. After that, in collaboration with Giessen University in Germany, we have integrated the SVC with a PTR. With such a system a lowest temperature of 1.19 K has been reached. Several ways to improve the system have been suggested.

¹ The lowest temperature with a PTR with two separate gas circuits has been achieved in Giessen University and is 1.27 K.

APPENDIX

The pressure drop in the rotary valve due to the flow resistance in its channels can be calculated as follows. We consider the rotating valve connected to the low-pressure side of the compressor, so we have a steady flow of gas at a pressure close to p_L . The pressure drop due to the dividing flow is written as (FIG. A.1a) [1]

$$\Delta p_d = -\frac{1}{2}\rho(v_1^2 - v_2^2) + \frac{1}{2}\rho v_1^2 K_{12} + \frac{1}{2}\rho v_1^2 \frac{f_{fr1}L_1}{d_1} + \frac{1}{2}\rho v_2^2 \frac{f_{fr2}L_2}{d_2}, \quad (\text{A.1})$$

where ρ is the density of the gas, v is the velocity, f_{fr} is the friction factor, L and d are the length and the diameter of a channel, and K_{12} is a dimensionless coefficient, expressed by

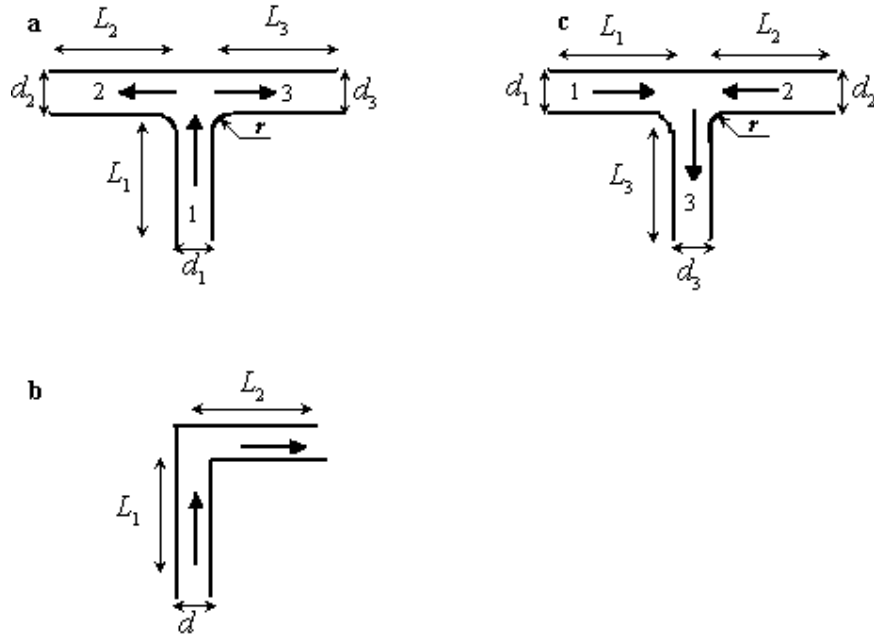


Figure A. 1. Various pipe junctions: **(a)** dividing flow, **(b)** miter bend, **(c)** combining flow.

$$K_{12} = 0.59 + \left[1.18 - 1.84 \left(\frac{r}{d} \right)^{1/2} + 1.16 \frac{r}{d} \right] \frac{v_2}{v_1} - \left[0.68 - 1.04 \left(\frac{r}{d} \right)^{1/2} + 1.16 \frac{r}{d} \right] \left(\frac{v_2}{v_1} \right)^2, \quad (\text{A.2})$$

where r is the radius of rounding. Indexes 1 and 2 stand for a branch, supplying flow to the junction. Here we assume, that $v_2=v_3$, $d_2=d_3$, and $L_2=L_3$. In our case $r=0$, so, equation A.2 reduces to

$$K_{12} = 0.59 + 1.18 \frac{v_2}{v_1} - 0.68 \left(\frac{v_2}{v_1} \right)^2. \quad (\text{A.3})$$

The pressure loss in a miter bend of 90° (see FIG. A.1b) is equal to

$$\Delta p_{mb} = \frac{1}{2} \rho v^2 \left[K_{Re} + \frac{f_{fr}(L_2 + L_1)}{d} \right], \quad (\text{A.4})$$

where

$$K_{Re} = K \left(\frac{2 \times 10^5}{Re} \right)^{0.2}. \quad (\text{A.5})$$

In our case for $Re < 2 \times 10^5$, $K=1.1$.

Finally, the pressure drop in the combining flow (FIG. A.1c) is calculated with

$$\Delta p_j = -\frac{1}{2} \rho (v_1^2 - v_3^2) + \frac{1}{2} \rho v_3^2 K_{13} + \frac{1}{2} \rho v_1^2 \frac{f_{fr1} L_1}{d_1} + \frac{1}{2} \rho v_3^2 \frac{f_{fr3} L_3}{d_3}, \quad (\text{A.6})$$

with

$$K_{13} = 1.19 - 1.16 \left(\frac{r}{d} \right)^{1/2} + 0.46 \frac{r}{d} - 1.73 \left(1 - \frac{r}{d} \right) \frac{v_1}{v_3} + \left(1.34 - 1.69 \frac{r}{d} \right) \left(\frac{v_1}{v_3} \right)^2. \quad (\text{A.7})$$

For $r=0$ equation 7 becomes

$$K_{13} = 1.19 - 1.73 \frac{v_1}{v_3} + 1.34 \left(\frac{v_1}{v_3} \right)^2. \quad (\text{A.8})$$

The scheme of the gas flow pass in the conventional rotary valve is shown in FIG. A.2. Typical values of the Reynolds number in our rotary valve are 4×10^4 – 5×10^4 . Hence, the friction factor is equal to 0.026 [1]. The valve is at room temperature. We consider a gas flow of 1 mol/s entering the rotary valve at $p_r=12$ bar. First the gas flow in the stator is divided in two. With the dimensions, indicated in FIG. A.2, and with equations A.1 and A.3 the pressure drop due to the dividing flow is equal to

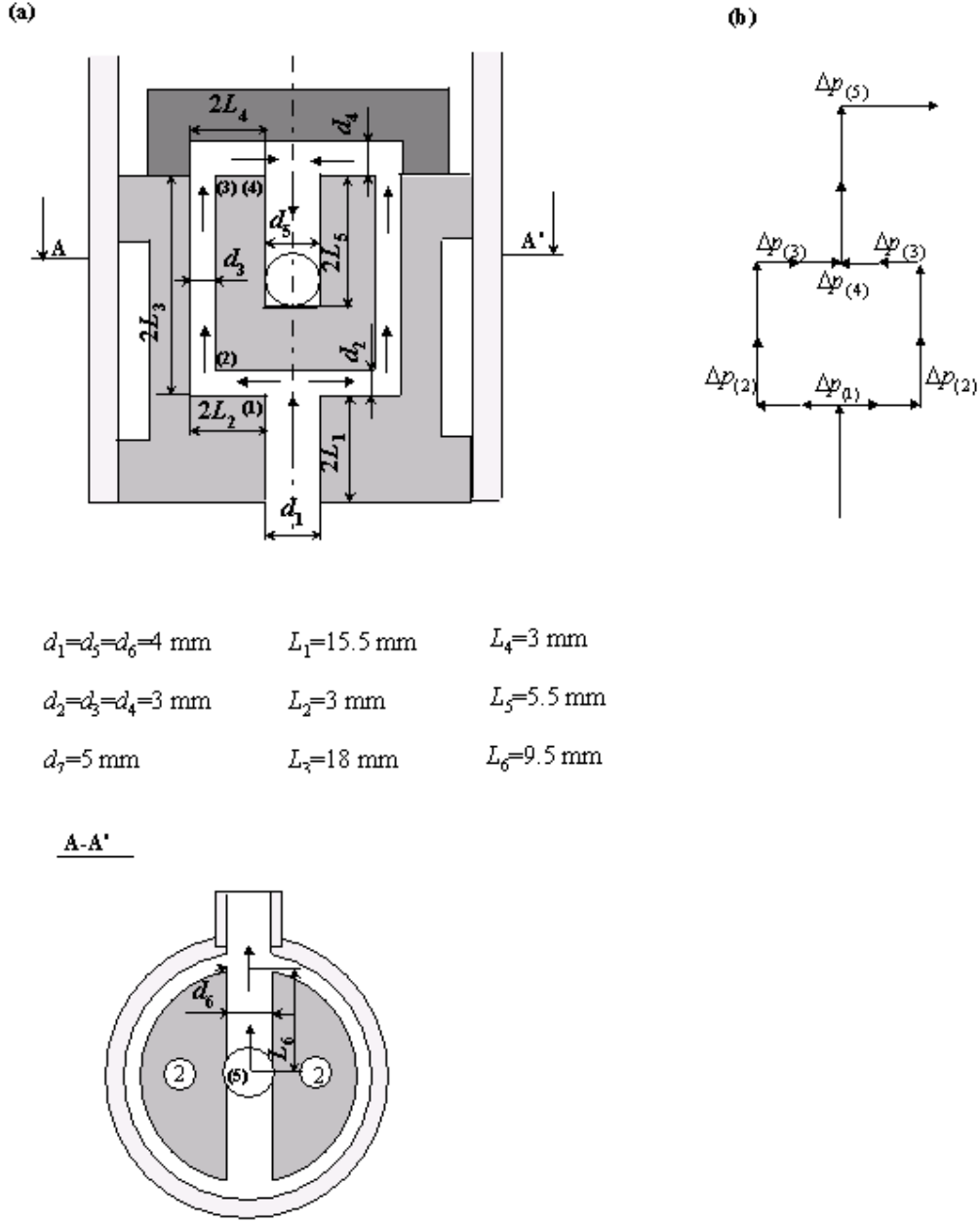


Figure A. 2. (a) Schematic diagram of the gas flow pass in the conventional rotary valve, when the system is connected to the low-pressure side of the compressor. (b) Equivalent diagram of the gas flow pass in the conventional rotary valve. The Δp_i refer to the various pressure drops in the corresponding flow-channel components.

$$\Delta p_{(1)} = 0.29 \text{ bar. (A.9)}$$

After that there are two miter bends, (2) and (3). With equations A.4 and A.5 they give pressure drops of

$$\Delta p_{(2)} = 2 \times 0.385 = 0.77 \text{ bar, (A.10)}$$

$$\Delta p_{(3)} = 2 \times 0.385 = 0.77 \text{ bar. (A.11)}$$

The combining flow (4) with equations A.6 and A.8 is calculated to be

$$\Delta p_{(4)} = 0.27 \text{ bar} . \text{ (A.12)}$$

In the joint (5) the gas flow is actually dividing in two parts. However, the resistance of the channel between the stator and the housing is large. So, most of the gas goes directly to the connection to the low-pressure side of the compressor. Thus, we assume, that the pressure drop in the joint (5) can be calculated with the expressions for a miter bend A.4 and A.5

$$\Delta p_5 = 0.091 \text{ bar} . \text{ (A.13)}$$

Combining expressions A.9-13, we get for the total pressure drop in the rotary valve, when it is connected to the low-pressure side of the compressor,

$$\Delta p_{tot}^{p_L} = 2.24 \text{ bar} . \text{ (A.14)}$$

The scheme of the gas flow pass, when it is connected to the high-pressure side of the compressor, is shown in FIG. A.3. We consider a gas flow of 1 mol/s entering the rotary valve at $p_H = 25$ bar. The gas flows into two channels with a diameter d_1 and a length L_1 . There is a miter bend in each of the two channels. With equations A.4 and A.5 the pressure drop, resulting from the bends, is

$$\Delta p_{(1)} = 2 \times 0.183 = 0.366 \text{ bar} . \text{ (A.15)}$$

The pressure drop due to the following combining flow can be calculated with equations A.6 and A.8

$$\Delta p_{(2)} = 0.143 \text{ bar} . \text{ (A.16)}$$

Therefore, with equations A.15 and A.16 the total pressure drop in the rotary valve, when it is connected to the high-pressure side of the compressor, is

$$\Delta p_{tot}^{p_H} = 0.51 \text{ bar} . \text{ (A.17)}$$

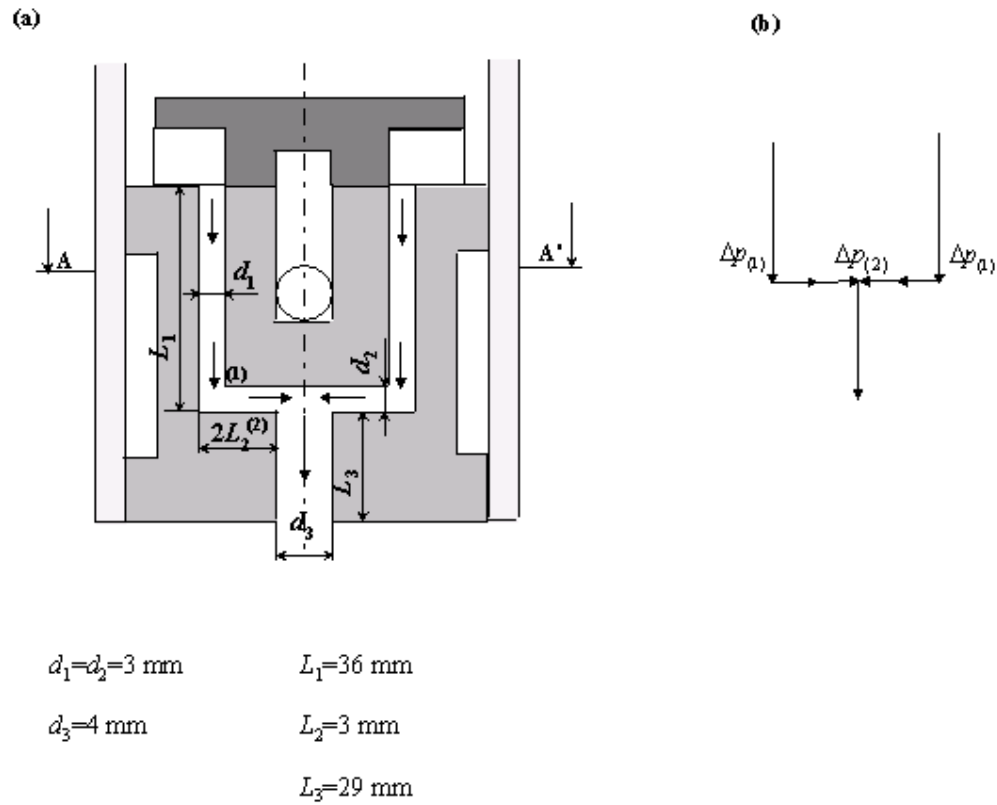


Figure A. 3. (a) Schematic diagram of the gas flow pass in the conventional rotary valve, when the system is connected to the high-pressure side of the compressor. **(b)** Equivalent diagram of the gas flow pass in the conventional rotary valve. The Δp_i refer to the various pressure drops in the corresponding flow-channel components.

REFERENCES

1. Blevins, R. D., "Applied fluid dynamics handbook", Krieger Publishing Company, USA, 1984.

SAMENVATTING

In dit proefschrift zijn verschillende aspecten van lage temperatuur cryo-cooling beschreven. Er is aandacht besteed aan pulsbuskoelers in het algemeen, regenerator materialen, en de integratie van een pulsbuskoeler (pulse tube refrigerator, PTR) met een supervloeibare vortex koeler (superfluid vortex cooler, SVC). De nadruk ligt op pulsbus koelers, welke geen bewegende delen hebben in het koude deel, waardoor ze een lange levensduur hebben en weinig mechanische en magnetische storingen teweeg brengen. Er is gebruik gemaakt van zowel ^4He als ^3He als werkend medium in de PTR, hetgeen zeer ongebruikelijk is in dit vakgebied.

Een van de doelen van het onderzoek was het verkennen van de fysica en de technologie van PTR's wanneer deze werken nabij hun laagst haalbare temperatuur. Om dit te kunnen onderzoeken zijn twee drietraps PTRs (PTR1 and PTR3) en één tweetraps PTR (PTR2) ontwikkeld. Met het eerste systeem, PTR1, is een laagste temperatuur gehaald van 2.19 K, gebruik makend van ^4He . Bij 4.2 K is een koelvermogen van 40 mW gemeten. Door een aantal modificaties aan te brengen (verhogen van de amplitude van de drukvariaties, gebruik van een titanium legering voor de pulsbus van de 3^e trap, optimalisering van instellingen van regelventielen) is het koelvermogen bij 4.2 K verhoogd tot 160 mW, wederom met ^4He .

De laagste temperatuur van 2.19 K, behaald met PTR1 met ^4He , is erg dicht bij de lambda overgangstemperatuur van ^4He (1.99 K bij een gemiddelde werkdruk in de PTR van 15 bar). Vlak boven het lambda punt heeft ^4He een negatieve volumetrische thermische expansie coëfficiënt.. Dit maakt het onmogelijk om met ^4He als werkend medium een temperatuur lager dan het lambdapunt te behalen. Om deze grens toch te kunnen passeren is ^3He gebruikt. Gebruik makend van ^3He in PTR1, is een laagste temperatuur behaald van 1.78 K, terwijl een koelvermogen van 65 mW gemeten is bij 4.2 K.

Het tweede systeem, PTR2, is tot stand gekomen door van PTR1 een enkele trap weg te laten. Op deze wijze werd het aantal tijdens experimenten in te stellen variabelen gereduceerd. Een aantal experimenten, zoals bijvoorbeeld het bepalen van de optimale stromingsweerstand van de regenerator, het vinden van optimale instelling van de regelventielen en het testen van geometrische modificaties aan de regenerator, zijn uitgevoerd met PTR2. Er is veel aandacht besteed aan het verbeteren van de roterende klep. Na de compressor is de roterende klep de grootste bron van verlies aan vermogen in GM-type PTRs. Een nieuw type 'contactloze' roterende klep is ontwikkeld. Bij gebruik van de nieuwe 'contactloze' roterende klep gaat nog slechts 12 % van het input vermogen verloren in de klep, tegenover 28 % met de conventionele klep.

Het ontwerp van PTR3 is gebaseerd op een 50% verkleining van PTR1. Dit terugschalen is gerealiseerd door de lengtes van de diverse buizen gelijk te houden, en de diameters te verkleinen. Als ontwerpeis is gesteld dat de performance van PTR3 tenminste vergelijkbaar zou moeten zijn met de performance van PTR1. In een eerste orde afchatting zou de laagste temperatuur gelijk moeten zijn, als gelijktijdig met het terugbrengen van het doorstroomd oppervlak met een factor twee, ook de stroming met een factor twee wordt gereduceerd. PTR3 is compact qua afmetingen en gewicht, vergt minder ingangsvermogen, en gebruikt slechts een kleine hoeveelheid werkgas zowel als regeneratormateriaal. Bovendien is het systeem zo ontworpen dat het flexibel is en eenvoudig te modificeren. Het volume van het lage temperatuurdeel van PTR3 (pulsbuis + regenerator) bedraagt slechts 0.28 liter. Door het verkleinen van PTR1 is de noodzakelijke hoeveelheid ^3He afgenomen van 220 tot 160 liter NTP. De laagste temperatuur die is behaald met PTR3 met ^4He is 2.13 K. Gevuld met ^3He is een laagste temperatuur van 1.73 K behaald. Dit is wereldwijd de laagste temperatuur, bereikt door een PTR met een enkel gas circuit¹. Koelvermogens van 80 mW bij 4.2 K met ^4He en 124 mW bij 4.2 K met ^3He zijn gemeten. De laagste temperaturen, zoals die zijn gehaald met PTR3 met ^4He en met ^3He , zijn vrijwel gelijk aan de temperaturen die zijn bereikt met PTR1. Er kan dus gesteld worden dat het schalen van de pulsbus koeler, gebaseerd op één dimensional model van de PTR, goed heeft gewerkt.

De regenerator is een zeer belangrijke component van een PTR. De regenerator bestaat uit een poreus materiaal met een hoge warmtecapaciteit. Bij lage temperaturen, echter, neemt de warmtecapaciteit van de meeste regenerator materialen sterk af, terwijl de warmtecapaciteit van het Helium toeneemt. Dit is lange tijd één van de obstakels geweest voor het bereiken van lage temperaturen. In samenwerking met de Universiteit van Tsukuba in Japan zijn potentieel betere regenerator materialen voor het sub-4 K temperatuurgebied onderzocht. De warmtecapaciteit is gemeten van een aantal monsters van rare-earth magnetische materialen. Van deze materialen lijkt GdAlO_3 de beste keuze voor sub-4 K toepassingen. Een hoge en redelijk scherpe piek in de warmtecapaciteit van TbFeO_3 maakt dit materiaal een goede kandidaat voor verder onderzoek naar de geschiktheid als potentieel regenerator materiaal.

In het derde deel van dit onderzoek is bestudeerd in hoeverre een PTR gebruikt kan worden als voorcoeler voor andere systemen, waarmee nog lagere temperaturen kunnen worden bereikt. Een PTR is gebruikt om een supervloeibare vortex koeler (SVC) voor te koelen. In principe is op deze wijze een koeler te construeren welke van kamertemperatuur koelt tot beneden 1 K, zonder bewegende delen in de kou, en zonder gebruik te maken van cryogene vloeistoffen. Het werkend medium in een SVC is supervloeibaar ^4He . De SVC is onafhankelijk van zwaartekracht en vereist nauwelijks additionele infrastructuur. In eerste instantie is de SVC voorgekoeld met een gepompt vloeibaar helium bad. Verschillende geometrieën van de koel componenten zijn getest, alsook de invloed van de werkdruk en de basistemperatuur op de prestaties van de koeler. Een laagste temperatuur van 0.88 K is bereikt. Naderhand is, in samenwerking met de Universiteit van Giessen in Duitsland, de SVC geïntegreerd met een PTR. Met deze combinatie is een laagste temperatuur van 1.19 K behaald. Er zijn verschillende suggesties gedaan om het systeem nog verder te verbeteren.

¹ De laagste temperatuur met een PTR met twee gescheiden gassystemen is behaald op de Universiteit van Giessen en bedraagt 1.27 K.

КРАТКОЕ СОДЕРЖАНИЕ

Эта работа посвящена различным аспектам криогенного охлаждения. Особое внимание уделено охлаждению с помощью пульсационных труб (pulse-tube refrigerator, PTR), а также регенерационным материалам и интеграции пульсационной трубы с вихревым рефрижератором, работающем на основе сверхтекучего гелия (superfluid vortex cooler, SVC). Пульсационная труба не содержит движущихся частей и механизмов в низкотемпературной части установки и поэтому имеет долгий срок службы и низкий уровень механических и магнитных помех. Одной из довольно уникальных особенностей этой исследовательской работы является то, что как ^4He так и ^3He использовались в установке качестве рабочей жидкости.

Исследование физики и технологии пульсационных труб, работающих в районе их низкотемпературного предела, являлось одной из целей этого проекта. Для этого были разработаны и построены две трехступенчатые пульсационные трубы (PTR1 и PTR3) и одна двухступенчатая пульсационная труба (PTR2). Используя ^4He в PTR1, была достигнута температура 2.19 К. Охлаждающая мощность 40 мВт была измерена при температуре 4.2 К. С определенными изменениями (увеличением амплитуды давления, использованием титановой третьей ступени, настройкой клапанов на максимальную мощность охлаждения) мощность была увеличена до 160 мВт при температуре 4.2 К.

Достигнутая с PTR1 температура 2.19 К находится близко к границе λ -перехода ^4He (1.99 К при среднем рабочем давлении пульсационной трубы, равном 1.5 МПа). Ниже границы λ -перехода ^4He имеет отрицательный коэффициент объемного расширения. В этом случае становится невозможным достичь температуру ниже λ -точки, используя ^4He . Этот барьер может быть преодолен при помощи использования ^3He . Используя ^3He в PTR1, были достигнуты температура 1.78 К и охлаждающая мощность 65 мВт при 4.2 К.

Двухступенчатая пульсационная труба PTR2 была получена путем исключения одной ступени из PTR1. Таким образом мы уменьшили количество переменных для оптимизации. Используя PTR2, был проведен ряд экспериментов, таких как определение сопротивления регенератора, нахождения оптимальных установок клапанов, изменение геометрии регенератора и так далее. Было проделано много работы по оптимизации ротационного клапана. Ротационный клапан – второй наибольший источник потерь энергии в пульсационных трубах типа Гиффорда-Мак-Магона (GM-type PTR) (наибольшим источником потерь энергии является компрессор). Был разработан новый тип ротационного клапана –

“бесконтактный” ротационный клапан. С использованием “бесконтактного” ротационного клапана потери энергии уменьшились до 12% от общей потребляемой мощности в сравнении с 28 % со стандартным клапаном.

Трехступенчатая PTR3 является уменьшенной копией PTR1 (объем PTR3 равен 50% объема PTR1). Уменьшение объема получено за счет уменьшения диаметров труб установки. Длина труб PTR3 и PTR1 одинакова. Из предварительных расчетов следовало, что при уменьшении площади поперечного сечения труб PTR1 на какой-либо фактор и при одновременном уменьшении потока на тот же фактор, температура холодного конца установки должна остаться неизменной. Также производительность уменьшенной установки (PTR3) должна быть по крайней мере равна производительности PTR1. PTR3 имеет небольшой размер и вес, потребляет мало энергии и требует небольшое количество рабочего газа и регенерационных материалов. Конструкция установки предусматривает возможность модификаций и легкого доступа к составляющим компонентам. Объем низкотемпературной части установки (3 пульсационные трубы + регенератор) составляет всего 0.28 л. Таким образом в результате уменьшения масштаба PTR1 количество требуемого рабочего газа уменьшилось с 220 л до 160 л при нормальных условиях. Это особенно важно в случае использования ^3He , цена которого приблизительно равна 125 \$/л.

С использованием ^4He в PTR3 была достигнута температура 2.13 К. После замены ^4He на ^3He температура понизилась до 1.73 К. Это рекордно-низкая температура, когда-либо достигнутая пульсационной трубой с единым циркуляционным потоком газа.¹ Охлаждающая мощность 80 мВт при 4.2 К была достигнута с ^4He и 124 мВт при 4.2 К - с ^3He . Температура холодного конца PTR3 с ^3He имеет практически такую же величину что и температура холодного конца PTR1 с ^3He . То же самое можно сказать и о температурах холодных концов PTR1 и PTR3 с ^4He . Таким образом, уменьшение объема PTR1, основанное на одномерной модели для пульсационных труб, имело положительный результат.

Одним из наиболее важных компонентов PTR является регенератор. Регенератор состоит из пористых материалов с высокой теплоемкостью. С понижением температуры теплоемкость большинства регенерационных материалов значительно уменьшается. В то же время теплоемкость гелия повышается. Этот факт являлся одним из основных препятствий на пути достижения низких температур регенеративными рефрижераторами. Совместно с университетом Тсукубы (Япония) мы исследовали ряд потенциальных регенерационных материалов на основе редкоземельных металлов для использования при температурах ниже 4 К. Согласно результатам измерений теплоемкостей образцов материалов мы пришли к выводу, что GdAlO_3 оказался наилучшим из исследованных материалов. Другой материал, TbFeO_3 , который продемонстрировал высокий, но довольно узкий максимум теплоемкости, рекомендуется для дальнейших исследований в качестве потенциального регенерационного материала.

В третьей части этой работы мы исследовали пульсационную трубу в качестве ступени предварительного охлаждения. Пульсационная труба была

¹ Самая низкая температура, достигнутая PTR с двумя различными циркуляционными потоками газа (^3He и ^4He), была достигнута в университете Гиссена (Германия) и имеет значение 1.27 К.

использована для преохлаждения вихревого рефрижератора, работающего на основе сверхтекучего ^4He (SVC). Полученная установка не содержит движущихся частей и механизмов в низкотемпературной части и имеет потенциал достижения температур ниже 1 К. Рабочие процессы в SVC не зависят от гравитации, что значительно облегчает процесс интеграции SVC и PTR.

Вначале был проведен ряд экспериментов, в которых SVC был преохлажден путем его помещения в емкость с жидким ^4He , пары которого были откачаны до достижения нужной базовой температуры (≈ 1.4 К). В этих экспериментах мы исследовали влияние размеров компонентов SVC, а также влияние давления рабочей жидкости и базовой температуры, на производительность рефрижератора. Была достигнута температура 0.88 К. На следующем этапе, совместно с университетом Гиссена (Германия), мы объединили SVC с PTR. В результате последующих экспериментов с полученной установкой была достигнута температура 1.19 К. В заключении было предложено несколько возможных путей усовершенствования установки.

ACKNOWLEDGMENTS

“Discoveries and improvements invariably involve the cooperation of many minds”
Alexander Graham Bell

Throughout my PhD research, resulted in writing of this thesis, I have received considerable support from my supervisor, Fons de Waele, my colleagues, family, and friends. Hereby, I would like to thank all of you for your help, understanding, encouragement, and friendship.

Carrying out this research (and I am sure it can be said about any research in general) required a lot of patience, hard work, and dedication not only from myself, but also from people, I have been working with. Many times we had to work literally days and nights with only a little hope for a good result. However, once getting a goal compensated all the frustrations and stresses on the way and motivated for a new challenge.

I would like to express my gratitude to Fons de Waele for being an excellent teacher and understanding and motivating supervisor. I have really learned a lot from you, Fons, from writing scientific articles to making good soldering joints and playing pool. However, I still have a long way of practising the last one in order to become a considerable pool opponent.

I would also like to thank my second supervisor, Prof. G. Thummes, for the opportunity to work in his group, fruitful discussions, and for a couple of wasted week-ends, which he spent with us in the lab, helping us to make a deadline.

Here, I would like to change the usual routine of acknowledgements, in which partners are being thanked as “last but not least”. I am incredibly grateful to Peter for being my very best friend and an outstanding discussion opponent. A great number of ideas resulted from our discussions and were successfully implied in my research. I thank you, Peter, for motivating me, teaching me to trust in myself, always being there for me, and helping me not to give up in the moments, when I was down.

I would like to thank Prof. Marcel ter Brake and Prof. Rini van Dongen for reading this thesis and helping me to improve it with their constructive remarks and suggestions.

The research project, described in Chapter 5, would not be possible without the collaboration with the University of Tsukuba, Japan, and in particular with Prof. H. Ikeda. I would like to thank Prof. H. Ikeda and Prof. Y. Matsubara, who helped to establish the collaboration. I would also like to thank Prof. Y. Matsubara for his interest in my work and for many useful discussions during his stay in our group.

There are a number of great physicists and cryocooler experts, who I would like to thank for helping me to understand certain aspects of low-temperature physics better and for valuable discussions. I am very grateful to Prof. R. Radebaugh, Prof. K. A. Gschneidner Jr., Prof. A.A. Arkharov, Prof. I.A. Arkharov, Prof. I.F. Kuzmenko,

Acknowledgments

Prof. K. Kopinga, Dr. J. Dam, Dr. J. Zeegers, Dr. L. Salerno, Dr. G. Kaiser, Dr. B. Helvensteijn, and many others. I would like to thank Prof. R. Radebaugh for being an excellent dance partner. Special thanks to Jacques Dam for a lot of help, professional support, being a good friend, and, of course, for taking fantastic photos of my dance performances.

I want to thank all current and former members of the low-temperature group for friendly and creative atmosphere, nice dinners out and certainly memorable annual barbeques. In particular, I would like to thank Manon Will for being an excellent roommate and a great board-game partner.

During the design, construction, and installation of the experimental set-ups I received a lot of technical support from the technicians. I thank Loek Penders, Leo van Hout, Peter Cappon, and Jos van Amelsvoort for their highly professional help. I also thank Jos de Laat and members of the Physics Faculty workshop: Marius Bogers, Henk van Helvoirt, Han van Dekker, Ginny Fransen - ter Plegt, Frank van Hoof and others for their continuous assistance in producing big and small parts for my set-ups and for the constructive discussions.

Further, I would like to thank all the students and PhD students, I worked with. I thank Rens, Laurens, Evi, Kris, and Koen for the good work during their traineeships, as well as for being fun to work with. I thank Uli, Frank, and Ning, who I worked with in Giessen University. Special thanks to my student assistants: Laurens and Joost. It would be much more difficult for me to successfully complete the projects without your help, including working overtime.

I want to thank my two “paranimfen” and also very good friends, Laurens and Misha, for their support, friendship, and contributions to my research. The outcome of Laurens’s great help during the regenerator materials project has been a successful publication in Cryogenics. And several nights, which Misha spent with me in the laboratory, resulted in reaching a lowest temperature of 1.73 K with my pulse-tube refrigerator. In addition to that I thank Misha and Laurens, as well as my other friends: Sveta, Wouter, Jenny, Alex, Valia, Vili, Ingrid, Ate, Walter, Cora, Marten, Anne, Patrique, Petra, Jorien, Arnoud, Jerome, Sibylle, Olya, Berry, David, Gabriel, and others, for great times together, including going out for dinners, concerts, movies, travelling, breakfast by the Eiffel Tower, etc., which always helped me to unwind. I would like to thank my dancing teacher, Suzanne, for great dance trainings, which always helped me to relax after a difficult working day.

I owe a tremendous debt to my parents, who greatly supported me throughout all five years of my research. Дорогие мама и папа, огромное спасибо вам за вашу помощь, поддержку, заботу и любовь.

Irina Tanaeva
Eindhoven, October 2004

CURRICULUM VITAE

Irina Tanaeva

- | | |
|---------------------------|---|
| May 5, 1976 | Born in Moscow, Russia |
| June 1993 | High school graduation: major in physics and mathematics. Diploma with distinction. |
| June 1998 | Moscow State Academy of Engineering and Computing Science, Russia. M.Sc. Applied Physics, major in cryogenic and vacuum engineering. Diploma with distinction. Graduation project “Development of a new type of distillation unit for an air separation plant”, performed at “Cryogenmash”, Russia. |
| June 1999 | Moscow State Open Teacher’s Training University, Russia. B.Sc. Philology. Diploma with distinction. |
| August 1999 – August 2004 | PhD research in Low Temperature group of Applied Physics Department of Eindhoven University of Technology, The Netherlands. Subject: “Low-temperature cryocooling”. Supervised by Prof. Dr. A.T.A.M. de Waele. |